AWARD NUMBER: W81XWH-15-2-0002

TITLE: Improvement and Extension of Auditory Hazard Models

PRINCIPAL INVESTIGATOR: Timothy Walilko, Ph.D.

CONTRACTING ORGANIZATION: Applied Research Associates, Inc.
Albuquerque, NM 87110

REPORT DATE: January 2019

TYPE OF REPORT: Final Report

PREPARED FOR: U.S. Army Medical Research and Materiel Command
Fort Detrick, Maryland 21702-5012

REPORT DOCUMENTATION PAGE

Form Approved
OMB No. 0704-0188

1. REPORT DATE	**2. REPORT TYPE**	**3. DATES COVERED**
January 2019	Final Report	1 Nov 2014 - 31 Oct 2018

4. TITLE AND SUBTITLE

Improvement and Extension of Auditory Hazard Models

5a. CONTRACT NUMBER

W81XWH-15-2-0002

5b. GRANT NUMBER

5c. PROGRAM ELEMENT NO.

6. AUTHOR(S)

[1]Tim Walilko, Ph.D., Ted Argo, Ph.D.

[2]Daniel J. Tollin, Ph.D., Nathaniel T. Greene, Ph.D.

[3]James Easter, P.E.

5d. PROJECT NUMBER

5e. TASK NUMBER

5f. WORK UNIT NUMBER

7. PERFORMING ORGANIZATION NAME(S) AND ADDRESS(ES) AND ADDRESS(ES)

[1]Applied Research Associates, Inc., 4300 San Mateo NE, Albuquerque, NM 87110

[2]University of Colorado Anschutz Medical Campus, 12631 E 17th Ave., MS B205, Aurora, CO 80045

[3]Cochlear Boulder LLC, 5445 Airport Blvd Ste 106, Boulder, CO 80301

8. PERFORMING ORGANIZATION REPORT NUMBER

9. SPONSORING / MONITORING AGENCY NAME(S) AND ADDRESS(ES)

U.S. Army Medical Research and Materiel Command

Fort Detrick, Maryland 21702-5012

10. SPONSOR/MONITOR'S ACRONYM(S)

11. SPONSOR/MONITOR'S REPORT NUMBER(S)

12. DISTRIBUTION / AVAILABILITY STATEMENT

Approved for Public Release; Distribution Unlimited

13. SUPPLEMENTARY NOTES

14. ABSTRACT

The Blast Auditory Model (BAM) is a comprehensive outer to inner ear model under development that translates the extreme range of acoustic exposures encountered in the modern military service environment to clinically relevant predictions of cochlear and synaptic damage that can be mapped to operationally relevant metrics such as the loss of speech discrimination. To make predictions the BAM propagates the user provided incident blast wave through the modeled auditory system that was derived using novel experimental methods that included the use of laser Doppler velocimetry and strategically placed fiber-optic pressure sensors in the outer, middle, and inner ear for both a chinchilla model and human temporal bones. To provide a clinically relevant metric, the pressure output in the inner ear is used to selectively degrade the function of an auditory nerve fiber model. Once the model is fully validated, BAM will provide engineers developing improved hearing protection devices as well as clinicians and industrial hygienists, a tool for exploring the relationship between high intensity noise exposures and resulting deficits in operational performance metrics.

15. SUBJECT TERMS

Auditory Models, Blast Exposure, Combat, Hair Cell Damage, Hearing Loss/Threshold Shifts, Hearing Protection Devices

16. SECURITY CLASSIFICATION OF:			**17. LIMITATION OF ABSTRACT**	**18. NUMBER OF PAGES**	
a. REPORT	**b. ABSTRACT**	**c. THIS PAGE**			**19b. TELEPHONE NUMBER** (include area code)
Unclassified	Unclassified	Unclassified	Unclassified	168	

TABLE OF CONTENTS

1 EXECUTIVE SUMMARY

The *Improvement and Extension of Auditory Hazard Models* program was a comprehensive evaluation of the auditory system from the outer to inner ear region that translates the response of the auditory system to clinically relevant predictions of cochlear and synaptic damage (Figure 1). The predicted damage is in a format that can be mapped in future programs to the loss of speech discrimination resulting from the exposure to high-intensity noise (i.e., blast overpressure). This program originally proposed to use experimental data to validate and improve the performance of the Auditory Hazard Assessment Algorithm for Humans (AHAAH) model (Price, 1998); however, a review of the experimental data suggested that the AHAAH model could not be modified within the scope of the current effort due to (1) a lack of information on the nonlinear response of the tympanic membrane to blast and (2) the controversy regarding the middle ear muscle contraction. These issues were either beyond the scope of the program or are being addressed in other ongoing efforts. To address the present need to predict the performance of hearing protection devices in terms of clinically relevant metrics, the phenomenological Blast Auditory Model (BAM) was derived here.

The BAM is designed to predict the propagation of an incident blast wave through the auditory system through a series of sequential submodels. The outputs of the model were verified experimentally using a combination of laser Doppler velocimetry and strategically placed fiber-optic pressure sensors in the outer, middle, and inner ear using both the chinchilla animal model and human temporal bones. For estimating the effect of hearing protection on energy transmitted to the middle and inner ear, the incident pressure measured on the surface of and under hearing protection, and in the ear canal, of post-mortem human specimens (PMHSs) was predicted using the developed model. To predict the pressure in the middle ear, measurements in both animal and PMHS were collected and used to develop a phenomenological nonlinear transfer function between the ear canal pressures under an HPD and pressures in the scala vestibuli (SV) within the inner ear. Using this approach, the BAM model can accurately capture the nonlinear behaviors of the middle ear which were not accounted for in existing electroacoustic models of the middle ear. The SV pressures calculated by BAM are correlated to inner and outer hair cell losses measured in the chinchilla at pressures that have been translated to an equivalent human exposures through a human-to-chinchilla transfer function that was developed within the program. This approach, unlike the AHAAH, allows for model validation by providing a methodology and transfer function for mapping animal-equivalent responses to human exposures. Furthermore, the use of this approach allows effects at exposure levels above the limits of human volunteer tests to be predicted and applied as part of the performance validation of the BAM encompassing the extreme exposure levels experienced in the military.

To provide a clinically relevant metric for the evaluation of HPD performance and physiological response to blast, the pressure output from actual SV measurements or the predicted pressure from the middle ear module of BAM can be used to degrade the function of an auditory nerve (AN) fiber model (Zilany et al., 2014; Bruce et al., 2018) by selectively reducing the function of model inner and outer hair cells. Using this approach, predictions of reductions in auditory functional performance may be validated via reconstructions of standard clinical batteries with and without auditory damage. For example, simulated speech coding deficits can be quantified with the Speech Intelligibility Index or other clinically relevant criteria to provide useful predictions of the ability to hear and understand commands and communication after blast exposure. These metrics are not

available with use of other models, which only predict engineering measures such as the summed displacement of locations along the basilar membrane.

The results of the effort provide a clear framework for further development of the BAM as an alternative to the AHAAH. However, for application of the BAM for auditory risk assessment additional work is required. These steps include: investigation of changes in auditory brainstem response (ABR) and distortion product otoacoustic emissions (DPOAE) response morphology in addition to simple changes in response thresholds; performance of sophisticated histological preparations to investigate synaptopathy and hidden hearing loss; and validation of model predictions against existing and retrospective reviews of hearing loss.

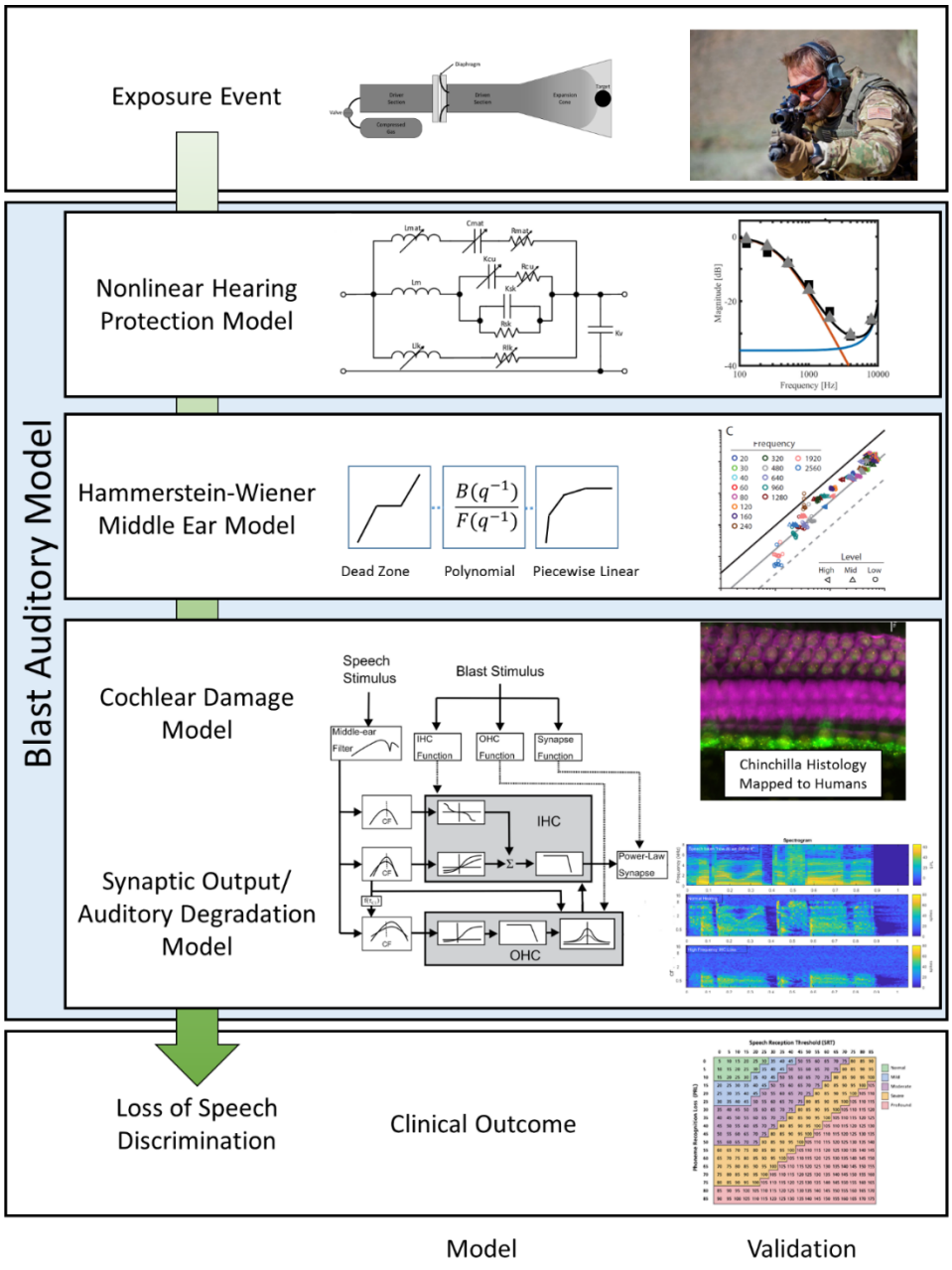

Figure 1. Flow diagram of the experimental tests conducted and numerical models developed to translate the response of the auditory system to clinically relevant predictions of cochlear and synaptic damage.

2 INTRODUCTION

The objective of this effort was to develop a deeper neuro-functional understanding of acoustic injury through a coordinated program of numerical modeling and focused experimental testing. To quantify the energy transmitted through the outer and middle ear, post mortem human surrogates (PMHS) and chinchillas were instrumented with pressure gauges in the ear canal and middle ear space, as well as in the scala tympani and scala vestibuli. To quantify hair cell loss associated with the exposure to blast, anesthetized chinchillas were exposed to blast overpressures calibrated to the equivalent blast exposure from whole-head PMHS tests conducted in a large-bore shock tube. The shock tube simulates a wide range of blast exposures commonly observed in a military environment. With the chinchilla exposures calibrated to a human equivalent exposure, the pressures measured in the outer and middle ear of the PMHS could be used to quantify the loss of hair cells and resulting changes in auditory systems responses. The model initially adopted as the foundation of the modeling task was the Auditory Hazard Assessment Algorithm for Humans (AHAAH) model. The program originally proposed was to use the experimental data to assess AHAAH function, and when required, improve the performance of the model for high-intensity sound exposures (i.e., blast). To meet the original objectives the program investigated sound propagation through hearing protection devices (HPD) using PMHS, measured middle-ear mechanics in human cadaver and anesthetized animal models were also used to assess assumptions and results predicted by the AHAAH model.

The findings of the testing confirmed several AHAAH predictions; however, the findings indicated that behavior of several AHAAH components, particularly the maximum displacement of the stapes, were inaccurate and required updating. Also, non-ossicular sound transmission pathways are not included in this model, leading to an underprediction of energy transmitted to the cochlea. These fundamental issues in the current AHAAH model were found to be unfixable with the existing body of data. It was determined that the most efficient approach to developing a deeper neuro-functional understanding of acoustic injury was the creation of a phenomenological model of sound transmission to the inner ear so that the relationship between hair cell loss and auditory transduction within the auditory nerve can be quantified. The new approach is based on the mechanical and physiological measurements collected within the program, as well as through the application of the existing data reported in the literature. The new model developed under this program is called the Blast Auditory Model (BAM).

The BAM addresses the limitations of previous models by adding nonlinear characteristics to the performance of HPD and the response of the middle ear. The model is also designed to interface with existing auditory nerve models in order to predict the degradation in auditory transduction within the auditory nerve. This new output may be used to interface with auditory nerve models to predict deficits in behavioral and physiological measures of auditory function, including speech intelligibility and spatial hearing ability, as well as physiological measures of auditory function including otoacoustic emission and auditory brainstem responses. The BAM, as an agnostic assessment of auditory system transduction, thus avoids several shortcomings of the strategy employed by AHAAH. The following are the technical accomplishments that have been completed to reach the objectives of the program.

3 KEYWORDS

Auditory Models, Blast Exposure, Combat, Hair Cell Damage, Hearing Loss/Threshold Shifts, Hearing Protection Devices

4 TECHNICAL ACCOMPLISHMENTS

The program was a systematic evaluation of the auditory system starting with the outer ear and working through the middle ear region, and into the inner ear, to understand the cause of hair cell loss due to noise exposure. The roadmap for the program is shown in Table 1 below. The following three specific aims were executed. The Program final report follows the format of the specific aims outlined in Table 1 from experimental testing using PMHS and chinchilla models to the development of a protocol for the evaluation of HPD performance to exposure to blast overpressure.

To quantify the energy transmitted through the outer and middle ear in **Specific Aim 1**, PMHS were instrumented with pressure gauges in the canal, middle ear space, as well as the scala tympani and scala vestibuli.

Next, to quantify hair cell loss associated with the exposure to blast, chinchillas were exposed to blast overpressures in Specific Aim 2. Pressure used in **Specific Aim 2** were calibrated to the equivalent blast exposure from whole-head PMHS tests conducted in a large-bore shock tube in Specific Aim 1 that simulated blast exposure in a military environment. With the chinchilla exposures calibrated to a human equivalent exposure, the pressures measured in the outer and middle ear of the PMHS were correlated with the loss of hair cells and resulting changes in auditory system function in the chinchilla model.

Based on these findings, protocols to quantify the degree of hearing loss expected, and the amount of protection provided by hearing protective devices to mitigate this damage (**Specific Aim 3**) were developed.

Table 1: Specific aims of the program that employed the use of both PMHS and Chinchilla models to quantify the response of the auditory system to blast exposure

Description
Specific Aim 1: Address inability to predict nonlinear response of auditory system for high-intensity noise exposure measured in the military environment to improve methodology for predicting the performance of HPD
Major Task 1: Measurement and Simulation of Blast Overpressure Wave through the external auditory canal with and without hearing protection devices
Subtask 1: Evaluate performance of four types of HPD using PMHS specimens against blast overpressure ranging from 1 to 12 psi generated by a large bore, compressed gas shock tube
Subtask 2: Establish methodology for deriving nonlinear parameters for electroacoustic model of outer ear capable of predicting pressures in the ear canal with and without HPD
Major Task 2: Measurement and Simulation of Blast Overpressure Wave through the middle ear
Subtask 1: Quantify nonlinear behavior of PMHS middle ear using laser-Doppler vibrometer (LDV) using blast wave emulator that deconstructed Subtask 1 blast waves into continuous waveform
Subtask 2: Establish methodology for deriving nonlinear transfer function for converting canal pressure into scala vestibuli pressure for estimation of hair cell loss associated with exposure to blast

Description
Specific Aim 2: Develop a neuro-functional understanding of acoustic injury by correlating human and animal auditory mechanisms and physiological responses measured experimentally to generated noise and blast events
Major Task 1: Quantifying Middle Ear Dynamics using Chinchilla Models
Subtask 1: Quantify nonlinear behavior of chinchilla middle ear using LDV using blast wave emulator that deconstructed Subtask 1 blast waves into continuous waveform
Subtask 2: Establish transfer function between chinchilla and human to relate observed hair cell loss in chinchillas to blast exposures in humans
Major Task 2: Quantify hair cell loss in Chinchilla resulting from exposure to blast overpressure
Subtask 1: Quantify nonlinear behavior of PMHS middle ear using LDV using blast wave emulator that deconstructed Subtask 1 blast waves into continuous waveform
Subtask 2: Establish methodology for deriving nonlinear transfer function for converting canal pressure into scala vestibuli pressure for estimation of hair cell loss associated with exposure to blast
Subtask 3: Establish methodology through the use of chinchilla to human transfer functions to predict the changes in hearing associated with predicted hair cell loss
Major Task 3: Integrate auditory nerve model to mechanical damage model for hair cell loss
Subtask 1: Quantify auditory brainstem responses, otoacoustic emissions, and histological measures of hair cell loss to determine association of hair cell loss generated by blast to changes in hearing
Subtask 2: Integrate auditory nerve model
Specific Aim 3: Develop a robust, validated system for the evaluation of hearing protective systems across the broad range of intensities and frequency spectra seen in real-world exposures
Major Task 1: Develop new protocol for HPD testing
Subtask 1: Develop new protocol for HPD testing
Subtask 2: Compare results to ANSI headform results

4.1 Specific Aim 1: Predicting the Nonlinear Response of Auditory System for Exposure to High-Intensity Noise

Injuries to the peripheral auditory system are among the most common results of high-intensity impulsive acoustic exposure (i.e., blast overpressure). Prior studies of high-intensity sound transmission by the ossicular chain have relied upon measurements in animal models, measurements at more moderate sound pressure levels (SPLs; i.e., < 130 dB SPL), and/or measured responses to steady-state noise. Here, we directly measure intracochlear pressure in human PMHS temporal bones with fiber optic pressure sensors placed in scala vestibuli (SV) and scala tympani (ST) during exposure to shock waves with peak positive pressures between ~7–83 kPa, with and without hearing protective device use. From the data collected, the insertion loss was calculated from conditions with hearing protection, relative to exposures without protection. These insertion loss calculations were used to develop a nonlinear hearing protection model in the

MathWorks Simulink programming environment. The following is a detailed description of the experimental testing to quantify changes in sound transmission through the outer and middle ear using a variety of commonly used hearing protection devices.

4.1.1 Major Task 1: Measurement and Simulation of Blast Overpressure Wave through the External Auditory Canal with and without hearing protection devices

To quantify the transmission of sound through the outer ear with and without HPD, eight full-cephalic human cadaver heads were exposed, face-on, to acoustic shock waves in a 45-cm diameter shock tube. Specimens were exposed to impulses with nominal peak overpressures of 7, 28, 55, and 83 kPa (171, 183, 189, and 192 dB pSPL), measured in the free field adjacent to the forehead. Specimens were prepared bilaterally by mastoidectomy and extended facial recess to expose the ossicular chain. Ear canal (EAC), middle ear, and intracochlear SPL were measured with fiber-optic pressure sensors, while surface-mounted sensors measured SPL and skull strain near the opening of each EAC and at the forehead. The use of temporal bone tissue was in compliance with the University of Colorado Anschutz Medical Campus Institutional Biosafety Committee, the Colorado Multiple Institutional Review Board (COMIRB EXEMPT 14-1464), and the U.S. Army Medical Research and Materiel Command (USAMRMC) Office of Research Protections (ORP). Tissue was obtained from cadavers undergoing autopsy with permission to use tissues and organs for research, including specific permission to expose those tissues to damaging energy (Lone Tree Medical Donation, Littleton, CO). The whole-head specimens evaluated had no history of middle ear disease (except presbycusis).

4.1.1.1 Temporal bone preparation for shock tube testing

Temporal bone preparation procedures were similar to several recent reports from our laboratory (e.g., Deveze et al., 2010; Greene et al., 2017; Greene et al., 2015; Mattingly et al., 2015; Maxwell et al., 2017). Briefly, the temporal bones were prepared bilaterally: The pinna and surrounding skin were reflected during preparation but left intact. Temporal bones were prepared with a canal-wall-up mastoidectomy with an extended facial recess. The facial canal was opened and the facial nerve removed to maximize access and visibility of the middle-ear structures, which were inspected for damage and abnormalities. The ossicular chain was not disturbed (including the stapedius muscle/tendon). The cochlear promontory was thinned near the oval and round windows in preparation for pressure probe insertion.

4.1.1.2 Instrumentation for measuring transmission of energy through auditory system

Sensor placement is illustrated in Figure 2A; specimens were outfitted with an array of sensors in the ears bilaterally, as well as on the surface of the skull, and in the air adjacent to the front surface of the head. The exposure level was measured in the free field adjacent to the specimen's forehead with a "pancake," or "splitter"-style, pressure probe (Endevco 8530C) oriented with the sensor surface 90° to the long axis of the shock tube. Surface sensors were attached ~2–3 cm above the pinna (in line, vertically, with the entrance of the ear canal) outside the area of coverage by a set of ear muffs, as well as centered on the forehead (on the horizontal circumference of the head determined by the left and right surface sensors, ~2 cm above the brow line). The skin overlying the skull in these locations was reflected. Strain gauges (Omega KFH-3-350-D17-11LM2S, Norwalk, CT) were secured to the skull with cyanoacrylate adhesive and were covered with the reflected flap of skin, which was sutured into place. Pressure gauges (Endevco 8515C-15, Irvine, CA) were similarly affixed to stainless steel plates, which were likewise secured to the skull with

cyanoacrylate adhesive, and the overlying skin was removed (Figure 2B). Wires were tightly sutured to the surface of the skin along the circumference of the head.

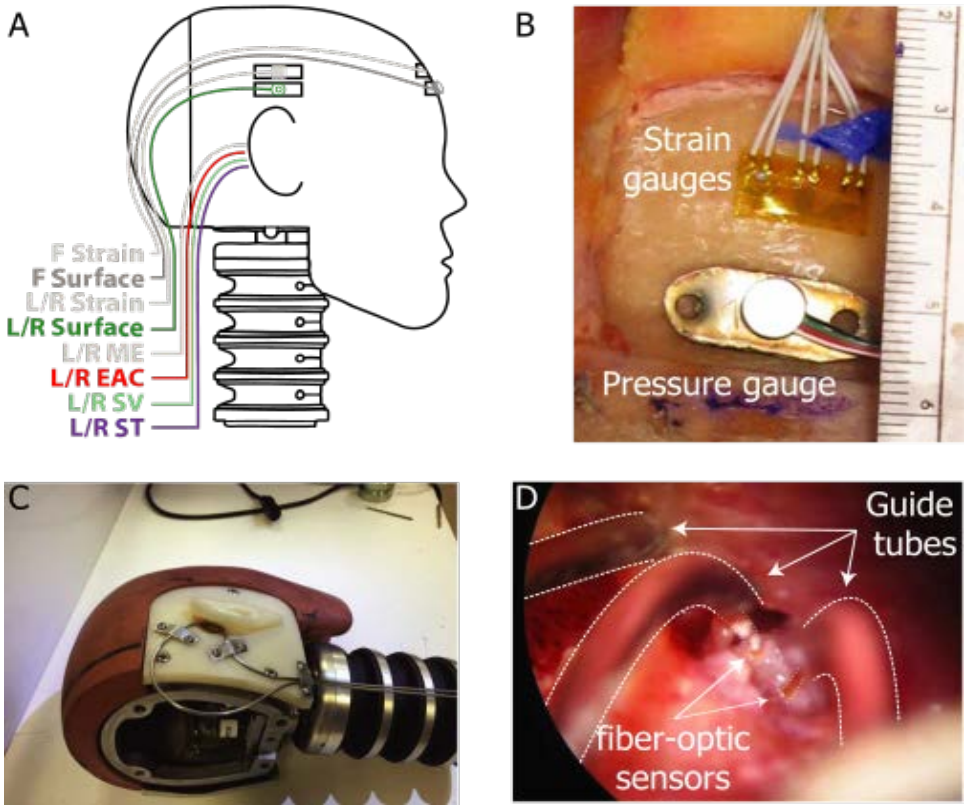

Figure 2. Locations and fixation methods for strain gauges and pressure sensors. (A) Strain gauges and surface-mount pressure gauges were placed in three locations on the skull (Front/Left/Right). Fiber-optic pressure sensors (FOP-M) were placed into both ear canals (L/R EAC) and both middle ear (L/R ME) cavities. Fiber-optic pressure sensors (FOP-M260) were inserted bilaterally into the scala vestibuli (L/R SV) and scala tympani (L/R ST). (B) Strain gauges and surface-mount pressure gauges were fixed to the surface of the skull in three locations with cyanoacrylate adhesive. (C) Stainless steel tubing was securely mounted to the skull to guide and protect the fiber-optic pressure sensors (shown on a modified Hybrid III head). (D) Fiber optic pressure sensors (bracketed by dotted lines) were inserted into the cochlea via small cochleostomies, sealed into the cochlea with alginate dental impression material, and fixed in place with cyanoacrylate adhesive along the length of the guide tube. (Note, strain gauge responses are not presented in this report.)

Prior to sensor placement in the ear, pre-test velocity measurements (see Section 4.1.1.3) were made on both ears. Fiber-optic pressure sensors were then inserted into the ear (into the external auditory canal, PEAC, SV, PSV, ST, PST, and middle ear (PME)), run through custom-fitted stainless steel guide tubes (demonstrated on a modified Hybrid III male head in Figure 2C). The guide tubes were run under the skin from the base of the skull into the mastoidectomy (through a channel cut in the bone) and fitted such that no deformation was introduced around the pinna (which could interfere with ear muff placement). The end of the guide tube terminated in a hole cut in the bony wall of the ear canal (for PEAC) and < 1 cm from the intended target (PSV and PST; Figure 2D). Fiber-optic sensors (FISO FOP-M-NS-1037A for PEAC and PME, and FOP-M260-NS-1036A for PSV and PST; FISO Inc., Quebec, Canada) were then inserted through the guide tubes, inserted underwater (to avoid introduction of air bubbles) into the cochlea via small cochleostomies made with a sharp pick (for PSV and PST) or until the sensor tip could just be seen (~100 µm) extending from the probe tube into the PME) or the ear canal (PEAC). The tip of the

PEAC probe was fixed in place within ~2 mm of the tympanic membrane (TM); the PME was placed ~1 cm posterior to the incus short process in the middle ear cavity. PSV and PST probes were sealed in place in the cochlea with alginate dental impression material (Jeltrate). Once placed, stapes and round window velocity measurements were repeated and compared to the pre-test responses. The reflected skin and pinna were then fixed back into place over the mastoidectomy with heavy suture, and the skin margin was re-sealed with cyanoacrylate adhesive. Optic fibers and sensor wires were then bundled together at the back of the head and affixed to the specimen support structure (shielded by the head and rubber/plastic covers), outside of the shock tube. In this manner, the sensors and the optic fibers were securely fixed in place and protected from damage.

All pressure sensors (both FISO and Endevco) were new (i.e., were not re-used from one specimen to the next) and came calibrated from their respective suppliers. Sensors were not re-calibrated on site and, if a sensor failed or provided faulty readings, was replaced (if possible) before subsequent measurements were collected. All sensors were zeroed to ambient pressure prior to each recording.

Motion of the sensor tips, as well as motion of the fiber optic cable, can introduce noise and artifact to the recorded signal. While it was not possible to eliminate all motion of sensor leads due to the high-intensity nature of the stimulus, care was taken to minimize motion of sensor tips and leads. Surface mount gauges were firmly affixed to the skull via stainless steel mounting plates and cyanoacrylate adhesive, and wire leads were tightly sutured to the scalp surface leading to the nape of the neck. Fiber optic pressure sensors were likewise firmly held in place within the guide tubes by applying cyanoacrylate adhesive to the far end of the guide tubes such that the liquid adhesive wicked into the guide tube via capillary action, while the guide tubes that were rigidly mounted to the skull in at least two places with stainless steel mounting plates and screws. Intracochlear pressure sensors were sealed inside the cochlea with alginate dental impression material. Each specimen was inspected following all recordings, and no evidence of probe motion (cracked or missing alginate material) was observed. Guide tubes from both ears were routed to the nape of the neck, where they were sutured together. All sensor leads ran through a section of flexible, clear PVC tubing and zip-tied together to form a single cable bundle that ran up the back of the neck (e.g., Figure 2C) to the aluminum mounting bracket, and zip tied along the leeward edge of the mounting bracket (Figure 4C). The bundle was routed to the steel support struts to which it was firmly attached by covering the length of the exposed cable with black adhesive vinyl tape. The cable bundle then passed into the shock tube suppressor and out to the data acquisition system via a cable pass-through. The cable bundle was allowed to flex behind the neck to allow relatively natural movement of the head in response to the exposure but was rigidly supported along all other segments to minimize motion and artifact.

4.1.1.3 Pre-test velocity measurements

At the beginning of each experiment, a number of velocity measurements were made in each ear in order to probe specimen condition. Velocity measurements were conducted as described previously (Greene et al., 2017; Greene et al., 2015; Mattingly et al., 2015): measured using a single-axis LDV (OFV-534 and OFV-5000; Polytec Inc., Irvine, CA), acoustic stimuli delivered to the ear canal via PVC tubing from a closed-field magnetic loudspeaker (TDT CF1; Tucker-Davis Technologies Inc., Alachua, FL), and the sound pressure level near the TM recorded with a probe-tube microphone (Type 4182; Brüel & Kjær, Nærum, Denmark). Stimulus presentation and data recordings were performed at a sampling rate of 96kHz, using an external sound card (Hammerfall Multiface II; RME, Haimhausen, Germany) modified to eliminate high-pass filtering

on the analog output and controlled using a custom program developed in MATLAB (MathWorks Inc., Natick, MA). Stimuli were three repetitions of one-second duration tone pips logarithmically spaced at four frequencies/octave between 100 Hz to 12 kHz, presented attenuated by 30 dB from full scale (approximately 90–110dB SPL).

Figure 3 shows a representative set of validation measurements in one ear (359L). Following the mastoidectomy and facial recess, but prior to making cochleostomies (opening the cochlea) and sensor placement, the average stapes velocity transfer function across the three repetitions (Figure 3A) was recorded (labeled PRE, circles) for comparison to prior reports in the literature (grey band: Mattingly et al., 2015; Rosowski et al., 2007). Similarly, the round window velocity (Figure 3B) was measured at a low frequency (400 Hz, 110 dB SPL) to verify opposite (180°) motion relative to the stapes to rule out the presence of air in the cochlea (Nakajima et al., 2009). Responses were then compared to velocities measured after pressure probe insertion and fixation (Figure 3A, labeled POST) to quantify any changes in these responses. Note, the orientation of the LDV laser could not be held constant between pre- and post-measurements due to the guide tube placement procedure, thus, some changes in transfer function magnitudes were expected; however, the shape of the magnitude curve did not change substantially across frequency after the pressure sensors were inserted and sealed into the cochlea. Response phases (not shown) matched prior reports and were essentially identical in pre- and post-measurements in all ears included for analysis. Finally, after the completion of all experimental procedures, the fiber optic probes and guide tubes were removed from the specimen to inspect for gross anatomical damage (Figure 3C; none was noted), and the bone between the SV and ST cochleostomies was removed to verify the position of the cochlear partition between the two (Figure 3D).

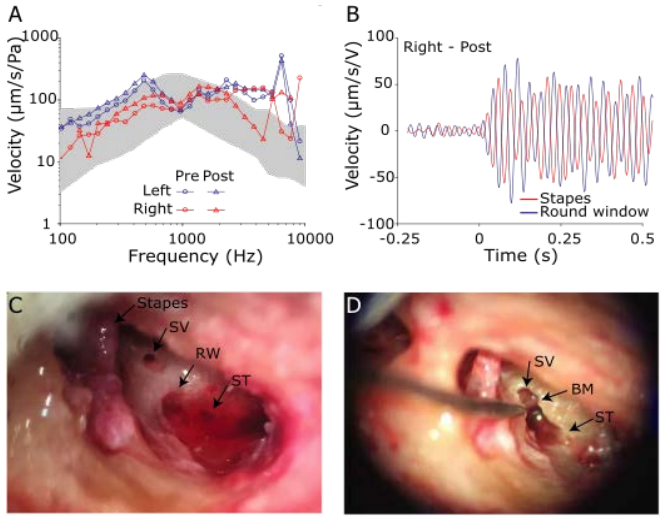

Figure 3. Validation procedures. (A) Stapes velocity transfer functions (HStap = VStap/PEAC; mean across three repetitions in specimen 359L) were measured before (○) and after (△) intracochlear pressure sensor insertion to verify comparable magnitudes (note that the angle of the LDV with respect to the stapes motion differed between measurements, thus absolute magnitudes could vary somewhat). Gray band represents the 95% confidence interval (CI) from (Rosowski et al., 2007). (B) Round window velocity (blue) was compared to Stapes velocity (red) at 400 Hz to verify a 180° phase difference. The stimulus was a 1s duration tone pip. (C) Cochleostomies were created near the base of the stapes and the round window (RW) to enter into the SV and ST, respectively. (D) After all experimental conditions were completed, intracochlear pressure probe placement was verified by dissecting away the bone between the two cochleostomies, and verifying that the basilar membrane (BM) was between the two fenestrations.

4.1.1.4 Shock wave exposure

When preparations and pre-test velocity measurements were complete, specimens were transported to the test apparatus. Acoustic shock waves were generated with a ~45-cm diameter shock tube with a ~2.4-m long expansion cone and spheroidal suppressor, mounted inside a ~16-m semi-trailer (Figure 4A; ARA Inc., Littleton, CO). Specimens were suspended upside-down from a steel and aluminum support structure inside the expansion cone of the shock tube and fixed in place facing the shock tube driver with the interaural axis horizontal to the ground (Figure 4B–C; demonstrated here with a Hybrid III dummy head). The shock tube was driven with compressed air and used Mylar (for 7-kPa peak exposures) or aluminum (for higher pressures) membranes that were allowed to rupture spontaneously. A wire mesh screen near the membrane prevented membrane material from contacting the specimen. Pressure was monitored in both the driver and driven segments, near the membrane. A high-intensity light source provided illumination for a Phantom v7.3 (Vision Research, Wayne, NJ) high-speed camera, which filmed at 2,000 frames/second through a transparent polycarbonate window in the expansion cone, time-locked to the shock wave exposure. Data acquisition was performed by a Hi-Techniques, Inc. (Madison, WI) meDAQ system operating at 1 MS/s. Recordings were triggered by the pressure sensor adjacent to the specimen's forehead.

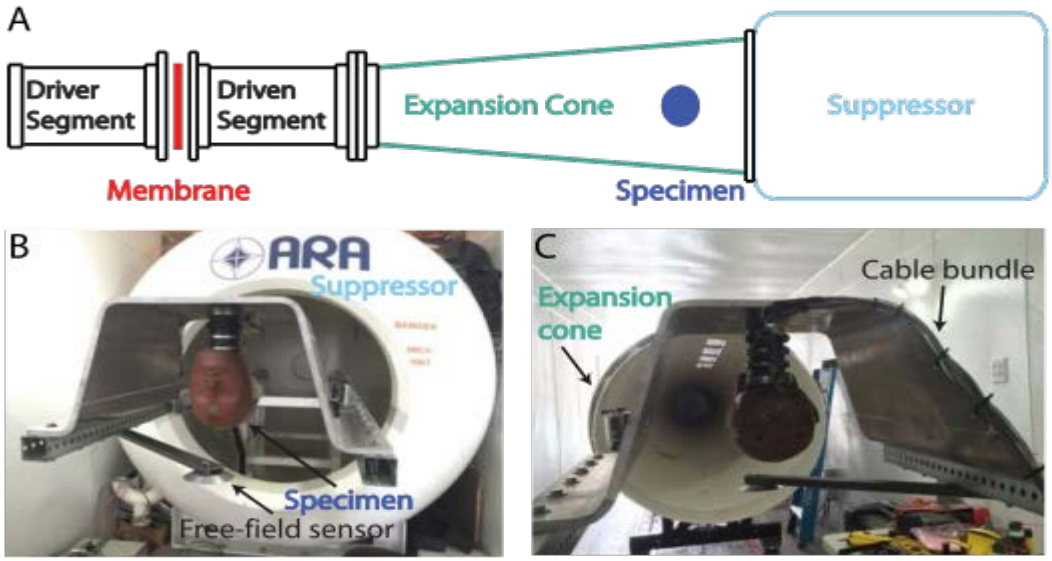

Figure 4. Shock waves were generated with a 45-cm diameter shock tube mounted inside a semi-trailer (A). The specimen (a Hybrid III dummy head shown here) was mounted (B) inside the expansion cone (C) of the shock tube, held in place upside-down inside an aluminum mount, affixed to a steel frame. A pancake-style, free field pressure gauge was mounted adjacent to the specimen's head (slightly forward of the forehead). The bundle of wires and fiber-optic cabling were run up the neck, along the back of the aluminum mount, and attached to the steel supports to protect the bundle from the shock wave.

Peak SPL (pSPL) values are calculated as: pSPL = 20*log10(Pp / 20 µPa), where Pp is the instantaneous peak pressure in Pascals (ANSI, 1973). Specimens were exposed to impulses with nominal peak overpressures of 7, 28, 55, and 83 kPa nominal peak pressures (171, 183, 189 and 192 dB pSPL). In general, exposure levels resulting from the 55 and 83 kPa nominal peak pressure exposures were more variable, and the sensor responses less consistent than the results collected at the lower levels, thus discussion of the responses to the higher two exposure levels is limited.

Specimens were exposed to these pressure levels in both an open-ear condition and with one or more HPDs fitted (3M E-A-R Classic, 3M Combat Arms, ARA ShotShield, and 3M Peltor over-the-head ear muffs with gel ear cup seals). In a subset of specimens, measurements were additionally made with an Advanced Combat Helmet (ACH) fitted to the specimen's head. Note, the results from measurements with HPD and helmet use are outside the scope of this report, and only results from open-ear, no-helmet conditions are presented in the results below. Preliminary results from HPD measurements have been presented elsewhere (Walilko et al., 2017).

No specimen was tested under all exposure conditions; instead, specimens were exposed to a pseudorandom set of conditions, starting with an open-ear, 7-kPa nominal peak pressure exposure and ending with an open-ear exposure at the highest condition tested for the day. Open-ear, 7-kPa nominal peak pressure exposures were repeated throughout the duration of testing in order to assess changes in the specimen's response after repeated exposures.

4.1.1.5 Pressure Results from Whole Head PMHS testing

Figure 5 demonstrates waveforms recorded during ~7 kPa and ~55 kPa nominal peak pressure exposures (6.3 kPa and 62.8 kPa actual peaks; red and blue lines, respectively) recorded by the free-field pressure sensor during testing. The shock waves (Figure 5A) approximated a Friedlander waveform (i.e., an "ideal" shock waveform consisting of a fast onset and short positive pressure component, followed by a shorter, lower magnitude negative component, given by the equation $P = PS(\exp(-t/\tau))(1-(t/\tau))$, PS = 62.8 kPa, τ = 2 ms; see inset) at the waveform onset (Chandra et al., 2012). Specifically, the shock waves generated reproduced the fast, positive pressure onset as well as the slower negative-going phase; however, the waveform showed ringing with a period of ~35 ms that was related to the length of the shock tube system and persisted for some time after the initial onset.

Measurements on the forehead showed incident peak pressures approximately twice that measured by adjacent free-field and EAC entrance sensors, as expected based on the sensor orientation (normal versus tangential to the shock wave propagation). At 7 kPa, EAC pressure showed gain, calculated from the frequency spectra, consistent with the ear canal resonance, and gain in the intracochlear pressures (normalized to the EAC pressure) were consistent with (though somewhat lower than) previously reported middle ear transfer functions. Responses to higher intensity impulses tended to show lower intracochlear gain relative to EAC, suggesting sound transmission efficiency along the ossicular chain is reduced at high intensities. TM rupture was observed following nearly every exposure 55 kPa or higher.

Intracochlear pressures reveal lower middle-ear transfer function magnitudes (i.e., reduced gain relative to the ear canal) for high SPL, thus revealing lower-than-expected cochlear exposure based on extrapolation from cochlear pressures measured at more moderate sound levels. These results are consistent with lowered transmissivity of the ossicular chain at high intensities and are consistent with our prior report measuring middle ear transfer functions in human cadaveric temporal bones with high-intensity tone pips.

Shock waves are characterized using two characteristic durations: the A-duration (the time interval between impulse arrival at the free-field sensor and the first negative-going zero crossing) is ~2 ms for both levels; and the B-duration (the duration to the last point on the waveform envelope 20 dB down from the peak) is ~250 ms for the 7 kPa, and ~80 ms for the 55 kPa peak impulses (following: Coles et al., 1968; Hynson et al., 1976). The onset time, the time of arrival at each sensor, is defined as the point at which the pressure exceeds a value 20 dB below the peak, or four standard deviations

of the response prior to the free field onset, whichever is lower. Median and first and third quartiles (25th and 75th percentiles) of the onset time, as well as A- and B- durations, are provided for each sensor for each of the four intensities in Table 2. Onset times generally decrease above 6.3 kPa and are relatively consistent at higher exposure levels. Notably, onset times are shortest in the front surface (FSurf) sensor and are comparable in the lateral surface (Surf), ear canal (EAC), and intracochlear pressure sensors (SV and ST) at 6.3 kPa. The intracochlear pressure sensors show somewhat shorter onset times than Surf or EAC sensors at higher exposure levels, but the interquartile range is relatively large, with substantial overlap across levels. A-durations are relatively consistent at ~2 ms across all four levels and across all seven sensors, whereas B-durations decreased substantially from ~200 ms to 50–100 ms with increasing level. The decrease in B-duration is evidence of a relative reduction of the ongoing low-frequency oscillations relative to the peak pressure at the onset of the exposure, suggesting that the shock wave intensity increases nonlinearly relative to the level of the ongoing reverberations within the shock tube. Note, only responses showing no evidence of sensor failure are included, thus the N varies from one condition to the next.

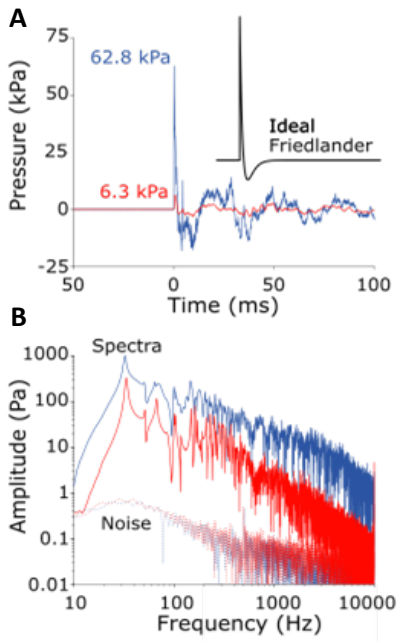

Figure 5. Example shock waves generated by the shock tube measured by the free-field pressure gauge during testing of specimen 359. (A) Time-domain recordings show a 7 kPa nominal peak pressure (red; 6.3 kPa actual), and a 55 kPa nominal peak pressure (blue; 62.8 kPa actual) shock wave exposures. An ideal Friedlander waveform with a 2-ms A-duration is shown in the inset. (B) The frequency spectra (solid) of the shock waves shown in A, along with the noise floors (dashed) estimated from the period preceding the exposure, reveal a high signal-to-noise ratio from ~10 Hz–10 kHz that extends to a wider range of frequencies with increasing SPL. Spectra are computed over a 1-s window beginning at the onset in the free-field sensor.

The frequency spectra (calculated from the first one second after the shock wave arrival, t = 0 to 1s and smoothed with a 1/8-octave wide moving average filter for visualization) of the shock waves (Figure 5B) reveal an overall trend towards low frequencies (i.e., < 200 Hz), in addition to a substantial peak at ~30 Hz corresponding to the resonant period of the shock tube system (solid red and blue lines show the spectra for the corresponding shock waves presented in Figure 5A). The signal was well above the noise floor (dotted lines), which was estimated from the recording immediately prior to the impulse, for frequencies between ~10 Hz–10 kHz for 7-kPa nominal peak

pressure impulses, and over a broader bandwidth for higher-level impulses. Note, measurements were collected in both ears in all specimens; here we treat each ear independently, and do not directly compare the two ears within each specimen, as small variations in head orientation or tissue condition/preparation in the two ears may cause slight differences in results between ears.

Table 2. Medians, first (Q1) and third (Q3) quartiles, and number (N) of Onset times, A-, and B-durations calculated for each pressure sensor, at each exposure level. All times are shown (in ms) relative to the free-field (Field) sensor. FSurf: front surface; Surf: surface sensor adjacent to the ear; EAC: external auditory canal, adjacent to the tympanic membrane; SV: scala vestibuli; ST: scala tympani; ME: middle ear; std dev: standard deviation; N: number of included measurements.

Onset (ms)

	7 kPa			28 kPa			55 kPa			83 kPa		
	Median (Q_1, Q_3)		N	Median (Q_1, Q_3)		N	Median (Q_1, Q_3)		N	Median (Q_1, Q_3)		N
Field	0.00	(-,-)	8	0.00	(-,-)	7	0.00	(-,-)	3	0.00	(-,-)	3
Fsurf	0.41	(0.37, 0.45)	8	0.31	(0.24, 0.34)	6	0.30	(0.28, 0.31)	3	0.21	(0.18, 0.31)	3
Surf	0.74	(0.64, 0.79)	16	0.51	(0.46, 0.58)	14	0.51	(0.49, 0.51)	6	0.44	(0.40, 0.64)	6
EAC	0.66	(0.59, 0.71)	14	0.55	(0.50, 0.61)	11	0.52	(0.51, 0.55)	3	0.44	(0.44, 0.47)	5
SV	0.66	(0.55, 0.73)	12	0.42	(0.34, 0.46)	11	0.36	(0.17, 0.39)	4	0.39	(0.25, 0.51)	5
ST	0.74	(0.64, 0.94)	13	0.45	(0.38, 0.52)	11	0.41	(0.31, 0.54)	4	0.35	(0.23, 0.40)	4
ME	0.86	(0.83, 1.12)	10	0.61	(0.52, 0.67)	8	0.55	(0.52, 0.57)	3	0.48	(0.45, 0.52)	3

A-Duration (ms)

	7 kPa			28 kPa			55 kPa			83 kPa		
	Median (Q_1, Q_3)		N	Median (Q_1, Q_3)		N	Median (Q_1, Q_3)		N	Median (Q_1, Q_3)		N
Field	2.03	(1.88, 2.14)	8	2.00	(0.68, 2.14)	7	3.05	(0.73, 3.20)	3	2.00	(1.94, 6.36)	3
Fsurf	2.26	(2.19, 2.80)	8	3.05	(2.56, 3.33)	6	2.93	(2.87, 3.27)	3	2.26	(2.07, 6.38)	3
Surf	2.64	(2.55, 2.69)	16	2.43	(2.27, 2.76)	14	2.34	(2.28, 2.68)	6	4.02	(2.32, 5.97)	6
EAC	2.46	(2.37, 2.59)	14	2.13	(1.62, 2.46)	11	3.20	(3.05, 4.77)	3	2.62	(0.70, 5.89)	5
SV	3.23	(2.31, 3.70)	12	2.94	(1.98, 3.25)	11	2.92	(1.96, 2.97)	4	3.37	(3.01, 5.81)	5
ST	2.95	(2.47, 3.66)	13	3.20	(2.87, 3.27)	11	2.86	(2.18, 2.92)	4	3.06	(1.72, 5.43)	4
ME	2.95	(2.68, 3.53)	10	3.03	(2.73, 3.22)	8	3.01	(2.78, 4.21)	3	3.24	(2.80, 6.50)	3

B-Duration (ms)

	7 kPa			28 kPa			55 kPa			83 kPa		
	Median (Q_1, Q_3)		N	Median (Q_1, Q_3)		N	Median (Q_1, Q_3)		N	Median (Q_1, Q_3)		N
Field	258	(256, 259)	8	49	(48, 115)	7	61	(56, 120)	3	54	(54, 54)	3
Fsurf	256	(205, 259)	8	266	(183, 425)	6	103	(63, 294)	3	27	(26, 29)	3
Surf	291	(256, 316)	16	116	(81, 136)	14	55	(53, 66)	6	86	(42, 90)	6
EAC	196	(181, 257)	14	81	(49, 141)	11	62	(60, 182)	3	116	(89, 258)	5
SV	364	(324, 405)	12	235	(177, 294)	11	117	(88, 137)	4	90	(38, 210)	5
ST	349	(266, 452)	12	189	(135, 323)	10	103	(82, 139)	4	149	(117, 225)	4
ME	289	(258, 324)	10	197	(195, 198)	8	117	(60, 119)	3	118	(117, 118)	3

4.1.1.6 Otoscopic examination results from PMHS heads exposure to blast

The external and in-ear condition of each specimen was inspected prior to the first, and after each, shock wave exposure. Two ears had TM perforations prior to testing and were excluded from further analysis (2/16). No visible damage was noted after any 7-kPa exposure (14/16 ears), and only one ear showed a perforation after a 28-kPa exposure (1/14 ears), which was likely caused by an experimenter rather than the shock wave. In contrast, TM rupture was observed after nearly every 55-kPa (4/5 ears) or 83-kPa (6/6 ears) peak exposure. Note, most specimens were exposed to both 7 kPa and 28 kPa, but no specimen was exposed to both 55 kPa and 83 kPa. Testing ceased once both TMs were perforated.

Figure 6 shows examples of the TM ruptures observed. The left column shows intact TM from three ears (411R, 359L, and 373L) shortly prior to the peak exposure causing each TM rupture. Note, the location and orientation of the fiber-optic pressure probe is visible at the top left (top) or

right (center, bottom) of each image. The center column shows the same ears after subsequent unprotected 55-kPa nominal peak exposure, and the right column shows an illustration demonstrating the orientation and location of each TM (colored area), the location of the fiber-optic sensor (grey bars), the location of the manubrium of the malleus (lighter area with a solid border), and the region in which the TM rupture(s) were visible (dotted lines). Several perforations are visible, showing the range of TM perforations observed in this study—top: a large perforation encompassing both anterior quadrants through which the cochlear promontory is visible (though out of focus), and two smaller perforations in each of the posterior quadrants; center: a circular perforation in the anterior-superior quadrant; bottom: a "slit-like" perforation in the anterior-inferior quadrant that extends outward radially from the center (Kuroda, 1993). In some cases, perforations broadened when subjected to additional exposures (not shown). In the results below, responses are only assessed if the TM was intact prior to the exposure (i.e., there was no pre-existing perforation).

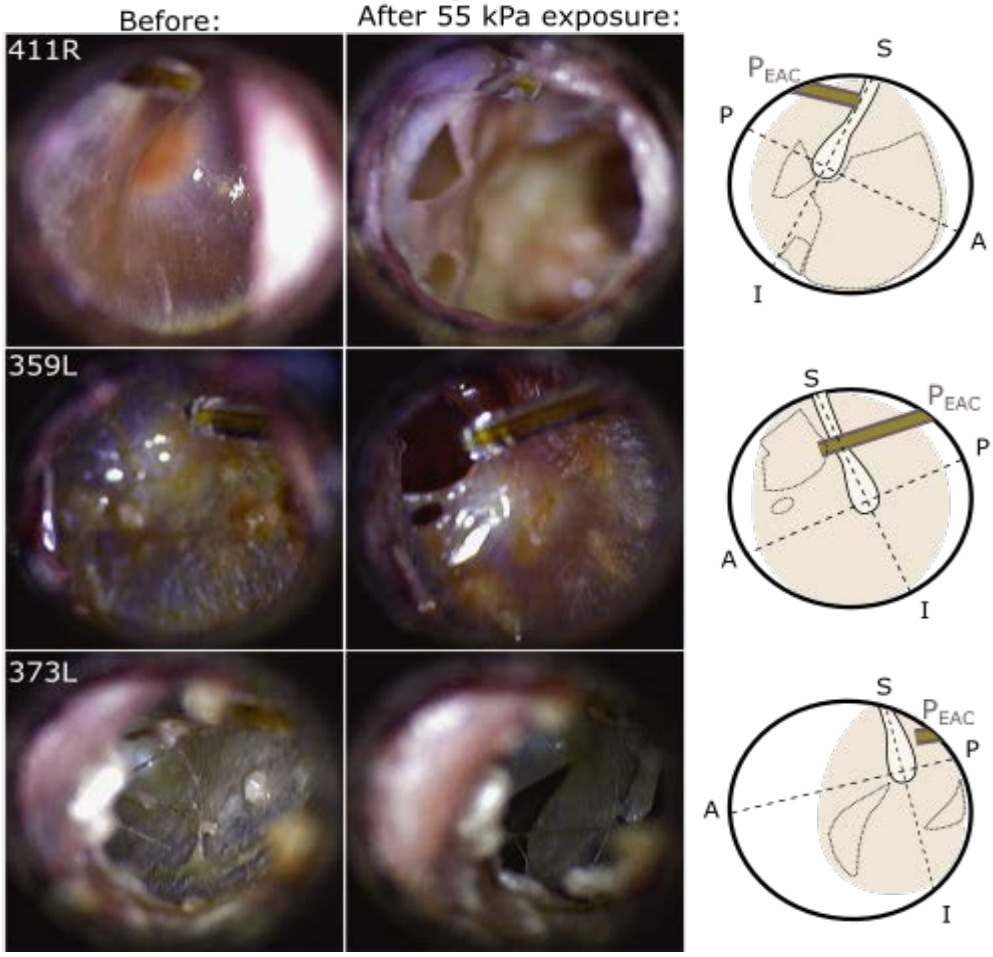

Figure 6. Photomicrographs of tympanic membranes taken before (left) and after (center) high level shock wave exposures from three specimens/ears (specimen number and ear (L or R) noted in the upper left of each panel). The external auditory canal fiber-optic pressure sensor (EAC) is visible in the upper left or right corners. The approximate position of the umbo, orientation of the manubrium (solid outline), and perforated area (dotted lines) is highlighted in an illustration (right) of each TM.

4.1.1.7 Measured PMHS response to various levels of blast

To quantify the nonlinear response of the head to varying levels of blast overpressure, the PMHS specimens were exposure to multiple Freelander pressure waves with peak pressures of 7, 28, 55, and 83 kPa. To ensure that the previous exposures to pressure did not change the response or structure of the tympanic membrane low pressure tests were performed every five tests to quantify the response of the auditory system and otoscopic examinations were performed after each exposure. A change in either the measured response or a perforated TM would stop the test series.

4.1.1.7.1 7-kPa nominal peak pressure

All eight specimens (16 ears) were exposed to 7-kPa nominal peak pressure shock waves at the beginning of each set of exposures, and again after certain larger exposures to verify the condition of the ears and probes throughout the duration of the experiment. If a response to the 7-kPa exposure changed substantially in one or more sensor channels, the sensor was repaired or replaced, if possible, or noted as a failure and excluded from subsequent analysis otherwise. Figure 7 shows the first 14 ms (Figure 7A) and first 400 ms (Figure 7B) of the responses of the pressure probes to a single 7-kPa nominal peak pressure exposure (ear 359L, the same as in Figure 3). The peak exposure level (computed from the free field pressure sensor) for this exposure was ~6.3 kPa, or ~170 dB pSPL. The pressure wave arrived at the free-field pressure sensor first (at time = 0 ms), followed by the front surface (forehead) sensor ('FSurface') at ~0.4 ms, and the remaining sensors at ~0.7 ms (see Table 2). The forehead surface sensor showed a somewhat higher pressure peak than the free-field sensor (~1.9 dB), presumably due to the sensor orientation (the shock wave angle of incidence is normal to the forehead). Two main differences between the in-ear sensors and the free-field/surface sensors are visible. First, the in-ear sensors showed substantially higher pressure peaks resulting from the gain of the pinna and ear canal (Wiener et al., 1946). In particular, the EAC sensors showed up to ~6 dB, and the intracochlear pressure sensors ~5.5 dB higher peak pressures than the free-field pressure sensor. Second, an oscillation with a ~1.5 ms period is visible (particularly between 8–14 ms) in Figure 7A (in addition to the ~30 ms fluctuation observed in Figure 7B) in the responses of the SV and ST sensors that is not present in the other curves. Note, a large negative peak is observed in the SV sensor at ~2.5 ms that appears to be a component of the 1.5-ms period oscillation, but was not observed in all specimens, thus may be either an artifact or a unique feature of this specimen.

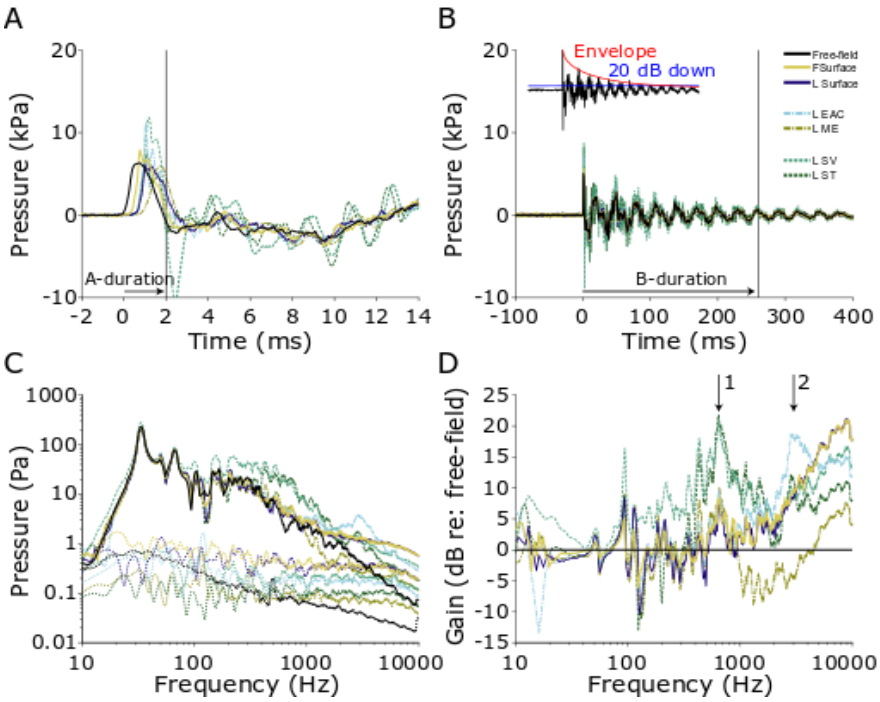

Figure 7. Pressures measured during a 7-kPa nominal peak pressure exposure in ear 359L. The first 14 ms (A) and 400 ms (B) of the recording are shown, illustrating the A- and B- durations (horizontal arrows) of the free-field pressure gauge measurement of the shock wave. For all sensors, A-duration (2.0 ms) is defined as the first zero crossing, while the B-duration (259.1 ms) is defined as the time to the last point exceeding 20 dB down from the peak (see inset). The frequency spectra (solid) and noise floors (dotted) of each sensor (C). The gain of each sensor relative to the free-field pressure gauge (D).

The frequency spectra, calculated over a 1s period beginning at shock wave arrival at the free-field sensor, and the difference in the spectra relative to that of the free-field sensor (in dB), are shown in Figure 7C–D (smoothed with a 1/8-octave wide moving average filter for visualization). The spectra are largely similar to the responses observed in the free-field sensor for low frequencies (i.e., < 200 Hz); however, the spectra deviate substantially from the free-field at higher frequencies. In particular, two distinct peaks in the gain plots, centered at 600–800 Hz and at 2–3 kHz, are visible in all signals. First, a substantial (~10 dB) peak at 2–3 kHz, representing the ear canal resonance, appears in the EAC probes. This gain propagates through the ear and is visible in the downstream pressure sensors. Second, a substantial peak (~20 dB) at 600–800 Hz, corresponding with the ~1.5 ms period oscillations visible in the time-domain plots, appears in the intracochlear pressures, indicative of the middle ear gain. Together, these effects increase the amplitude of signals entering the cochlea by 10–20 dB, relative to the incident sound pressure level, for frequencies above ~300 Hz. Lower frequency sounds show little or no difference relative to the incident exposure. Note, all signals are well above the noise floor for frequencies between ~10 Hz–10 kHz.

The relative peak pressure amplitudes (computed from waveforms) are compared across sensor location and across exposure level in Table 3. Mean and standard deviation of the peak pressure measured in the free field is shown at left and reveals peak pressures comparable to the nominal peak pressure exposures by which responses are grouped (i.e., mean exposure was 7.6 ± 1.9 kPa for the 7-kPa nominal peak pressure exposure condition). Responses of the other sensors are reported in dB gain relative to the free field sensor, as reported above. In general, peak pressure responses are higher in the front surface sensor, comparable in the lateral surface sensors, higher

in the ear canals, and lower in the intracochlear pressures (SV and ST) and middle ear sensors than the free field sensor, but responses are variable, with standard deviations exceeding means for most measures.

Table 3. Mean and standard deviation (SD) of peak pressure (in kPa) measured in the free field for each exposure level, and the gain in peak pressure level for each sensor relative to the free field pressure gauge (in dB re: free field). Abbreviations are defined in Table 2.

		Peak Pressure (kPa)						
		Field	FSurf	Surf	EAC	SV	ST	ME
7 kPa	Mean	7.59	+2.7	+0.3	+3.9	-2.7	-2.5	-3.1
	SD	1.89	1.7	1.4	5.3	5.3	5.3	6.9
	N	16	16	16	14	13	13	11
28 kPa	Mean	31.19	+4.8	+1.3	+4.8	-4.6	-5.1	-8.0
	SD	3.1	1.4	1.5	6.9	6.2	6.5	9.3
	N	14	14	14	12	11	11	9
55 kPa	Mean	57.5	+4.3	+1.4	-0.6	-0.5	-0.6	-11.5
	SD	4.46	0.6	1.7	5.8	2.1	4.2	17.5
	N	6	6	6	4	4	4	4
83 kPa	Mean	92.63	+4.6	-9.5	-6.4	-6.5	-6.0	-7.3
	SD	1.82	2.5	13.3	3.0	5.0	6.6	1.2
	N	6	6	6	6	5	5	3

4.1.1.7.2 28-kPa nominal peak pressure

Seven of the eight specimens (14 of the 16 ears) were exposed to the 28-kPa nominal peak pressure exposure condition. Figure 8 shows the first 14 ms (A) and first 400 ms (B) of the responses of the pressure probes to a single 28 kPa nominal peak pressure exposure (ear 411R). The peak pressure level (calculated from the free field sensor) for this exposure was close to ~37.6 kPa, or ~185 dB pSPL. Similar to the 7-kPa exposure, the pressure wave arrived at the free-field pressure sensor first (t = 0); however, the intensity of the shock wave was higher, thus the speed of the wave front was higher and the delay to each of the sensors shorter relative to the 7-kPa stimulus—the front surface (forehead) sensor was delayed by ~0.3 ms and the remaining sensors ~0.5 ms relative to free-field. Once again, the front surface (forehead) sensor (~4.5 dB) and the EAC pressure sensors (~2.6 dB) showed higher peak pressures than the free-field sensor; however, compared to the lower intensity exposure the shock wave rise-time was shorter, the peaks sharper, and the B-duration shorter (as described in Section 4.1.1.4 and Table 2). The intracochlear pressure sensors showed somewhat lower peak pressures than the free-field sensor (~ -1 dB). This decrease is prominent for higher frequency components of the response, as revealed in the frequency spectra (Figure 8C–D; smoothed with a 1/8-octave wide moving average filter for visualization). Peak pressures showed a similar trend as the 7-kPa exposure—peak pressures were higher in the front surface and ear canal sensors, and intracochlear and middle ear pressures were lower than the free field sensor (Table 3).

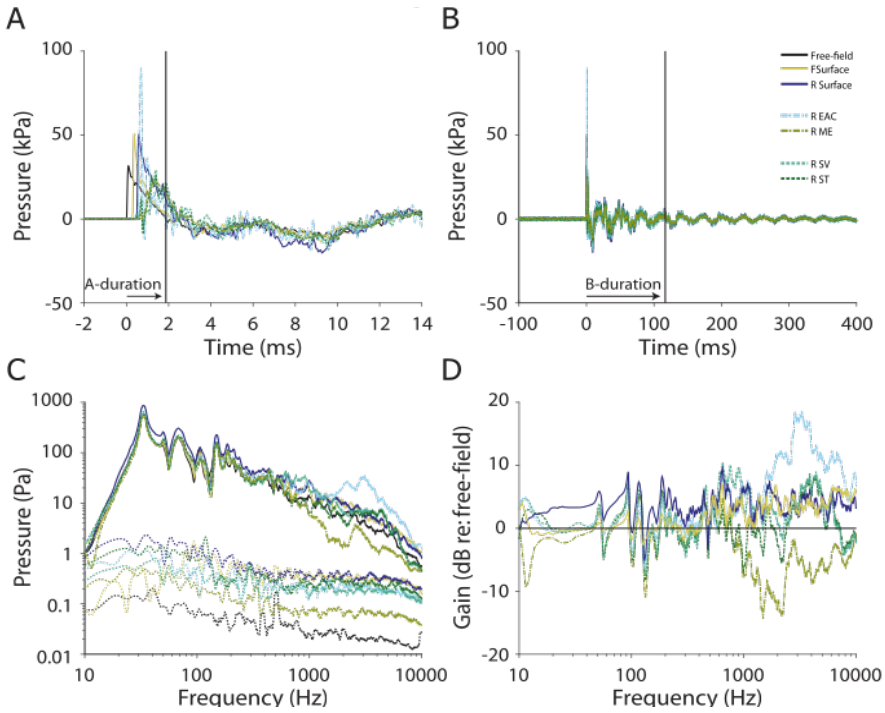

Figure 8. Pressures measured during a 28-kPa nominal peak pressure exposure in ear 411R. The first 14 ms (A) and 400 ms (B) of the recording are shown, illustrating the A- and B- durations (horizontal arrows; 2.1 ms and 48.4 ms, respectively) of the free-field pressure gauge measurement of the shock wave. The frequency spectra (solid) and noise floors (dotted) of each sensor (C). The gain of each sensor relative to the free-field pressure gauge (D).

4.1.1.7.3 55-kPa and 83-kPa nominal peak pressures

Three of the eight specimens were exposed to the 55-kPa, and three specimens to the 83-kPa (six of the 16 ears each), nominal peak pressure shock waves (two specimens were not exposed to either due to previous damage). Figure 9 shows the first 400 ms (A) and first 14 ms (B) of the responses of the pressure probes to a single 55-kPa nominal peak pressure exposure (ear 359L, the same as Figure 7 and Figure 3). The 55-kPa nominal peak pressures were somewhat more variable than the lower levels (e.g., Table 3), and the peak exposure level in this specimen was ~62.8 kPa, or ~190 dB pSPL. Similar to the 28-kPa exposure, the pressure wave arrived at the free-field pressure sensor first, at the forehead sensor delayed by ~0.3 ms, and at the remaining sensors delayed by ~0.5 ms (Table 2).

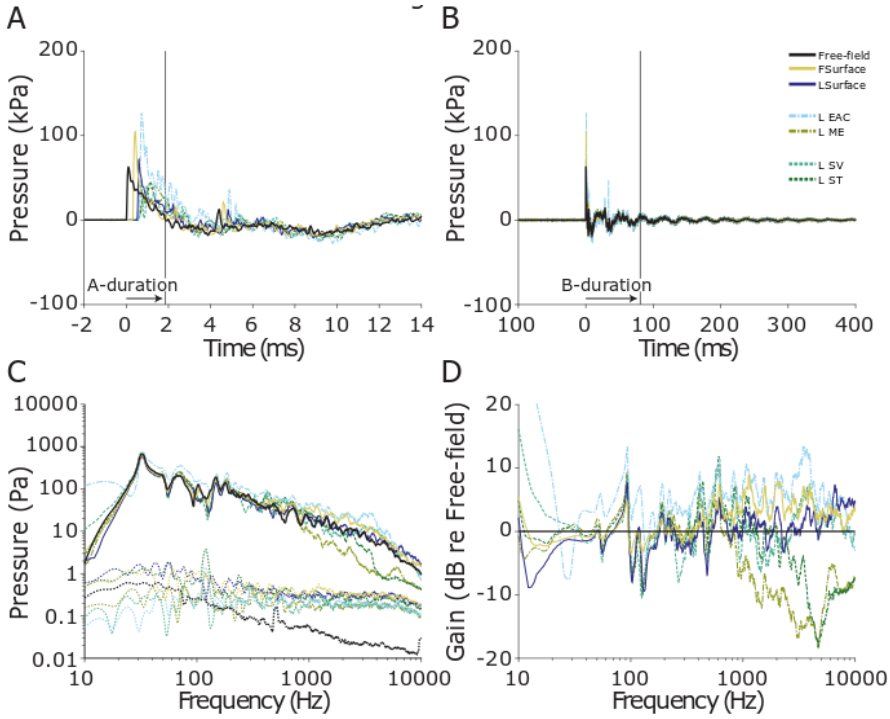

Figure 9. Pressures measured during a 55-kPa nominal peak pressure exposure in ear 359L (same as Figure 6). The first 14 ms (A) and 400 ms (B) of the recording are shown, illustrating the A- and B- durations (horizontal arrows; 3.1 ms and 62.4 ms, respectively) of the free-field pressure gauge measurement of the shock wave. The frequency spectra (solid) and noise floors (dotted) of each sensor (C). The gain of each sensor relative to the free-field pressure gauge (D).

4.1.1.8 Evidence for a bone-conducted component of shock wave propagation

In the 28-kPa and 55-kPa nominal peak exposures shown in Figure 8 and Figure 9, a small disturbance is visible in both intracochlear pressure sensors at ~0.3–0.4 ms. These responses are shown expanded in Figure 9A and B, respectively. This pressure arrives in the cochlea 0.1–0.15 ms prior to the air-conducted shock wave arrival at the entrance or within the ear canal (~0.5 ms), thus must be the result of an alternate sound conduction pathway such as through the skull bone (which has a speed of sound of ~3 km/s for the longitudinal mode (White et al., 2006), nearly an order of magnitude faster than the ~343 m/s speed of sound in air at 20°C), stimulating the cochlea directly. This pressure typically arrives in both SV and ST sensors simultaneously and generally revealed an increase in sound pressure level, as illustrated in Figure 9A. Note, the speed of sound increases with increasing shock wave peak overpressure, thus the 343 m/s estimate provided here represents a lower bound on the speed of sound in air. This bone-conducted sound pressure is quickly over-ridden by the air-conducted pressure wave arrival at 0.5–0.6 ms, thus we cannot directly differentiate their contributions to the overall sound pressure observed. Nevertheless, these early sound pressures observed are substantial, although L SV showed a somewhat higher peak than L ST, rising to ~2.2 kPa and ~2.5 kPa (in Figure 9A and B, respectively) by the time the shock wave is visible in the EAC sensor at ~ 0.5 ms. Similar pressure increases preceding shock wave arrival in the EAC are observed in all measurements during exposures 28 kPa or higher, although absolute pressures and time courses vary somewhat across specimens/ears.

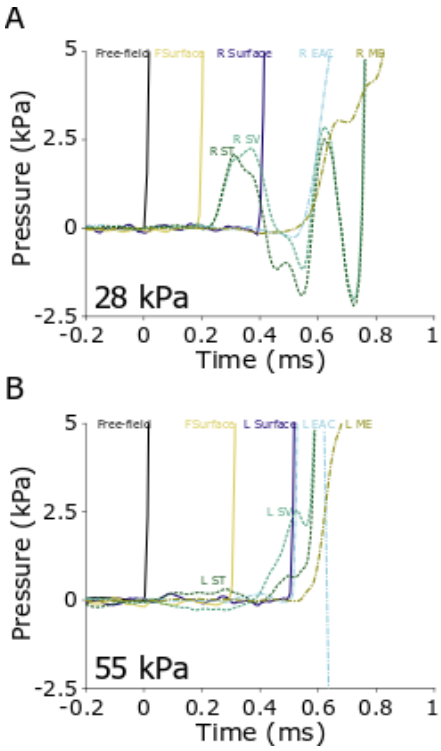

Figure 10. Pressures measured during the 28-kPa (A) and 55-kPa (B) nominal peak pressure exposures, from Figure 8 (ear 411R) and Figure 9 (ear 359L), respectively, expanded to show the first 1 ms after the shock wave arrival at the free field sensor. Note the pressure change in SV and ST appears after the increase in FSurface, but prior to that in the EAC in both examples indicating a non-ossicular (likely bone-conducted) component to the sound transmission. Note, results in A and B are from two different specimens, and absolute arrival times vary between A and B.

4.1.1.9 Intracochlear pressure transfer functions

In order to more directly compare results to prior reports (e.g., Greene et al., 2017), intracochlear pressure transfer functions (HSV/ST/Diff) were calculated from the frequency spectra of PSV Figure 11A; HSV), PST (Figure 11B; HST) and PDiff (Figure 11C; HDiff, the complex difference between SV and ST), by normalizing to PEAC, the sound pressure level in the corresponding ear canal. Figure 11shows transfer function magnitudes (top) and phases (bottom) for the three examples (from two ears) shown in Figure 7–Figure 9 (measured during the 7-, 28-, and 55-kPa nominal peak pressure exposures). Transfer function phase was calculated from the complex component of the frequency spectrum (calculated from a 1-s window after response onset in the free-field sensor), represents the delay between the EAC and each sensor, and was unwrapped using the Matlab function *laplacianUnwrap.m*, available on the Mathworks file exchange website (Bouwman and Bakker, 2016). Both magnitude and phase responses are smoothed with a 1/5-octave wide moving average filter for visualization. Responses are superimposed onto the range of normal responses observed previously in the literature at moderate sound pressure levels (light grey, Nakajima et al., 2009), as well as the responses recorded at somewhat higher levels and lower frequencies (dark grey, Greene et al., 2017), measured with short tone pips. The responses shown in grey represent the range of responses expected for normal, healthy temporal bones (that is, stimuli were presented at levels that elicit responses that vary linearly with sound pressure level), thus deviations from these responses represent nonlinearities in the sound transmission pathway.

Transfer function magnitudes for the 7-kPa exposure (blue) were generally consistent with the prior reports, although magnitudes were somewhat lower for high frequencies (> ~600 Hz) during the impulse noise pressures in the HSV and HDiff. Responses to the 28-kPa nominal peak pressure exposures revealed reduced transfer function magnitudes in all three measures, particularly showing a decrease in the frequency range showing maximum gain (~600 Hz–2 kHz) such that the gain was relatively constant (at or below zero dB re: EAC) across frequencies in all three transfer functions. The 55-kPa peak exposure level showed an additional (small) decrease in gain across frequency relative to the 28-kPa exposure. A notable deviation from the prior reports is visible in HSV for the 55 kPa exposure, which showed an increasing rather than decreasing phase angle for frequencies greater than 1 kHz. This phase disparity generally increased with level, and may be an artifact of the phase unwrapping algorithm, or evidence of the bone conducted sound transmission altering the response at the exposure onset.

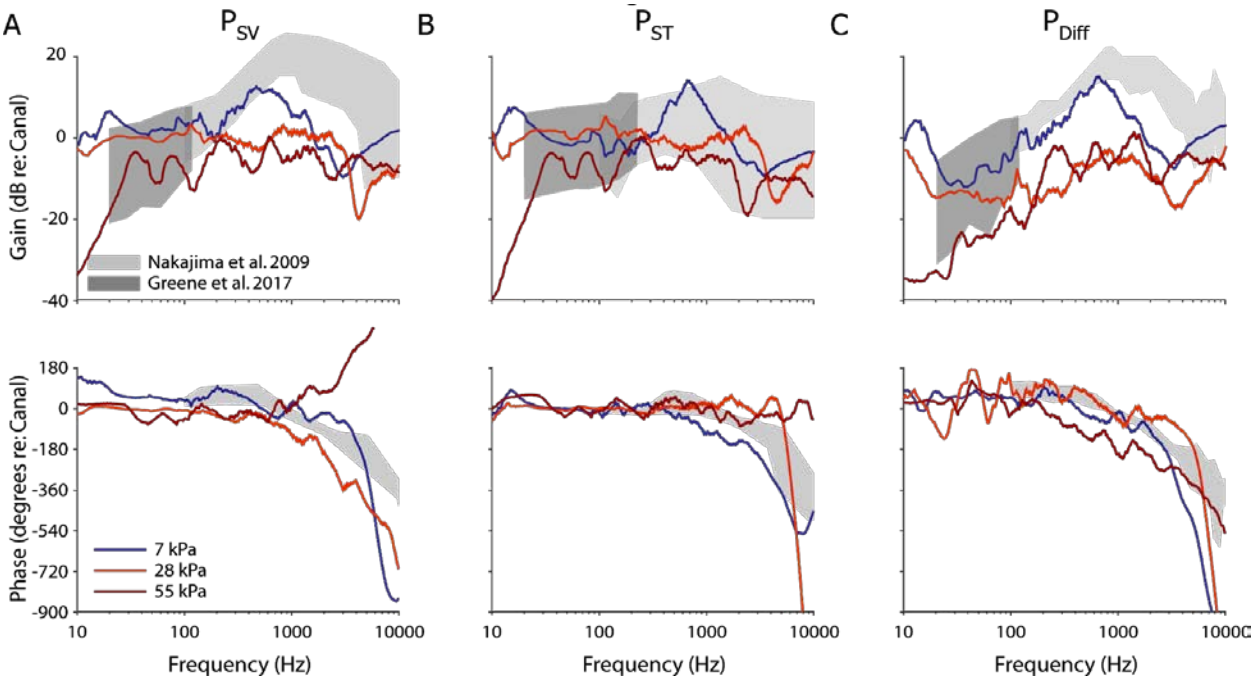

Figure 11. Example intracochlear pressure transfer function magnitudes and phases for the specimens and exposures shown in Figure 7–Figure 9 (i.e., responses in ears 359L, 411R, and 359L during 7-kPa, 28-kPa, and 55-kPa nominal peak pressure exposures respectively). Responses are shown superimposed onto the range of responses observed to moderate sound pressure level tone pips (gray shading) reported previously (dark: Greene et al., 2017; light: Nakajima et al., 2009).

Responses are summarized across the population of specimens/ears in Figure 12. As in Figure 11, transfer function magnitude (top) and phase (bottom) are shown for PSV (Figure 12A; HSV), PST (Figure 12B; HST) and PDiff (Figure 12C; HDiff). The median ± interquartile range of responses for each of the intracochlear pressure transfer function magnitudes (top) and phases (bottom) are show for the 7-kPa (blue) and 28-kPa (red) peak pressure exposures. Responses from 55-kPa and 83-kPa exposures were comparable to those of the 28 kPa, but are excluded here for clarity (and due to the small number of exposures; n = 4 and n = 3, respectively). Transfer function magnitudes are consistently lower during the higher exposures than during 7-kPa exposures in all three measures. PSV and PST show a substantial decrease between approximately 400 Hz–1 kHz, decreasing by a mean (± standard deviation) of -8.8 ± 1.1 dB and -9.2 ± 2.0 dB, respectively. This decrease is substantially larger than at lower frequencies (30–400 Hz), where the decrease was

only -3.0 ± 1.9 dB and -4.4 ± 2.2 dB, respectively. PDiff, on the other hand, shows a more consistent decrease across frequencies, showing declines of -9.6 ± 2.2 dB and -7.8 ± 1.3 dB in the 30–400 Hz and 400–1000Hz bands, respectively. PSV and PDiff were lower in magnitude than previously reported, even for the 7-kPa exposure, which may indicate the nonlinearity may begin at a lower intensity than we tested here, or may reflect the difference in methodology between measurements (e.g., steady-state versus impulse noise exposure). Overall, the 7-kPa and 28-kPa peak pressure exposure transfer function magnitudes are comparable to the ~140 dB SPL and the ~160 dB SPL steady-state tone exposures described previously (Greene et al., 2017).

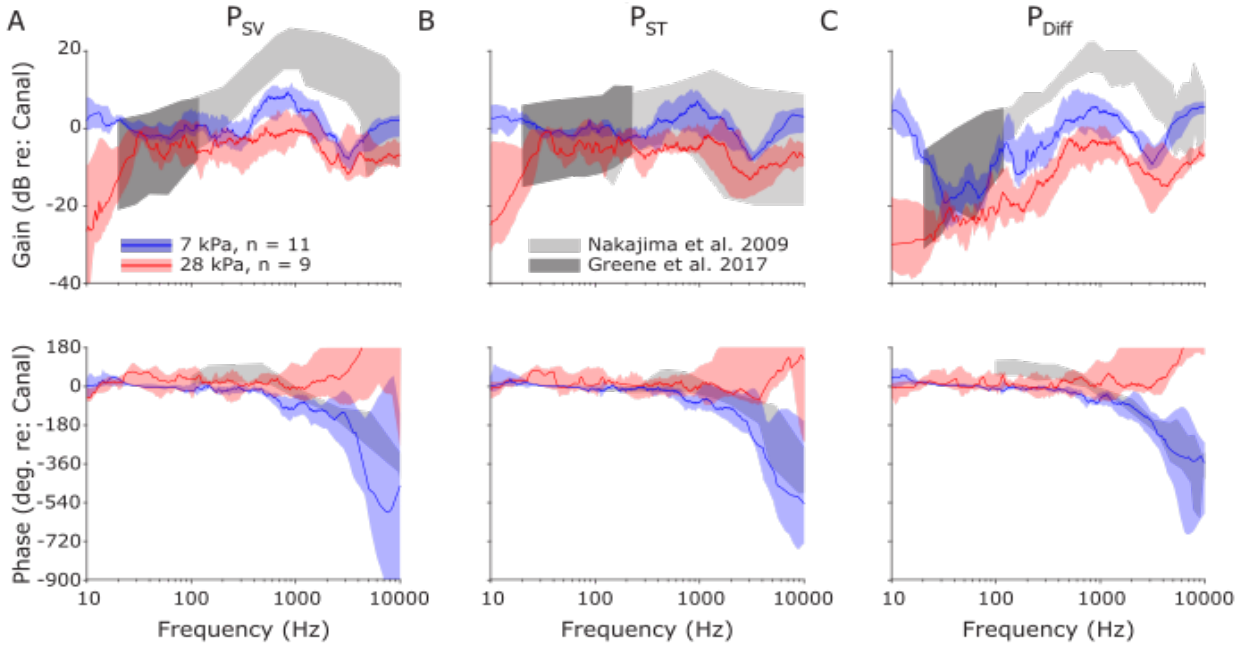

Figure 12. Median and interquartile ranges for intracochlear pressure transfer function magnitudes for all specimens tested, shown for 7 kPa and 28 kPa nominal peak pressure exposures. Responses are shown superimposed onto the range of responses observed to moderate sound pressure level tone pips (gray shading) reported previously (Greene et al., 2017; Nakajima et al., 2009).

Transfer function phases were generally consistent with prior reports (Greene et al., 2017; Nakajima et al., 2009) to tone stimuli, particularly for low frequencies (< ~1 kHz); transfer function phases for the 28 kPa (and 55 kPa and 83 kPa) exposure appear to deviate from the prior reports at higher frequencies (> 1 kHz), showing an increasing phase with frequency suggesting a phase lead in the intracochlear pressures compared to EAC. This deviation (and the large variability across subjects) may be due to noise in the signal, errors in the phase unwrapping algorithm, or evidence of a substantial contribution from a non-ossicular sound conduction pathway (e.g., via bone conduction). Evidence for this final possibility is visible in the shorter intracochlear pressure onset times relative to EAC (Table 2).

4.1.1.10 Findings from Hearing Protection Assessments

To determine the non-linear parameters within the AHAAH hearing protection module, four different types of HPD were evaluated. For performance comparisons, the response measured using each type of protection was compared against the empty ear. Table 4 is a brief description of the HPDs that were used in the PMHS testing.

Table 4. Description of the four types of hearing protection devices evaluated in the effort, including in the ear (ITE) and outside the ear (OTE) configurations.

<table>
<tr><th>Equipment</th><th>Sound Attenuation/Frequency Response at Non-Blas Level</th><th>Picture</th></tr>
<tr><td>ITE-1 = 3M E-A-R Classic Roll-Down Foam Earplug</td><td>
<table>
<tr><th></th><th>125</th><th>250</th><th>500</th><th>1000</th><th>2000</th><th>3150</th><th>4000</th><th>6300</th><th>8000</th><th>NRR</th></tr>
<tr><td>Mean</td><td>37.4</td><td>40.9</td><td>44.8</td><td>43.8</td><td>36.3</td><td>41.9</td><td>42.6</td><td>46.1</td><td>47.3</td><td rowspan="2">29</td></tr>
<tr><td>S.D.</td><td>5.7</td><td>5</td><td>3.3</td><td>3.6</td><td>4.9</td><td>3</td><td>3.1</td><td>3.5</td><td>2.7</td></tr>
</table>
</td><td>  </td></tr>
<tr><td>ITE-2 = 3M Combat Arms Earplug in Open (Nonlinear) Position</td><td>
<table>
<tr><th></th><th>125</th><th>250</th><th>500</th><th>1000</th><th>2000</th><th>3150</th><th>4000</th><th>6300</th><th>8000</th><th>NRR</th></tr>
<tr><td>Mean</td><td>4.1</td><td>4.5</td><td>11</td><td>18.7</td><td>24.9</td><td>29.8</td><td>25.8</td><td>18.7</td><td>26.5</td><td rowspan="2">7</td></tr>
<tr><td>S.D.</td><td>2.7</td><td>2.8</td><td>3.9</td><td>3.2</td><td>3.3</td><td>2.7</td><td>3.3</td><td>3.6</td><td>3.3</td></tr>
</table>
</td><td>  </td></tr>
<tr><td>ITE-3 = ARA ShotShields in Open (Nonlinear) Position</td><td>
<table>
<tr><th></th><th>125</th><th>250</th><th>500</th><th>1000</th><th>2000</th><th>3150</th><th>4000</th><th>6300</th><th>8000</th><th>NRR</th></tr>
<tr><td>Mean</td><td>22.4</td><td>21.3</td><td>24.2</td><td>22.2</td><td>22.6</td><td>27.5</td><td>23.5</td><td>31.1</td><td>38</td><td rowspan="2">15</td></tr>
<tr><td>S.D.</td><td>3.9</td><td>3.8</td><td>4</td><td>3.5</td><td>3.3</td><td>3.8</td><td>3.1</td><td>4.4</td><td>3.8</td></tr>
</table>
</td><td>  </td></tr>
<tr><td>OTE = 3M ComTac XP/ComTac III, No Power</td><td>
<table>
<tr><th></th><th>125</th><th>250</th><th>500</th><th>1000</th><th>2000</th><th>3150</th><th>4000</th><th>6300</th><th>8000</th><th>NRR</th></tr>
<tr><td>Mean</td><td>15.2</td><td>17.6</td><td>24.9</td><td>30.5</td><td>33.4</td><td>39.3</td><td>41.4</td><td>46.2</td><td>45.8</td><td rowspan="2">21</td></tr>
<tr><td>S.D.</td><td>4.2</td><td>2.7</td><td>2.3</td><td>3.8</td><td>4.1</td><td>3</td><td>3.4</td><td>3</td><td>4.7</td></tr>
</table>
</td><td>  </td></tr>
</table>

To quantify the performance of the four HPD evaluated, the PMHS data collected was processed to determine the insertion loss for each HPD. Insertion loss is the difference between the maximum estimated pressure for the open-ear condition and the maximum pressure measured when a hearing protector is placed for the same condition on the same PMHS. To calculate the insertion loss, the pressure time wave in Figure 13 was decomposed into its frequency components in Figure 14 for both the empty unconcluded ear and for the case when the ear canal was occluded with a HPD. The insertion loss was calculated by subtracting the occluded frequency components from the empty ear case paired by the pressure at the surface of the head. This process was completed for each hearing protection all four pressure conditions (Figure 15).

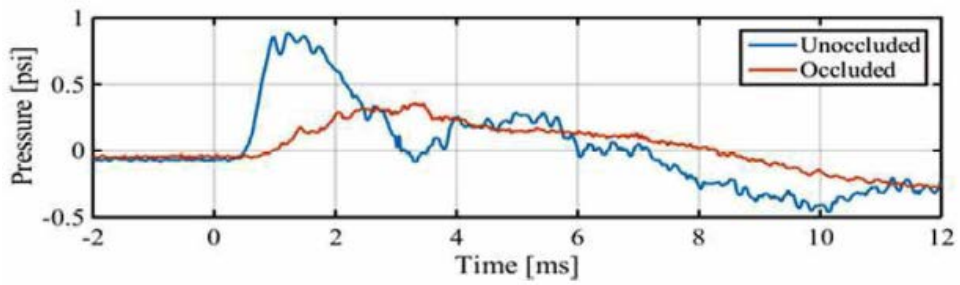

Figure 13. Comparison of the pressure time trace from sensor in ear canal with and without hearing protection device.

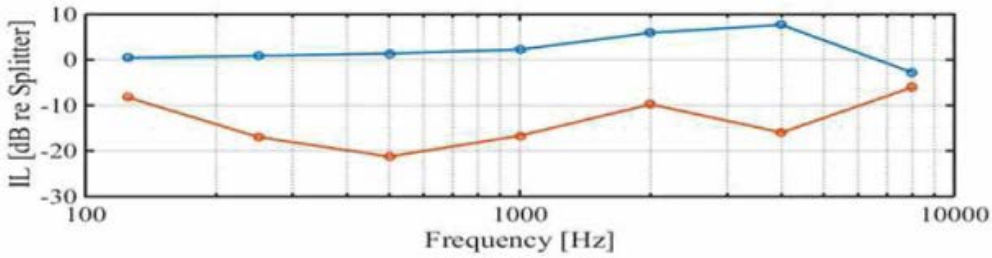

Figure 14. Comparison of the pressure in ear canal with and without hearing protection device in the frequency domain.

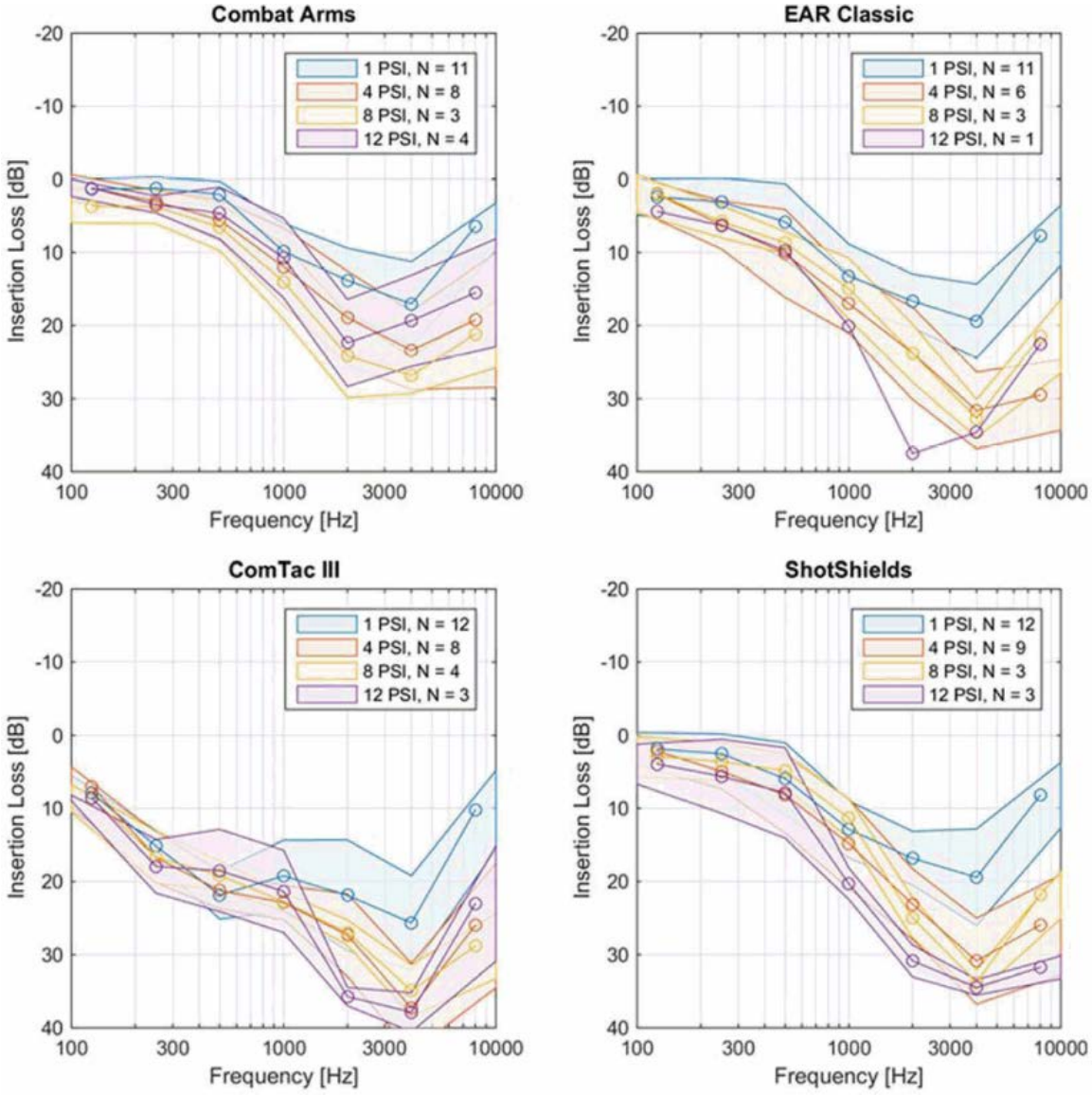

Figure 15. Insertion loss curves for the four different hearing protection devices.

4.1.1.11 Development of a Nonlinear Hearing Protection Device Module

The experimental and insertion loss data presented in the previous sections was used to improve a hearing protection module (HPM) designed for evaluation of hearing at high-intensity impulsive pressure levels and not derived from experimental data at those levels. The most common electro-acoustic model for the human auditory system is the AHAAH model—a non-empirical model that uses electronic elements to represent the biophysical functions of the respective structures within the ear. For an electro-acoustic model, voltages represent pressure, currents represent volume velocity, and charges represent volume displacement. Using electric elements that include inductors, resistors, and capacitors, the pressure changes in the ear can be simulated and represented by changes in voltage throughout the circuit. The pressures collected in this effort allowed researchers to empirically validate the model using PMHS and ANSI S12.42-compliant shock tube data and modify/change the parameters of the individual elements to better represent the biological function of the structures within the ear.

In this effort, the Insertion Loss (IL) curves provided by an HPD were deconstructed into a three-piston model (Figure 16). Each "piston" (Skin, Device, Air Leak) occupies a different portion of the 100-Hz to 10-kHz frequency band typically associated with hearing protection. In Figure 17, the IL data from the Combat Arms hearing protection that was evaluated for the different pressure levels tested are represented by the blue circles. MATLAB was used to fit the three piston resonator circuit with the natural frequencies of each piston indicated by the vertical lines.

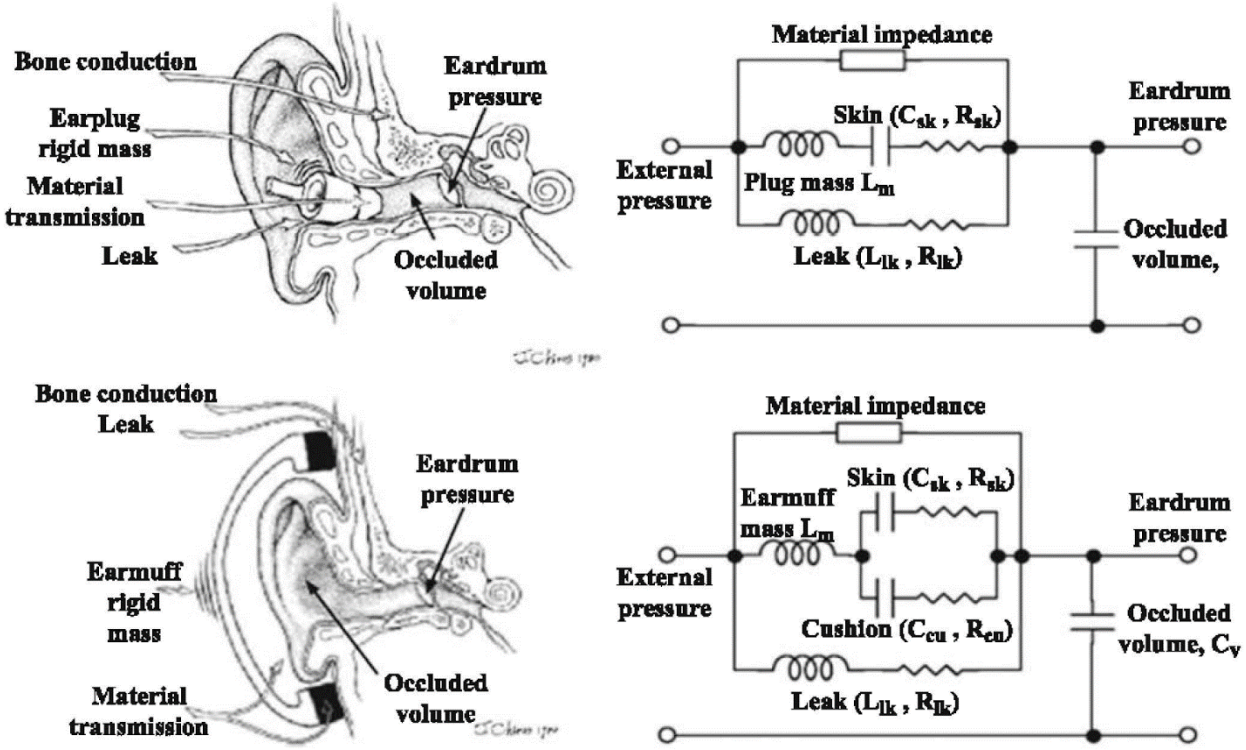

Figure 16. Schematic of the three piston hearing protection module illustrating how electrical elements are used to represent the hearing protection device and the biological function of the structures within and surrounding the ear canal (from Kalb 2013).

Using curves such as the ones shown in Figure 17, nine frequency bands for hearing protection improvements during impulse noise exposure generated by blast can be identified. From 7 kPa to 55 kPa the "leak" path is always present, suggesting a possible area for improvement for HPD. Also observable is that the "Material" adds protection above 2 kHz as pressure increases; unfortunately, the bulk of the energy in the pressure wave is in lower frequency bands suggesting that the development of new materials for the HPD may not reduce the risk of hearing damage. The last piston "skin" shows negligible transmission. This is most likely due to the viscoelastic properties of the tissue that damp out the energy prior to reaching the sensory structures of the ear.

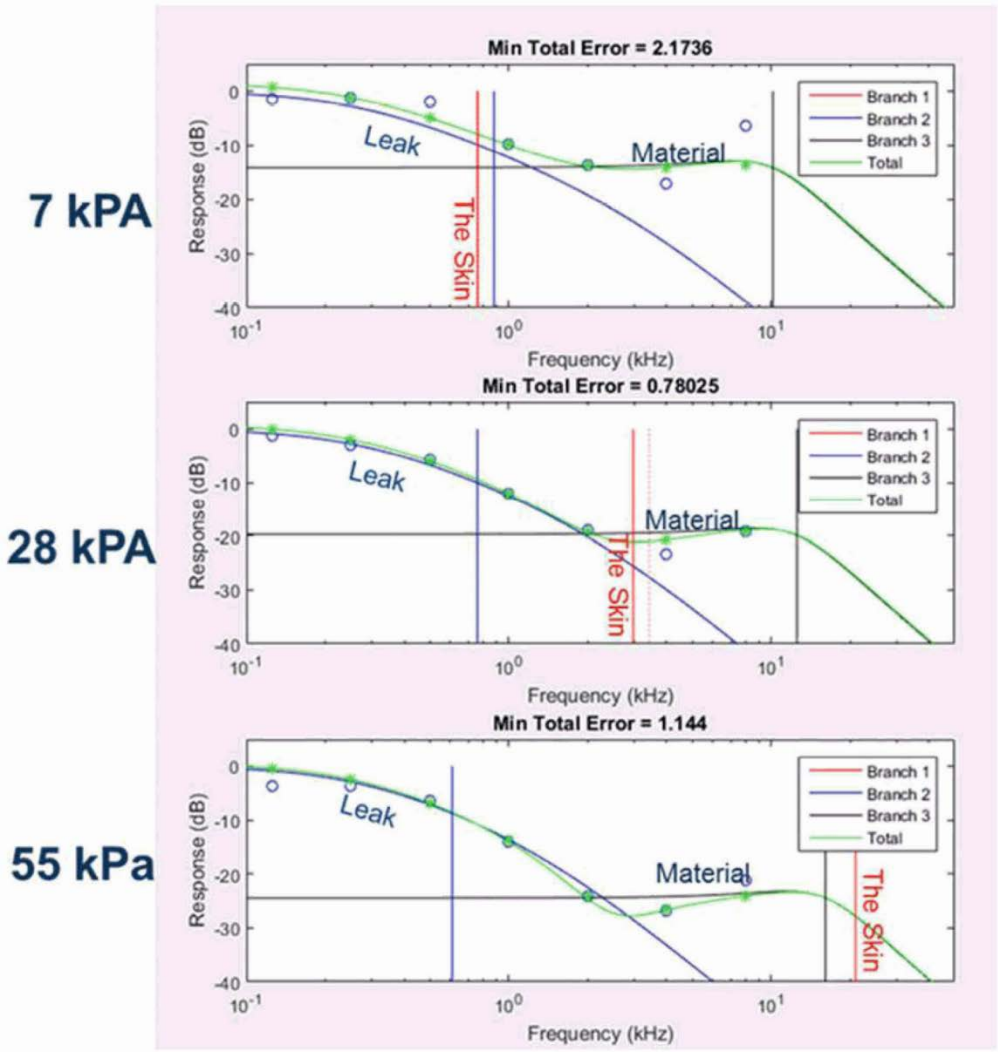

Figure 17. Output in the frequency domain from the three branch resonator circuit for the Combat Arms HPD broken down by pathway illustrating how the energy is transmitted through and around the hearing protection for various levels of blast pressure.

Currently all 11 electro-acoustic component values (EACV) shown in Figure 18 have been derived from insertion loss curves measured using standard Real Ear Attenuation at Threshold (REAT) or similar methods. As the methodology was determined for calculating the EACVs, it was observed that the order in which they are determined influences the values selected. This suggests that the number of EACVs to be determined is too large for the IL curves used for the derivation, making the model overdetermined and hence unstable. The section below describes how the methodology developed under this effort reduces the number of derived EACVs from 11 to 6 to increase the accuracy and stability of the predictions.

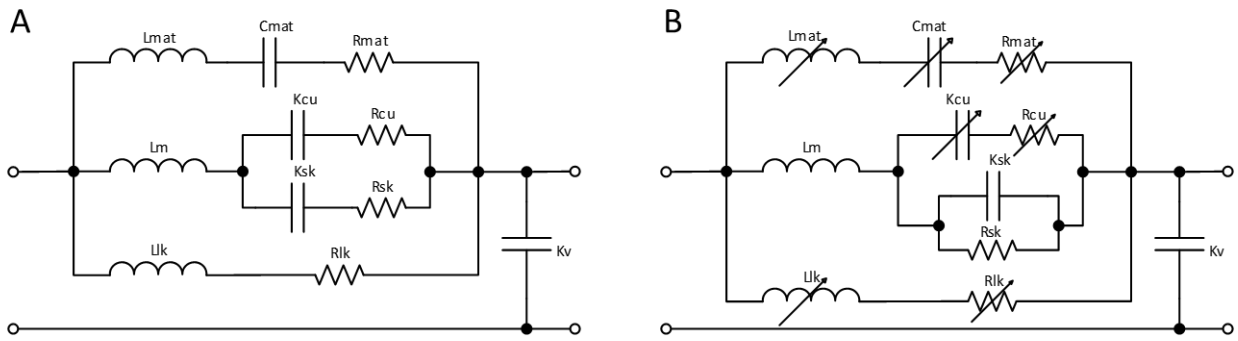

Figure 18. Hearing protection modules for the AHAAH model are composed of linear and nonlinear electroacoustic elements. Left – HPD module proposed by Fedele and Kalb. Right – Modified HPD module developed under this program.

4.1.1.11.1 Descriptions of Model's Three Branches

4.1.1.11.1.1 Branch 1 - Leak

The leak path consists of an inductor/resistor pair representing the movement of air between the hearing protection and the skin. A capacitor representing the compliance of the air in the ear canal cavity is also included in this path.

The compliance of the air in the ear canal cavity is based on the compressibility of gas and the volume of the gas behind the hearing protection. The gas volume for each hearing protection device was measured and found to be similar for each device. The value for the compressibility is held fixed at 1e5 dyne/cm^5. This reduces the ear canal from a variable to a fixed value.

The leak inductor/resistor path is modeled by separate inductance and resistance models for fluid flow through a slot as a function of pressure. The resistive (real) portion of this impedance is modeled using the same function as Fedele and Kalb (2015), taken from Sivian (1935),

$$Z_{RE} = 150\left(1 + \frac{U}{203}\right)^{1.17}, \tag{1}$$

where

$$U = \frac{P}{\rho c} \tag{2}$$

for pressure P air density ρ, and speed of sound in air c.

The inductive (imaginary) portion of the impedance is modeled after Sivian's work as well. In this case, the imaginary portion of the fluid flow through a rectangular slot is used. It is assumed that the slot is bent into an annulus and that the impedance of the annulus is equivalent to the impedance of a slot. The imaginary portion of the impedance is defined by Sivian as

$$Z_{IM} = \rho\omega\left\{\frac{1}{4g_w g_h} + \frac{1}{3\pi g_w^2 g_h^2}\left[(g_w^2 + g_h^2) - (g_w^2 - g_h^2)^{3/2} + 3g_w g_h\left(g_h \log\frac{g_w(g_w^2+g_h^2)^{1/2}}{g_h} + g_w \log\frac{g_{wh}(g_w^2+g_h^2)^{1/2}}{g_w}\right)\right]\right\} \tag{3}$$

for g_h and g_w defined as the slot height and width, respectively. For this algorithm, the gap width is equivalent to the circumference of the ear canal and gap height is the difference in radius

between the ear canal and the HPD. In this algorithm, the diameter of the ear canal is held fixed at 0.83 cm, but the gap height is allowed to vary from an initial value of 0.75e-3 cm. This reduces the leak path from two undetermined variables to one.

4.1.1.11.1.2 Branch 2 - Material

This branch consists of an inductor, capacitor, and resistor representing the mass, compliance, and resistance of the hearing protection device. Each of these values are allowed to vary in the optimization algorithm.

4.1.1.11.1.3 Branch 3 - Rigid Body

The rigid body branch is composed of an inductor representing the mass of the HPD, a resistor and capacitor representing the viscosity and elasticity of the skin supporting the HPD, and a resistor and capacitor representing the viscosity and elasticity of the ear cup supports present for earmuffs. These elements are represented as follows.

- The cushion of the ear cup supports is composed of a compliance and resistance pair. These values are allowed to vary when using the optimization algorithm.
- The mass of the hearing protection was determined experimentally for each HPD tested. These values were held fixed in the optimization algorithm, thereby reducing the free variables by two.
- The Maxwell model for the skin is shown in Figure 19. This is a validated biomechanical model for skin based on small deformations. These values are held fixed in the optimization algorithm, thereby reducing the number of parameters by one.

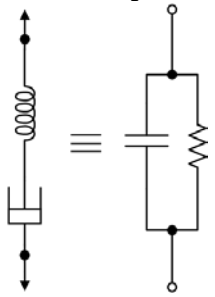

Figure 19. Mechanical Maxwell model representing the response of the skin to high intensity blast and the equivalent electrical model.

To implement the hearing protection module into the Blast Auditory Model, the circuit model is fit to the octave band attenuation calculated as the difference between the measured pressures in the freefield and inside the ear canal.

4.1.1.11.2 Fit the HPD Module to the Measured Insertion Loss

To predict the performance of HPDs, the eleven electroacoustic parameters in the linearized hearing protection module are adjusted until the attenuation prediction matches the measured octave band attenuation values. This match is optimized through a combination of reduction in the number of fit parameters and by applying an automated fit routine that systematically adjusts the model parameters until the difference between the model and the octave band insertion loss is minimized. The optimized parameters are then used in the regression analysis to model their level-dependent behavior.

4.1.1.11.3 Determine Fixed Parameters

To reduce the number of free parameters available in the fitting routine, parameters in the hearing protection module may be fixed as constants based on measurements or tabulated physical values as follows.

- M_m: HPD mass is derived from physical measurement of the mass of the hearing protection device (insert devices) or individual ear cup (circumaural devices). Converted to specific acoustic impedance L_m by dividing by the cross sectional area of the HPD.
- K_{sk}: Stiffness of the skin in the Maxwell skin model is taken from Kwon et al. (2006). Conversion to specific acoustic impedance through division by cross sectional area of skin yields 5e-12 cm^5/dyne.
- R_{sk}: Resistance of the skin in the Maxwell skin model is taken from Kwon. Conversion to specific acoustic impedance through division by cross sectional area of skin yields 2.03e6 dyne-s/cm^5.
- K_V: The occluded volume under the hearing protection was measured for a variety of insert hearing protection devices and fixed at a value of 1e5 dyne/cm^5.

4.1.1.11.4 Optimize for Free Parameters

After assigning values to the fixed parameters, the remaining free parameters are systematically varied to match the modeled attenuation to the measured attenuation values for each exposure level. As the parameters are varied, the resulting frequency-dependent pressure in the ear canal behind the hearing protection is calculated. This pressure is then propagated to the tympanic membrane and middle ear of the AHAAH model.

A flow chart depicting the steps for optimizing the fit parameters is shown in Figure 20. Each step is designed to minimize the total error between the modeled attenuation and measured attenuation. Each branch of the model is sequentially optimized in a ‘fit step,’ which is repeated for four iterations.

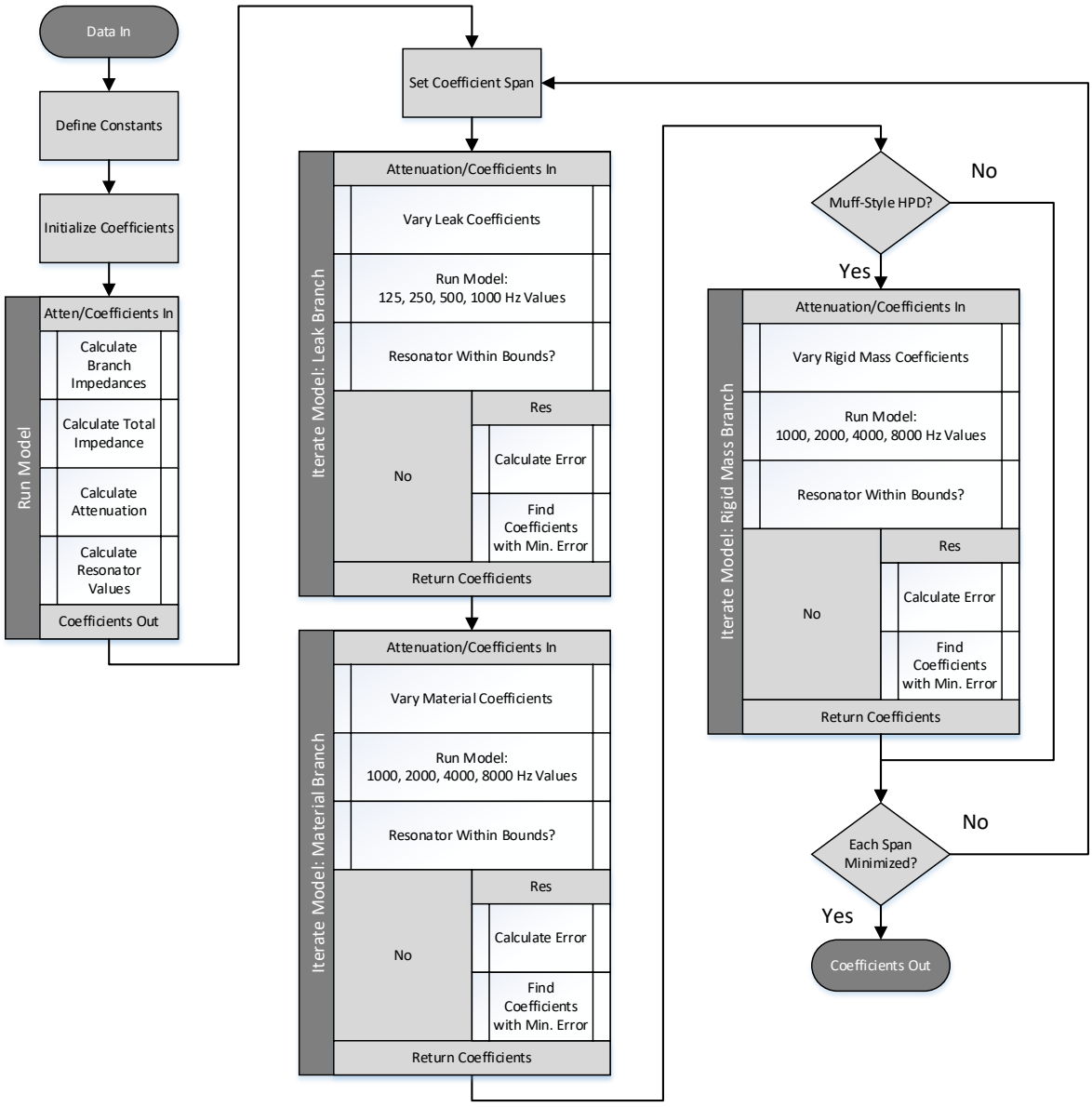

Figure 20. The coefficient optimization routine for a given HPD and exposure level is performed using this sequence of steps.

4.1.1.11.5 Initialization

Fitting coefficients will be performed for the lowest exposure level first. Once the optimization routine is completed for an exposure level, the next higher exposure level will be optimized using the previous fit as its initial parameters. For the first fit, the model is initialized with the default coefficients in Table 5, which are based on the specific hearing protection device. ARL-TR-6748 (Fedele and Kalb 2015) contains tables of coefficients for an array of hearing protection devices derived from fits to REAT (ANSI S12.6, 1984) IL measurements. These coefficients should be used for all hearing protection devices included in the tables with the “generic” muffs and plugs used for devices that have not been included.

Table 5. Initial parameters for the optimization routine are selected from the fixed model parameters described in Fedele and Kalb 2015.

Branch	Element	Initial Value	Source
1	L_{mat}	Device-Specific	Fedele 2015
1	M_{mat}	Device-Specific	Fedele 2015
1	R_{mat}	Device-Specific	Fedele 2015
2	L_m	Device-Specific	Lab Measurement
2	K_{cu}	Device-Specific	Fedele 2015
2	R_{cu}	Device-Specific	Fedele 2015
2	K_{sk}	2e11 dyne/cm^5	Kwon 2006
2	R_{sk}	2.03e6 dyne-s/cm^5	Kwon 2006
3	L_{lk} (Imaginary Impedance)	0.75e-3 cm gap height	Sivian 1935
3	R_{lk} (Real Impedance)		Sivian 1935
3	K_v	1e5 dyne/cm^5	Lab Measurement

Once the initial coefficients have been selected, the frequency-dependent lumped element impedance for each element should be calculated as follows:

Resistance:

$$Z_R = R_{ac} = \frac{R}{S^2} \tag{4}$$

Compliance:

$$Z_K = \frac{K_{ac}}{j\omega} = \frac{K}{j\omega S^2} \tag{5}$$

Mass:

$$Z_L = j\omega L_{ac} = \frac{j\omega L}{S^2} \tag{6}$$

In the element impedances, the subscript ac refers to the specific acoustic impedance and is equivalent to the element value normalized by the cross-sectional area *S*. In these formulas, *j* is the imaginary constant and ω is the angular frequency in radians/second. Upon calculating the element impedances, standard methods for solving electrical circuits can be used to determine the impedance for each branch and for the system as a whole.

The intent of this model is to determine the amount of pressure arriving in the ear canal behind the hearing protection such that it can be propagated through the middle and inner ear sections of the model to predict hearing injury. Therefore, the output of the hearing protection module, the attenuation due to the HPD, is the pressure drop across the K_v element compared with the freefield value which is analogous to the voltage drop in a standard electrical circuit formulation compared with the source voltage.

4.1.1.11.6 Model Iteration

To find a global minimum for the model, the elements in the branches are systematically fit in steps to the frequency range in which they govern the response. First, the gap height in the leak

branch is varied to fit the 125-, 250-, 500-, and 1000-Hz octave band portion of the attenuation. Then, the three material parameters in the material branch are varied to fit the 1000-, 2000-, 4000-, and 8000-Hz octave band portion of the attenuation. Finally, the earmuff suspension parameters are varied to fit the 500-, 1000-, and 2000-Hz band portions of the attenuation.

The iteration cycle is repeated four times to systematically increase the goodness of fit of the model-data comparison. To determine the goodness of fit between the calculated attenuation and the experimentally measured attenuation, an error estimate is made. An average of the deviation of the modeled attenuation from the measured attenuation is used. In each iteration, this elements resulting in the minimum of this value are propagated to the next fitting step.

Due to the large number of fit parameters and the smaller number of data points, the fit parameters are allowed to vary widely during each iteration cycle. In the first of the four iterative cycles, allowable values for each parameter are allowed to span six orders of magnitude centered on the value propagated from the previous fit step. In subsequent iterations the allowable span is reduced such that in iteration two, the span is three orders of magnitude, iteration three is 1.5 orders of magnitude, and iteration four is one order of magnitude. This scheme allows the parameters for each branch to affect the fit of subsequent fit steps while being affected by previous fit steps.

To ensure the calculated values are physically reasonable, the resonance frequency and quality factor of the oscillator formed by each of the three branches is also calculated:

$$f_{res} = \frac{1}{\omega}\sqrt{\frac{K}{L}} \tag{7}$$

$$Q = \frac{1}{R}\sqrt{KL} \tag{8}$$

The resonance frequency and quality factor for each branch is bounded to a physically reasonable range and limited from values outside of these bounds. The bounds for the resonance frequencies and quality factors for each branch are shown in Table 6. Fit steps generating element values which caused the quality factor and resonance frequency to fall outside of these ranges were discarded and the coefficients from the previous fit step were carried forward.

Table 6. The resonance frequency and quality factor of the oscillator formed by each branch is bounded to ensure the elements maintain physical relevance.

Branch	Q_{min}	Q_{max}	f_{min} (Hz)	f_{max} (Hz)
Material	0.5	10	1000	20000
Rigid Mass	0.5	10	1000	5000
Leak	0.01	10	None	2000

4.1.1.11.7 Fitting Results

An example output of the fitting routine is shown in Figure 21 for a nonlinear universal fit insert HPD for four sequential exposure levels from 171 dBP to 192 dBP. The model has fit the gray triangles to the data represented by the black squares in octave bands. In each case, the orange line represents the contribution of the leak branch to the total impedance, the blue line represents the contribution of the material branch to the total impedance, and the black line represents the continuous impedance curve. A line representing the rigid body branch is not visible at this scale for this HPD. In this example, the leak branch varies little, thereby demonstrating a leak with a

consistent gap width around the device. The material branch demonstrates increased attenuation with exposure level due to both the level-dependent design of the device.

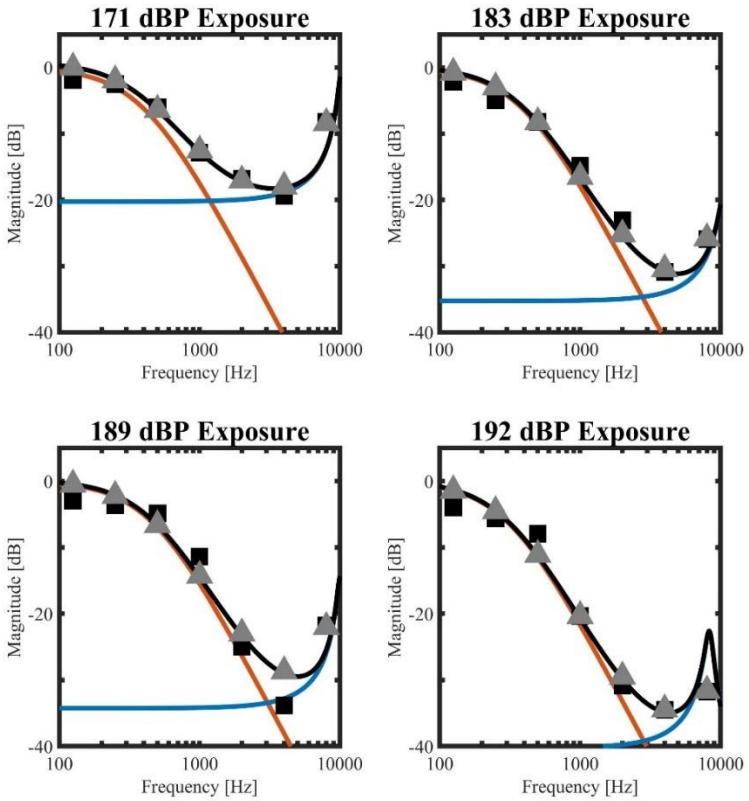

Figure 21. The optimization routine varies the elements of the HPD module to compare the module result (gray) with the measured data (black). Each branch of the model is varied sequentially; the resultant response for the low frequency (orange) and high frequency (blue) are shown. This process is repeated for each exposure level.

4.1.1.11.8 Regression Analysis of Model Coefficients

The optimization routine produces the elements of the HPD module that most closely resemble the measurements for each exposure level. Nonlinear behavior of the elements, however, must be determined by finding a relationship that can be implemented in the Simulink model. Although element values for different test fixtures and sources may be determined by the optimization routine, since the optimization routine is operating on attenuation, a relative measurement which will be independent of source or test fixture, rather than pressure, an absolute measurement that may vary from fixture to fixture or source to source, the results may be combined to form one set of coefficients or split out by fixture or source.

To determine the behavior of the elements at levels that were not tested, a linear regression is performed on each element with respect to exposure level in dBP,

$$E = e^{A*P+B} \quad (9)$$

where E is the element value, P is the exposure level in dBP, and A and B are the linear fit coefficients. Figure 22 demonstrates a fit (gray lines) to PMHS data for 171-dBP, 183-dBP, 189-dBP, and 192-dBP exposures (black dots). Linear elements, such as K2 and R3 do not vary with the fit generating a pressure-independent line at a single element value. Nonlinear elements

demonstrate slopes with both positive and negative behavior and are implemented in the model regardless of the sign of the coefficient.

The regression analysis performed on each coefficient demonstrates a limitation of this approach. The slopes of the coefficients may produce nonphysical element values when extrapolating the coefficients outside the range of incident pressures measured; therefore, model predictions for incident pressures outside of the range used in the regression analysis should be considered carefully to ensure the that coefficients generate physically meaningful predictions.

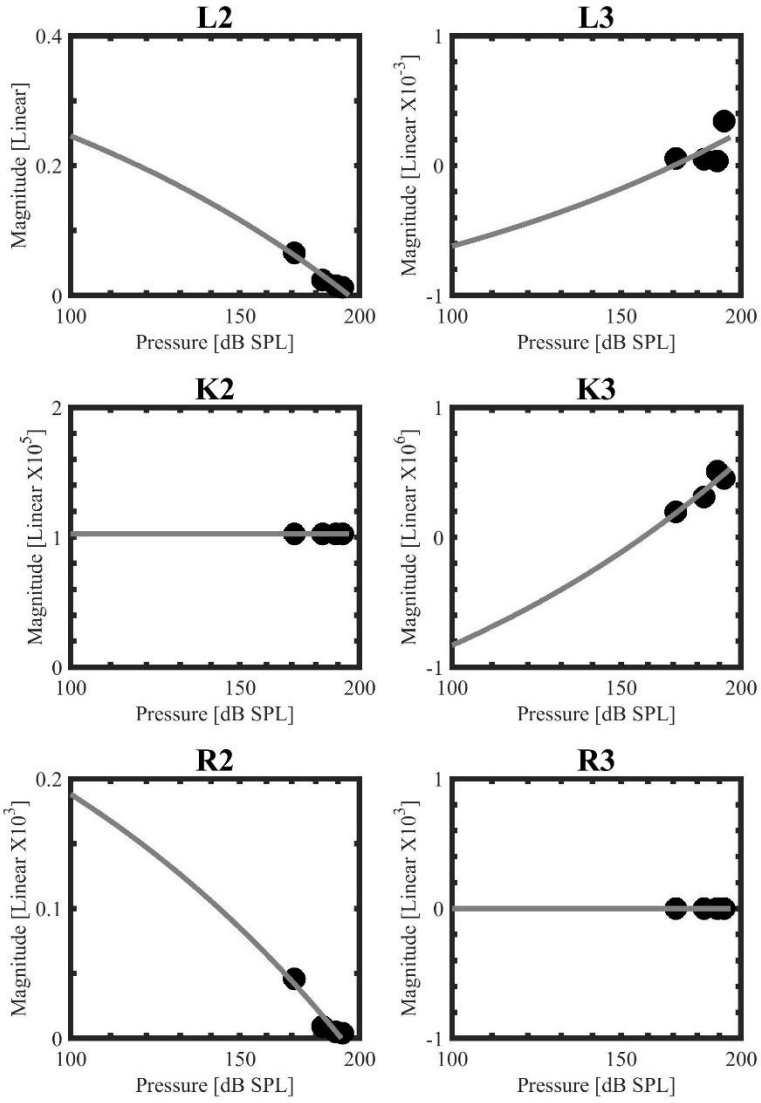

Figure 22. Linear regressions were performed on each of the calculated coefficients to determine how the nonlinearity was is included in the appropriate elements. Some elements remain linear while others display nonlinear behavior.

4.1.1.11.9 Implement the Regression Coefficients into a Simulink Model of the HPD Module

The Simulink model for the ARA nonlinear hearing protection model is shown in Figure 23. A pressure source is programmed to import a pressure-time history recorded from a free field measurement and the solver is programmed to find a solution at each time step. Nonlinear elements are arranged in the same manner as the circuit schematic of the nonlinear model shown in Figure

18. Other model elements are probes to observe the instantaneous pressure, including a probe to measure the pressure deposited into the ear canal compliance. This pressure is equivalent to the pressure measured in the ear canal during testing and is used as the solution to the model.

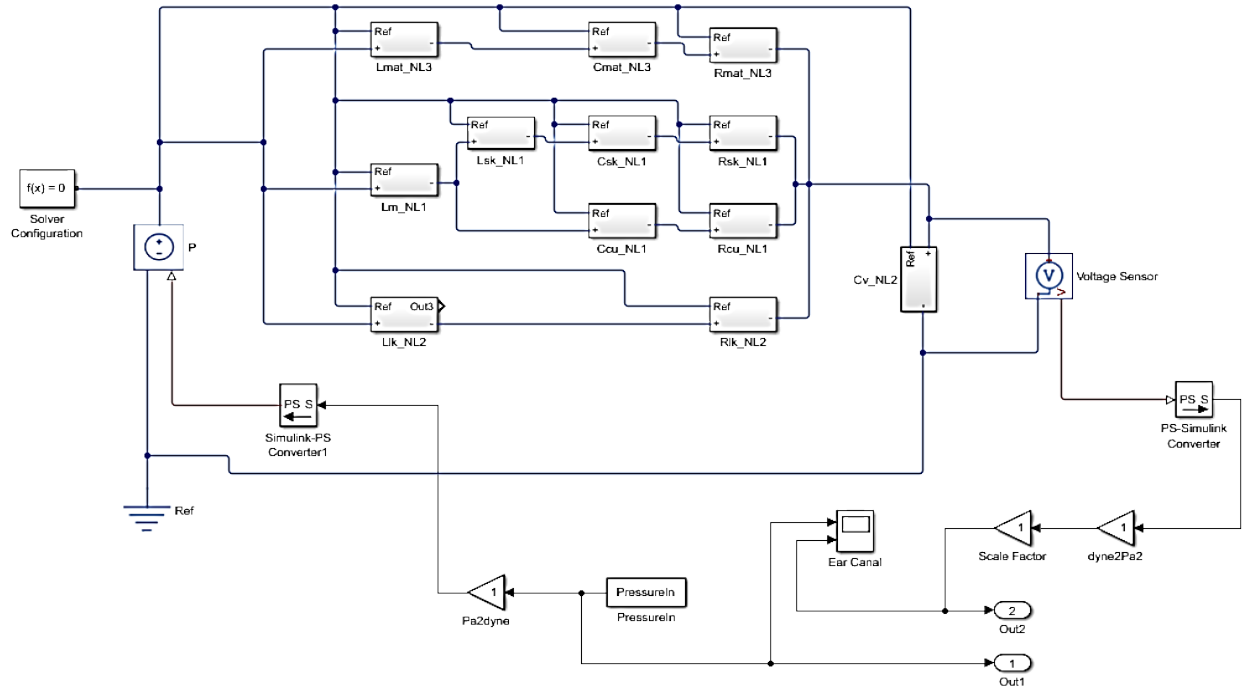

Figure 23. ARA's Nonlinear HPD Simulink Model consists of the nonlinear elements, solver, and monitoring probe points.

A typical implementation of a nonlinear element is shown in Figure 24. Coefficients for the element are imported and interpolated based on the instantaneous pressure, then combined. The linear coefficients are implemented using the same elements as the nonlinear coefficients, but using $A = 0$ for the linear term. Use of the same element construct allows the model to be used for linear and level-dependent devices with no changes. The coefficient is then applied to the element; in this example, the element is an inductor.

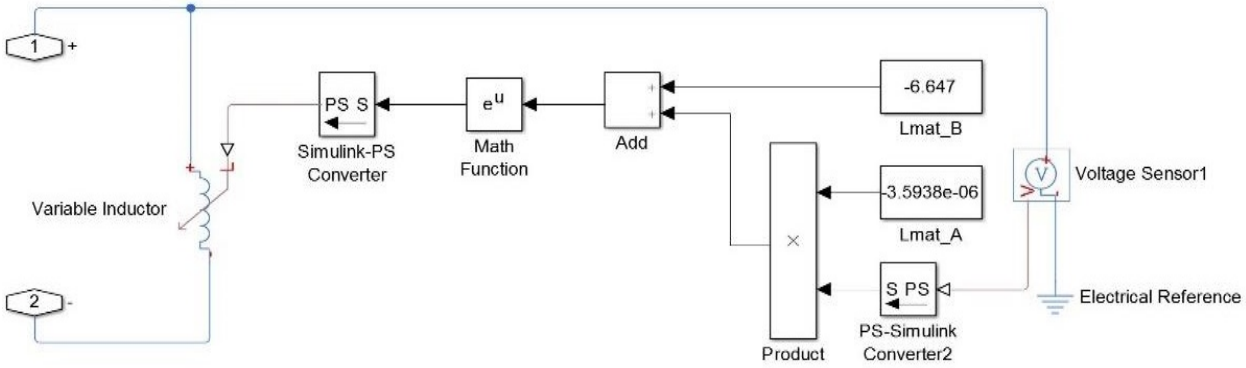

Figure 24. Element implementation for ARA's Simulink model consists of coefficient lookup and interpolation routines.

Exercising the model for a pressure-time history of interest produces the information shown in Figure 25. In each subplot, the blue lines represent the model output and the orange lines represent

the measurement. The top pane shows the general time-domain agreement between the model and measurement for a level-dependent earplug at a 183-dBP (4-psi) exposure. The center subplot shows the frequency-domain spectrum for both measurement and model which is further decomposed into one third octave bands in the lower subplot. In this example, good agreement between the measurement and model is seen in the time domain signals; the frequency spectra show good agreement between 1 kHz and 3 kHz with the model over-predicting the amount of pressure propagating through the HPD above and below this band.

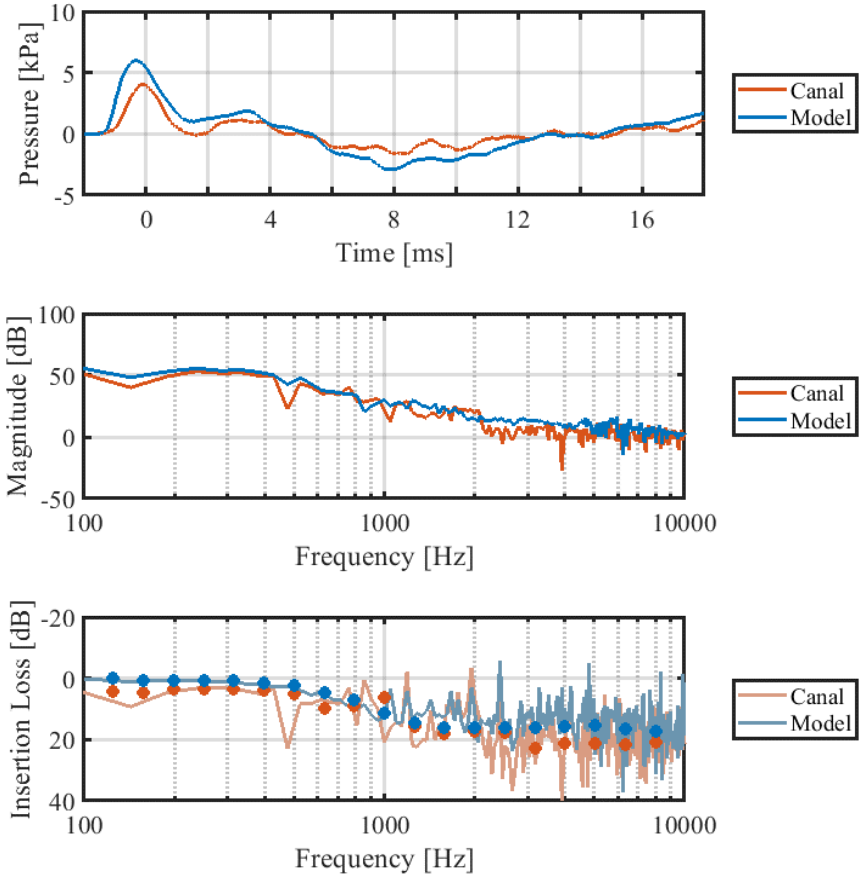

Figure 25. Simulink Model Output. Top – Time domain waveform. Center – Frequency Spectrum. Bottom – Continuous frequency and one-third octave band-limited insertion loss.

4.1.1.11.10 Model Results

Measurements of four hearing protection devices and the open ear were conducted to validate the model. Each of these devices is commonly used by the U.S. Army or was developed at the Army's behest. Table 4 is a brief description of each of the hearing protectors. Each of these devices was evaluated using both PMHS and ANSI test fixtures; results from PMHS testing are shown in the following sections.

In the following sections, model predictions are compared to the measured pressure in the ear canal behind the HPDs in PMHS specimen targets using the Mobile Shock Tube as a source. Incident pressures used to form the regression coefficients were from 171-, 183-, 189-, and 192-dBP tests. In each of the results figures for the specific HPDs, blue lines represent the measured pressure in the ear canal, orange lines represent the predictions of the linear AHAAH HPD module ('AHAAH Linear'), yellow lines represent the predictions of the ARA model presented in this protocol with

all coefficients held constant ('ARA Linear'), and purple lines represent the results from application of the full nonlinear model ('ARA Nonlinear').

4.1.1.11.10.1 Open Ear

Open ear measurements were performed for the 171-dB exposure only; higher exposure levels with the open ear frequently damaged, but did not rupture, the tympanic membrane. Since regression through multiple exposure levels was not possible, the ARA linear and nonlinear models are the same for the open ear.

The data-model comparison for the open ear for one example 171-dBP exposure is shown in Figure 26. The peak pressure and A-duration are accurately captures by both the AHAAH linear and ARA models. Overall trends in the shape, even at long times (~15 ms to 20 ms) are accurately recorded. Both the AHAAH linear and ARA nonlinear models demonstrate a small amount of extra high frequency energy which is apparent sporadically throughout the waveforms, such as that apparent near 3 ms. This noise is at approximately 100 kHz, well above the range of human hearing and may be related to the time step utilized when running the models. In any event, it would be imperceptible to humans and only damaging at much higher intensities.

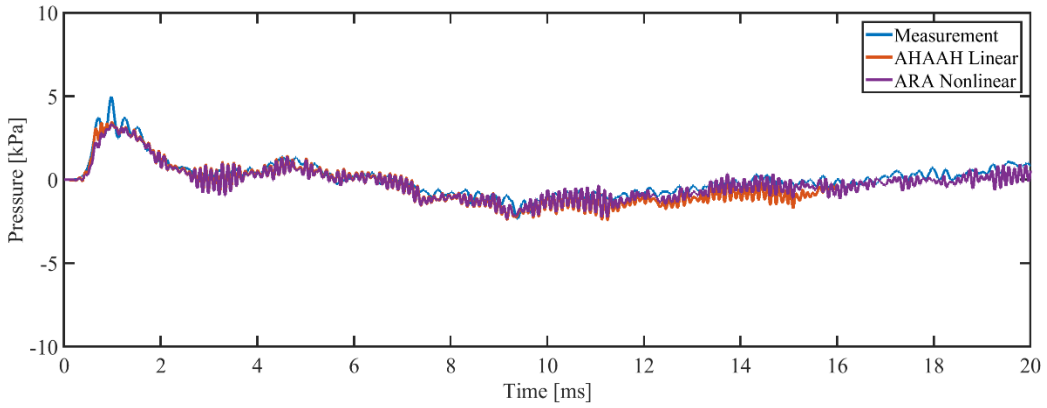

Figure 26. Data-model comparison for the Open Ear for a 171-dBP exposure sows good agreement between the measurement, AHAAH Linear and ARA nonlinear models.

4.1.1.11.10.2 Over-the-Ear HPD

The data-model comparison for the Peltor Comtac III earmuff with gel cushions is shown in Figure 27 for a 183-dBP exposure. The ARA model with linearized elements matches the measured A-duration well, however, the peak pressure is over-predicted by a factor of two and the strength of the shock is much stronger. The AHAAH linear model and the ARA model with nonlinear elements both capture the general shape of the measured pressure consisting of two gentle humps and a return to a near-quiescent after approximately 12 ms. The peak pressure using these models is over-predicted by approximately 10%.

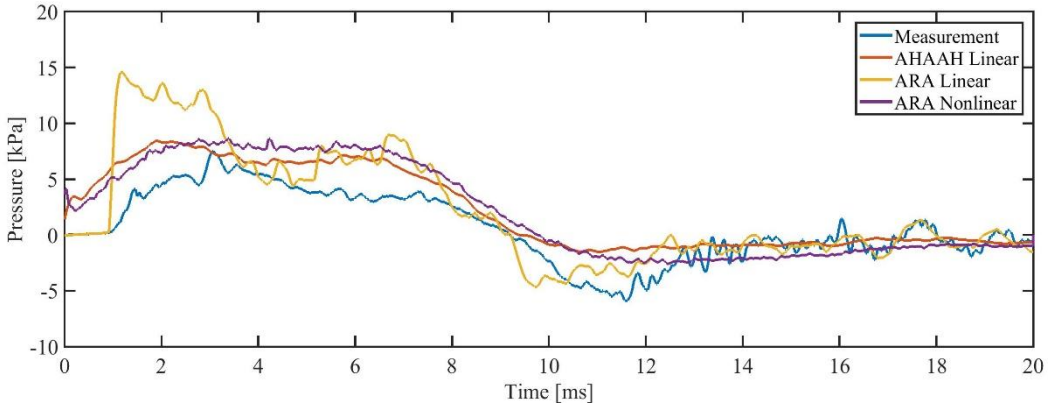

Figure 27. Data-model comparison for the Comtac III for a 183-dBP exposure. The data is matched well by the ARA nonlinear model and the AHAAH linear model. The ARA model with linear coefficients does not well represent the data.

4.1.1.11.10.3 In-the-Ear HPDs

The data-model comparison for the 3M Combat Arms is shown in Figure 28 for a 183-dBP exposure. The linear AHAAH model and linearized ARA model both accurately predict the A-duration and shape of the measured pressure as demonstrated by a two hump positive phase and negative phase all arriving at equivalent times. These models over-predict the peak pressure, however by 100% for the AHAAH linear model and 60% for the ARA linear model. The ARA nonlinear model accurately predicts the peak pressure and the general shape of the measured pressure, but prediction of the fine structure is poor.

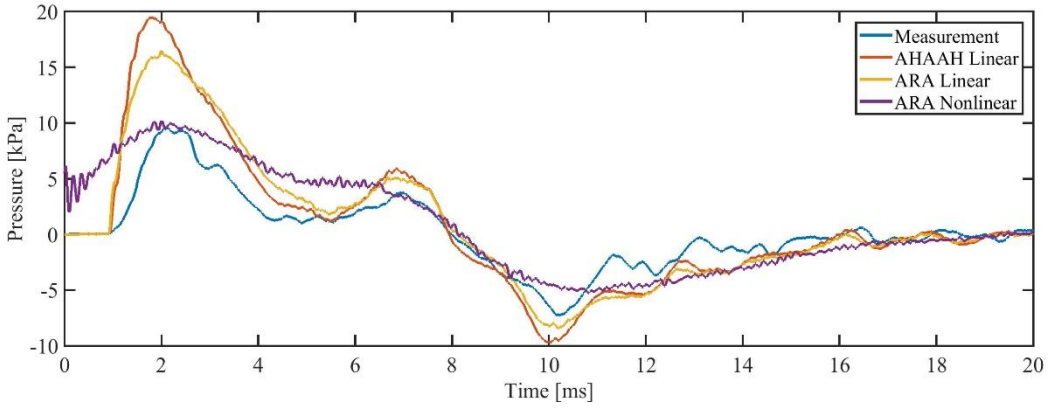

Figure 28. Data-model comparison for the 3M Combat Arms for a 183-dBP exposure. The A-duration is well captured by the AHAAH and ARA linear models, but the peak pressure is well captured by the ARA nonlinear model.

The data-model comparison for the ARA ShotShields is shown in Figure 29 for a 183-dBP exposure. The AHAAH linear model was implemented with the generic insert HPD coefficients for this case and the data-model comparison is poor. The ARA linear and ARA nonlinear models both capture more of the structure with the linear ARA model providing the best prediction of both A-duration and peak pressure. This hearing protection device has a constant attenuation down to low frequencies at approximately 15 dB to 20 dB. In the HPD model, the low frequency leak branch must use a very small gap to produce this attenuation which may become nonphysical when the linear regression extrapolates for lower pressures, such as the small jump near 7 ms.

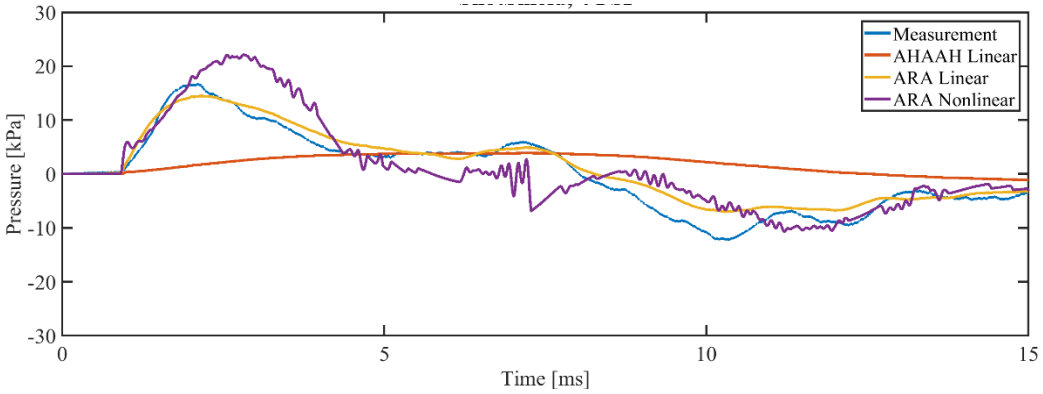

Figure 29. Data-model comparison for the ShotShields for a 183-dBP exposure. The behavior of the measured pressure is poorly predicted by the linear AHAAH model, but predicted more accurately by the ARA model.

The data-model comparison for the 3M E-A-R Classic foam earplugs is shown in Figure 30 for a 183-dBP exposure. The AHAAH linear model predictions are poor and do not represent the measured pressure. The ARA linear model under-predicts the peak pressure by 30%, yet captures the general shape of the measured pressure with respect to the A-duration and negative phase. The ARA nonlinear model accurately predicts the peak pressure and negative phase peak pressure of the measurement, though it over-predicts the A-duration by approximately 20%.

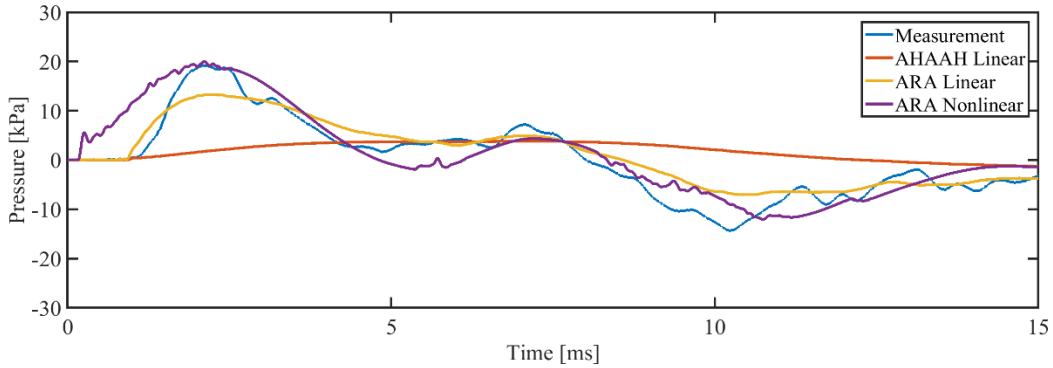

Figure 30. Data-model comparison for the E-A-R Classic for a 183-dBP exposure. The ARA nonlinear model captures the peak pressure and fine structure of the measured pressure with the ARA linear and AHAAH linear models providing poorer predictions.

4.1.1.11.10.4 Comparison between Test Fixtures and PMHSs

This protocol presents a method for evaluating hearing protection devices that is not tied to either the source generating the overpressure or the target holding the hearing protection. As an example of the comparison between PMHSs and a test fixture, the results of a data-model comparison for a 183-dBP exposure are shown in Figure 31. In each of these cases, the nonlinear model was used and the regressions were performed over the 132-dBP to 183-dBP band for the test fixture and over the 171-dBP to 192-dBP band for the PMHSs. As shown, both sets of equipment produce reasonable predictions of the measured pressure; each captures the general shape, peak pressure, and A-duration. The ANSI test fixture under-predicted the peak pressure by approximately 10%, but matched the amplitude of the remainder of the measured pressure wave. The PMHS prediction matched the peak pressure, but overestimated the A-duration by approximately 15%. The PMHS prediction does not match the shape of the measured pressure as well, likely due to the coefficient regression being performed over multiple PMHSs with different physiology and tissue properties,

which would introduce more variability into the data. The predictions based on the test fixture data were acquired using a much more consistent piece of test hardware, which generated better behaved coefficients as demonstrated by the tighter fit.

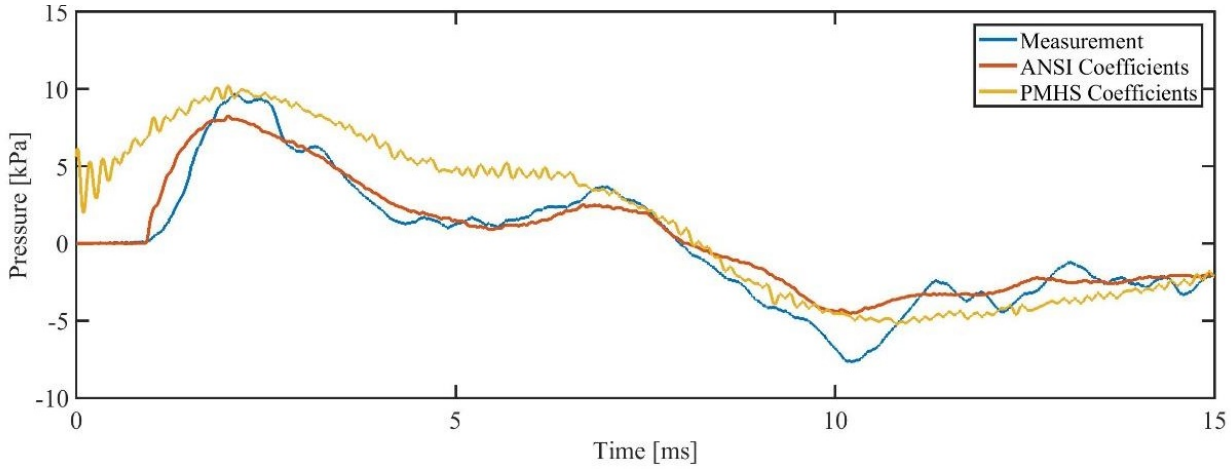

Figure 31. The model output (blue) for coefficients generated from ANSI test fixture (orange) and PMHS (yellow) measurements produce different predictions for a 183-dBP exposure. The ANSI coefficients better predict the measured pressure in the ear canal compared to the PMHS coefficients due to the variability in PMHS geometry and tissue parameters.

4.1.1.11.11 Limitations of the Updated HPD Module

- Measurements and regressions were only performed over the 85- to 192-dB exposure range. Results may not be valid for exposures outside of this pressure range.
- Coefficients were derived for four hearing protection devices. Use of other devices will require collection of additional data
- Measurements within PMHSs may produce insertion loss values, which differ from mechanical test fixtures due to the differences in material properties. Combination of insertion loss data from both sources may produce regressions with higher error than if each dataset were treated separately
- The order in which the fitting routine conducts its optimization search may affect the results for some hearing protection devices due to the presence of local minima in the model parameter space.

Development of a nonlinear middle ear model was performed using data collected in human cadaver and anesthetized chinchilla (described in Section 4.2.1). The overarching strategy has been: assess middle ear transfer functions in human cadaver and chinchilla to determine the relationship (i.e., develop the chinchilla to human transfer), assess hearing loss resulting from impulse noise exposures in anesthetized chinchillas, and determine human-equivalent impulse noise exposure dose-response functions for inner ear sensory tissue.

4.1.2 Major Task 2: Measurement and Simulation of Blast Overpressure Wave through the middle ear

To quantify the transmission of sound through the middle ear, 15 hemi-cephelic PMHS heads were exposed to high-intensity sound waves generated by a custom-built sound concentrating horn. Specimens were prepared by mastoidectomy and extended facial recess to expose the ossicular chain. Sound pressure measurements were made in scala vestibuli (PSV), tympani (PST), and

external auditory canal (PEAC), concurrently with LDV measurements of the stapes (VStap). Stimuli were moderate to high intensity (up to ~170 dB SPL), low frequency tones (20–2560 Hz). The use of temporal bone tissue was in compliance with the University of Colorado Anschutz Medical Campus Institutional Biosafety Committee, the Colorado Multiple Institutional Review Board (COMIRB EXEMPT 14-1464), and the U.S. Army Medical Research and Materiel Command (USAMRMC) Office of Research Protections (ORP). Tissue was obtained from cadavers undergoing autopsy with permission to use tissues and organs for research, and specific permission to expose those tissues to damaging energies (Lone Tree Medical Donation, Littleton, CO).

To numerically simulate the response of the middle ear to predict the energy transmitted to the inner ear, two approaches were tried; the first was to modify the elements within the AHAAH model to mimic the measured response and the development of a middle ear transfer function that converts the canal pressure into an intracochlear pressure. The approach taken and presented in this report was the development of a middle ear transfer function. To predict the large stapes displacements measured during high-intensity sound exposure, the nonlinear response of both the tympanic membrane and stapedial ligaments need to be taken in account and modeled. Quantifying the response of the tympanic membrane and the subsequent development of a numerical model to predict its response to blast was beyond the scope of this program. The transfer function was adopted as a logical alternative since no damage is observed in the middle ear after exposure to the range of blast tested in this effort.

4.1.2.1 Quantifying the Energy Transmitted through the Middle Ear - Temporal bone preparation

Prior to temporal bone preparation, the specimens were thawed in warm water and the external ear canal and tympanic membrane were inspected for damage. The pinna and surrounding soft tissue were removed in order to improve access for the mastoidectomy. Similar to Tringali et al. (2010), temporal bones were prepared with a canal-wall-up mastoidectomy with extended facial recess, separated by a remaining buttress of bone, in order to visualize the body of the incus, the long-process of the incus, the stapes, and the round window, which were inspected to rule out damage and abnormalities. The facial canal was opened and the facial nerve removed immediately posterior to the oval and round windows to maximize exposure of the stapes and round window structures. The round window was inspected and false membrane removed, if present. Finally, the cochlear promontory near the oval and round windows was thinned in preparation for pressure probe insertion.

The hemi-cephalic specimens were fastened to a flat plate affixed via a dual-axis goniometer stage (Thorlabs, Inc., Newton, NJ) to a steel base plate. The specimen was positioned so that the pressure probes would enter the cochlea nearly vertically to prevent air insertion into the cochlea. Cochleostomies were created under a droplet of water using a fine pick. Fiber-optic pressure sensors (FOP-M260-ENCAP, FISO Inc., Quebec, Canada) were inserted through the bony wall of the cochlea until just within the fluid (~100μm) of the SV and ST using micromanipulators mounted on a horizontal bar affixed to the base plate. Sensors were sealed to the cochlea with alginate dental impression material (Jeltrate). Velocity of the stapes was measured with a single-axis laser Doppler vibrometer (LDV; HLC-1000 and CLV-700; Polytec Inc., Irvine, CA) positioned with a joystick-controlled aiming prism (HLVMM2) mounted to a dissecting microscope (Carl Zeiss AG, Oberkochen, Germany) parallel to the microscope's line of sight. The LDV was aimed at the stapes capitulum, and oriented at ~45º from the direction of the piston-like

stapes motion. Microscopic (45–63 μm diameter) glass beads (P-RETRO-xxx, Polytec Inc., Irvine, CA) were placed on the stapes to ensure a strong LDV signal.

Following the conclusion of each experiment, the placement of both pressure probes was verified by carefully removing the bone between the two cochleostomies. The location and orientation of the basilar membrane was carefully assessed, and the compartment into which the probes projected was identified.

4.1.2.2 Sound presentation

All experiments were performed in a double-walled, sound-attenuating chamber (IAC Inc., Bronx, NY). Sounds were generated digitally and presented to the specimen with a ~30-cm subwoofer (Morel UW 1258) driven by a 300 W amplifier (Keiga KG5230), attached to a custom-built sound concentrating horn constructed of off-the-shelf PVC and copper components, their diameters tapering approximately exponentially from ~30 cm to ~1.25 cm over the course of ~12 m. The sound presentation system was coupled to the ear with a section of silicone tubing (11 mm OD) tapered on one end to fit within the ear canal, stabilized with cyanoacrylate adhesive, and sealed with Jeltrate. The sound pressure level in the external ear canal was measured with both a probe-tube microphone (Type 4182, Brüel & Kjær, Nærum, Denmark) and a fiber-optic pressure probe (FOP-M-BA, FISO, Inc.), which were positioned approximately 1 cm from the tympanic membrane through small holes in the silicone tubing adapter, and sealed in place with Jeltrate. Note, the pressure probe was included because the microphone signal clips at levels above ~164 dB SPL. The frequency response of the sound delivery system was approximately flat from ~15–100 Hz, above which the level declined roughly linearly, decreasing by approximately 25 dB at 1 kHz. Stimuli were high level, low frequency tones, presented in 17 steps between 20 Hz–5 kHz, with peak levels exceeding 170 dB SPL below 100 Hz (the highest level tone produced was 173.4 dB SPL at 80 Hz). Sounds were presented and data were collected with an external sound card (Hammerfall Multiface II, RME, Haimhausen Germany), sampled at 44100 Hz, and controlled by a custom-built program in MATLAB (Mathworks, Natick, MA).

4.1.2.3 Data collection and analysis

All acquired signals were band-pass filtered between 10 Hz and 5 kHz with a second order Butterworth filter for data analysis. Signals were recorded and averaged across ten repetitions of each stimulus condition. Responses were quantified through Fourier analysis, where the response is evaluated at the stimulus frequency. Spectra are calculated from the segment of the recording during which the stimulus was presented (adjusted for the acoustic transmission delay along the waveguide). Velocity and pressure transfer functions were calculated in a manner consistent with a method described in an established standard (ASTM, 2014). Briefly, measured values of stapes velocity (VStap), as well as scala vestibuli (PSV) and scala tympani (PST) sound pressures (in the frequency domain), are presented with respect to the sound pressure level in the external auditory canal (PEAC). Corresponding transfer functions (HStap, HSV, and HST) were computed from the responses of these measures to pure tone stimuli, using methods described previously (Deveze et al., 2013; Nakajima et al., 2009), e.g., equations below:

$$HStap = VStap/PEAC \quad (10)$$

$$HSV = PSV/PEAC \quad (11)$$

$$HST = PST/PEAC \quad (12)$$

Similarly, the differential intracochlear pressure transfer function was calculated as the complex difference between PSV and PST, normalized to the sound pressure level in the external auditory canal (Nakajima et al. 2009).

$$HDiff = (PSV - PST)/PEAC \quad (13)$$

The magnitude of the stapes velocity was adjusted using a cosine correction (Chien et al. 2006) based on an estimate of the included angle between the stapes primary axis (i.e., the direction of piston-like motion) and the orientation of the LDV laser (typically ~45º). Displacement was calculated (in the time-domain) in MATLAB using a trapezoidal approximation to the integral of the LDV velocity signal. Responses are only shown for frequencies at which the signal-to-noise ratio was greater than 10 dB, calculated by comparing measurements made immediately before and during sound presentation. Fiber optic pressure probes were factory calibrated, and the sensitivity verified by comparing sensor output normalized to the velocity (measured with the LDV) of a small cup of water driven by a Brüel & Kjær shaker (Type 4810) across the range of frequencies tested at comparable magnitudes to those presented during experiments. Sensor output was stable both within and across experiments, and no drift in sensor output was noted.

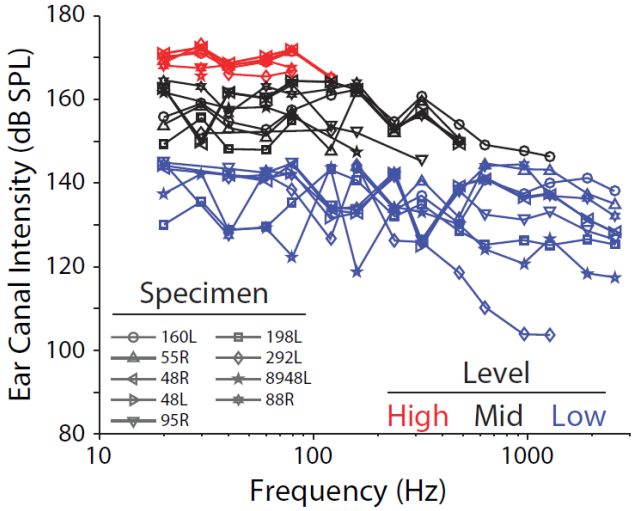

Figure 32. Sound pressure levels in the ear canal (PEAC) during recordings. Specimen number is indicated by marker symbol. Sets of recordings with roughly comparable levels are grouped by color and are analyzed independently in subsequent analyses (grouped as Low < 145 dB SPL, Mid 145 dB SPL and < 165 dB SPL, and High 165 dB SPL). Lines link the responses of individual specimens within each level group.

The sound pressure levels recorded in the ear canal near the tympanic membrane for each set of measurements, for the nine specimens meeting inclusion criteria, are shown in Figure 32. Inclusion criteria included: similarity of HStap to the 95% CI range reported previously (Rosowski et al. 2007), where responses consistently above this range suggest increased mobility of the ossicular chain (possibly due to damage) and responses consistently below this range suggest reduced mobility (potentially resulting from ossicular fixation due to otosclerosis); similarity of HSV, HST, and particularly HDiff to the range of responses reported previously (Nakajima et al. 2009), where deviations (particularly low HDiff) suggest that pressure probe placement was incorrect; appropriate probe placement as verified via dissection (see above); lack of visible damage to the tympanic membrane or middle ear structures.

Sounds were digitally generated and attenuated down from the maximum in discrete attenuation steps (i.e., 30-, 50-, or 70-dB attenuation, thus absolute SPL varied somewhat). The output of the

loudspeaker system is biased towards low frequencies, thus low-frequencies (< 100 Hz) tended to show the highest levels at a given attenuation level. Analysis is performed based on the responses of each specimen to sound pressure levels grouped into three categories based on the sound pressure level of the sound stimulation at low (< 100 Hz) frequencies. In figures to follow, low-level measurements, i.e., the lowest levels presented to each specimen (< 145 dB SPL), are shown as blue lines, mid-level measurements (black) were those with sound presentation levels between 145–165 dB SPL, and high-level measurements (red) were those above 165 dB SPL. Responses were recorded to ten repetitions of each stimulus, presented in order from low to high frequencies (one presentation of each frequency per repetition) and from low to high levels (completing all repetitions of each level before increasing). Reducing the attenuation further (and thus increasing input signal level) resulted in substantial harmonic distortion of the sound produced, and constant or decreasing sound pressure level in the ear canal; for this reason the highest level assessed was close to 170 dB SPL in all specimens. In the following section, responses to each of these three levels will be assessed in both the time and frequency domains.

4.1.2.4 Responses in the time- and frequency-domains

Velocity of the stapes capitulum, as well as sound pressure in the SV and ST near the oval and round windows are presented for nine temporal bones during presentation of low-, mid-, and high-level, low-frequency tones. Six additional specimens showed one or more transfer functions that deviated substantially from prior reports, thus were excluded from analysis. Two early specimens (160L, 55R) were not tested at all levels, thus do not appear in all figures. One additional specimen (292L) showed substantially lower HStap in the range of frequencies reported previously at the low level, but showed responses at lower frequencies and higher levels that were more consistent with prior reports, thus are included in the analyses. The following analyses are roughly grouped based on the sound pressure level in the EAC, as shown in Figure 32 (i.e., < 145 dB SPL for Low, ≥ 145 and < 165 dB SPL for Mid, and ≥ 165 dB SPL for High).

Figure 33 shows representative recordings from one example specimen (48L) in response to 10 superposed repetitions of 30 Hz (Figure 33A) and 80 Hz (Figure 33B) tones at the Low sound pressure level (blue SPLs in Figure 32). The signal sent to the loudspeaker amplifier is shown at the top, followed by the superposed waveforms recorded from the microphone (green) and fiber-optic pressure probe (blue) in the ear canal near the TM (shown together to demonstrate the consistency across recording devices), the displacement of the stapes from the LDV, and the scala vestibuli (PSV) and scala tympani (PST) sound pressures. Consistent with previous reports in human cadaver and small animals, motion of the stapes shows harmonic distortion at this level (Dallos et al., 1966; Guinan and Peake, 1967; Huang et al., 2012; Rosowski et al., 2007; Voss et al., 2000). This distortion is clearly visible at integer multiples of the fundamental frequency in the magnitude of the frequency spectrum (shown normalized to the maximum) at right and below, though all harmonics are >15 dB below the fundamental in all signals. The DStap spectra reveals somewhat higher magnitude harmonics than either of the intracochlear pressures, which may be evidence of non-piston-like motion of the stapes (a feature that may be more prominent due to our measurement on the stapes head).

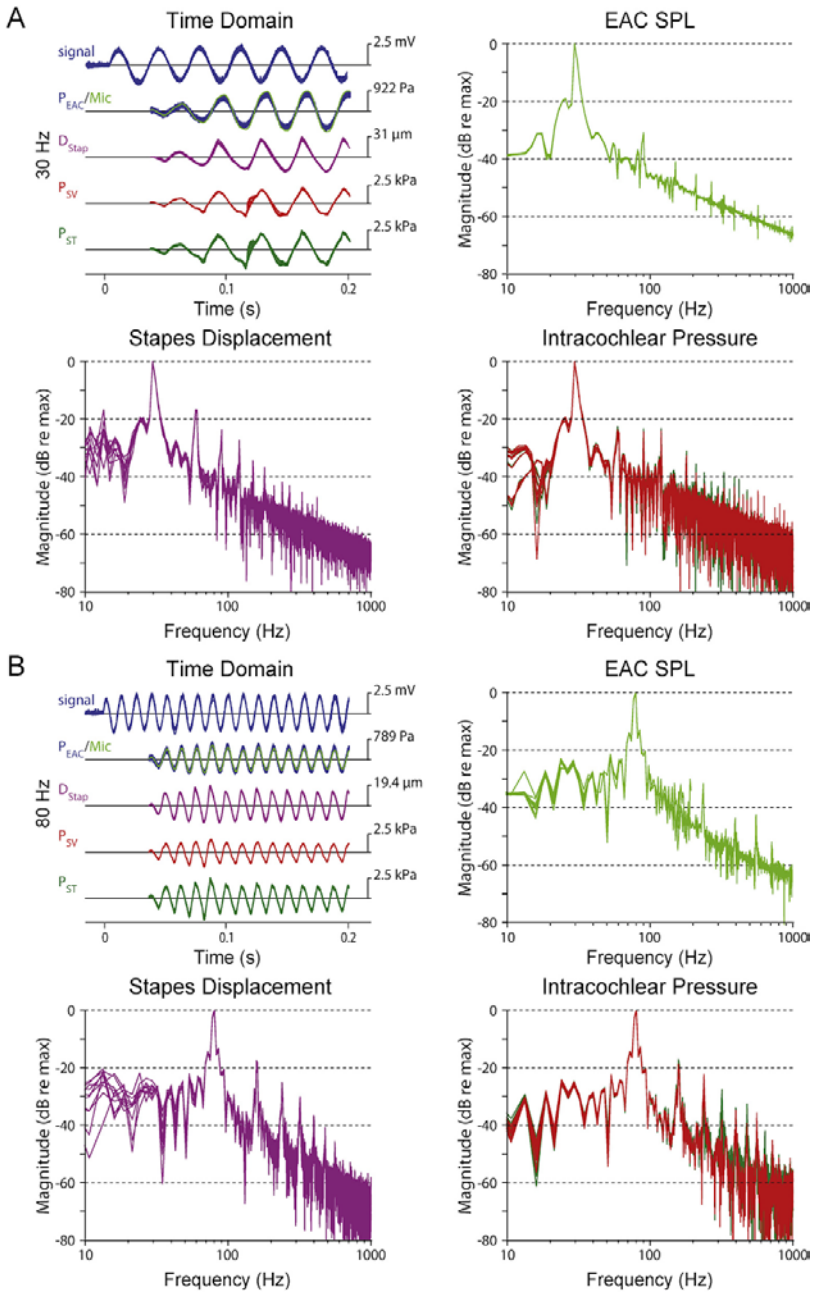

Figure 33. Examples of the stimulus waveform (signal, blue), sound pressure in the external auditory canal near the tympanic membrane recorded with a probe-tube microphone (Mic, light green), and a fiber optic pressure sensor (PEAC, blue) stapes displacement (DStap, violet), and intracochlear pressures measured in the scala vestibuli (PSV, red) and scala tympani (PST, green), recorded during ten presentation of a 30 Hz (A) and 80 Hz (B) tones presented at Mid (~150 dB SPL) sound pressure levels in specimen 48L. Each line represents the response recorded to a single stimulus presentation. The frequency spectrum of each signal is shown in panels not labeled "Time Domain" (at right and below), normalized to the amplitude at the stimulus frequency. For clarity, the output spectrum of the fiber optic pressure sensor in the EAC is not shown on the EAC SPL panels.

Stapes velocity (HStap), as well as scala vestibuli (HSV), scala tympani (HST), and the differential (HDIFF = (PSV–PST)/PEAC) sound pressure transfer functions were computed as the ratio of each measure to the sound pressure level in the EAC. Figure 34 shows the mean HStap(A), HSV (C), HST (D), and HDIFF (B) magnitude at Low levels presented for seven of the nine (excluding

160L and 55R) temporal bones that met inclusion criteria. Responses for each specimen were highly consistent across repetitions (± 1 standard deviation is smaller than the size of each marker), thus error bars are excluded from these plots. Recordings were stable over the course of ten repetitions, and are shown superimposed on the 95% confidence intervals/range of responses from prior reports (gray shading; Nakajima et al., 2009 for panels Figure 35B–D; Rosowski et al., 2007 for panel A). In general, transfer function magnitudes in all four responses rose with frequency towards a peak near 1 kHz, and showed lower responses to lower frequency tones. Interestingly, the difference between HSV and HST was smaller at lower (i.e., <100 Hz) than at higher frequencies, and in a minority of specimens the absolute magnitudes reversed at the lowest frequencies, showing somewhat higher peak sound pressures in the scala tympani than scala vestibuli (e.g., specimen 48R), similar to previous observations (Nakajima et al. 2009). Nevertheless, HDIFF was generally consistent with the previous reports (Greene et al. 2015; Mattingly et al., 2015; Nakajima et al., 2009) in the range of frequencies tested previously.

Figure 35 shows transfer function phase of each response at the Low level (i.e., the phase of each signal with respect to the sound pressure level in the ear canal (PEAC)). Responses are superimposed on the 95% confidence intervals/range of responses from prior reports (Nakajima et al., 2009 for panels B-D; Rosowski et al., 2007 for panel A). HStap phase was stable at just under 90º with respect to the sound presentation for frequencies below approximately 200Hz, and declined with higher frequency stimulation. Likewise, HSV and HST phase were stable between 0º–45º for low frequencies that declined with higher frequency tones. HDIFF phase was somewhat more variable across specimens, but was generally ~90º–180º at low frequencies that decreased at higher frequencies, consistent with prior reports (Nakajima et al. 2009).

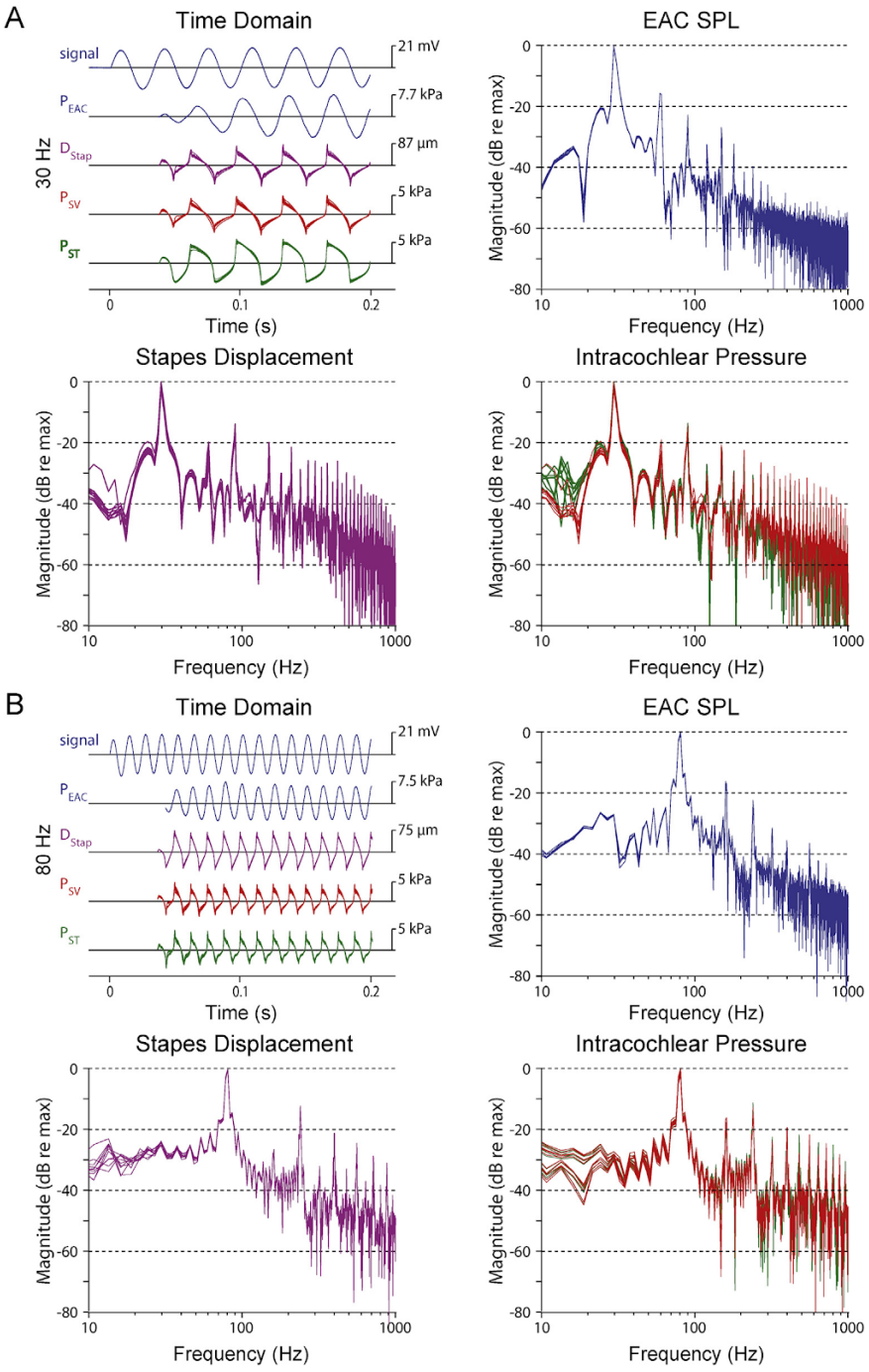

Figure 34. Examples recordings during presentation of a 30 Hz (A) and 80 Hz (B) tone presented at High (~165 dB SPL) sound pressure levels. Data are presented in the same format, for the same specimen as Figure 32 (48L). For clarity, responses from the EAC microphone are not shown since the signal clipped at high levels.

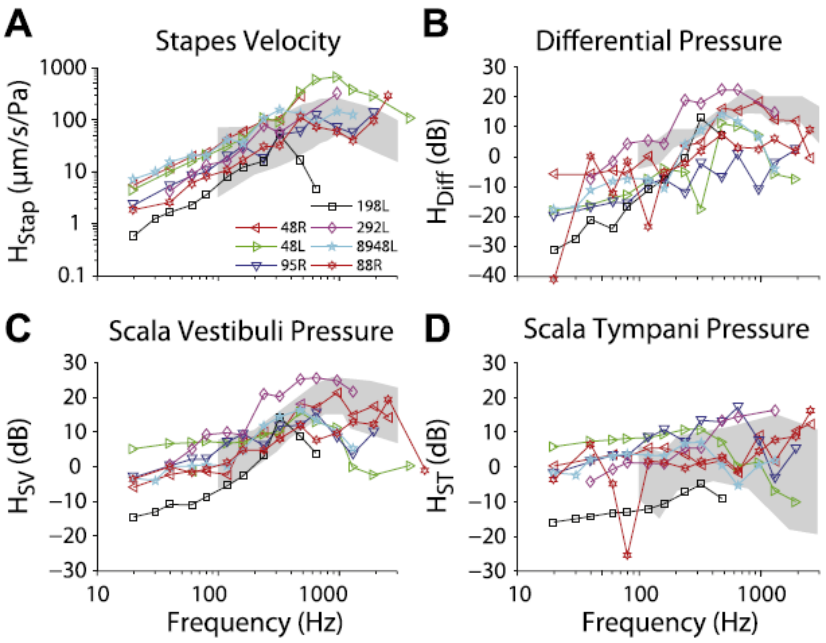

Figure 35. Stapes velocity (HStap), (B) differential (HDiff), (C) scala vestibuli (HSV), and (D) scala tympani (HST) sound pressure transfer function magnitudes recorded at the low level (<145 dB SPL). Responses shown are the mean across ten repetitions for each specimen (indicated by marker symbol and line color), and correspond to blue lines and markers shown in Figure 32. Gray bands represent the 95% CI for stapes velocity from Rosowski et al. (2007), and the range of responses reported for intracochlear pressures by Nakajima et al. (2009).

Figure 34 shows representative waveforms of 30 Hz and 80 Hz tones presented at the Mid level (black SPLs in Figure 32) for the same specimen as in Figure 33 (48L). In contrast to waveforms at the Low SPLs, which closely resemble PEAC, these response waveforms show substantial harmonic distortion that is either not present, or much lower in magnitude, in the ear canal sound pressure waveform. Nevertheless, PSV and PST waveforms appear to remain consistent with one another, as well as with DStap. The even numbered harmonics (2f, 4f, etc.) are less prominent than the odd harmonics (3f, 5f, etc.) in all signals, consistent with the shape of the waveform, and are lower in magnitude relative to the fundamental in the stapes displacement than in the intracochlear pressure measurements. Importantly, although the second harmonic is visible in the response of the EAC pressure probe, it remains approximately 20 dB lower in magnitude than the fundamental frequency of the response. Also note that for Mid and High SPL conditions the microphone signal is limited by the power supply, resulting in a clipped signal at high-pressure magnitudes, thus the EAC pressure probe is used rather than the microphone for these conditions, and the microphone signal is not shown.

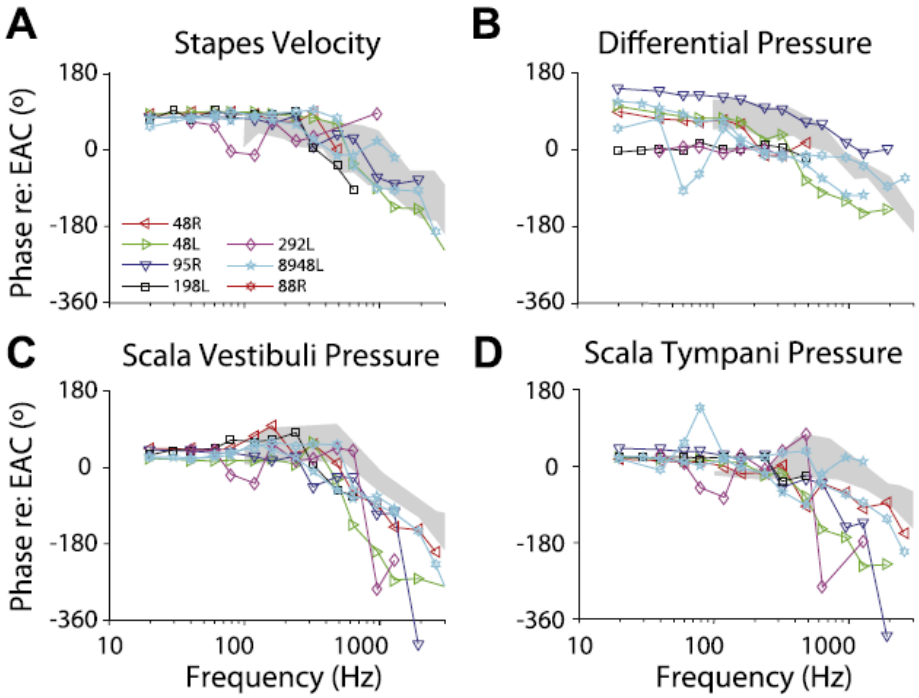

Figure 36. (A) Stapes velocity (HStap), (B) differential (HDiff), (C) scala vestibuli (HSV) and (D) scala tympani (HST) sound pressure transfer function phases recorded at the Mid sound presentation level (~150 dB SPL). Responses shown are the mean across ten repetitions for each specimen (indicated by marker symbol and line color), and correspond to blue lines and markers shown in Figure 31. Gray bands represent the 95% CI for stapes velocity from Rosowski et al. (2007), and the range of responses reported for intracochlear pressures by Nakajima et al. (2009).

Transfer function magnitudes calculated for responses to the Mid SPLs are shown in Figure 37. Responses are once again superimposed onto the 95% CI range (gray bands) of responses observed previously (Nakajima et al., 2009 for panels B-D; Rosowski et al., 2007 for panel A). Transfer function magnitudes are not directly affected by the harmonic distortion observed in Figure 36, since the transfer function at each frequency is computed from the magnitude at the fundamental frequency only. Similar to the Low SPL condition, responses in HStap, HSV, and HST are comparable to those prior reports over the range of frequencies tested; however, HDIFF shows a somewhat lower magnitude in most specimens compared to some (e.g., Nakajima et al., 2009), but not all (Greene et al. 2015; Mattingly et al., 2015) prior reports. Similarly, all responses show somewhat reduced magnitudes compared to the Low stimulation level (Figure 34), particularly for low frequency tones; that is, stapes velocity and intracochlear pressure increase at a slower rate than EAC sound pressure level above 145 dB SPL. Transfer function phases (not shown) were comparable to those observed at Low levels (Figure 35).

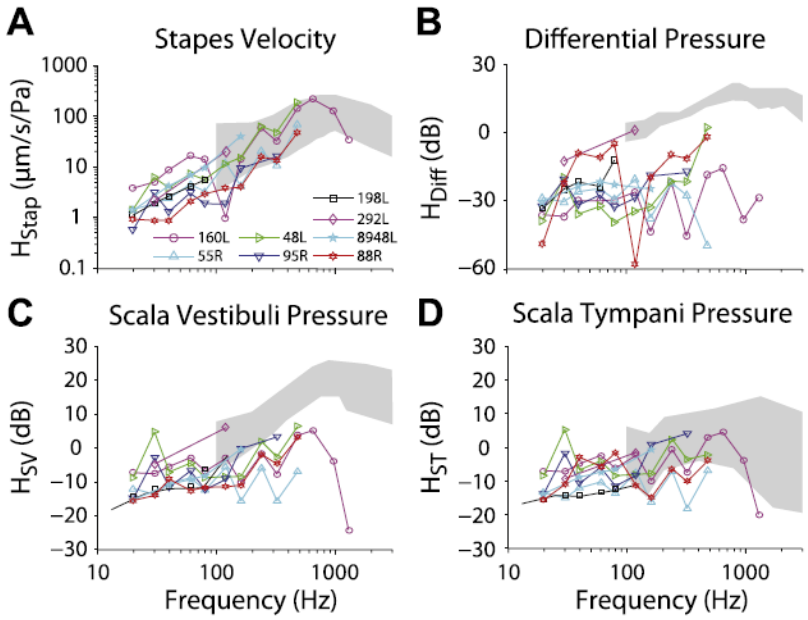

Figure 37. (A) Stapes velocity (HStap), (B) differential (HDiff), (C) scala vestibuli (HSV) and (D) scala tympani (HST) sound pressure transfer function magnitudes recorded at Mid (<~165 dB SPL) sound pressure levels. Responses shown are the mean across ten repetitions for each specimen (indicated by marker symbol and line color), and correspond to black lines and markers shown in Figure 32. Gray bands represent the 95% CI for stapes velocity from Rosowski et al. (2007), and the range of responses reported for intracochlear pressures by Nakajima et al. (2009).

In order to explore this observed magnitude decrease with stimulus level further, the mean (±SEM) transfer function magnitudes (computed on the real component of the transfer function, in the logarithmic magnitude domain) across the population of specimens are shown in Figure 38 for Low (blue), Mid (black), and High (red) SPL conditions. In general, transfer function magnitudes showed similar trends with frequency across levels, with magnitudes showing similar peaks in magnitude around 1kHz (for Low and Mid levels); however, the overall magnitude decreased with increasing stimulus level for all four measures.

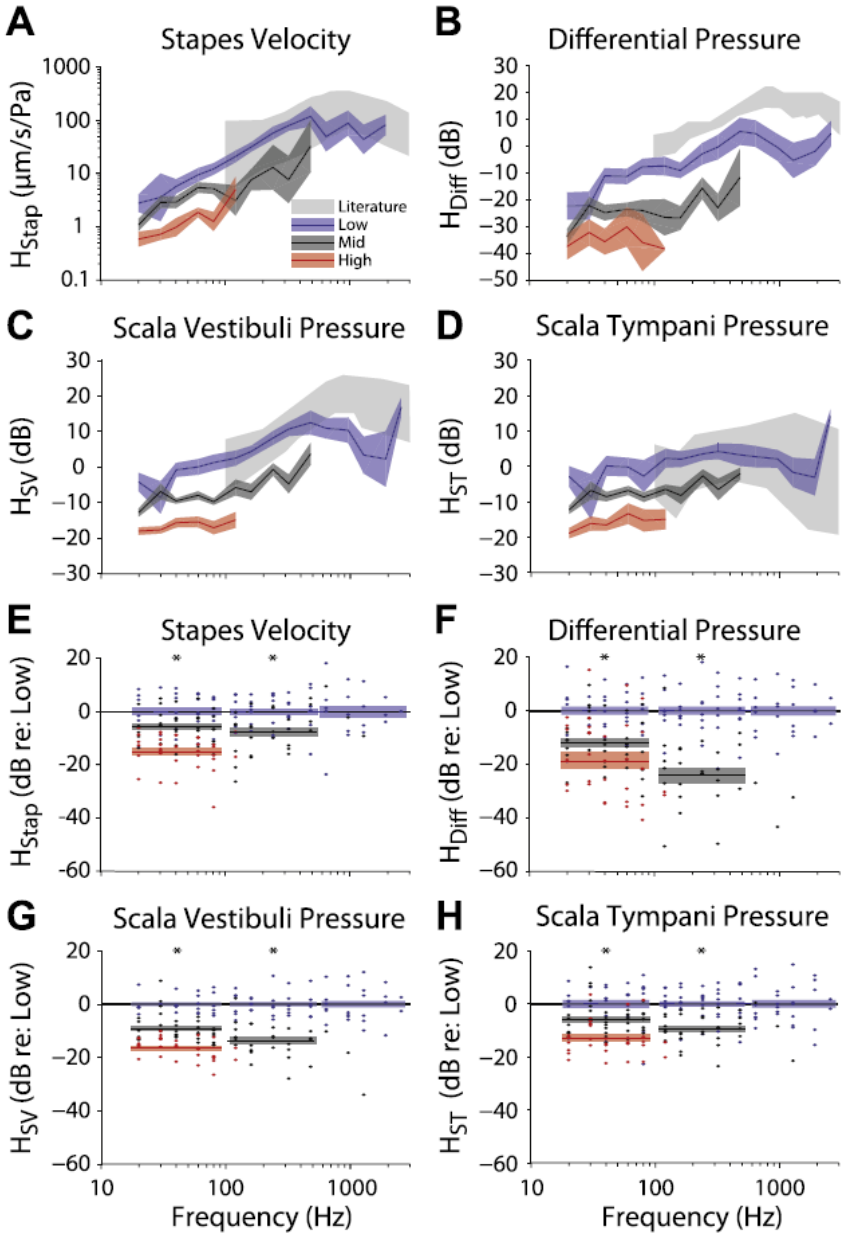

Figure 38. Comparison of transfer function magnitudes across the three stimulus levels presented for (A) Stapes velocity (HStap), (B) differential (HDiff), (C) scala vestibuli (HSV), and (D) scala tympani (HST) pressures. Lines and colored areas represent the mean and SEM range, respectively, for TF magnitude across specimens. Gray bands represent the 95% CI for stapes velocity from Rosowski et al. (2007), and the range of responses reported for intracochlear pressures by Nakajima et al. (2009). Transfer function magnitudes are shown normalized to the mean Low response (in dB) at each frequency measured for (E) stapes velocity, (F) differential, (G) scala vestibuli, and (H) scala tympani pressures. Dots indicate measurements from individual specimens, colored bars indicate the mean ±SEM of the normalized responses at each level (for frequencies <100 Hz, >100 Hz and <500 Hz, and >500 Hz), and asterisks indicate significance as assessed via one-way ANOVA within each frequency band. Note, comparisons including High level responses (red) were only made within the lowest frequency band, and comparisons of Mid and Low levels were not computed at the highest frequency band.

ln order to further assess these changes with level across frequency, the responses of specimen (dots) are shown as a function of frequency, relative to the mean response across specimens (in dB) observed at the Low level, in Figure 38E–H. Mean (± SEM) is shown for each measurement

for each stimulus level (indicated by color) in three frequency bands: (1) <100 Hz, (2) >100 Hz and <500 Hz, and (3) ≥500 Hz. Low responses were only assessed at the lowest frequency band, and Mid responses were only assessed at the low and mid frequency bands, due to the small number of responses in those bands. The change in transfer function magnitudes across levels was assessed with a one-way ANOVA with EAC SPL group (i.e., Low, Mid, or High) as the independent, and transfer function magnitude as the dependent variables. For the sake of brevity, we only summarize the results of these statistical comparisons here; the ANOVA indicated significant (Bonferroni corrected) main effects for all four measures ($F_{2,92} > 17$, $p < 0.001$) for both low- and mid-frequency bands (indicated with an asterisk), and post hoc testing with a Tukey's HSD test reveals that each level group is significantly different from one another in each case. These reductions in transfer function magnitudes suggest that the magnitude of the fundamental frequency at Mid and High SPLs does not increase linearly with stimulus level, as observed in the harmonic distortion observed in Figure 36, consistent with a limitation of the response at high EAC sound pressure levels. The frequency and level dependence of this effect will be explored further in the next section.

Figure 39 similarly shows the mean (± SEM) transfer function phases calculated for the Low, Mid, and High SPL conditions. Likewise, statistical analysis (one-way ANOVA) was performed on the phases normalized to the Low response. Transfer function phases were largely unaffected by the level for low frequencies (i.e., <100 Hz; $F_{2,92} < 3$, $p > 0.05$), except in HDiff ($F_{2,92} = 7.1$, $p = 0.0014$), which shows a shift in mean from approximately +45° for Low and Mid, and approximately –45° for High SPL stimulation. At higher frequencies, phase is highly consistent at Mid and Low levels, and may decrease more rapidly with increasing frequency than has been reported in a prior report (Nakajima et al. 2009; gray bands), potentially suggesting longer group delays than previously reported (which could result from either methodological differences, or a level dependent effect).

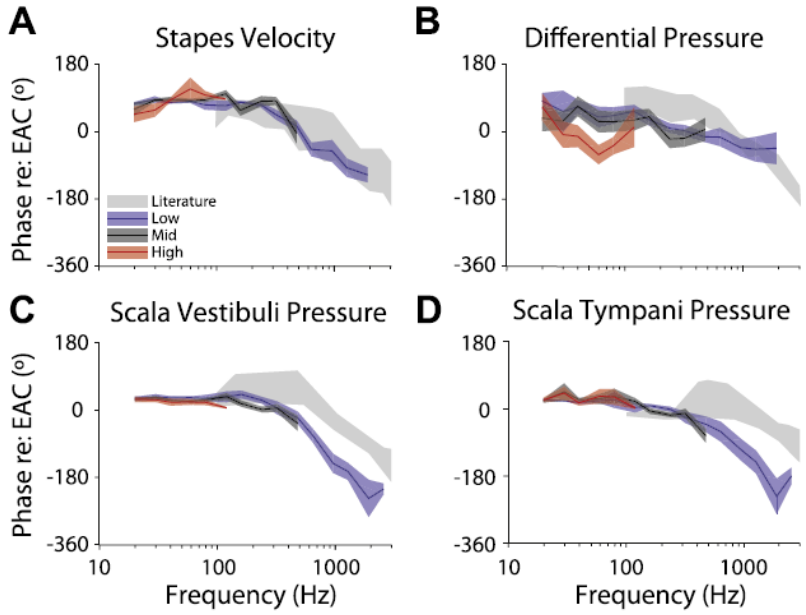

Figure 39. Comparison of transfer function phases (relative to PEAC SPL) across the three stimulus levels presented for (A) stapes velocity, as well as (B) differential, (C) scala vestibuli, and (D) scala tympani sound pressures. Lines and colored areas represent the mean and ±SEM range, respectively, for TF phase across specimens. Gray bands represent the 95% CI for stapes velocity from Rosowski et al. (2007), and the range of responses reported for intracochlear pressures by Nakajima et al. (2009).

4.1.2.5 Linearity of stapes displacement and scala vestibuli pressure with SPL

In the following sections, we focus our analysis on the responses of stapes displacement (DStap) and scala vestibuli pressure (PSV) directly to assess the linearity of the input to the cochlea at high sound pressure levels. Figure 40A shows the peak-to-peak DStap amplitude, measured in each trial recorded in one specimen (48L), as a function of sound presentation level (recorded level in dB SPL on the abscissa, level groups from Figure 32 are indicated with markers). Responses are shown for all three stimulus levels Low (O), Mid (^), and High (<). Responses are superimposed over an arbitrarily drawn 20 dB/decade line indicating a linear relationship (Guinan and Peake, 1967). Similarly to those previous results in the cat, DStap increased proportionally with sound pressure level up to ~150 dB SPL, above which displacement deviates from the 20 dB/decade line (towards higher EAC SPLs for a given DStap). Note this analysis is complicated by the aggregation of responses recorded at multiple frequencies. In particular, responses below 1 kHz can be reasonably well fit with a single line, since the ratio of DStap to PEAC is reasonably similar; however, the higher frequency responses would be better fit by a line with a somewhat lower y-intercept.

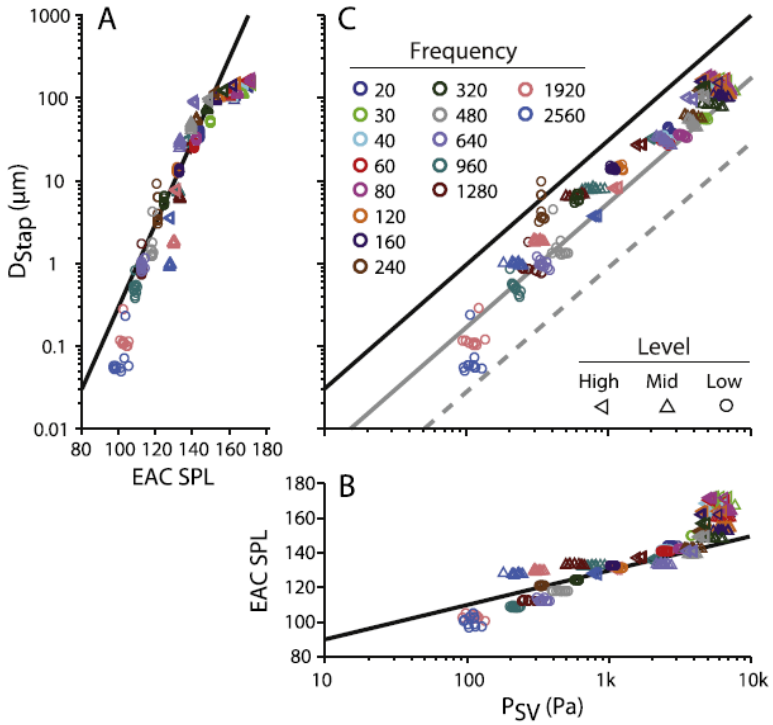

Figure 40. Peak-to-peak stapes displacement (DStap) (A) and scala vestibuli pressure (PSV) (B) as compared to PEAC SPL, and to one another (C), for specimen 48L, across the three levels tested (identified by marker shape), separated by frequency (in Hz, identified by marker color). Markers represent the response to a single stimulus presentation, and all repetitions for a given stimulus are shown. Diagonal lines represent: in (A): (DStap), an arbitrary 20 dB per decade line; in (B): (PSV), an arbitrary 20 dB per decade line; and in (C): the diagonals in A and B transferred onto these axes (black), as well as this line shifted towards higher pressures by 10 (gray solid) and 20 dB (gray dashed).

Intracochlear sound pressure level was similarly assessed by plotting the peak-to-peak PSV amplitude as a function of PEAC SPL (with the axes transposed) in Figure 40B. Responses are shown for the same conditions as for the displacement measurements presented at left, and are shown superimposed on an arbitrarily drawn 20 dB/ decade line. PSV rises linearly with increasing PEAC SPL up to ~150 dB SPL, above which PSV deviates from the 20 dB/decade line (towards

higher PEAC SPLs for a given PSV), similar to DStap. As in Figure 40A, the observed growth with SPL is complicated by the frequency dependence of the middle-ear gain and cochlear input impedance, which may explain the observed deviations from the straight line at lower levels.

The relationship between DStap and PSV is assessed in Figure 40C. Straight lines are drawn at locations corresponding to the straight lines in the left and bottom plots (black), as well as at 10 dB (gray) and 20 dB (dashed gray) higher PSV for reference. PSV consistently increased with DStap, with the responses generally falling along a single straight line across the range of displacements/pressures observed. In particular, while both DStap and PSV show a departure from proportionality at ear canal sound pressure levels above ~150 dB SPL, this nonlinearity appears comparable in magnitude in the two measures, thus the relationship between DStap and PSV remains consistent even at the highest levels tested (High, < symbols). Once again, the deviations from this straight line likely indicate the frequency dependence of the relationship between DStap and PSV.

4.1.2.6 Relationship between stapes displacement, scala vestibuli pressure, and SPL

The above plots of DStap and PSV reveal a general trend away from proportionality with PEAC SPL for levels greater than ~150 dB SPL. In order to further explore this dependence on level, the peak-to- peak DStap and PSV from one specimen (160L) are shown as a function of PEAC SPL in Figure 41A and B, respectively. Here, lines connect the mean responses (standard deviation is smaller than the broader line widths) assessed at the two high highest SPLs tested for each frequency, where both color and line width indicate stimulus frequency. The black lines are the same 20 dB per decade lines shown in Figure 40A–B. As observed in Figure 40, the responses observed in Figure 41 show substantial frequency dependence (particularly PSV). Nevertheless, two main points can be assessed from these plots (and are described in the following paragraphs): the maximum responses (DStap and PSV) observed, and an estimate for the SPL at which these responses saturate.

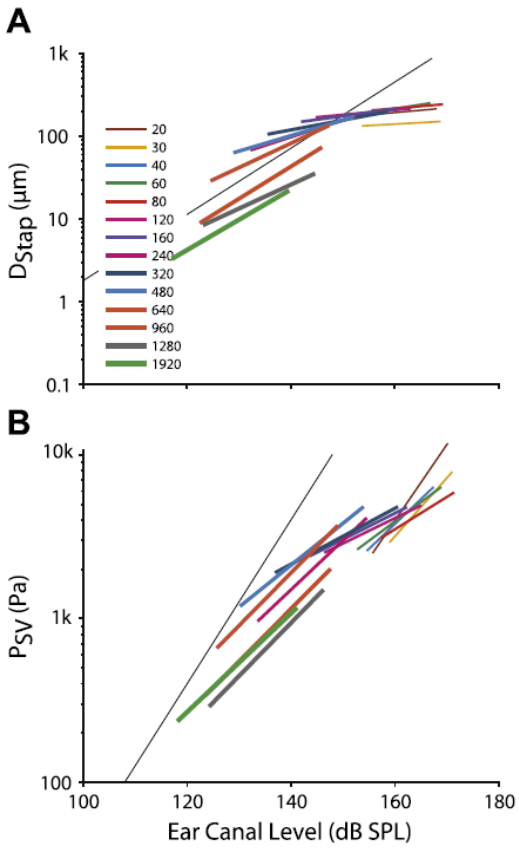

Figure 41. Mean of (A) DStap, and (B) PSV, for each frequency presented, as a function of PEAC SPL for one specimen, 160L. Frequency is represented by both color and line thickness. Responses are shown for the two lowest levels presented at each frequency (independent of the level classification outlined in Figure 32). Diagonal lines are the same arbitrary 20 dB per decade lines as in Figure 40.

First, since both DStap and PSV saturate at high PEAC SPLs, the asymptote of each response can be predicted based upon the maximum observed stimulus magnitude (not shown). Mean DStap maximum (±standard deviation), at any frequency or level, across the nine specimens was 133.0 ± 36.3 mm, which is substantially higher than prior estimates from small animals (e.g. ~20 mm in the cat: Guinan and Peake, 1967; ~30 mm in rabbit: Yamamoto, 1953). Mean PSV maximum was more variable across the nine specimens tested at 12.16 ± 9.03 kPa, and generally did not approach a clearly defined asymptote. It is unclear whether no asymptote was observed because EAC SPLs were not sufficiently high to reach saturation, or whether maximum pressures may continue to rise with increasing PEAC SPL. It is likely, however, that the observed PSV responses are more susceptible to variability due to the greater frequency dependence. Note that higher frequency responses tended to show lower amplitudes than low frequency responses at a given SPL, thus the maximum values reported here may not hold for higher frequencies.

Second, the PEAC SPLs at which DStap and PSV saturate cannot be measured at all frequencies here due to the low response of our loudspeaker above a few hundred Hz; however, they can be estimated by assessing the rate of change in response amplitude with level, since we assume these responses should rise linearly with SPL for low levels, but should saturate and show no increase at higher levels. The responses of each specimen were sampled relatively sparsely in level, thus a direct measurement of the asymptote value for each frequency is not possible. An estimate of the level at which these responses asymptote was calculated for each specimen by comparing the

slopes of the response at each frequency to the expected slopes (20 dB/dec.) shown in Figure 40A–B. Of note, this analysis assumes frequency independence over the range of frequencies tested (i.e., that each frequency will produce a similar DStap and PSV for a given PEAC SPL). Qualitatively, the slopes of these straight lines for DStap and PSV shown in Figure 41 are comparable to the 20 dB per decade lines from Figure 40A–B for PEAC SPLs < ~150 dB SPL, and, consistent with a response asymptote, DStap line slopes approached zero when either level was above ~150 dB SPL. PSV slopes are more variable, with responses that appear to decrease towards zero at higher PEAC SPLs, revealing the frequency dependence of this measure.

The relationship between intracochlear pressure and ossicular motion has not been thoroughly examined at the high levels and low frequencies assessed in this report, but since the stapes footplate provides the input to the scala vestibuli via the oval window, and since the two show similar dependence on sound pressure level in the ear canal at moderate levels, it is natural to assume a direct, positively correlated relationship between the two. No direct comparison of DStap and PSV has been reported, but indirect evidence is found in the reports of Nakajima et al. (2009), who reported a linear relationship between PIC and PEAC for tones presented between 80 and 130 dB SPL, and Aibara et al. (2001) who reported VStap for sound presentation between 60 and 120 dB SPL with no mention of level effects. Since both VStap and PSV are apparently linearly related with PEAC in these reports (Nakajima et al., 2009), one can thus assume that the two are linearly related in the range of sound pressure levels tested (60–130 dB SPL). .

As a way to compare DStap and PSV, prior reports have presented the cochlear input impedance, defined as: ZC = PSV/(VStap x AFP), where AFP is the area of the stapes footplate, which is typically assumed to be 3.2 mm^2 (Nakajima et al., 2009; Von Bekesy, 1960). Those prior studies report ZC that is relatively flat across frequency in the range of 10–100 GOhms, which is consistent across the range of stimulus levels tested (although level dependence does not appear to have been thoroughly assessed in these reports). Figure 42 shows the mean (±SEM) ZC (assuming AFP = 3.2 mm^2) across the population of specimens included in the current study, at the low, mid, and high level stimulation presentations. Responses are superimposed onto lines representing the mean responses observed in three prior reports (Merchant et al., 1996; Nakajima et al., 2009; Aibara et al., 2001). Results are assessed in the similar manner as the transfer functions in Figure 38 and Figure 39 (i.e. normalizing ZC to the mean ZC at the Low stimulus level, and assessing ZC in the frequency bands <100 Hz, 100 Hz, and < 500 Hz). Overall, low frequency (<1 kHz) responses are consistent with these prior reports, while higher frequencies deviate towards lower ZC (possibly related to the poor response of our loudspeaker system at these levels). One-way ANOVAs reveal that there is no significant change in ZC in either the low or mid frequency bands across level. Note, while ZC appears generally level independent, it shows substantial frequency dependence, which may underlie the lack of a clear saturation point in PSV with increasing EAC SPL as shown in Figure 40 and Figure 41. Assessment of individual frequencies with level should thus reveal a clear saturation point in PSV, but is not possible with this data set due to the sparse level sampling. Nevertheless, the similarity between these impedances and those prior reports suggests that the proposed relationship between DStap and PSV is consistent even at levels at which substantial distortion from a saturating nonlinearity appears in both responses.

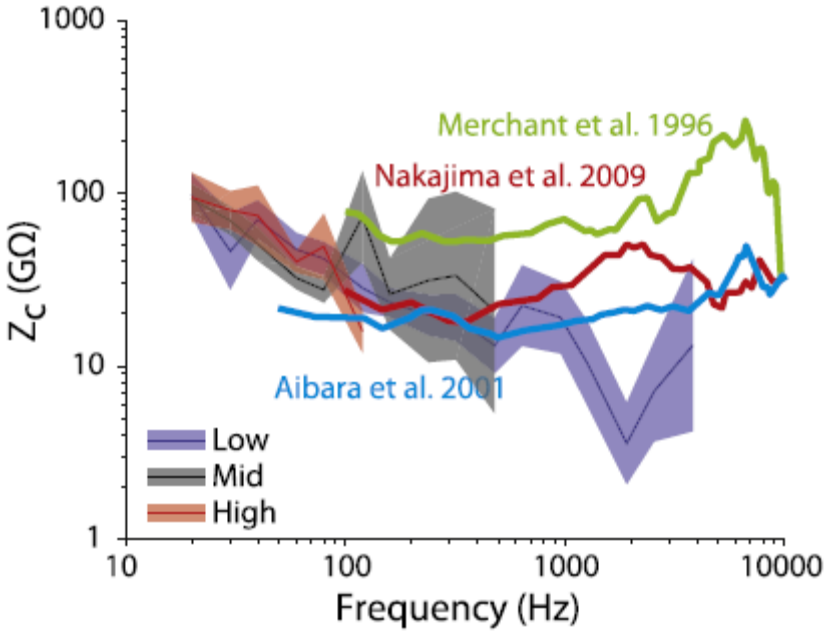

Figure 42. Mean (±SEM) cochlear input impedance (ZC = PSV/(VStap x AStap)) as a function of frequency for the three level bands tested (thin lines and shaded areas in blue: Low; black: Mid; red: High). Responses are superimposed onto the mean ZC from three prior reports (heavy lines in blue: Aibara et al., 2001; green: Merchant et al., 1996, and red: Nakajima et al., 2009).

The general strategy is as follows: An exposure waveform is applied to the outer ear/hearing protection module, the output of the hearing protection module is decomposed into frequency bands and applied to the nonlinear filters comprising the middle ear module, and the output of the middle ear module thus provides estimates of the inner ear exposure levels across these frequency bands. These exposure levels are compared to the human-equivalent dose-response functions developed in the chinchilla testing to determine deficits in inner and outer hair cell function. Finally, these hair cell degradation functions are applied to a phenomenological model of auditory nerve function to simulate the effects of degraded hair cell function on physiological measures of auditory function.

4.1.2.7 Development of a human middle ear transfer function

The computational approach adopted for this effort was to simplify the simulation of blast wave propagation, and thus the prediction of injury, by employing system identification to find a closed-form transfer function for the middle ear. A system model of a chosen functional form was derived for each frequency from each data set. The resulting transfer functions were combined to form a composite transfer function giving good prediction of PSV resulting from a given pressure waveform at the External Auditory Canal (PEAC). This transfer function enables an accurate and computationally efficient means of simulating the energy transferred to the sensory organ of the cochlea from a given blast event.

4.1.2.7.1 Data and models

The data used for system identification of the middle ear transfer function were derived from testing of PMHS specimens (human temporal bones) using a high-intensity sound source, an LDV to measure stapes velocity, and a fiber-optic probe to measure pressures in the SV and ST. The details of experimental methods and apparatus are given in the related publications, and in earlier

reports. Datasets used for system identification comprised four presentation levels and forty-three frequencies:

- Presentation levels (nominal EAC): 120, 125, 140, 145 dB SPL
- Frequencies: 1/4-octave intervals, 10 Hz to 12800 Hz

For each dataset at a given presentation level and frequency, PEAC and PSV were extracted as input and output, respectively, for use in finding an appropriate model and transfer function relating the two. MATLAB's System Identification Toolbox was used for this purpose. A number of linear and nonlinear models were explored, including

- Discrete-time model
- Linear Auto-Regressive Exogenous (ARX)
- Nonlinear ARX
- Nonlinear Hammerstein-Wiener

After evaluation of the respective models' performance and accuracy, the Hammerstein-Wiener model was chosen for further development. This model allows greater flexibility in choosing the type of nonlinearity than do the other models. A variety of nonlinearities may be chosen for the input (Hammerstein model) and the output (Wiener model). Between the two lies a linear polynomial model characterized by its poles (F-vector) and zeros (B-vector) and delay. For the example shown here, we will assume a nonlinear Hammerstein-Wiener (H-W) model (idnlhw in MATLAB) with the following properties:

- B-vector length = 8 (7 zeros + 1)
- F-vector length = 6 (6 poles)
- Delay = 0
- Input nonlinearity = dead zone
- Output nonlinearity = piecewise linear

4.1.2.7.2 Integration of models

A composite transfer function was generated by replacing the linearized central block of the H-W model with one in which each element of the B- and F-vectors is the mean of that element across all 43 frequencies. The resulting transfer function does combine the high- and low-frequency responses of the 43 test frequencies, yielding a prediction of PSV very consistent with the data.

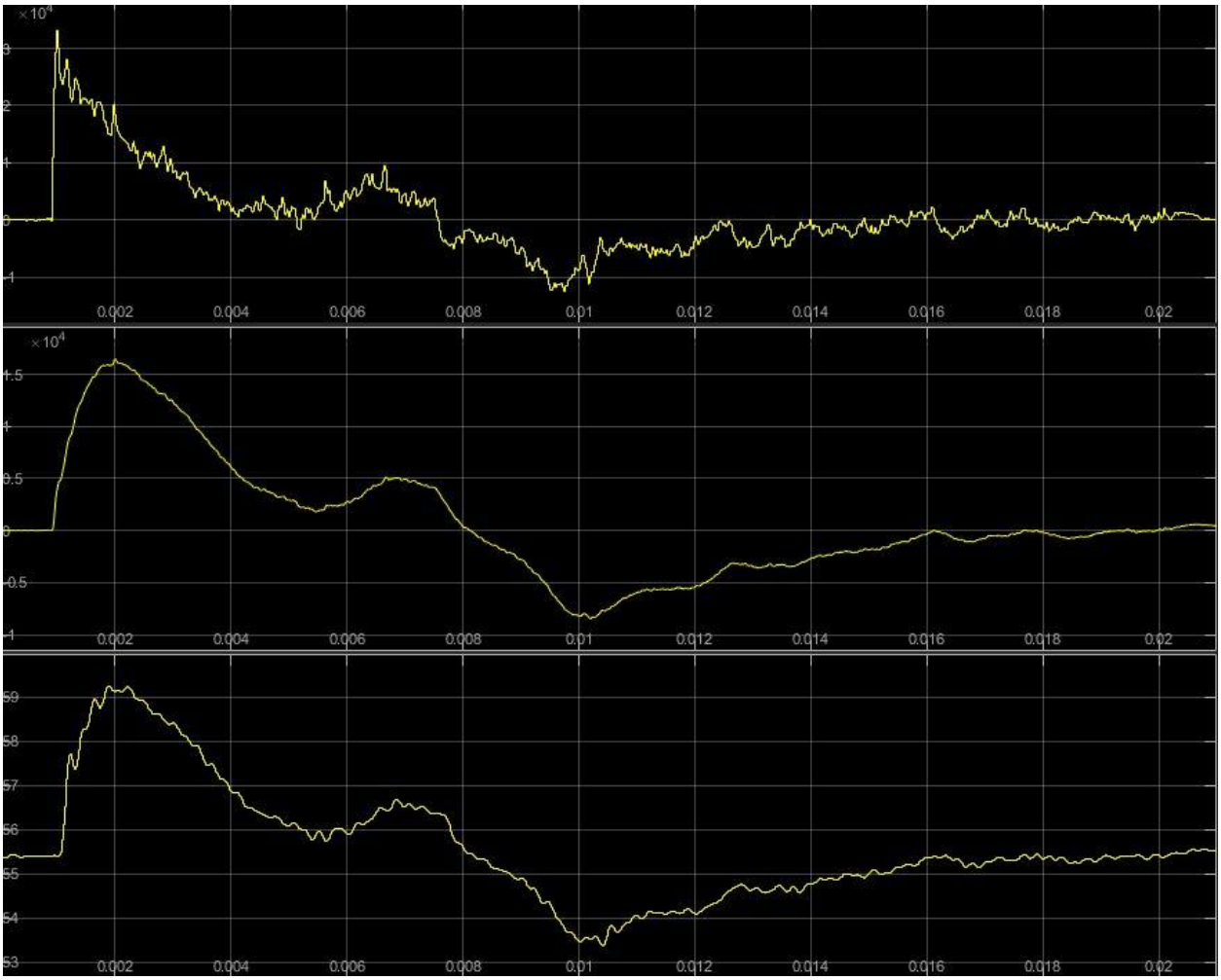

Figure 43. Top to bottom: Incident pressure, predicted PEAC and predicted PSV.

The results obtained with Simulink are sufficiently in keeping with observation that this approach is considered successful. Using a middle ear transfer function obtained in this manner, the simulation is expected to yield good prediction of inner ear pressures (PSV) and lead to useful modeling of auditory injury (hair cell loss and auditory degradation) as the result of blast exposure.

4.1.2.7.3 Application of models

Forty-three nonlinear Hammerstein-Weiner models were generated using data acquired from a human right temporal bone (437R) at 145 dB SPL nominal presentation level. To test the accuracy of the individual frequency models, each frequency model was used in a block representing the middle ear in the Simulink representation of the auditory system (Figure 44). A sample of the individual transfer functions is shown in Figure 45. The nonlinear Hammerstein-Wiener model at each frequency captures the middle ear's response, with SV pressure as the output variable. It was observed that those taken at higher frequencies captured the initial pressure rise accurately, but not the sustained peak, while those from lower frequencies did predict the peak, but at a greater group delay than shown by the data.

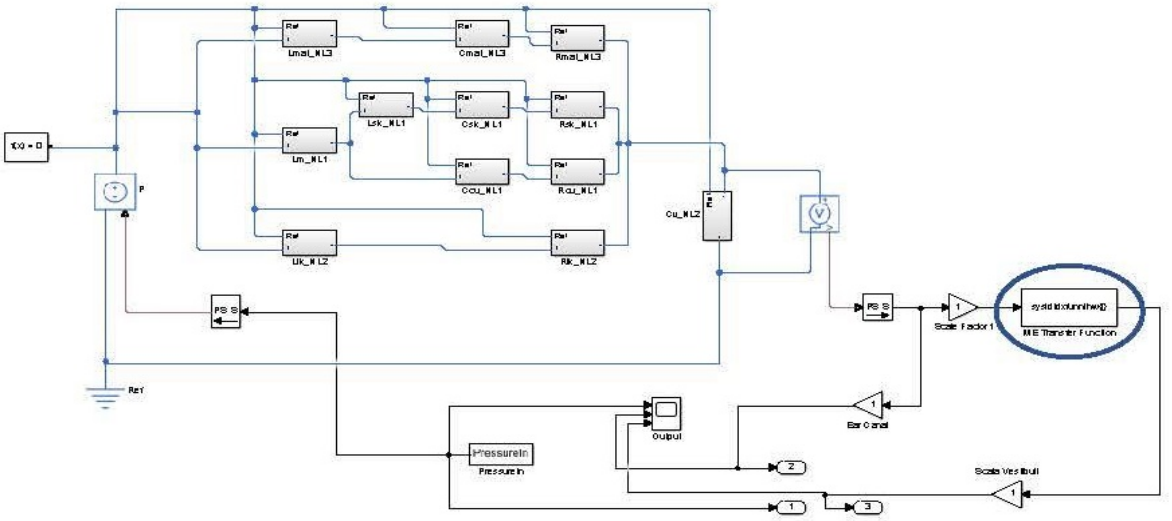

Figure 44. Simulink Model with Middle Ear Transfer Function (circled).

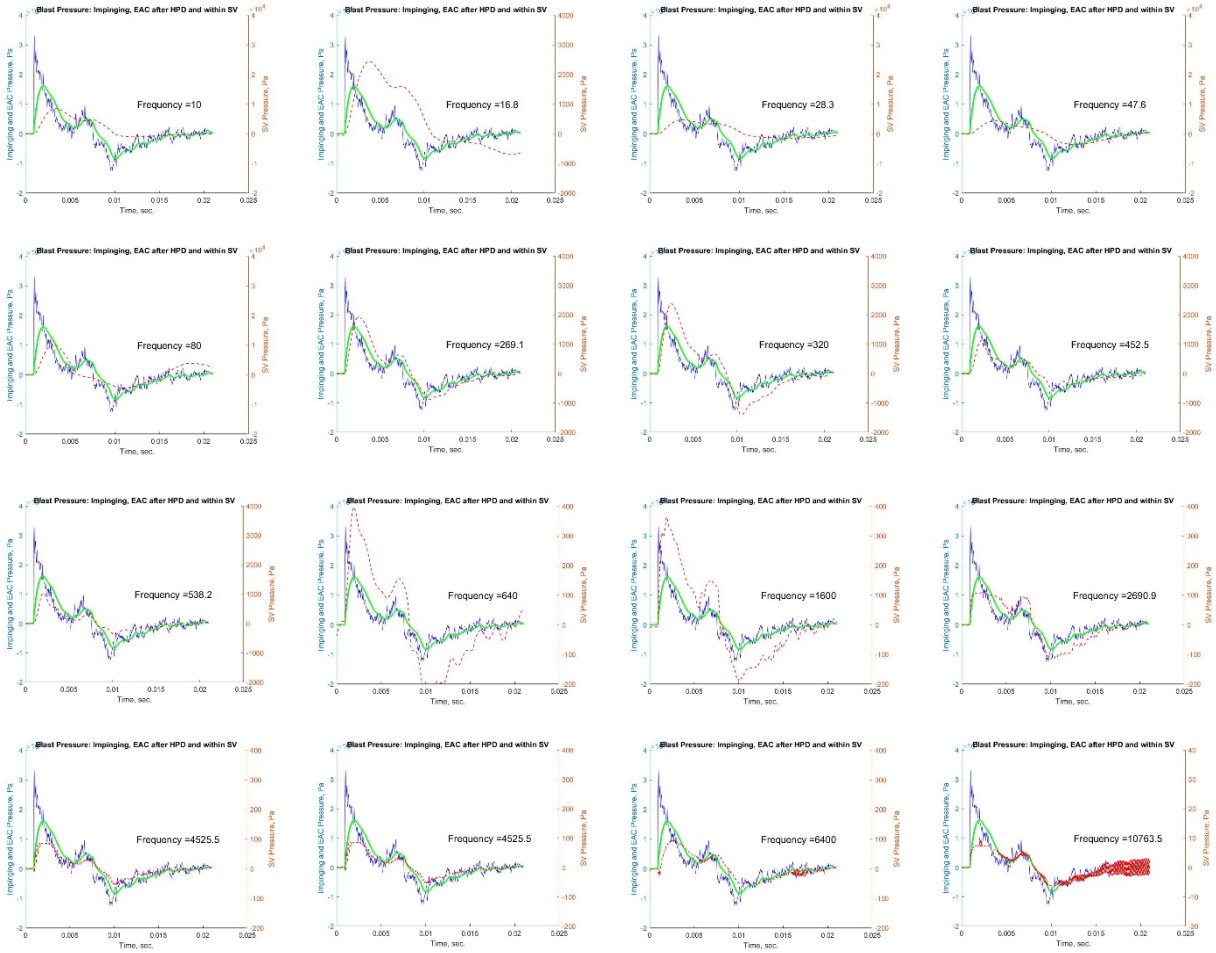

Figure 45. Cross-section of individual frequency transfer functions: Incident pressure (blue), predicted PEAC (green, solid) and predicted PSV (red, dashed). Each model is derived from PMHS data at the frequency shown.

4.2 Specific Aim 2: Develop a neuro-functional understanding of acoustic injury by correlate human and animal auditory mechanisms and physiological responses measured experimentally to generated noise and blast events

In Specific Aim 1, the pressure and energy transmitted through the human inner and middle ear were characterized using a combination of experimental testing and numerical modeling. To understand the effect of pressure on hair cell loss and auditory function, a chinchilla model was used in parallel with the human experimental testing. Chinchillas are often used in studies of hearing due to the similarity between the chinchilla and human audiograms. Prior to this study, their suitability for use in research for auditory trauma from blast noise was unknown. For Specific Aim 2, the first task was to quantify the middle ear dynamics of the chinchilla using the same methodology used in Section 4.1.2.2 for humans. Once the transfer function between human and chinchilla was established, the data was used to understand in human equivalent levels the effect of blast on inner ear hair cell loss and resulting auditory nerve function. The following sections describe how the pressures measured in the human were used to estimate the associated hair cell loss and auditory function using a chinchilla model.

4.2.1 Major Task 1 Quantifying Middle Ear Dynamics using Chinchilla Models

4.2.1.1 Chinchilla preparation for testing middle ear response to blast

To quantify the middle ear dynamics of the chinchilla the experiments followed the general methodology outlined by (Chan et al., 2016). Six adult cadaveric chinchillas were used for this study. The chinchillas had been frozen shortly after euthanasia, and were fully thawed before measurements. The skull of the chinchilla was opened to expose the bulla and allow access to the middle ear ossicles and the turns of the cochlea. The tensor tympani and stapedius muscles were left intact.

Pressures in the scala vestibuli were measured by inserting small-diameter (250 μm), off the shelf fiber optic pressure probe (FOP-M260-ENCAP, FISO Inc., Quebec, Canada) into a small hole drilled in the vestibuli near the oval window. To measure scala tympani pressure, the posterior bulla was opened and a small hole was drilled near the round window. The fiber optic pressure sensors were precisely positioned and held in place using micromanipulators (Kopf, Tujunga, CA), and were sealed in place after insertion with Jeltrate alginate impression material.

4.2.1.2 Sound presentation for Chinchilla testing

All experiments to quantify middle ear response were performed in a double-walled sound attenuating chamber (IAC Inc., Bronx, NY). Sounds were generated and data collected using a Hammerfall Multiface II soundcard (RME, Haimhausen, Germany), and signals were designed and analysed in custom-built programs in MATLAB. Sound stimuli consisted of 29 logarithmically spaced tones with frequencies between 10 and 1280 Hz.

The low-frequency, high intensity sound delivery system was similar to that described by Greene et al. (2017). Sounds were presented to the specimen with a ~30 cm subwoofer (Morel UW 1258) driven by a 300 W amplifier (Keiga KG5230) and two Selenium D408Ti 2-Inch Titanium Horn Drivers driven by a Crown amplifier (XLi 3500), all three drivers attached to a custom-built stainless steel sound concentrating horn, and were directed into the ear canal with flexible copper tubing. The total length of the sound concentrating horns and copper tubing was ~3 m; its diameter tapered from ~30 cm to ~1.25 cm.

The loudspeaker system was adapted to fit the ear canal of the chinchilla by terminating the copper tubing with an ear speculum, which further reduced the diameter to around 5 mm. A sound was then directed to the ear canal via a small silicone tube which was fed through a foam earplug to provide an effective seal. Tones with frequencies below 800 Hz were generated by the subwoofer, while tones above 800 Hz were generated by the horn drivers.

In order to maximize the sound levels produced, the output level of the speaker system was not calibrated to achieve a consistent sound level across frequency. Instead the output voltage to the speakers was attenuated by a fixed amount, and this attenuation was reduced from full scale to produce different outputs. The output from the speakers was therefore not a constant sound pressure level across all frequencies, but follows the characteristics of the sound presentation system. Although results are grouped and presented by nominal presentation level, responses are normalized to the actual sound pressure level measured in the EAC.

The speaker output is highest at the lower frequencies, with the peak output being just above 180 dB SPL at around 100 Hz. The maximum output from the subwoofer then drops to 130–150 dB SPL around 700–800 Hz.

The sound pressure level was measured using a G.R.A.S. 46BH 1/4-inch microphone (frequency range 10–20,000 Hz, dynamic range 54–194 dB) connected to the sound card via a G.R.A.S. 12AA power module (G.R.A.S., Denmark). The microphone was equipped with a custom probe tip, which was inserted into the ear canal alongside the silicone tube delivering the sound. The sound pressure level was therefore measured near the tympanic membrane at the same point as the sound enters the ear canal.

4.2.1.3 Chinchilla Measurement Procedure

After opening the bulla, the chinchilla middle ear was inspected for signs of abnormality. To ensure the cochlea was behaving normally (i.e., no air had infiltrated the cochlea), glass beads were placed on the stapes footplate and the round window, and a laser Doppler vibrometer (Polytec, OFV 5000, Irvine CA) was used to measure the displacements at both points in response to a series of low frequency low intensity tones to ensure that the displacements of these structures were out of phase.

Cochleostomies were then created, and the pressure probes were inserted and fixed in place as described above. The posterior bulla was left open during the measurements. After the probes were inserted the laser vibrometer was again positioned to measure the displacement of the stapes footplate.

Tones were initially presented with the signal attenuated by 60 dB; the attenuation was then sequentially decreased in steps of 5 dB towards zero, thus increasing the sound pressure level presented by the loudspeaker. Each tone was presented for a duration one second, and was repeated three times. These three repetitions were averaged in the time domain to determine the sound pressure levels in the ear canal and cochlea.

After the measurements were completed the pressure probes were removed and their placement in the cochlea (ST or SV) was verified by dissecting away the bone overlying the cochlea. The tympanic membrane and the ossicles were also examined after the measurements for signs of damage. All six specimens showed appropriate pressure probe placement, no signs of damage, and no cracking of the bone overlying the cochlea was observed during the cochleostomies.

4.2.1.4 Chinchilla transfer functions in response to low-frequency, high-intensity sound

Intracochlear sound pressure levels showed a strong dependence on excitation frequency. In order to simplify presentation, the following results are grouped into discrete octave, wide-frequency bands. The analysis only includes data points for which the signal to noise ratio was greater than 10 dB, which was calculated by comparing measurements made immediately before and during tone presentations.

Figure 46 shows the evolution of intracochlear sound pressure with increasing PEAC for different frequency bands. This figure includes data from all six chinchillas, although not all frequencies are shown. In Figure 46, A shows Scala Vestibuli Pressure (P_{SV}) vs PEAC, B shows Scala Tympani Pressure (P_{ST}) vs PEAC, and C shows the differential Pressure (P_{Diff} = PSV–PST) vs PEAC. Frequency bands are indicated with varying colors, as indicated in the legend. A black dotted line has been added to show a ratio of 1:1 (a linear increase with PEAC).

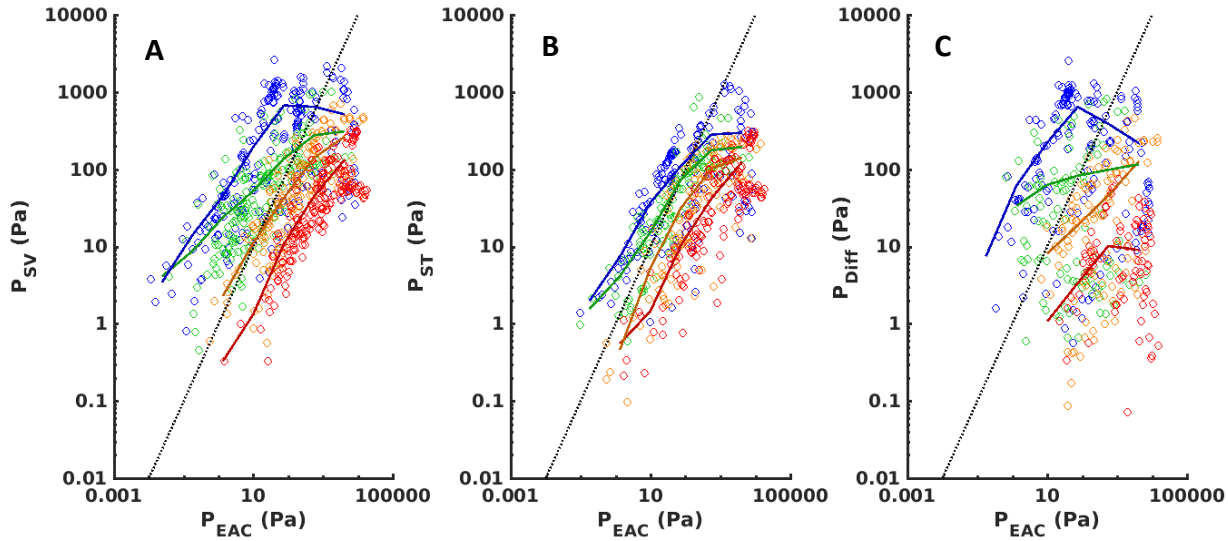

Figure 46. Scala vestibuli (PSV), scala tympani (PST), and differential (PDiff) intracochlear pressure as a function of ear canal Pressure (PEAC) for different frequency bands (red: 10-20 Hz; yellow: 40-80 Hz; green: 160-320 Hz; blue: 640-1280 Hz). Individual measurements (circles) are shown alongside a mean (solid colored line) calculated by a binning process based on applied ear canal pressure. A black dotted line showing a ratio of 1:1 between PEAC and intracochlear pressure has been added for reference.

The solid colored lines are added to give a clearer impressing of the trends in the data. These lines were created through a data binning process. Data was placed into bins based on PEAC, and the mean was calculated.

The strong relationship between stimulation frequency and intracochlear pressure magnitude is clearly visible as a vertical offset across frequency bands. For any given PEAC, the intracochlear pressure was larger with higher excitation frequency (up to 1280 Hz). At excitation frequencies between 640 Hz and 1280 Hz, the scala vestibuli pressure reached ~1000 Pa, while the highest pressures recorded between 10 Hz and 20 Hz were ~300 Pa. Pressures in the scala vestibuli were larger than those in the scala tympani.

At the highest frequencies tested (640 Hz–1280 Hz), much greater variation in the data is visible. This is partly due to their being more variation between individual specimens at higher frequencies. In particular, one specimen showed noticeably lower response levels than others.

Intracochlear pressures increased linearly with increasing PEAC, but saturated at the highest levels tested. The PEAC at which PSV and PST showed this saturation may show a slight dependence on the excitation frequency: at the highest frequency band (640 Hz–1280 Hz) the intracochlear pressures show signs of beginning to saturate at around 100 Pa, while at the lowest frequencies they do not begin to saturate until the ear canal pressure is over 1000 Pa. The slope of each function represents the gain of each intracochlear pressure relative to PEAC, and this gain decreased as PEAC increased. PDiff (Figure 46C) also increases with increasing PEAC, this indicates that intracochlear pressure gain relative to PEAC is greater for PSV than for PST.

Figure 47 shows the relationship between the middle ear transfer function magnitude (the ratio of intracochlear pressure to pressure in the ear canal), for different frequency bands, as a function of PEAC. As with Figure 46, different colors represent different frequency bands, as indicated in the legend. Figure 47A shows the scala vestibuli transfer function (PSV/PEAC), Figure 47B shows the scala tympani transfer function (PST/PEAC), and Figure 47C shows the differential pressure transfer function (PDiff/PEAC). The solid colored lines were calculated in the same way as for Figure 46.

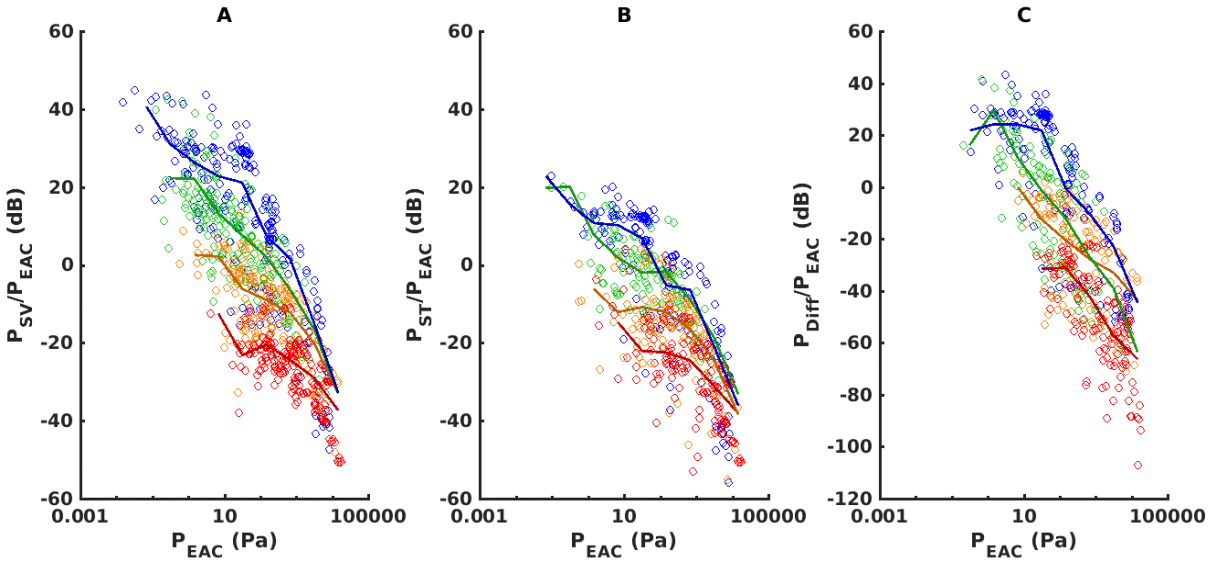

Figure 47. The ratio of intracochlear pressures to ear canal pressure as a function ear canal pressure (PEAC) for different frequency bands. As in Figure 46, individual markers show individual measurements while the solid colored line shows the mean calculated by a binning process based on applied ear canal pressure. Frequency ranges as in Figure 46.

In general, a gradual decrease in the transfer function magnitude with increasing PEAC was observed for moderate level sounds, and a sharp decline was observed for the highest sound exposures in all frequency bands. However the rate at which the transfer function fell was not equal across frequency. At the lowest PEAC the middle ear gain, given by the scala vestibuli transfer function, was around +40 dB at frequencies between 640 Hz and 1280 Hz, and -15 dB at frequencies between 10 and 20 Hz. At the highest PEAC tested, the middle ear gain was ~ -40 dB in all four frequency bands. PST and PDiff transfer functions show similar trends with gains peaking around +20 dB for low PEAC, and declining to ~ -50 dB and -70 dB respectively at the highest PEAC.

In Figure 48, we can see the relationship between stapes footplate displacement and pressures in the ear canal and scala vestibuli across different frequency bands measured in a subset of animals

(3/6). A black dotted line has been added to show a ratio of 1:1 as in Figure 46 (a linear increase with PEAC). In Figure 48C, a grey dotted line has also been added by shifting the black line to a higher pressures.

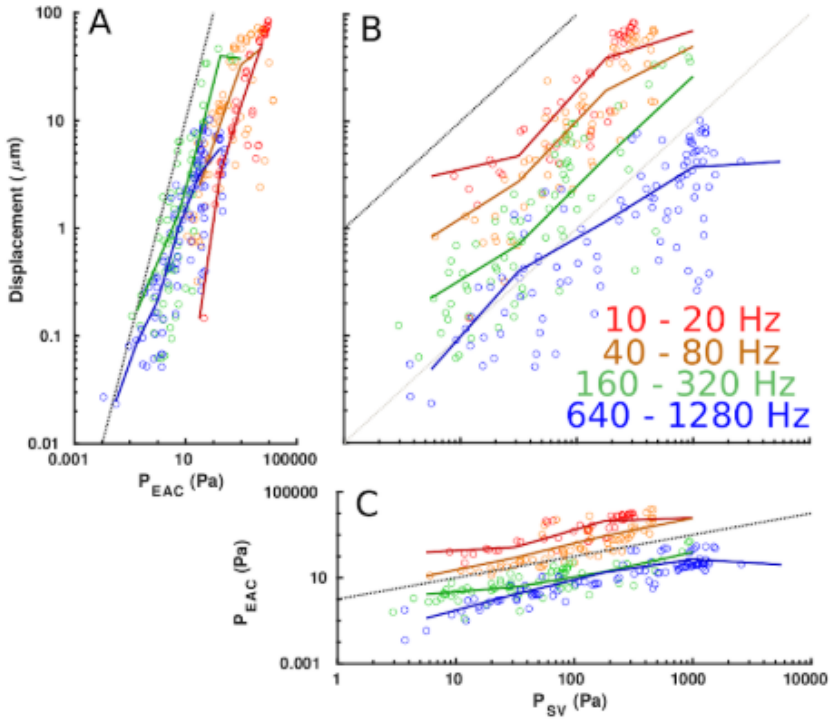

Figure 48. Stapes footplate displacement (A) and scala vestibuli pressure (C) as a function of ear canal pressure, and as a function of one another (B). The colored circles shows the individual measurements (circles) while the solid colored line shows a mean calculated by a binning process.

In general, footplate displacement increases linearly with increasing PEAC and PSV. There is some evidence that for the lowest frequencies tested, ranging from 10 Hz–80 Hz, the stapes footplate displacement begins to saturate for PEAC just below ~1000 Pa (~150 dB SPL).

Figure 49 shows scala vestibuli transfer function magnitude (A) and phase (B) as a function of stimulus frequency. The data here has been divided into groups based on PEAC presentation level (following Greene, 2017). The data in blue shows all measurements with a PEAC below 125 dB SPL, green shows data gathered between 125 and 145 dB SPL, orange shows data gathered between 145 and 165 dB SPL, and red shows all data above 165 dB SPL. The solid line shows the mean at each frequency (the mean number of samples is just over eleven) and the shaded area represents one standard deviation above and below the mean.

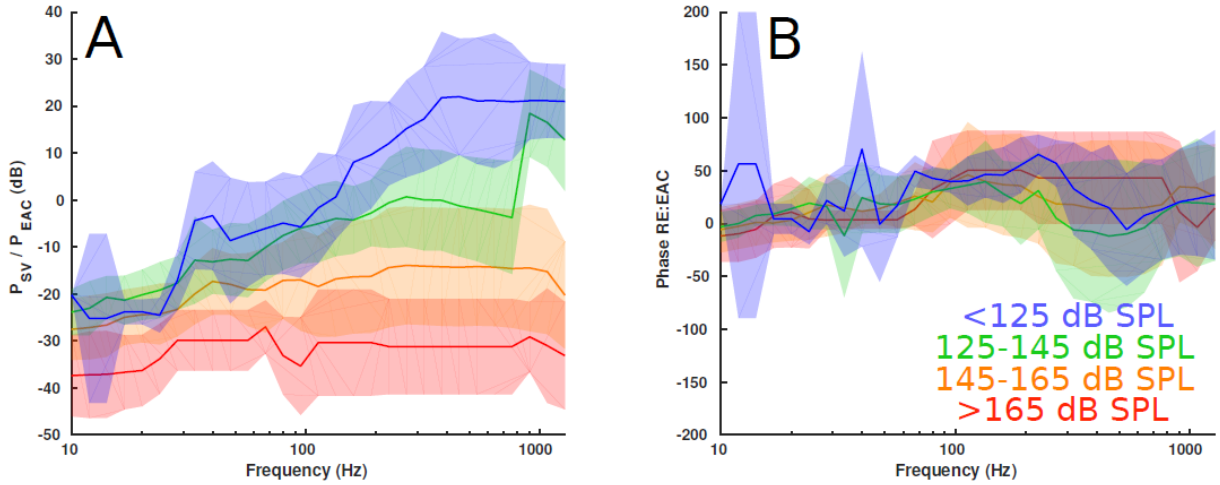

Figure 49. Scala vestibuli transfer function magnitude (A) and phase (B) as a function of stimulus frequency. Data is divided into groups based upon the pressure in the ear canal (distinguished by color as indicated in the legend) and averaged over each stimulation frequency to produce the solid colored lines. The colored shaded areas indicate one standard deviation either side of the mean.

Transfer function magnitudes varied with both frequency and applied PEAC SPL. In general we observed lower transfer function magnitudes with increasing PEAC, and higher transfer function magnitudes with increasing frequency. At the highest PEAC (red line, above 165 dB SPL) the transfer function was -38 dB at 10 Hz, and -31 dB at 1000 Hz. At the lowest PEAC (blue line, below 125 dB SPL) the mean transfer function was around -20 dB at 10 Hz, and +22 dB at 1000 Hz. Thus the transfer function magnitude appears to increase for higher frequencies, but this frequency dependence was itself strongly dependent upon the sound pressure level applied.

With PEAC below 125 dB SPL the transfer function varied by as much as 45 dB across frequency, while above 165 dB SPL, the transfer function varied by only ~10 dB across frequency. As was seen in Figure 47, the transfer function appears much flatter across frequency with higher ear canal sound pressure levels. The phase (Figure 49B) remains around zero until 100 Hz and then appears to increase slightly before returning to zero at 300–500 Hz. No substantial differences in the phase were visible across PEAC.

4.2.1.5 Comparison of chinchilla and human intracochlear pressures and transfer functions

Human data was taken from Greene et al. (2017). Compared to humans, intracochlear pressures in chinchillas showed lower pressures, but comparable frequency and level dependence. Figure 50 shows PSV for both chinchilla (red) and human (blue) specimens for three different frequency bands. Figure 50A shows data from 20–40 Hz,B shows 80–160 Hz, and C shows 320–640 Hz. We were unable to compare higher frequencies due to insufficient data, whereas interleaved frequencies (not shown) showed responses intermediate between those shown. The y-axis shows PSV, while the x-axis shows PEAC. The circles indicate individual measurements, while the solid line shows the mean PSV calculated over different PEAC bins as in previous figures. The average number of data points in each bin was around 26. A black dotted line has been added to show a ratio of 1:1 as in Figure 46 (a linear increase with PEAC).

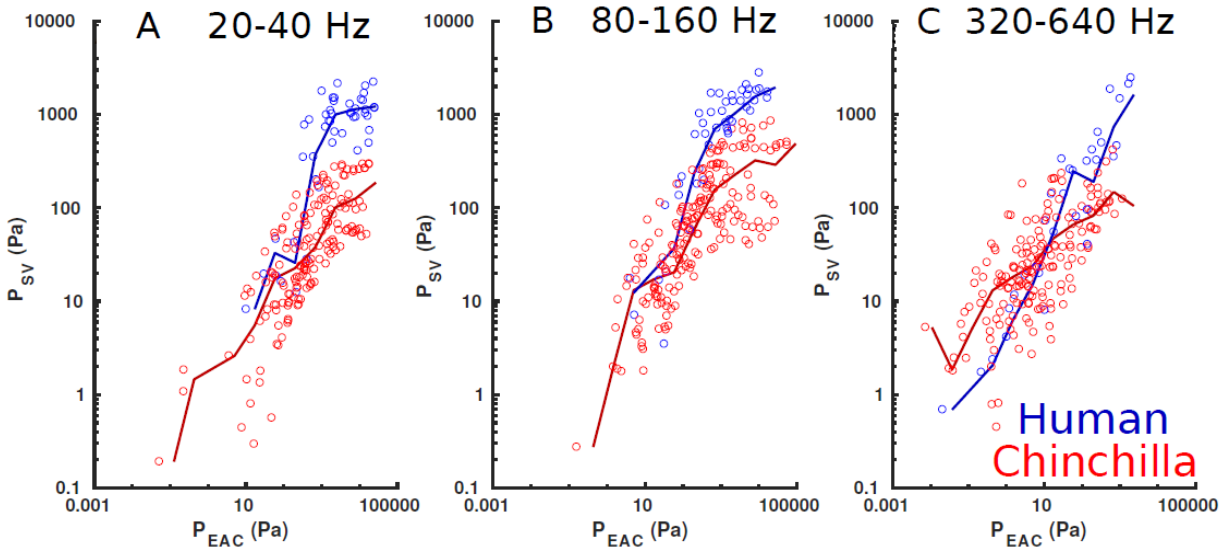

Figure 50. Scala vestibuli pressures measured in both chinchilla (red) and human (blue). Each subplot shows data within different frequency bands as indicated in the titles. The human data has previously been reported in Greene (2017). Individual measurements (circles) are shown alongside a mean (solid colored line) calculated by a binning process based on applied ear canal pressure. A black dotted line showing a ratio of 1:1 between PEAC and intracochlear pressure has been added for reference.

Overall, the chinchilla pressures were lower than the human pressures, particularly at very high PEAC. The maximum PSV observed increases with frequency, suggesting the largest PSV is found at the higher frequencies in chinchillas and in humans; however, no clear saturation in PSV is visible for frequencies between 320 and 640 Hz in either species, which is likely due to the inability of the loudspeaker system used to produce sufficient ear canal pressures at these frequencies.

Figure 51 compares transfer function magnitudes with increasing PEAC between chinchillas (red) and humans (blue) for the same three different frequency bands, as in Figure 50. The y-axis shows the transfer function magnitude: the top row (A–C) shows PSV transfer function; the middle row (D–F) shows PST transfer function magnitude; and the bottom row (G–I) shows differential pressure transfer function magnitude. The x-axis shows PEAC. The circles indicate individual data points.

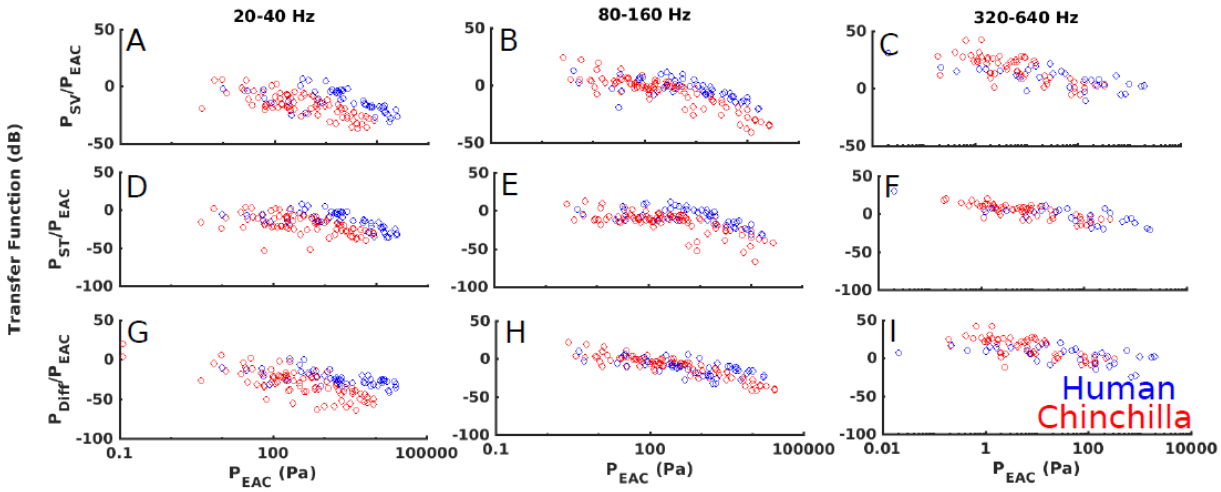

Figure 51. The ratio of scala vestibuli (A, B, C), scala tympani (D, E, F), and differential (G, H, I) pressure to ear canal pressure measured in both chinchillas (red circles) and humans (blue circles). Each column shows data in a different frequency band as indicated in the titles.

Similar trends in the data are visible when comparing humans to chinchillas, although the human transfer function magnitudes appear to grow larger than those in chinchillas as PEAC increases across all but the highest frequencies. At low pressures and at higher frequencies, the human and chinchilla data mostly overlaps.

Lastly, in Figure 52, we can see the ratio of chinchilla to human intracochlear pressures (chinchilla to human transfer function) against ear canal sound pressure level (A) and Frequency (B). The ratio is found by first calculating the mean PSV across different PEAC bands (the same mean values as are plotted in Figure 50). Only data from 20–640 Hz is included as there was an insufficient amount of comparable data at higher and lower frequencies.

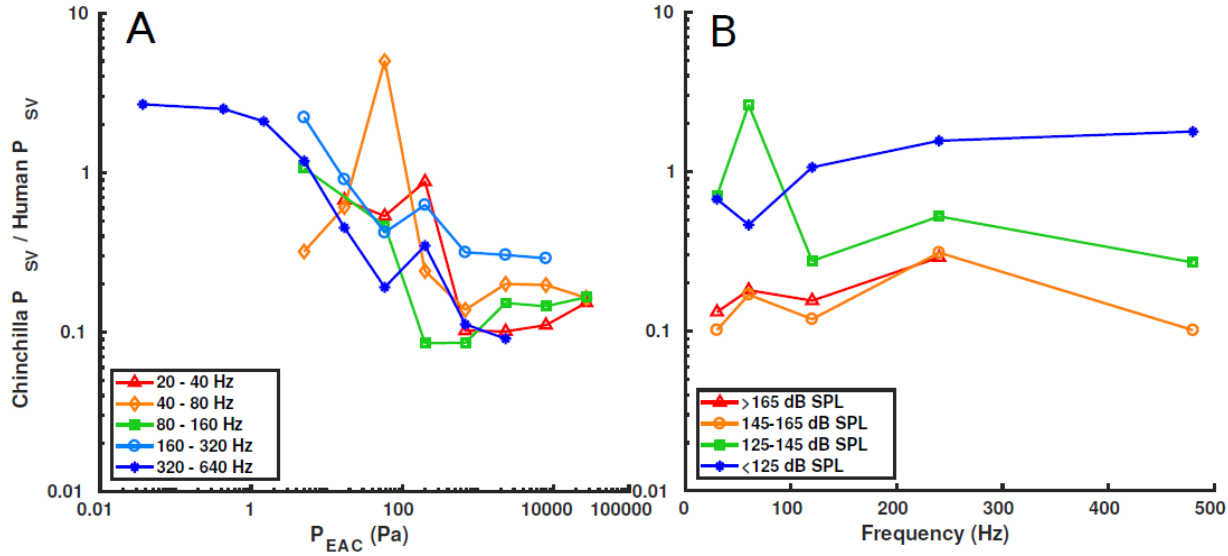

Figure 52. The ratio of chinchilla to human intracochlear pressures (chinchilla to human transfer function) against ear canal sound pressure level (A) and Frequency (B). In A, the data is divided into different frequency bands, while in 34B it is divided into groups based upon applied ear canal pressure (as in Figure 49).

In Figure 52A, we can see the level dependence of the chinchilla to human transfer function. The transfer function appears to first fall with increasing PEAC, but then saturates. As a whole, the data appears to follow a sigmoid function, with the transfer function being flatter with low and high PEAC. The transfer function begins to fall at a PEAC of around 1–2 Pa (320–640 Hz), and levels off somewhere around 1000 Pa.

In Figure 52B, we can see how the transfer function varies across frequency. In this figure we have separated the measurements based on PEAC, as in Figure 49. The measurements have then been averaged over each octave. In general the transfer function appears flat over frequency, but falls with increasing PEAC. At the lowest SPL levels (<125 dB SPL) human and chinchilla responses are comparable thus the transfer function is around 1–2, while at the highest levels (>165 dB SPL) the transfer function is around 0.1–0.2.

4.2.1.6 Suitability of the chinchilla as compared to other common animal models

We made measurements of stapes displacement in response to low-frequency, high-intensity sounds in chinchillas (Chinchilla lanigera), guinea pigs (Cavia porcellus), Mongolian gerbils (Meriones unguiculatus), laboratory rats (Rattus norvegicus) and laboratory mice (Mus musculus). In total, we used four of each species. Specimens were not killed for this study, but instead were salvaged from known sources and had no known hearing defects or had any undergone any procedures that may damage hearing. All specimens had been frozen shortly after death and were fully thawed before beginning measurements.

After the specimen carcass had fully thawed, the skull of each animal was opened to expose the bulla and allow access to the middle ear ossicles and the cochlea. The tensor tympani and stapedius muscles were left intact.

Stapes displacement was measured with a laser Doppler vibrometer (LDV, OFV-534; Polytec Inc., Irvine, CA) attached to a surgical microscope (Leica M400 E) with a polytec HLV MM2 unit. Small (45–63 μm diameter) glass beads (P-RETRO-xxx, Polytec Inc., Irvine, CA) were placed on the stapes to enhance the strength of the laser signal.

Sound presentation and data collection were identical to that described in the previous section, and the measurement procedure was also identical, except that no intracochlear pressures were measured. In these measurements, we were also able to position the animal’s head so as to optimize the LDV measurements angle.

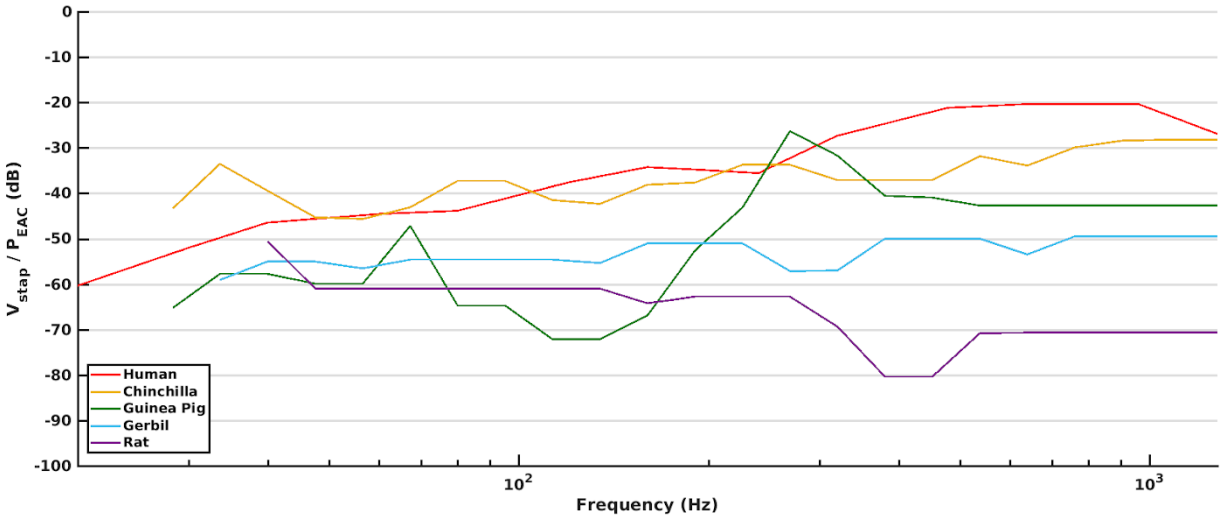

Figure 53. Shows the ratio of stapes velocity to ear canal sound pressure level, for ear canal sound pressure levels below 125 dB SPL.

The middle ear transfer function (the ratio of stapes velocity to ear canal pressure) shows large differences across species, as can be seen in Figure 53. The transfer function shows a tendency to increase with increasing frequency in all species except the rat, where it appears to decline. The magnitude of the transfer function is largest for humans and smallest for rats. The chinchilla transfer function appears overlap the human transfer function across most frequencies.

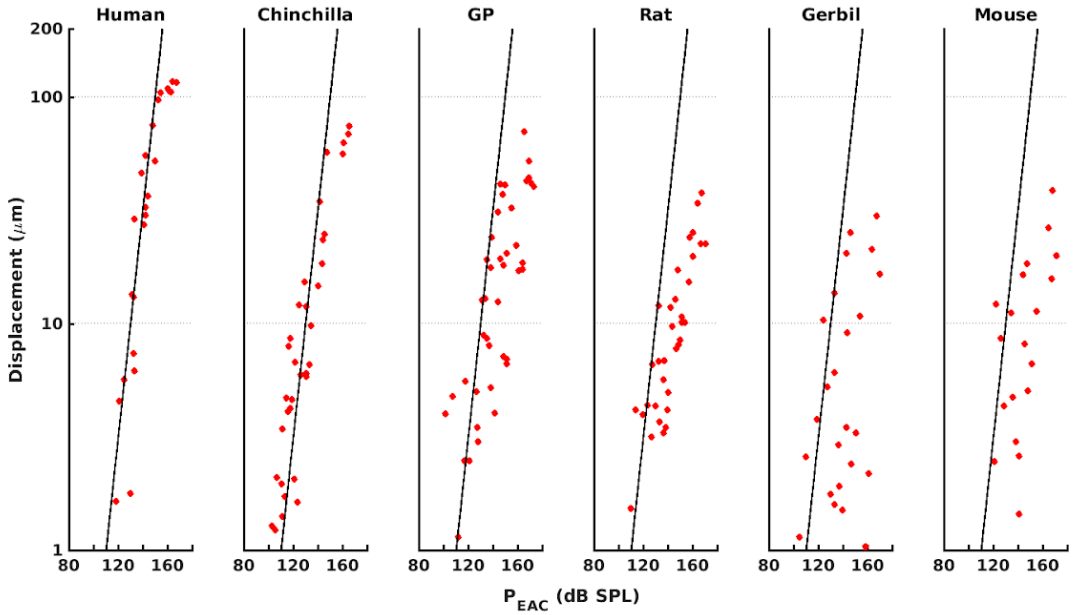

Figure 54. Peak to peak stapes displacement against ear canal sound pressure level for each species.

Measurements of the peak stapes displacement at each applied ear canal sound pressure level are shown in Figure 54. Clear differences can be seen across species, with the human having the largest displacements and the rat, gerbil, and mouse having the lowest overall displacements.

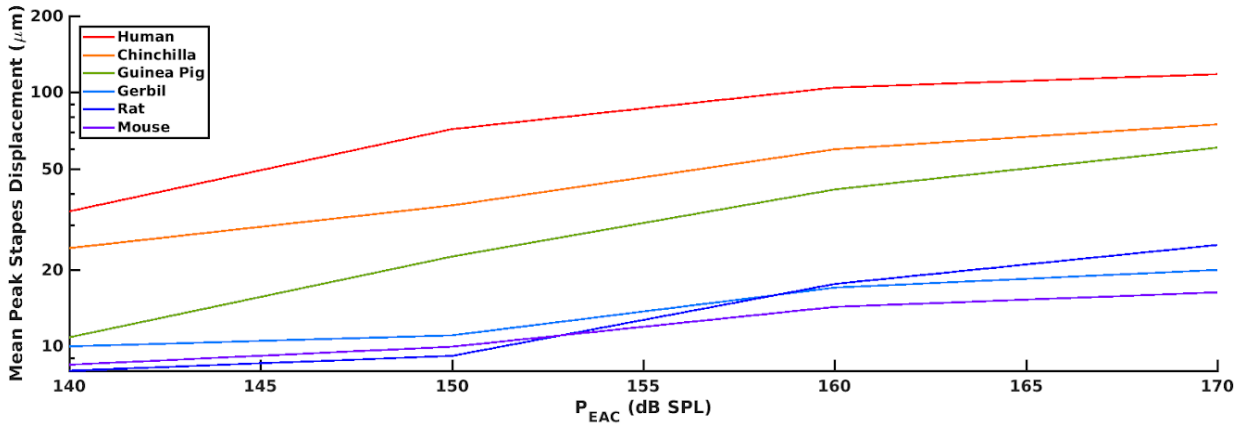

Figure 55. Shows how the mean peak stapes displacement changes with increasing ear canal intensity.

Another way to display the data from Figure 54 is shown in Figure 55. Here we have plotted mean peak stapes displacement at each applied sound pressure level. The mean was calculated for every 10 dB increase in applied sound pressure level by averaging all measurements ±5 dB. For all species measured, the mean peak stapes displacement increases with applied sound pressure, but does also show a tendency to saturate for some species, in other words the rate at which the displacement increases is declining with increasing sound pressure level.

4.2.2 Major Task 2: Estimate Human Hearing Loss from Animal Exposure Results

The work from the previous task shows the chinchilla transfer function appears to overlap the human transfer function across most frequencies and was found to be an appropriate model for estimating hearing loss resulting from exposure to blast. In this task, a variety of measurements were used to provide insight into the blast intensities that will cause permanent hearing damage in humans using the chinchilla model. The findings will be used to develop models to estimate the expected type and degree of human hearing loss for a given exposure to blast.

4.2.2.1 Chinchilla hearing loss assessment

In order to determine blast exposures in chinchillas that produce permanent hearing loss (i.e., loss that did not recover 21–28 days post blast exposure), a variety of measurements to assess the hearing ability of 24 chinchillas before and after exposure to blasts of varying intensities were used. These results will be used in combination with the previously described pressure measurements in both chinchillas and humans to predict the blast intensities that will cause permanent hearing damage in humans. The damage to the cochlear structures in response to blast are expected to have functional consequences. First, behavioral hearing ability should be disturbed. Second, hair cell functionality should be altered. Finally, sound-evoked responses of the auditory nerve should be comparably altered.

The impulse was generated in a small-bore shock tube. The intensity of each impulse was measured using a G.R.A.S. 46BH 1/4-inch microphone connected to the sound card via a G.R.A.S. 12AA power module (G.R.A.S., Denmark). The microphone was place above the head of the animal, and between the two ears. Impulse intensities ranged from 0.7 psi to 6.7 psi.

The hearing ability of the chinchillas was assessed in a number of ways: behavioral audiograms; auditory brainstem response (which assesses auditory nerve and more central auditory brainstem

function); distortion product otoacoustic emissions (which assess hair cell function); and immunohistochemistry.

4.2.2.2 Chinchilla Behavioral Audiograms

Prior to blasting, chinchillas were trained to respond to tones so as to allow measurement of their audiograms. Chinchillas were placed in box that was divided into two halves with a barrier. An Xbox Kinect (Microsoft, Redmond, WA) was used to monitor the position of the chinchilla (determining which side of the box it was currently in). Tones were then played from a speaker placed on top and in the center of the box and, if the chinchilla remained in the same side of the box during the tone presentations, a small current was passed through the floor of that side of the box. If the chinchilla jumped to the other side during the tone presentation, the chinchilla would avoid the shock.

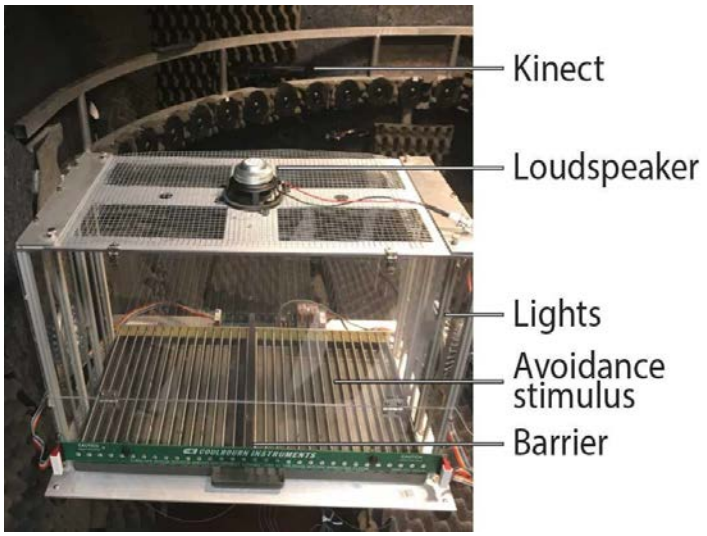

Figure 56. Chinchilla behavioral fixture used to quantify behavioral response to tones before and after exposure to blast overpressure.

Chinchillas were placed in the box daily for around ten minutes. Tones were played at 500, 1000, 2000, 4000, 8000, and 16000 Hz, and at a sound pressure level of 60–70 dB, for around two weeks in order to fully train the animals to avoid the shock by jumping in response to the tones. After the training period was complete, the sound pressure level was gradually lowered, and measurements repeated several times, until we found the minimum sound pressure level at which the animals would reliably respond. This was repeated approximately four weeks following blast exposure.

4.2.2.3 Auditory Brainstem Response (ABR)

To measure ABRs, the chinchillas were first anesthetized with an intraperitoneal injection of ketamine (30mg/kg) and xylazine (5mg/kg). Three platinum subdermal needle electrodes were then inserted under the skin; the apex electrode was placed between the ears (vertex) with a reference electrode at the nape, and a ground electrode was placed on the hind leg. Sounds were then played into the ears and the signals from the electrodes were recorded.

Signals were designed in custom-built MATLAB software and consisted of Gaussian-windowed tone bursts (Gabor clicks). These were presented at a rate of around 30Hz, at frequencies of 0.5, 1, 2, 4, 8, and 16 kHz, and at sound pressure levels from 30 to 90 dB SPL.

ABRs were measured one week before the blast, and then one, two, and three weeks post blast.

4.2.2.4 Distortion Product OtoAcoustic Emissions (DPOAEs)

DPOAEs were measured with EMAV: Otoacoustic Emission Averager (Neely and Liu, 1994). The Etymotic ER-10B+ microphone and Etymotic ER2 earphones were used to produce the stimulus tones and to measure the otoacoustic emissions.

The EMAV software was used to generate two primary tones (F1 and F2), which were sent to the two ER2 earphones and then to the ear canal via the ER10B. DPOAEs were recorded at six F2 frequencies: 0.5, 1, 2, 4, 8, and 16 kHz. The ratio F2/F1 was 1.22. The sound pressure level of the stimulus was also varied so as to find DPOAE thresholds. DPOAEs were measured immediately before and after blast exposure, and then at one, two, and three weeks post blast.

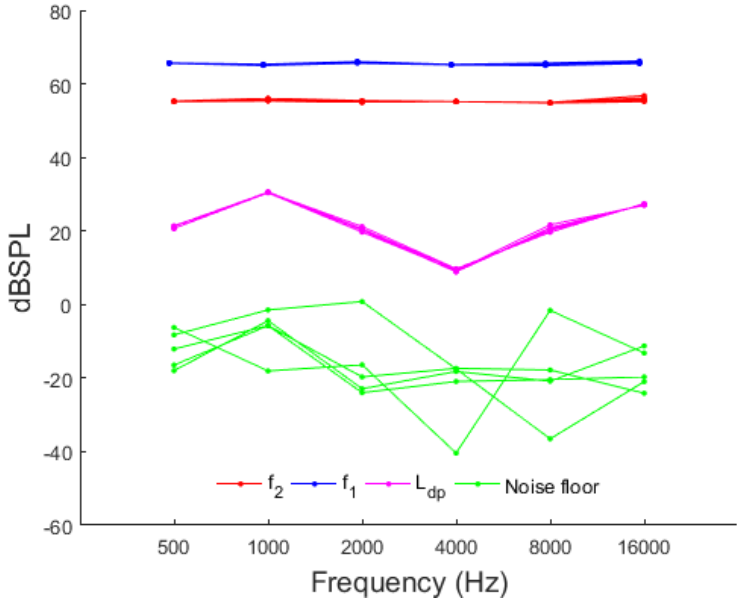

Figure 57. Example of Otoacoustic Emission data collected and used to quantify DPOAE changes associated with exposure to blast overpressure

Figure 57 shows sound level on the y-axis and frequency on the x-axis. The noise floor of the recordings at the measured frequencies are shown in green. The resulting DPOAE level (Ldp) from tone presentation is displayed in magenta. The levels of the tones f1 and f2 are show in blue and red, respectively.

The DP-gram here originated from a normal-hearing, female chinchilla. The data exhibits quality OHC emissions due to the change in response with frequency, the low standard deviation of the emissions, and the roughly 20-dB difference between Ldp and the noise floor.

4.2.2.5 ImmunoHistoChemistry (IHC)

After the final measurements of behavioral audiograms, the animals were euthanized and their cochleae were removed and prepared for immunohistochemistry.

After the bulla was removed from the skull, it was opened and inspected for visible signs of damage. A small hole was made in the cochlea and then it was placed in Paraformaldehyde for two hours following which it was placed in Ethylenediaminetetraacetic acid (EDTA) for one week in order to decalcify.

4.2.2.6 Behavioral audiograms

Figure 58 shows behaviorally measured thresholds of hearing (in dB SPL) for brief tones as a function of frequency in three different chinchillas. The red curve shows baseline thresholds prior to blast exposure while the blue curve shows threshold measured between three and four weeks post exposure. A control animal exposed to no blast (0 psi), but otherwise was subjected to all of the procedures necessary for blast exposure and showed no changes in hearing threshold as expected. An animal exposed to 1.95 psi exhibited shifts in threshold of ~15 dB SPL across the frequencies tested. And an animal exposed to 4.88 psi exhibited shifts in threshold ranging from ~20 dB at low to ~50 dB or more for high frequencies. Results suggest that exposures >~2 psi can produce permanent hearing loss in chinchilla the magnitude of which appears to scale with increasing exposure above 2 psi.

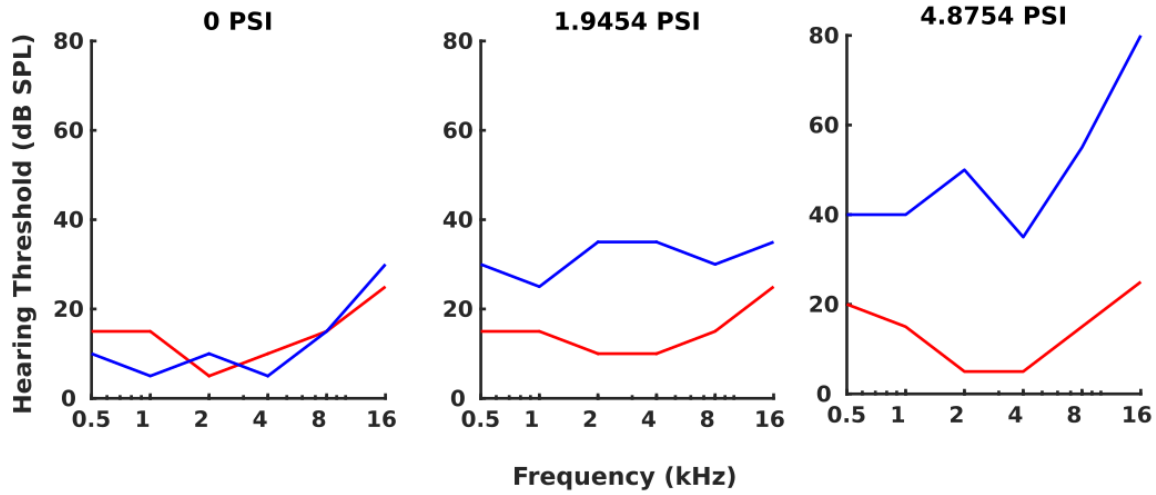

Figure 58. Threshold hearing shifts in Chinchilla with increasing magnitude of blast exposure

4.2.2.7 Auditory brainstem response thresholds

Figure 59 shows the ABR waveforms recorded from a chinchilla before (pre-blast, blue line) and one week after (post-blast, red line) exposing it to a blast of ~3.25 psi. The two graphs show data from the left and right ears. These ABRs were produced by presenting clicks with a sound pressure level of 90 dB SPL, which was ~60 dB above the threshold in the pre-blast condition. A clear ABR is visible before the blast but appears almost entirely absent one week post blast. These observations, along with similar post-blast deficits in the DPOAE measurements, have allowed us to determine the blast psi in chinchilla at which significant and permanent damage to the peripheral auditory system (e.g., hair cells and auditory nerve fiber) begins to occur from. These initial observations are guiding our current sets of experiments. The data also demonstrates that our laboratory-based blast tube setup is capable of causing permanent hearing damage that persists for weeks post blast.

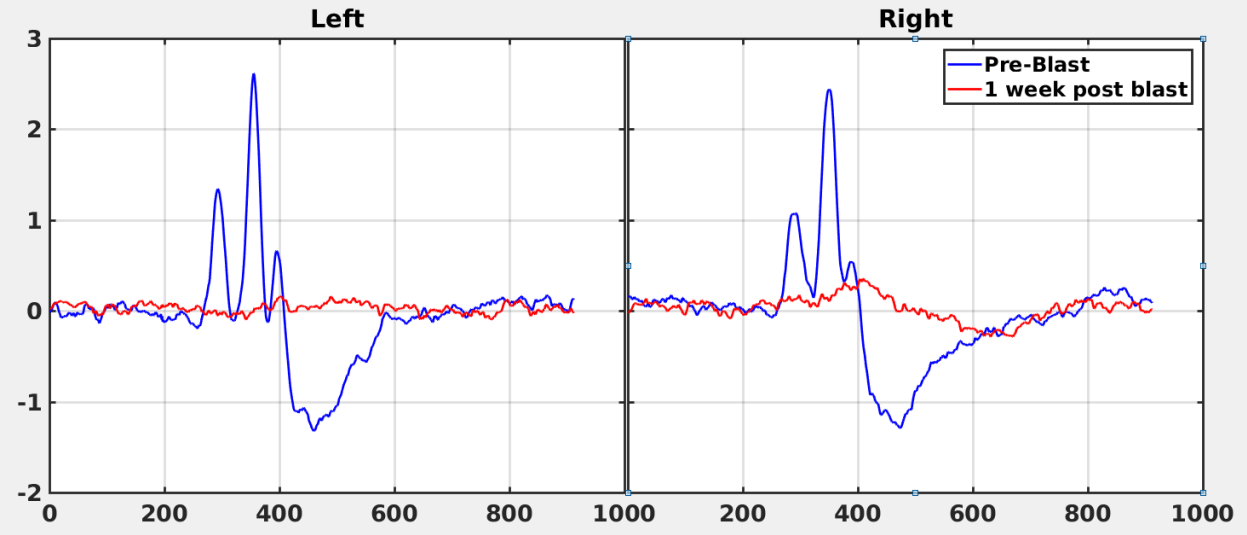

Figure 59. ABR waveforms recorded from a chinchilla before and after exposure to blast

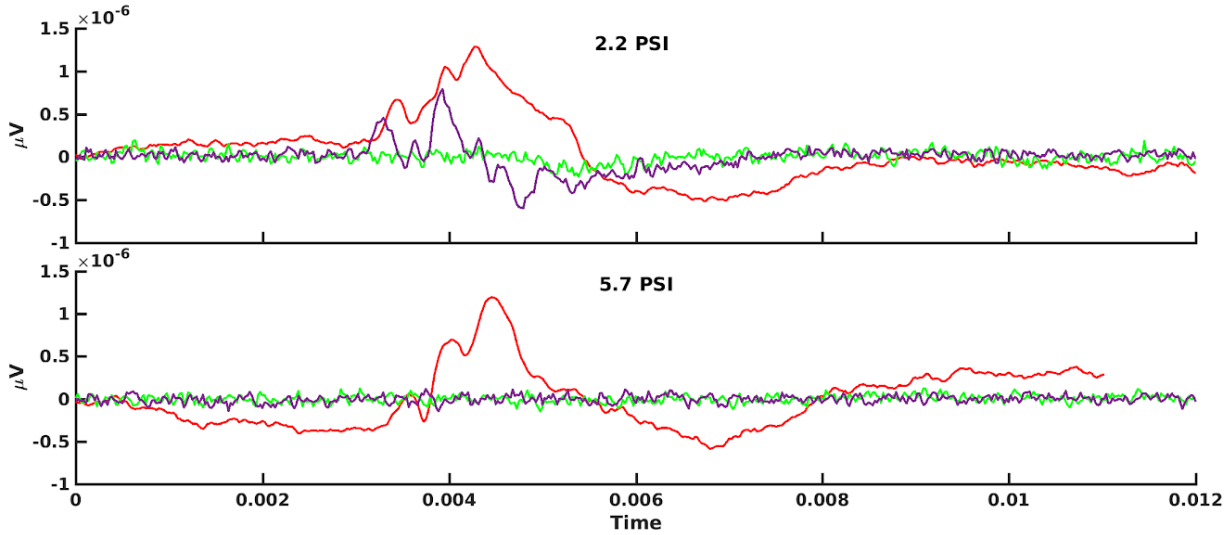

Figure 60. ABR data for two chinchillas exposed to blast

Figure 60 shows ABR data for two chinchillas exposed to blast of 2.2 and 5.7 psi. In this graph, the red line shows the ABR signal prior to blasting, the green line shows one week post blast, and the purple line shows three weeks post blast. These ABRs show the signal measured for a 4 kHz tone pip into the ear at 70 db SPL. In the top graph (2.2 psi blast) the ABR signal is almost entirely absent one week post blast, but a significant recovery is seen two weeks later. Note, however, that the amplitude of Wave I of the ABR in the 2.2 psi condition had not fully recovered to pre-blast levels, perhaps indicating synaptopathy (i.e., 'hidden hearing loss'), or a reduction in the number of auditory nerve fibers. In the bottom graph (5.7 psi) the ABR signal has entirely disappeared after the blast, and showed no signs of recovery even after three weeks.

4.2.2.8 Distortion product otoacoustic emissions

Figure 61 shows the level of the DPOAEs in two chinchillas (the same two chinchillas as were shown for the previous ABR measurements) before and after exposure to blast. The left figure shows a chinchilla exposed to 2.2 psi, while the right figure shows one exposed to 5.7 psi. The red

line shows data acquired before the blast, orange shows immediately after the blast, green shows one week post blast, and purple shows three weeks post blast. The solid lines shows the level of the DPOAEs, dotted lines shows the noise level. Exposure to 2.2 psi shows a small change in the level of the DPOAEs of ~10–20 dB for frequencies >2 kHz. DPOAE levels remain above the noise at all points before and after the blast. Exposure to 5.7 psi shows a more dramatic change in the level of the DPOAEs. Immediately following the blast, the DPOAEs are not visible above the noise, and no recovery is seen after three weeks.

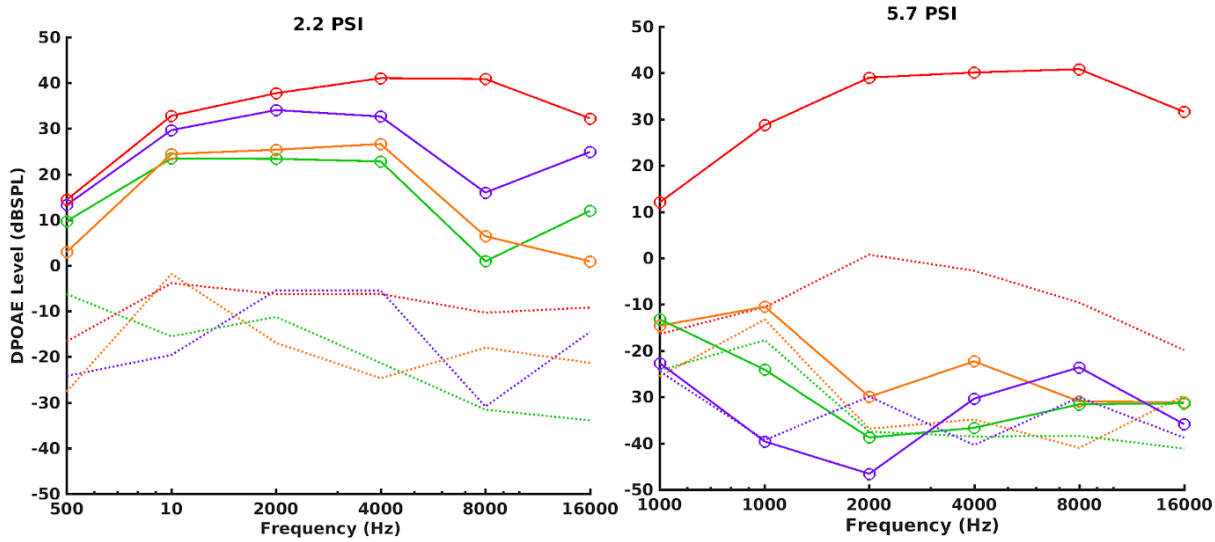

Figure 61. Level of the DPOAEs in two chinchillas before and after exposure to blast

4.2.2.9 Histological estimation of hair cell loss

Loss of hair cells was assessed in chinchillas exposed to shock waves and allowed to recover for at least three weeks. Sections of basilar membrane were isolated from the base, the middle, and the apical turns of each cochlea, and stained with phalloidin, etc., to stain for intact hair cells and synapses (Figure 62). Hair cell counts, estimates of hair cell losses for inner hair cells (IHCs), and each of the three rows of outer hair cells (OHCs) were correlated with shock wave exposure level.

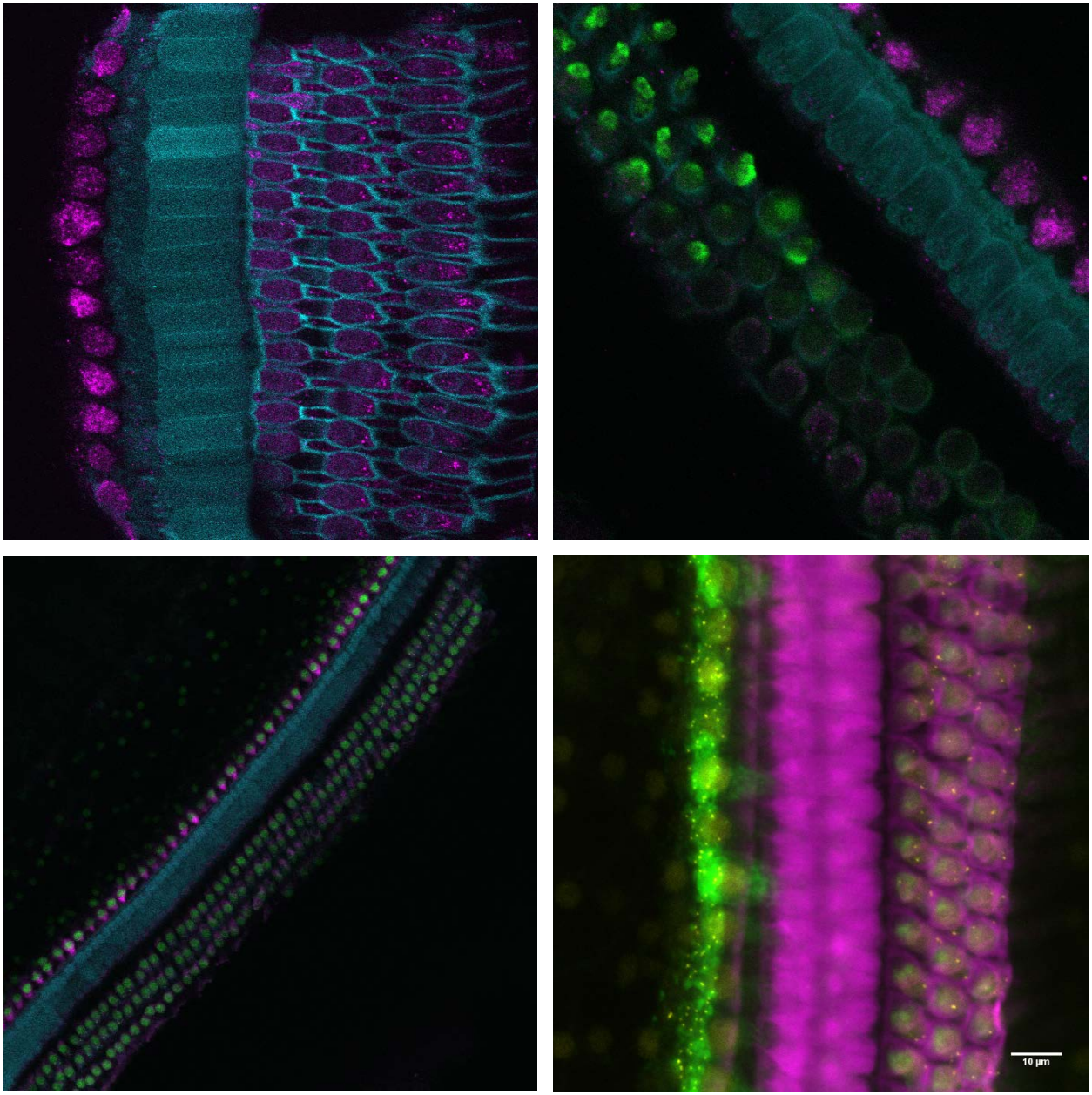

Figure 62. Photomicrographs representing images of the cochlea in four representative animals.

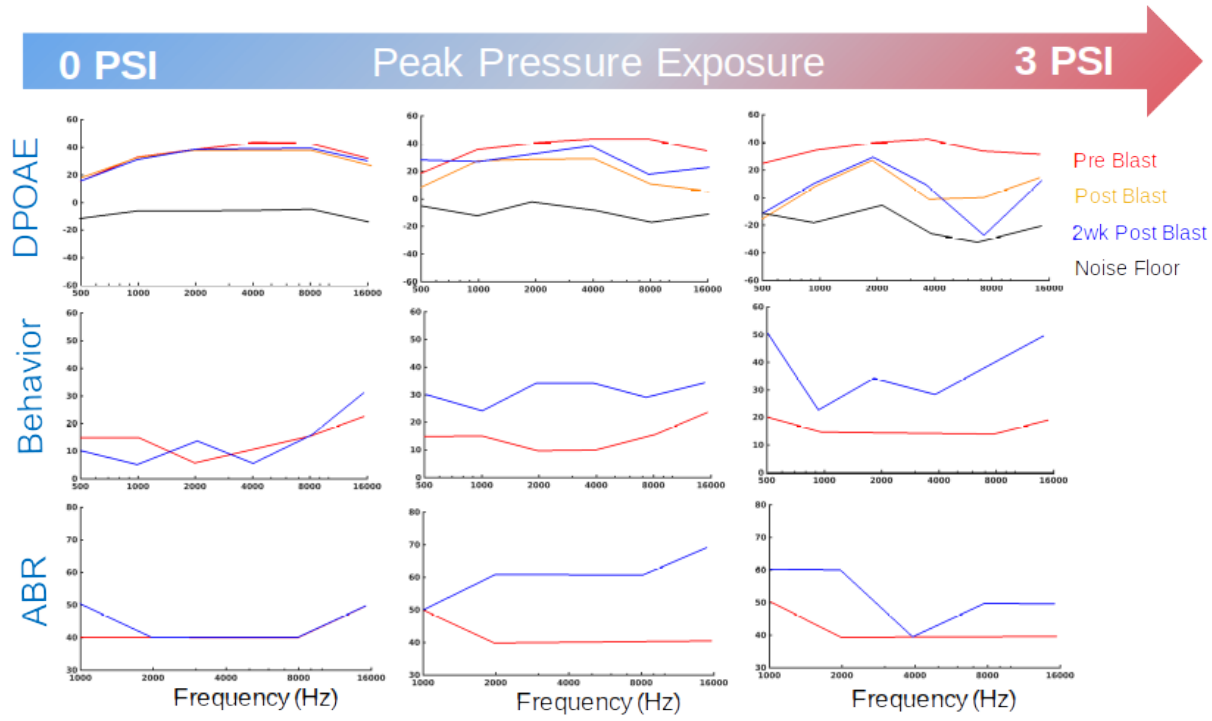

Figure 63. Outcome measure changes for three different chinchillas exposed to different levels of blast

The permanent change in perceptual hearing capabilities implies permanent blast-induced damage to the auditory periphery (e.g., hair cells, auditory nerve). Figure 63 (top row) shows example data of the level of the DPOAEs in the same three chinchillas before and after exposure to blast. The left column shows a control chinchilla exposed to 0.0 psi, while the middle and right figure shows one exposed to ~1–2 psi and >2 psi, respectively. The red line shows data acquired before the blast, orange shows immediately after the blast and blue two weeks post blast. The solid lines shows the level of the DPOAEs, black lines shows the noise level. Exposure to 1–2 psi shows a small change in the level of the DPOAEs of ~10–20 dB for frequencies >2 kHz. DPOAE levels remain above the noise at all points before and after the blast. Exposure to >3 psi shows a more dramatic change in the level of the DPOAEs. Immediately following the blast, the DPOAEs are not visible above the noise, and no recovery is seen after two weeks.

Figure 63 (middle row) shows behaviorally measured thresholds of hearing (in dB SPL) for brief tones as a function of frequency in three different chinchillas. These three animals summarize the functional changes to auditory characteristics as a function of blast exposure level (top arrow). The red curve shows baseline thresholds prior to blast exposure while the blue curve shows threshold measured after two weeks post exposure. The left column shows results for a control animal exposed to no blast (0 psi), but otherwise was subjected to all of the procedures necessary for blast exposure, showed no changes in hearing threshold as expected. Animals exposed to ~1–2 psi exhibited shifts in threshold of ~15 dB SPL across the frequencies tested. An animal exposed to ~>3 psi exhibited shifts in threshold ranging from ~20 dB at low to ~50 dB or more for high frequencies. Collectively, the results suggest that exposures >~2 psi can produce permanent hearing loss in chinchilla the magnitude of which appears to scale with increasing exposure above ~1 psi.

Together, the results above (along with data not shown) imply that substantial damage to the hair cells begins to occur by exposures of at least ~1–2 psi and predict modest increases in hearing thresholds of ~10–20 dB SPL. Exposures >~3 psi produce more severe damage, the magnitude of which appears to scale with exposure level (e.g., increased exposure level leads to increased hearing loss). These results are consistent with the observed changes in perceptual hearing thresholds observed above for comparable exposure levels. A signature of this damage would also be expected to be seen in the responses of the auditory nerve fibers, as assessed by the ABR.

Finally, Figure 63 (bottom row) shows ABR threshold data. In this graph, the red line shows the ABR signal prior to blasting and the blue line shows two weeks post blast. As expected, ABR thresholds are comparable in the control animal (left column). For higher blast exposure levels, there is an increase in ABR thresholds that is generally comparable to the increases seen in the DPOAEs and the behavioral audiogram

4.2.2.10 Dose-response function development

Hearing loss dose-response curves (DRCs) were estimated by fitting logistic functions to each of the behavioral, physiological, and histological estimates of auditory function degradation described in Sections 4.2.2.1-4.2.2.9. DRCs were estimated by fitting (least squared) a four-parameter logistic function of the form:

$$f(x) = ymax - \frac{ymin - ymax}{1 + e^{-(x-a)/b}} \quad (14)$$

where ymax and ymin represent the upper and lower asymptotes, a represents the center point, and b represents the steepness of function. This function was fit to each datasets using the MATLAB (Mathworks) curve fitting toolbox. Data were calculated as the change in each response, at each measured time point, for each frequency, relative to the baseline (pre-exposure) measurement. In each case, ymin and ymax were set to reasonable values, and *a* and *b* left as free parameters. The log-transformed peak pressure of the shock wave was used as the independent variable. Below, DRC estimates are shown for each parameter. Markers indicate individual data points, and colored lines indicate the estimated DRC for the data at each corresponding frequency. Two plots (rows) are shown for each time point (columns) collected, representing hearing loss and proportion of normal function as a function of exposure level.

4.2.2.10.1 Behavioral thresholds

Behavioral responses were estimated at the beginning and end of data collection (four weeks after exposure) due to the amount of time required for data collection. Figure 64 shows dose response functions for behavioral thresholds, estimated with ymin set to zero (no change), ymax set to 120 dB SPL (profound hearing loss), and for each frequency tested (colors). Audiometric thresholds typically declined with increasing exposure level such that DRCs showed a 50% decrease by ~5–10 psi peak pressure at all frequencies.

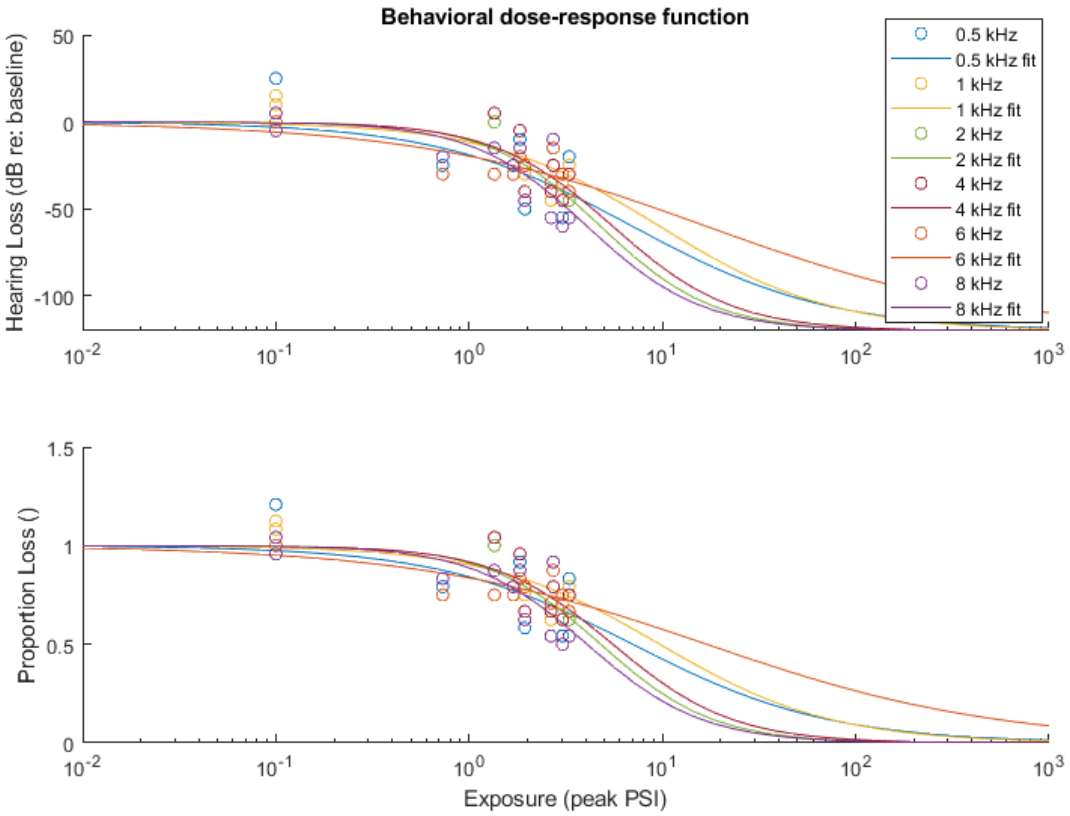

Figure 64. Dose response functions for behavioral thresholds

4.2.2.10.2 ABR thresholds

ABR response thresholds were estimated at the beginning and at one, two, and three weeks after shock wave exposure. Figure 65 shows DRCs estimated for changes in ABR thresholds following exposure. ABR DRCs were estimated with ymin set to zero (no change), ymax set to 120 dB SPL (profound hearing loss), and for each frequency tested (colors). ABR data tended to be noisier and thresholds therefore more variable, thus DRC estimates were less consistent than behavioral DRCs.

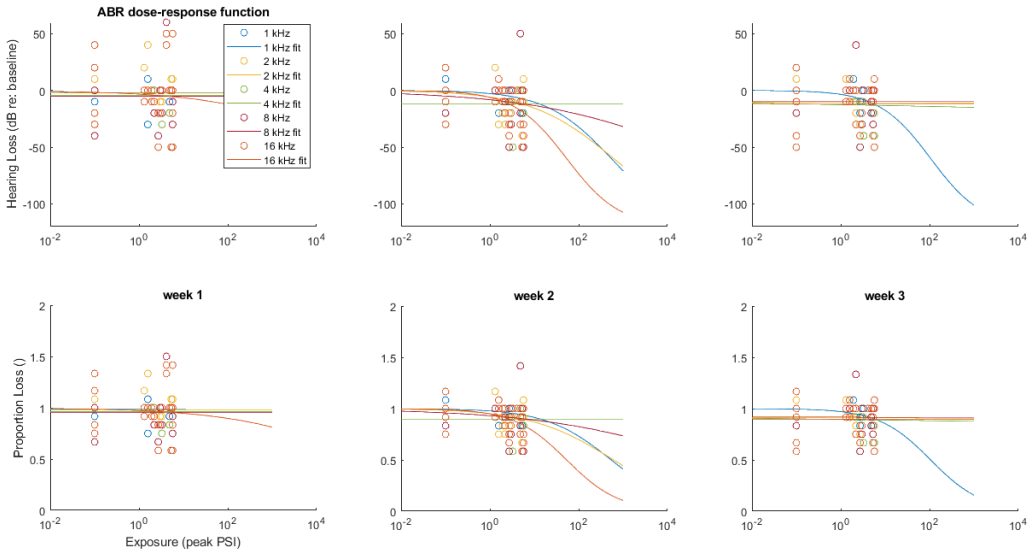

Figure 65. Dose response functions for auditory brainstem responses

4.2.2.10.3 DPOAE thresholds

DPOAE response thresholds were estimated at the beginning and at one, two, and three weeks after shock wave exposure. Figure 66 shows DRCs estimated for changes in DPOAE thresholds following exposure. DPOAE DRCs were estimated with ymin set to zero (no change), ymax set to 100 dB SPL (profound hearing loss), and for each frequency tested (colors). DPOAE data tended to be noisier and thresholds therefore more variable, thus DRC estimates were less consistent than behavioral DRCs, but more consistent than ABR threshold data. Notably, DPOAE DRCs tended to show steeper slopes in Weeks 1 and 2 than in Week 3, suggesting functional recovery.

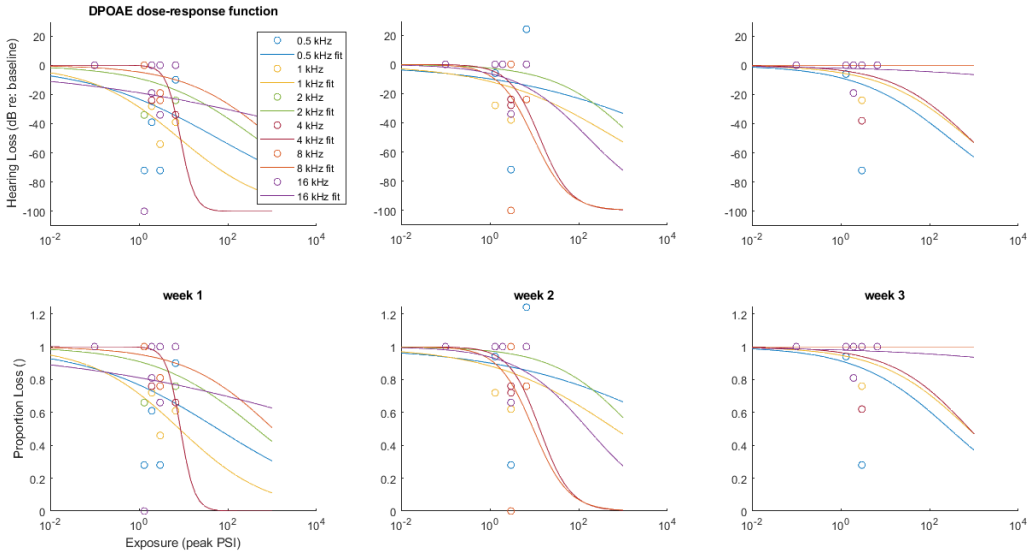

Figure 66. Dose response functions for distortion product otoacoustic emissions

4.2.2.10.4 Histological estimates of hair cell loss

The proportion of inner and outer hair cells surviving at the end of each recovery period (four weeks) was assessed in at least three positions along the cochlea, roughly near the base, the middle, and near the apex of the cochlear spiral (corresponding to high, mid, and low-frequency sensitive regions). Figure 67 shows dose response functions for both inner (blue) and outer (red) hair cell survival, for basal, mid, and apical cochlear sections. The majority of available data are from basal (high frequency) sections. The basal and mid OHC DRCs estimate a 50% survival at ~3–10 psi, whereas IHC DRCs show much higher survival rates (50% > 100 psi), likely due to insufficient data to make an informed estimate.

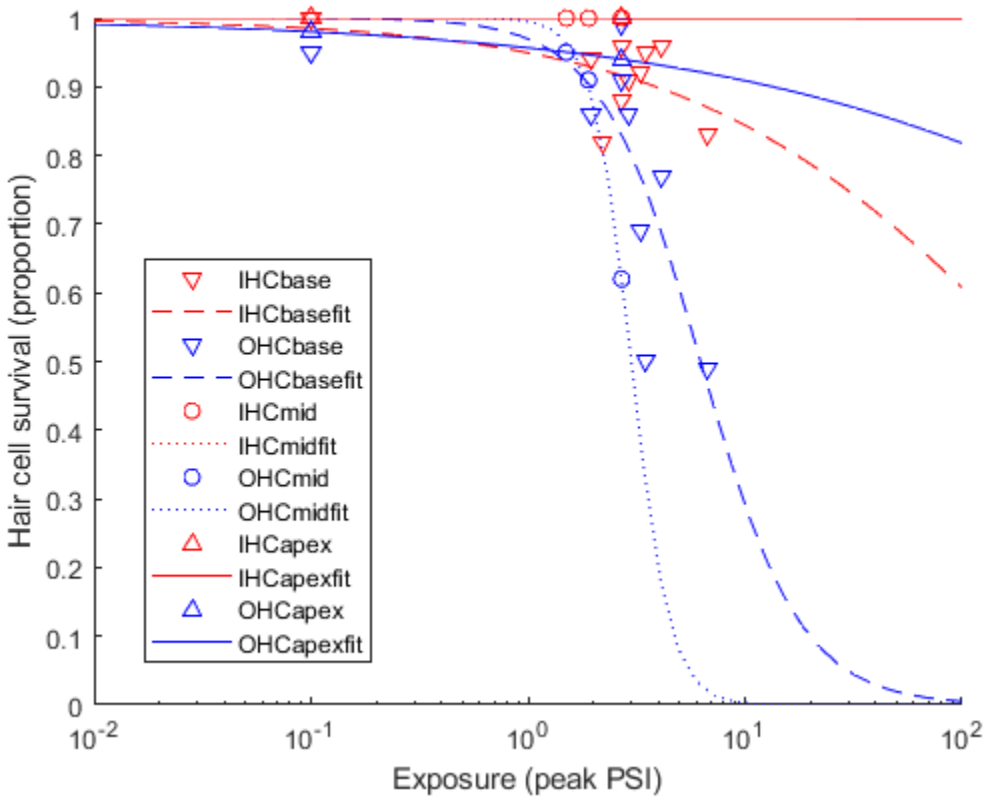

Figure 67. Inner and outer hair cell dose response functions.

4.2.2.11 Hearing loss model development

Estimates of human hearing loss for a given noise exposure were made using the chinchilla to human transfer function, and the DRCs (particularly for hair cell loss) defined above. Briefly, we begin with the assumption that scala vestibuli pressure drives hearing loss. We estimate scala vestibuli pressure in the human ear above, and to estimate hearing loss, with the exposure level that would generate an equivalent scala vestibuli pressure in the chinchilla cochleae must be determined. Hearing loss may then be estimated using the chinchilla dose-response functions described above.

4.2.2.11.1 Human and chinchilla middle ear transfer functions

To determine the exposure required to generate the observed human scala vestibuli pressures (PSV) in the chinchilla requires knowledge of the chinchilla middle ear transfer function (HME) since it directly relates scala vestibuli (PSV) into the ear canal pressure (PEAC).

Where:

$$PSV_{Ch} = HME_{Ch} \times PEAC_{Ch} \quad (15)$$

$$PSV_{H} = HME_{H} \times PEAC_{H} \quad (16)$$

We determined the nonlinear, level-dependent middle ear transfer function for humans, HME_H, above; however, have not performed the same analysis in the chinchilla, thus have not calculated HME_{Ch}. If we apply the same exposure to both human and chinchilla ears, PEAC,

$$PEAC = \frac{PSV_{Ch}}{HME_{Ch}} = \frac{PSV_{H}}{HME_{H}} \quad (17)$$

Rearranging thus yields the level-dependent relationship between chinchilla and human PSV, the chinchilla to human transfer function, H_{Ch2H}:

$$H_{Ch2H} = \frac{PSV_{Ch}}{PSV_{H}} = \frac{HME_{Ch}}{HME_{H}} \quad (18)$$

We assume that scala vestibuli pressure drives the observed hearing loss, as it represents the input to the cochlea, thus if we instead set the human and chinchilla PSV equal to one another we may relate the equivalent $PEAC_{Ch}$ exposure required to elicit the observed PSV_H by dividing by H_{Ch2H}:

$$PEAC_{Ch} = \frac{PSV_{Ch}}{HME_{Ch}} = \frac{PSV_{H}}{HME_{Ch}} \quad (19)$$

From this relationship it is relatively straightforward to show that the ear canal sound pressure levels in the chinchilla may be found by scaling the ear canal exposure level in humans by the chinchilla to human transfer function:

$$PEAC_{Ch} = PEAC_{H} \times \frac{1}{H_{Ch2H}} \quad (20)$$

Thus the equivalent chinchilla exposure, $PEAC_{Ch}$, is thereby found by simply multiplying the human exposure, $PEAC_H$, by the inverse of the chinchilla to human transfer function, H_{Ch2H}.

4.2.2.11.2 Chinchilla to human transfer function, H_{Ch2H}

The inner ear model assumes that the PSV exposure in chinchilla resulting in hearing loss (manifesting as any of the above measures; e.g., hair cell loss) will produce a comparable hearing loss in the human PSV; however, the transmission of sound to the chinchilla and human inner ears differs substantially, as we have revealed experimentally. The chinchilla to human transfer function, H_{Ch2H}, specifies the relationship between chinchilla and human PSV at equivalent PEAC exposure levels.

Figure 68 shows the time (left) and frequency (right) domain representations of waveforms, representing the output of each major stage of the model. The incident wave, an 8-psi peak overpressure shock wave recorded in the ARA mobile shock tube, was used as input to the model. The external ear model then estimated the sound pressure level at the tympanic membrane in the human ear canal (EAC), and the middle ear model estimated the sound pressure level in the human scala vestibuli (HSV). A discrete Fast Fourier Transform (FFT) was applied to each of these waveforms to obtain the frequency-domain representation of each signal.

The chinchilla scala vestibuli pressure (CHSV) was set equal to the human scala vestibuli pressure (HSV), and the chinchilla ear canal exposure (CHEAC) estimated by scaling the EAC pressure at each frequency with the inverse of H_{Ch2H}, as described below.

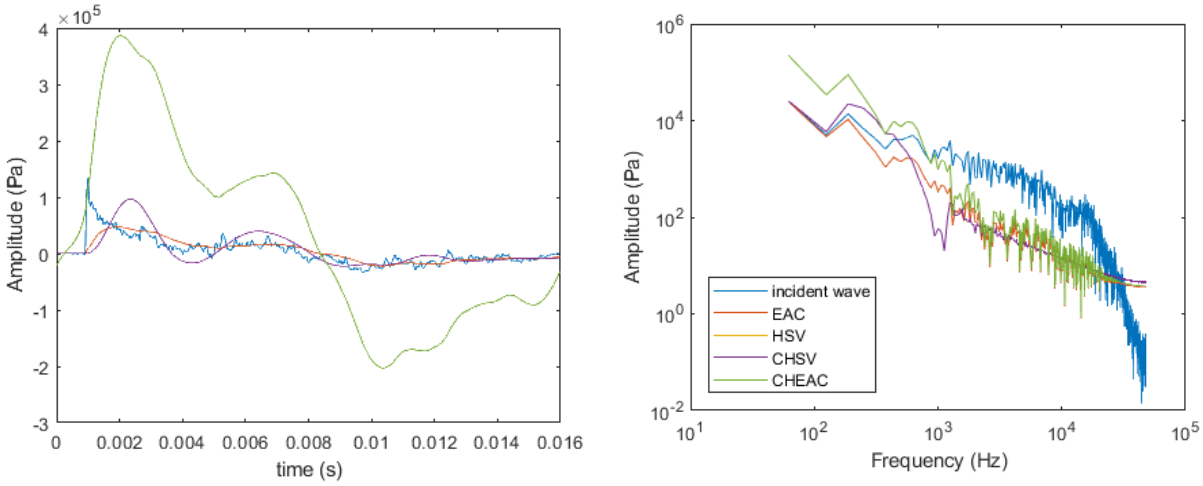

Figure 68. Time and frequency domain representations of the incident wave input, and modeled ear canal (EAC), human scala vestibuli (HSV), and chinchilla scala vestibuli (CHSV) pressures.

H_{Ch2H} was estimated by fitting a sigmoidal function, to the PSV_{SV}/PSV_H vs frequency responses shown above in Figure 52A, of the form:

$$f(x) = ymax - \frac{ymin-ymax}{1+(a/x)^b} \quad (21)$$

where:

$$x = \log_{10}(EAC)+1 \quad (22)$$

The fit (least squares) was performed using the MATLAB curve fitting toolbox by first log-transforming the human-chinchilla ratio data (and adding 1), setting ymax to 1, ymin set to 0, and leaving a and b free to be set by the fitting algorithm. A scaling factor (H) for each frequency present in the frequency representation of HSV is defined by Equation 23:

$$H(SPL) = 1 / 10^{((1-\frac{(0-1)}{1+(a/x)b})-1)} \quad (23)$$

where

$$x = abs(EAC/nfft) \quad (24)$$

The result is a scaling factor (H) that varies between 1 and 10 that represent the frequency dependent ratio between HSV and CHSV at each frequency present in the EAC. For the above

8-psi incident peak pressure exposure the scale factors present are shown in Figure 69 (circles), along with the hypothetical scale factor at all possible EAC SPLs (black line).

To convert the HSV to CHSV pressure, each frequency component of the HSV was simply multiplied by the appropriate scale factor. The time domain waveform of the CHSV was then calculated with a discrete inverse-Fast Fourier Transform (Figure 68). Finally, auditory function is estimated by applying the calculated CHSV to the DRCs estimated in the prior section.

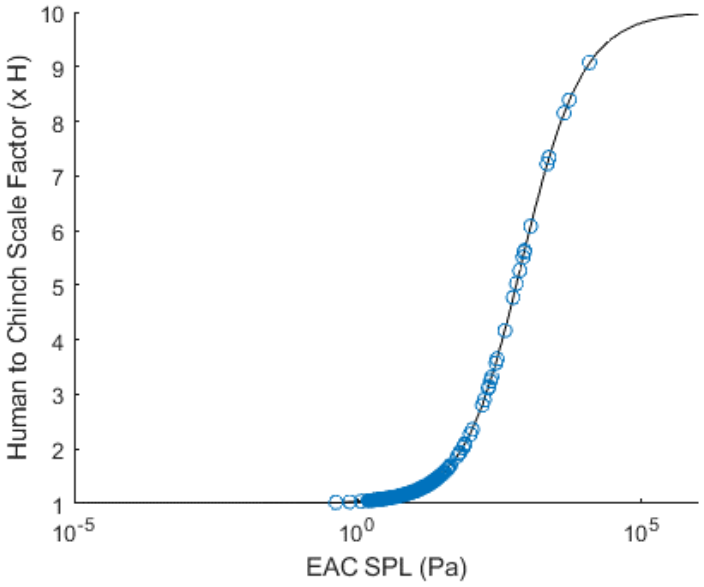

Figure 69. Human to chinchilla scaling factor (i.e., CHSV to HSV ratio) at each frequency calculated by the FFT, dependent upon the SPL in the EAC.

4.2.2.11.3 Hair cell function estimation

To demonstrate the application of the calculated CHSV to estimating degradation in auditory function, we have applied estimates of degraded hair cell function to an existing phenomenological model of auditory nerve function. This model includes parameters that specify inner and outer hair cell function from 1 (normal), to 0 (no remaining function). To calculate these values, we used the DRC calculated in Figure 67. For simplicity, we used the DRC from outer hair cells (OHCs) near the base of the cochlea (baseOHC) for estimates of both OHCs and IHCs (after shifting upwards in level). specifically, outer (cohc) and inner (cihc) hair cell functions were calculated as:

$$cohc(x) = 1 - \frac{1}{e^{-(x-ohca)/ohcb}} \quad (25)$$

$$cihc(x) = 1 - \frac{1}{e^{-(x-ihca)/ihcb}} \quad (26)$$

where:

$$x(f) = \log_{10}(\text{cumulative sum}(PCHSV(f))) \quad (27)$$

PCHSV is the magnitude of the amplitude spectra of the calculated chinchilla scala vestibuli pressure, *ohca* and *ohcb* represent the *a* and *b* parameters for the OHC fit, and *ihca* = *ohcb*+0.25 and *ihcb* = *ohcb*. Results of the 8-psi exposure from above are shown in Figure 70, which shows the hypothetical OHC (blue) and IHC (red) functions as a function of SV pressure (solid lines), and the values of the calculated *cohc* and *cihc* for each frequency component (dots). These

functions thus estimate that OHC function will be degraded by up to ~90%, and IHC function degraded by ~75% for a single, 8-psi exposure.

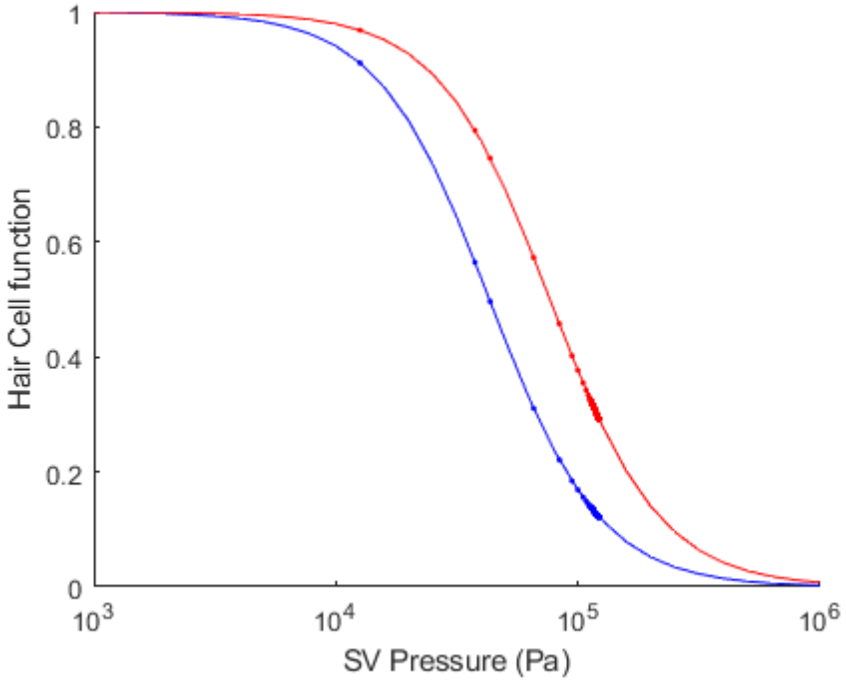

Figure 70. Estimate of human hair cell survival for an 8-psi exposure

4.2.2.12 Auditory nerve model

A phenomenological model of auditory nerve function, developed by colleagues at the University of Rochester, McMaster University, and the University of Malay, was chosen to form the basis of our inner ear model.

4.2.2.12.1 Hair cell degradation

Dose response functions are used to determine the proportion of inner (cihcs) and outer (cohcs) hair cell function remaining, between 1 (normal) to 0 (no function).

Estimates were made of a and b for the IHC and OHC logistic fits, and a simple function created to determine the cihcs (inner hair cell) and cohcs (outer hair cell) remaining function parameters, for each auditory nerve fiber frequency (CF), given an applied stimulus. The function takes in three parameters: (1) the auditory nerve fiber CFs to be modeled; (2) the exposure frequencies; and (3) the exposure SPLs of the stimulus applied. cihcs and cohcs may thus vary as a function of frequency.

Auditory nerve output is then simulated. Figure 71 shows results for three exposure levels, roughly sampling the effects of OHC function reductions of 10%, 50%, and 90%: peak pressures at 1 psi, 6 psi, and 35 psi. Responses after a 1-psi exposure show little change relative to baseline (not shown), thus the mean-rate neurogram (left) shows a reasonably robust representation of the audiogram (top). For a 6-psi exposure, the neurogram representation has lost some of its high-frequency information, and the response is a bit more “smeared” spectrally. The 3-psi exposure response has lost most of the response altogether, suggesting a profound hearing loss.

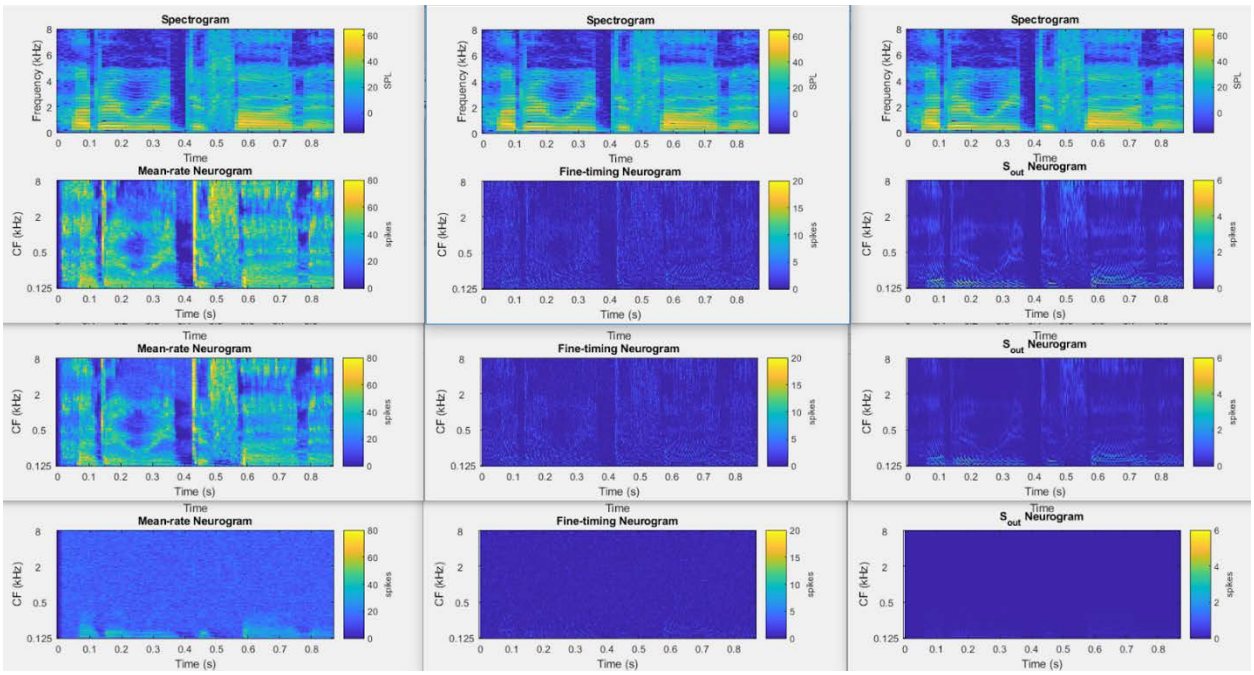

Figure 71. Example neurograms for an undamaged and damaged cochlea.

4.2.2.12.2 Acoustic waveform reconstruction

Finally, the acoustic waveform is reconstructed from the neurogram to determine the effect of legibility of the speech waveform via the speech intelligibility index (SII). Waveform reconstruction is performed using an inverse short-time Fourier transform, with the neurogram providing the amplitude spectra, and the original spectrogram providing the phase spectra. Waveforms may then be assessed for legibility, and deficits relative to the unexposed, full function model output are determined, thereby provide a direct estimate of speech reception threshold shifts expected from a given noise exposure. This, and similar functional metrics of hearing loss are expected to better correlate with operationally relevant performance than more basic estimates of hearing loss, such as displacement or strain along the basilar membrane.

4.2.2.12.3 Integration into the Blast Auditory Model (BAM)

Each of the model module described above are combined to form the foundation of the BAM. BAM is thus a phenomenological model of sound exposure that produces anatomical, physiological, and behavioral estimates of hearing loss. These results may then be directly compared with laboratory measurements to develop and validate model predictions.

4.3 Specific Aim 3: Development of a Hearing Protection Evaluation Protocol

A hearing protection evaluation protocol was developed to instruct the hearing protection community on the method for testing and modeling hearing protection devices using the BAM. The protocol outlines the hearing protection module development, testing methods, and combination of the model and data to produce predictions of hearing protection device performance. The protocol in its entirety is included as Appendix 2: Hearing Protection Evaluation Protocol to this report.

4.4 Next Steps

We believe that the results of the effort described in this report provide a clear framework for a hearing loss model to replace the AHAAH in damage risk criteria; however, there are several clear steps that should be taken to (1) further develop and validate BAM predictions and (2) to extend the model to make results more meaningful and universal.

1. Additional animal experiments to improve dose-response estimates
    a. Investigate changes in ABR and DPOAE response morphology in addition to simply changes in response thresholds
    b. More sophisticated histological preparations to investigate synaptopathy
    c. Perform studies at higher exposure levels
    d. Perform studies with multiple exposures
2. Validate model predictions against existing and retrospective reviews of hearing loss
3. Incorporate synaptopathy into the model auditory nerve to predict hidden hearing loss
4. Incorporate models of ABR, auditory brainstem, and auditory perception as model outputs

5 Training and Professional Development Opportunities

Nothing to report.

6 Dissemination of Results to Communities of Interest

Results from this research were disseminated to the following scientific communities:

- Military health science community – Podium and poster presentations at the Military Health System Research Symposium
- General acoustics community – Podium and poster presentations at meetings of the Acoustical Society of America, peer-reviewed manuscripts
- Otolaryngology research community – Podium and poster presentations at the Association for Research in Otolaryngology meetings, peer-reviewed manuscripts
- Experimental mechanics community – Podium presentation at the Society for Experimental Mechanics
- Military blast injury community – Podium presentation at the first Japan-U.S. Technical Information Exchange Forum on Blast Injury
- Middle ear research community – Podium and poster presentations at the Middle Ear Mechanics in Research and Otology, peer-reviewed manuscripts

7 Plans for the Next Reporting Period

Nothing to report.

8 IMPACT

8.1 What was the impact on the development of the principal discipline(s) of the project?

Hearing loss and tinnitus are the top two diagnoses among Service Members of Operations Enduring Freedom and Iraqi Freedom (U.S. Department of Veterans Affairs, 2012). They are also the most prevalent disabilities recorded for Service Members who served during World War II, the Korean Conflict, the Vietnam Era, and during peacetime periods. Among Veterans, impairment of the auditory system is consistently documented as the second most prevalent bodily system injury after musculoskeletal disabilities. Service-connected disability for hearing loss and tinnitus

continues to rise annually, as does the total amount spent on these disabilities (U.S. Department of Veterans Affairs, 2012). Estimates approach $1.2 billion of entitlement for compensation and care of hearing loss and auditory system injuries in over 1.8 million Veterans in 2012 alone (U.S. Department of Veterans Affairs, 2012). Despite efforts to emphasize and improve military hearing conservation programs (HCPs), between 10% and 18% of Service Members enrolled in such programs annually have been diagnosed with significant threshold shifts in their hearing, representing a prevalence of two to five times higher than rates in comparable civilian, industrial HCPs (Groenewold, 2011). The majority of these injuries, and the costs associated with the injury, can be mitigated with the design and use of proper hear protection devices.

The specific aims of the program are to develop a neuro-functional understanding of acoustic injury through modeling and experimental testing. Cadaveric human whole heads were instrumented with pressure sensors and strain gauges, and the heads were exposed to high-level shock waves with and without hearing protection. Insertion loss was calculated from conditions with hearing protection, relative to exposures without protection. The hearing protection model was then developed in the MathWorks Simulink programming environment. For estimations of hearing loss, the chinchilla model was successfully used to develop a chinchilla-to-human transfer function for the pressures in the scala vestibuli allowing the animal model to be used to understand the human physiological response to blast. As a result, DPOAEs to infer outer hair cell loss in response to a human relevant blast exposure in chinchilla were measured. This and the electrophysiological 'audiograms' via the auditory evoked brainstem response measured in chinchilla allowed the establishment of a threshold for hair cell loss that is clinically based and whose operational and long term effects can be quantified through the use of the auditory never model being incorporated into the BAM model. In the existing models such as AHAAH, the loss of hair cells is inferred from theoretical strain predicted in the basilar membrane instead of measured hairless loss in response to blast exposure in this program.

Once the BAM model is validated for performance across all military exposure levels, the model can be used as a tool whose output is clinically relevant. This model can then be used for exploring the relationship between high-intensity noise exposures and resulting deficits to assess the level of protection provided by a variety of hearing protection devices for multiple weapons systems. The availability of a clinically relevant tool than can be used to assess multiple weapon systems and scenarios provides the commanders and decision makers the ability to selection or require the design of, the optimal protection device for the military event.

8.2 What was the impact on other disciplines?

Concurrent injuries to the auditory system as a result of acute blast trauma and resultant traumatic brain injury (TBI) accounted for one-quarter of all injuries among marines during Operation Iraqi Freedom (Gondusky and Reiter, 2005). Blast-related TBI produces significantly greater rates of hearing loss and tinnitus compared with non-blast-related TBI, affecting up to 60 percent of these patients (Lew et al., 2007). In addition, a considerable population of blast-trauma patients with central auditory system injury may have been misdiagnosed because of the lack of assessment criteria for this population and because of logistical testing difficulties with polytrauma patients.

Through the modeling and experimental testing conducted in this program, alternative pathways allowing energy to be transmitted into the inner ear and potentially into the brain tissue itself have been identified. The strain measurements in the whole head experiments have shown that the strain in temporal bone and the pressure in the inner ear region increase prior to the arrival of measured dynamic changes in the middle ear. If the energy is being transmitted through the temporal bone

it is possible similar energy is being transmitted through the frontal, occipital and other bones of the skull increasing the risk of blast induced neurological injury. Additionally the identification of changes in auditory processing associated with blast in the chinchilla model that has been calibrated to a human equivalent exposure to eventually help differentiate auditory process disorders from symptoms identified with traumatic brain injury.

8.3 What was the impact on technology transfer?

Previous codes were written in obsolete programming languages that were difficult to interpret and update as the knowledge of the community advanced. The BAM model and supporting code has been written in the popular MATLAB programming code. This was a conscious decision so that the code can be either used in the native MATLAB format or exported to C++. Because of this decision other in the community will be able to use the code without needing to use LS-Dyna or other finite element codes that required extensive training to use. Additionally with the interface between the enhanced AHAAH model that predicts the mechanical response of the auditory system with the detailed physiological mode of the auditory-nerve fiber a useful tool for testing our understanding the underlying mechanical and physiological processes in the auditory periphery after expose to high intensity noise.

8.4 What was the impact on society beyond science and technology?

The foundation of the program was modeling supported by extensive experimental testing that included PMHS and anesthetized animal testing. As a result of this approach a robust methodology for the evaluating the performance of hearing protective systems across the broad range of intensities and frequency spectra seen in real-world exposures was developed. The BAM model ultimately developed takes into account the nonlinear effects that are inherent in current hearing protection but were lacking in previous models. The approach taken in this program can be applied to the mitigating the other effects of blast overpressure exposure in the military such as blast induced traumatic brain injury using the appropriate human and animal models.

9 ACCOMPLISHMENTS

Table 7 is the contractually required SOW for the program. All of the listed accomplishments below were completed within the period of performance for the program.

Table 7. Statement of Work

Description
Specific Aim 1: Develop a neuro-functional understanding of acoustic injury encompassing the dynamics of the peripheral auditory system, through sensory transduction, to central auditory processing.
Major Task 1: Measurement and Simulation of Blast Overpressure Wave through the External Auditory Canal
Subtask 1: Submit documents for local IRB review
Subtask 2: Submit IRB approval and necessary documents for HRPO review
Milestone #1: HRPO approval received
Subtask 3: Measurement of blast on PMHS at CU Health Science Center • Walilko's team will provide instrumentation, data collection, and data analysis • Tollin's team will provide facilities for testing and surgical expertise for preparation of eight specimens

Description
Milestone #2: Co-author manuscript on result of blast on PMHS
Subtask 4: Fabrication of shock wave emulators ● Argo's team will design and build the improved shock wave emulator ● Tollin's team, with Easter consulting, will determine specifications for the shock wave emulator and will provide suitable test facilities
Subtask 5: Improve EAC and HPD response within AHAAH ● Argo will integrate hearing protection into the AHAAH model ● Walilko, with Easter consulting, will integrate the improved EAC into the AHAAH model
Milestone #3: Improved EAC and HPD inclusion in the AHAAH model
Specific Aim 2: Develop an animal model, correlating human and animal auditory mechanisms and physiological responses to noise and blast events.
Major Task 1: Quantifying Middle Ear Dynamics using Both PMHS and Chinchilla Models
Subtask 1: Submit documents for local IACUC review
Subtask 2: Submit documents for local IRB review
Milestone #4: Local animal/human use approvals received
Subtask 3: Submit documents for ACURO review
Subtask 4: Submit documents for HRPO review
Milestone #5: Sponsor animal/human use approvals received
Subtask 5: Characterization of PMHS middle ear response ● Walilko/Argo's team will guide PMHS studies and provide instrumentation and data collection/analysis support ● Tollin's team, with Easter consulting, will perform LDV measurements on 12 PMHS temporal bones
Milestone #6: Co-author manuscript on result of temporal bone testing
Subtask 6: Quantify chinchilla middle ear response ● Walilko's team will guide chinchilla studies and provide instrumentation and data collection/analysis support ● Tollin's team will perform LDV measurements on chinchilla middle ear
Milestone #7: Author manuscript on result of chinchilla middle ear tests
Subtask 7: Address non-linearities of AHAAH middle ear ● All co-PIs will assist in integration of nonlinear elements into the AHAAH model
Milestone #8: Improved middle ear nonlinearity inclusion in the AHAAH model
Subtask 1: Measurements of auditory brainstem responses
Subtask 2: Measurements of otoacoustic emissions
Subtask 3: Histological determination of hair cell loss
Milestone #9: Author manuscript on result of chinchilla auditory response tests
Subtask 4: Predict damage correlated to central auditory function ● All co-PIs will analyze data and determine methods for inclusion into AHAAH
Milestone #10: AHAAH model with improvement to the audio processing portion of the algorithm
Specific Aim 3: Develop a robust, validated system for the evaluation of hearing protective systems across the broad range of intensities and frequency spectra seen in real-world exposures.
Major Task 1: Extending and Improving Performance of Auditory Hazard Model
Subtask 1: Develop new protocol for HPD testing ● Walilko will contribute laboratory space and experimental equipment and assist in data analysis ● Argo's team will develop test protocols and compare data to AHAAH model predictions
Milestone #11: AHAAH model correlated with experimental data on HPDs ready for distribution to stakeholders for evaluation

10 CHANGES/PROBLEMS

10.1 Changes in approach and reasons for change

Nothing to report

10.2 Actual or anticipated problems or delays and actions or plans to resolve them

Nothing to report

10.3 Changes that had a significant impact on expenditures

- Purchase of ANSI S12.42-compliant shock tubes were approved for both the University of Colorado and Applied Research Associates, Inc.
- Purchase of MATLAB modules was approved for Applied Research Associates, Inc.

10.4 Significant changes in use or care of human subjects, vertebrate animals, biohazards, and/or select agents

10.4.1 Significant changes in use or care of human subjects

Nothing to report

10.4.2 Significant changes in use or care of vertebrate animals

Our lab, along with others, have successfully measured behavioral responses to auditory stimuli using the pre-pulse inhibition (PPI) of acoustic startle paradigm in humans and also many common laboratory animals including mice, rats, and guinea pigs (Koch, 1999). Panel B shows an example of the startle behavior elicited by exposing a guinea pig to different startle sound SPLs. Startle response amplitude is measured as the RMS amplitude of the waveform recorded from an accelerometer mounted beneath the animal platform between 100–200 ms after the startle sound.

Guinea pigs startle reliably (e.g., large amplitude, inset of B, blue line) for intense startle SPLs (red, green and blue data points) but startle less for lower intensity stimuli (inset of B, red line). While there is some habituation in guinea pig startle amplitude from trial-to-trial, the overall trend of the responses are maintained—louder sounds produce larger startle than fainter sounds.

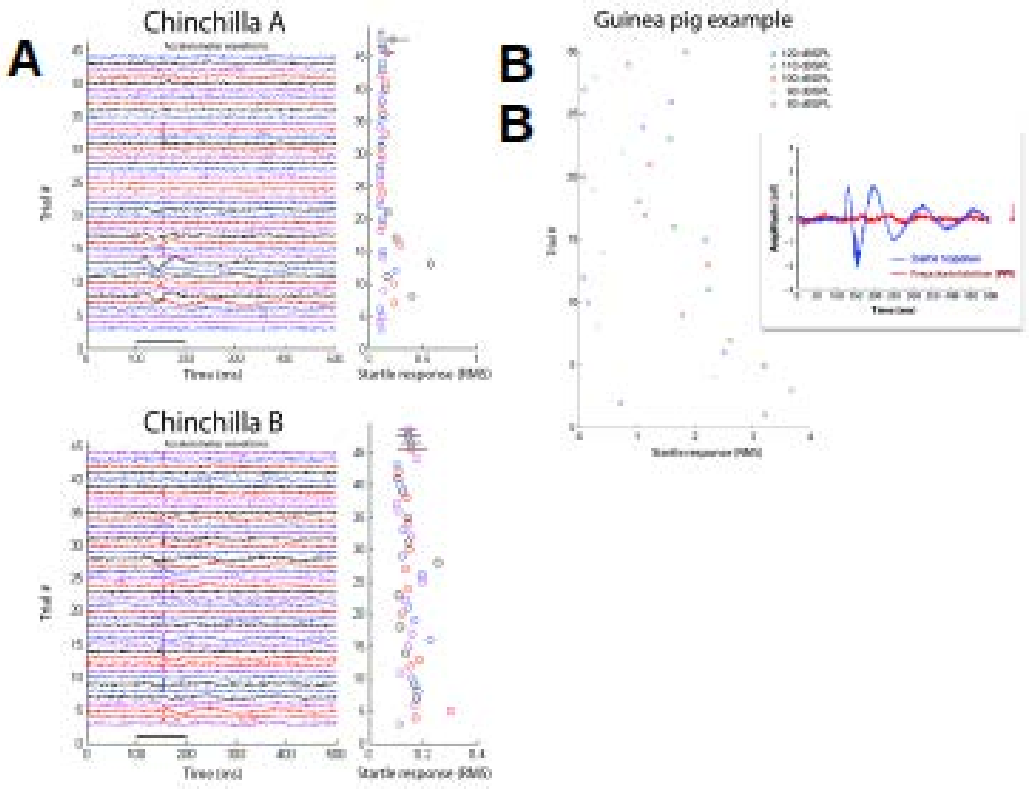

Figure 72. Startle behavior elicited by chinchilla and guinea pig.

Our attempts to use the startle response method in chinchillas produced variable, low-amplitude (unusable) responses. Results from two sessions with two different chinchillas are shown in panel A. In both animals, the overall amplitude of the startle is very low, about an order of magnitude less than that produced by guinea pigs using the same stimuli. In an attempt to overcome the lack of robust acoustic startle in chinchilla, a puff of air to the cheek was combined with the loud acoustic startle sound. Relative to control condition where no aversive startle stimuli (sound + air) were presented (purple traces and data points, indicating RMS amplitude in the 100–200 ms window), there was little increase in startle amplitude when the aversive startle stimuli were presented at different sound SPLs (other color traces and data points). In effect, chinchillas exhibit a lengthy freezing behavior which thwarts using startle response as a means to measure auditory perception in this species.

In response, we submitted an amendment to our current approved animal protocol. In the amended protocol we propose to implement instead an active avoidance behavioral paradigm to measure the audiogram, which is described in Section 4.2.2 of this report.

10.4.3 Significant changes in use of biohazards and/or select agents

Nothing to report

11 PRODUCTS

11.1 Publications, conference papers, and presentations

11.1.1 Journal publications

1. Greene, N. T., Alhussaini, M. A., Easter, J. R., Argo IV, T. F., Walilko, T., & Tollin, D. J. (2018). Intracochlear pressure measurements during acoustic shock wave exposure. *Hearing research*.
2. Peacock, J., Alhussaini, M. L., Greene, N. T., & Tollin. D. J. (2018). Intracochlear pressure in response to high intensity, low frequency sounds in chinchilla. *Hearing research. 367*:213-222.
3. Banakis Hartl, R. M., Mattingly, J. K., Greene, N. T., Farrell, N. F., Gubbels, S. P., & Tollin, D. J. (2017). Drill-induced cochlear injury during otologic surgery: intracochlear pressure evidence of acoustic trauma. *Otology & Neurotology, 38*(7), 938-947.
4. Greene, N. T., Jenkins, H. A., Tollin, D. J., & Easter, J. R. (2017). Stapes displacement and intracochlear pressure in response to very high level, low frequency sounds. *Hearing research, 348*, 16-30.
5. Maxwell, A. K., Banakis Hartl, R. M., Greene, N. T., Benichoux, V., Mattingly, J. K., Cass, S. P., & Tollin, D. J. (2017). Semicircular canal pressure changes during high-intensity acoustic stimulation. *Otology & Neurotology, 38*(7), 1043-1051.
6. Walilko, T. J., Lowe, R. D., Argo, T. F., Meegan, G. D., Greene, N. T., & Tollin, D. J. (2017). Experimental evaluation of blast loadings on the ear and head with and without hearing protection devices. *Mechanics of Biological Systems and Materials, 6*, 101-109
7. Hartl, R. M. B., Mattingly, J. K., Greene, N. T., Jenkins, H. A., Cass, S. P., & Tollin, D. J. (2016). A preliminary investigation of the air-bone gap: Changes in intracochlear sound pressure with air-and bone-conducted stimuli after cochlear implantation. *Otology & Neurotology, 37*(9), 1291.
8. Greene, N. T., Mattingly, J. K., Banakis, R. H., Tollin, D. J., & Cass, S. P. (2016). Intracochlear Pressure Transients during Cochlear Implant Electrode Insertion. *Otology & Neurotology, 37*(10), 1541-1548.
9. Mattingly, J. K., Greene, N.T., Jenkins, H.A., Tollin, D.J., Easter, J.R., & Cass S.P. (2015). Effects of Skin Thickness on Cochlear Input Signal using Transcutaneous Bone Conduction Implants. *Otology & Neurotology, 36*(8):1403-11.
10. Brown, A. D., Beemer, B. T., Greene, N. T., Argo IV, T., Meegan, G. D., & Tollin, D. J. (2015). Effects of active and passive hearing protection devices on sound source localization, speech recognition, and tone detection. *PloS one*, *10*(8), e0136568.

11.1.2 Books or other non-periodical, one-time publications.

Nothing to report

11.1.3 Other publications, conference papers and presentations.

1. Argo, T. F., Walilko, T., Tollin, D. J., Greene, N.T., & Easter, J.R. (2018, August). *A hearing protection device evaluation protocol for the auditory hazard assessment*

algorithm for humans. Presented at 2018 Military Health Science and Research Symposium (MHSRS), Kissimmee, FL.

2. Peacock, J., Greene, N. T., & Tollin, D. J. (2018, August). *Auditory trauma from blast: Measurements in chinchillas and how they compare to humans*. Presented at 2018 Military Health Science and Research Symposium (MHSRS), Kissimmee, FL.
3. Walilko, T., Greene, N. T., Argo, T. F., Easter, J. R., & Tollin, D. J. (2018, August). *Development of a new auditory injury model for quantifying inner ear damage mechanisms*. Presented at 2018 Military Health Science and Research Symposium (MHSRS), Kissimmee, FL.
4. Greene, N., Alhussaini, M., Easter, J., Tollin, D., Argo, T., & Walilko, T. (2018, July). *Stapes displacement and intracochlear pressure in response to high level, high frequency sounds*. Presented at the 8th International Symposium on Middle Ear Mechanics in Research and Otology, Shanghai, China.
5. Argo, T. F., Greene, N. T, Easter, J., Tollin, D. J., & Walilko, T. (2018, May 10). *Quantifying the insertion loss of hearing protection using a compressed gas shock tube*. Presented in a special symposium "Hearing Protection: Impulse Peak Insertion Loss, Specialized Hearing Protection Devices" at the 175th Meeting of the Acoustical Society of America, Minneapolis, MN.
6. Walilko, T., Tollin, D., Argo, T., & Easter, J. (2018, February 12). *Modeling the Middle Ear Dynamics that Results from Exposure to High Intensity Impulsive Noise*. Presented at the Association for Research in Otolaryngology Midwinter Meeting, San Diego, CA.
7. *Walilko, T., Argo, T., Greene, N., Tollin, D., & Easter, J.* (2018, February 2). *Progress of the Improvement and Extension of Auditory Hazard Models program*. Presented to Congressionally Directed Medical Research Programs (CDRMP) at Ft. Detrick, MD.
8. Tollin, D. J. (2018, February 24). *Mechanisms of auditory injury due to acoustic blast*. Presented to the National Center for Rehabilitative and Auditory Research (NCRAR) and Oregon Health and Sciences University (OHSU), Portland, OR.
9. Walilko, T.J., Argo, T.F., Meegan, D., Greene, N.T., & Tollin, D.J. (2016, August). *Quantifying the Nonlinear Characteristics of Hearing Protection Devices against Blast Overpressure*, Presented at Military Health Science and Research Symposium (MHSRS), Orlando, FL.
10. (*) Walilko. T., Lowe, R., Argo, T., Greene, N., & Tollin, D. (2016, June 6). *Experimental Evaluation of Blast Loadings on the Ear and Head Protected With Hearing Protection*. Keynote address at Society of Experimental Mechanics XIII International Congress, Orlando, FL.
11. (*) Walilko, T., Argo, T., Wiri, S., Maxwell, A., Greene, N., Tollin, D., VandeVord, P., Hulbert, L., & Zai, L. (2016, June 13). *Integration of Human and Animal Models to Systematically Evaluate Blast Loadings of the Neurological System*. Presented at Japan-USA Technical Information Exchange Forum on Blast Injury, Toyko, Japan.
12. Greene, N. T., Mattingly, J. K., Banakis Hartl, R. M., Tollin, D. J, & Cass, S. P. (2016, May 20). *Intracochlear Pressure Transients During Cochlear Implant Electrode Insertion*. Presented at the American Neurotology Society 51st Annual Meeting, Chicago, IL.
13. Banakis Hartl, R. M, Mattingly, J. K., Greene, N. T., Jenkins, H. A., Cass, S. P., & Tollin D. J. (2016, May). *Investigating the air-bone gap: Changes in intracochlear sound pressure with air- and bone-conducted stimuli after cochlear implantation*. Accepted at the American Neurotology Society 51st Annual Meeting, Chicago, IL.

14. Greene, N. T., Hussaini, M. A., Walilko, T. J., Argo, T. F., Easter, J. R., & Tollin, D. J. (2016, February 20). *Intracochlear Sound Pressure Levels during Acoustic Shock Wave Exposure*. Presented at the Thirty-ninth Annual Mid-Winter Research Meeting of the Association for Research in Otolaryngology (ARO), Vol 39, San Diego, CA.
15. Anbuhl, K. L., Greene, N. T., Ferber, A. T., Benichoux, V., Brown, A. D., & Tollin, D. J. (2016, February 20). *Temporary unilateral conductive hearing loss during development impairs auditory spatial discrimination ability and information processing in neurons of the inferior colliculus.* Submitted to the Thirty-ninth Annual Mid-Winter Research Meeting of the Association for Research in Otolaryngology (ARO), Vol 39, San Diego, CA.
16. Easter, J. R., Greene, N. T., Tollin, D. J., & Cass, S. P. *Stapes velocities and intracochlear pressures for differing modes of stimulation with an implantable middle ear hearing device*. Submitted to the Thirty-ninth Annual Mid-Winter Research Meeting of the Association for Research in Otolaryngology (ARO), Vol 39, San Diego, CA.
17. Banakis Hartl, R. M., Greene, N. T., & Tollin DJ. *Investigating the Weber phenomenon: Intracochlear sound pressure with acoustic and bone conducted stimuli*. Submitted to the Thirty-ninth Annual Mid-Winter Research Meeting of the Association for Research in Otolaryngology (ARO), Vol 39, San Diego, CA.
18. Greene, N. T. (2016, January 24). *Investigating the Mechanisms of Residual Hearing Loss Following Cochlear Implant Insertion*. Presented at the Ultimate Colorado Midwinter Meeting, Vail, CO.
19. Greene, N. T., Jenkins, H., Tollin, D. J., & Easter, J. (2015, July 1). *Ossicular chain motion during low frequency and high intensity sound stimulation*. In Abstracts of the 7th International Symposium on Middle Ear Mechanics in Research and Otology, Aalborg Denmark.
20. (*) Brown, A. D., Beemer, B. T., Greene, N. T., & Tollin, D. J. (2105, May 18). *Effects of active and passive hearing protective devices on sound source localization, tone detection, and speech recognition*. In Abstracts of the 169th Meeting of the Acoustical Society of America, Pittsburgh PA.

11.2 Website(s) or other Internet site(s)

Nothing to Report

11.3 Technologies or techniques

1. Development of a loudspeaker-based blast wave emulator
2. Development of techniques for measuring intracochlear pressures during very high-level noise and blast wave exposures

11.4 Inventions, patent applications, and/or licenses

Nothing to report

11.5 Other Products

The Blast Acoustic Model software was developed in Mathworks Simulink. The model is capable of predicting damage to the synapses and hair cells within the cochlea when exposed to blast with and without hearing protection.

12 PARTICIPANTS & OTHER COLLABORATING ORGANIZATIONS

12.1 What individuals have worked on the project?

Name: Ted Argo, Ph.D.

Project Role: Program Manager

Researcher Identifier: NA

Nearest person month worked: 12

Contribution to Project: Contributed to and reviewed quarterly and annual reports, planning meetings with subcontractors, development/review of test plans, acoustic modeling of blast wave emulator, construction and testing of blast wave emulator, scheduling of facilities and equipment, optimization of HPD module search algorithm, HPD evaluation protocol, scientific presentations

Name: Doug Meegan, Ph.D.

Project Role: Acoustic/Blast SME

Researcher Identifier: NA

Nearest person month worked: 6

Contribution to Project: Review of modeling, implementation of insertion loss optimization routine, review of operating procedures, internal program quality review

Name: Tim Walilko, Ph.D.

Project Role: Principle Investigator

Researcher Identifier: NA

Nearest person month worked: 10

Contribution to Project: Wrote quarterly and annual reports, planning meetings with subcontractors, development/review of test plan, instrumentation of PMHS testing, review of approvals documentation, implementation of changes to the AHAAH model

12.2 Has there been a change in the active other support of the PD/PI(s) or senior/key personnel since the last reporting period?

Nothing to report

12.3 What other organizations were involved as partners?

12.3.1 University of Colorado Health Science Center

Location of Organization	Anschutz Medical Campus 13011 E 17th Place Aurora, CO 80045
Partner's contribution to the project	Provided the medical expertise, equipment, and laboratory space required for the evaluation of various types of HPD under a variety of pressure overpressure conditions using eight instrumented PMHS heads. Additional expertise in carrying out temporal bone measurements. Chinchilla behavioral and physiology measurements.
Facilities	Center for Surgical Innovation (CSI) at the University of Colorado is a multidisciplinary surgical training center that was used in this program as a location for storing biological specimens prior to and after testing. CSI was also used as the space for preparing each specimen including performing the mastoidectomy, cochleostomy, and instrumentation of each specimen prior to testing.
Collaboration	Daniel J. Tollin, Ph.D. Nathaniel T. Greene, Ph.D.

12.3.2 Cochlear Boulder, LLC

Location of Organization	5445 Airport Blvd Boulder, CO 80301
Partner's contribution to the project	Consulted on the development of the test matrix as well as the analysis of the experimental test data. Assisted in model development.
Collaboration	Jim Easter

13 SPECIAL REPORTING REQUIREMENTS

13.1 Quad charts

A quad chart is attached as an appendix below.

14 REFERENCES

Aibara, R., Welsh, J. T., Puria, S., & Goode, R. L. (2001). Human middle-ear sound transfer function and cochlear input impedance. *Hearing Research, 152*(1-2), 100-109.

ANSI. (1973). *American National Standard Psychoacoustical Terminology [ANSI S3.20-1973]*. New York: American National Standards Institute.

ANSI. (1984). *Method for the Measurement of the Real-Ear Attenuation of Hearing Protectors [ANSI S12.6-1984]*. New York, NY: American National Standards Institute.

ASTM. (2014). *Standard Practice for Describing System Output of Implantable Middle Ear Hearing Devices [ASTM F2504-05(2014)]*. West Conshohocken, PA: ASTM International. Retrieved from www.astm.org

Bouwman, J. G., & Bakker, C. J. (2012). Bouwman, J. G., & Bakker, C. J. (2012). Alias subtraction more efficient than conventional zero-padding in the Fourier-based calculation of the susceptibility induced perturbation of the magnetic field in MR. *Magnetic resonance in medicine, 68*(2), 621-630.

Bruce, I. C., Erfani, Y., & Zilany, M. S. (2018). A phenomenological model of the synapse between the inner hair cell and auditory nerve: Implications of limited neurotransmitter release sites. *Hearing Research, 360*, 40-54.

Chan, P., Ho, K., & Ryan, A. F. (2016). Impulse noise injury model. *Military Medicine, 181*(suppl_5), 59-69.

Chandra, N., Ganpule, S., Kleinschmidt, N. N., Feng, R., Holmberg, A. D., Sundaramurthy, A., . . . Alai, A. (2012, September). Evolution of blast wave profiles in simulated air blasts: experiment and computational modeling. *Shock Waves, 22*(5), 403-415.

Chien, W., Ravicz, M. E., Merchant, S. N., & Rosowski, J. J. (2006). The effect of methodological differences in the measurement of stapes motion in live and cadaver ears. *Audiology and Neurotology, 11*(3), 183-197.

Coles, R., Garinther, G. R., Hodge, D. C., & Rice, C. G. (1968). Hazardous exposure to impulse noise. *Journal of the Acoustical Society of America, 43*(2), 336-343.

Dallos, P. J., & Linnell, C. O. (1966). Subharmonic Components in Cochlear-Microphonic Potentials. *Journal of the Acoustical Society of America, 40*(1), 4-11.

Deveze, A., Koka, K., Tringali, S., Jenkins, H. A., & Tollin, D. J. (2010). Active middle ear implant application in case of stapes fixation: a temporal bone study. *Otology & Neurotology, 31*(7), 1027-1034.

Fedele, P., & Kalb, J. (2015). *Level-dependent nonlinear hearing protector model in the Auditory Hazard Assessment Algorithm for Humans [ARL-TR-7271]*. Adelphi, MD: U.S. Army Research Laboratory.

Gondusky, J. S., & Reiter, M. P. (2005). Protecting military convoys in Iraq: an examination of battle injuries sustained by a mechanized battalion during Operation Iraqi Freedom II. *Military medicine, 170*(6), 546-549.

Greene, N. T., Jenkins, H. A., Tollin, D. J., & Easter, J. R. (2017). Stapes displacement and intracochlear pressure in response to very high level, low frequency sounds. *Hearing research, 348*, 16-30.

Greene, N. T., Mattingly, J. K., Jenkins, H. A., Tollin, D. J., Easter, J. R., & Cass, S. P. (2015). Cochlear implant electrode effect on sound energy transfer within the cochlea during acoustic stimulation. *Otology & neurotology, 36*(9), 1554.

Groenewold, M. R., Tak, S. W., & Masterson, E. (2011). Severe Hearing Impairment Among Military Veterans-United States, 2010 (Reprinted from MMWR, vol 60, pg 955-958, 2011). *JAMA, Journal of the American Medical Association, 306*(11), 1192-1194.

Guinan, Jr., J. J., & Peake, W. T. (1967). Middle-ear characteristics of anesthetized cats. *Journal of the Acoustical Society of America, 41*, 1237-1261.

Huang, C. C., Lin, C. D., Wang, C. Y., Chen, J. H., Shiao, Y. T., & Tsai, M. H. (2012). Gustatory changes in patients with chronic otitis media, before and after middle-ear surgery. *Journal of Otolaryngology & Otology, 126*(5), 470-474.

Hynson, K., Hamernik, R. P., & Henderson, D. (1976). B-duration impulse definition: Some interesting results. *Journal of the Acoustical Society of America, 59*(S1), S30.

Kalb, J. T. (2013). *An electroacoustic hearing protector simulator that accurately predicts pressure levels in the ear based on standard performance metrics [ARL-TR-6562]* . Aberdeen Proving Ground, MD: U.S. Army Research Laboratory, Human Research and Engineering Directorate.

Koch, M. (1999). The neurobiology of startle. *Progress in Neurobiology, 59*(2), 107-128.

Kuroda, R. (1993). Clinical study on perforation of the tympanic membrane and discussion based on experimentally induced tympanic rupture. *Nippon Jibiinkoka Gakkai Kaiho, 96*(9), 1490-1500.

Kwon, H. J., Kwon, Y. H., & Kim, Y. H. (2006). Biomechanical skin measurement system for analysis viscoelasticity. In *Key Engineering Materials, Vols. 326-328* (pp. 777-780). Trans Tech Publications.

Lew, H. L., Jerger, J. F., Guillory, S. B., & Henry, J. A. (2007). Auditory dysfunction in traumatic brain injury. *Journal of Rehabilitation Research & Development, 44*(7).

Mattingly, J. K., Greene, N. T., Jenkins, H. A., Tollin, D. J., Easter, J. R., & Cass, S. P. (2015). Effects of skin thickness on cochlear input signal using transcutaneous bone conduction implants. *Otology & neurotology, 36*(8), 1403.

Mattingly, J. K., Greene, N. T., Jenkins, H. A., Tollin, D. J., Easter, J. R., & Cass, S. P. (2015). Effects of skin thickness on cochlear input signal using transcutaneous bone conduction implants. *Otology & Neurotology, 36*(8), 1403.

Maxwell, A. K., Banakis Hartl, R. M., Greene, N. T., Benichoux, V., Mattingly, J. K., Cass, S. P., & Tollin, D. J. (2017). Semicircular canal pressure changes during high-intensity acoustic stimulation. *Otology & Neurotology, 38*(7), 1043-1051.

Merchant, S. N., Ravicz, M. E., & Rosowski, J. J. (1996). Acoustic input impedance of the stapes and cochlea in human temporal bones. *Hearing Research, 97*(1-2), 30-45.

Nakajima, H. H., Dong, W., Olson, E. S., Merchant, S. N., Ravicz, M. E., & Rosowski, J. J. (2009). Differential intracochlear sound pressure measurements in normal human temporal bones. *Journal of the Association for Research in Otolaryngology, 10*(1), 23.

Neely, S. T., & Liu, Z. (1994). Otoacoustic emission averager. *Tech. Memo No. 17*.

Price, G. R. (1998). Welcome to the ARL Auditory Hazard Assessment Algorithm–Human (AHAAH) Version 1, 0. *Ear Model Users Manual*.

Price, G. R., & Kalb, J. T. (1998). Welcome to the ARL Auditory Hazard Assessment Algorithm—Human (AHAAH) Version 1.0. In *Ear Model Users Manual.*

Rosowski, J. J., Chien, W., Ravicz, M. E., & Merchant, S. N. (2007). Testing a method for quantifying the output of implantable middle ear hearing devices. *Audiology and Neurotology, 12*(4), 265-276.

Sivian, L. J. (1935). Acoustic impedance of small orifices. *The Journal of the Acoustical Society of America, 7*(2), 94-101.

Tringali, S., Koka, K., Deveze, A., Holland, N. J., Jenkins, H. A., & Tollin, D. J. (2010). Round window membrane implantation with an active middle ear implant: a study of the effects on the performance of round window exposure and transducer tip diameter in human cadaveric temporal bones. *Audiology and Neurotology, 15*(5), 291-302.

U.S. Department of Veterans Affairs. (2012). *Annual Benefits Report: Fiscal Year 2012.* Washington, DC: Veterans Benefits Administration. Retrieved Oct 23, 2018, from www.benefits.va.gov/REPORTS/abr/docs/2012_abr.pdf

Von Békésy, G., & Wever, E. G. (1969). *Experiments in hearing* (Vol. 8). New York: McGraw-Hill.

Voss, S. E., Rosowski, J. J., Merchant, S. N., & Peake, W. T. (2000). Acoustic responses of the human middle ear. *Hearing Research, 150*(1-2), 43-69.

Walilko, T. J., Lowe, R. D., Argo, T. F., Meegan, G. D., Greene, N. T., & Tollin, D. J. (2017). Experimental evaluation of blast loadings on the ear and head with and without hearing protectino devices. *Mechanics of Biological Systems and Materials, 6*, 101-109.

White, P. J., Clement, G. T., & Hynynen, K. (2006). Longitudinal and shear mode ultrasound propagation in human skull bone. *Ultrasound in medicine & biology, 32*(7), 1085-1096.

Wiener, F. M., & Ross, D. A. (1946). The pressure distribution in the auditory canal in a progressive sound field. *Journal of the Acoustical Society of America, 18*(2), 401-408.

Yamamoto, S. (1953). Yamamoto, S. (1953). Supplement to the physiology of conduction apparatus of rabbits the maximum value of the movement of the stapedial basis. *Hiroshima J Med Sci, 12*, 259-273.

Yankaskas, K. (2013). Prelude: Noise-induced tinnitus and hearing loss in the military. *Hearing Research, 295*, 3-8.

Zilany, M. S., Bruce, I. C., & Carney, L. H. (2014). Updated parameters and expanded simulation options for a model of the auditory periphery. *Journal of the Acoustical Society of America, 135*(1), 283-286.

15 APPENDICES

15.1 Appendix 1: Quad Chart

Improvement and Extension of Auditory Hazard Models

ERMS/Log Number **13063022**

Award Number: **W81XWH-15-2-0002**

PI: Tim Walilko, Ph.D. **Org:** Applied Research Associates, Inc. **Award Amount: $** 2,320,452

Study/Product Aim(s)

- Develop a neuro-functional understanding of acoustic injury encompassing the dynamics of the peripheral auditory system, through sensory transduction, to central auditory processing.
- Develop an animal model, correlating human and animal auditory mechanisms and physiological responses to noise and blast events.
- Develop a robust, validated system for the evaluation of hearing protective systems across the broad range of intensities and frequency spectra seen in real-world exposures.

Approach

Phase 1 – Simulation of blast through EAC to improve cochlea parameters in AHAAH model as well as validate output from in-ear shock emulator.

Phase 2 – Quantify middle ear bone dynamics to increase the fidelity of the parameters in the model representing the stapes and annular ligament

Phase 3 – Extend AHAAH model using auditory evoked potentials and behavior data from Chinchilla model to improve the understanding of cognition of high amplitude sound including any nonlinear effects:

Phase 4 – Improve AHAAH model to predict risk of injury for high impulse noise and identify the appropriate type of hearing protection for real-world exposures

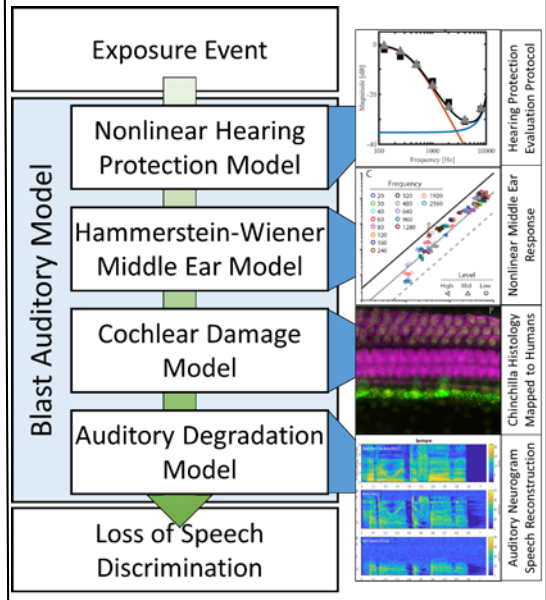

The Blast Auditory Model developed under this program predicts the propagation of a blast wave through the auditory system using a series of sequential submodels. The outputs of the model were verified experimentally using laser Doppler vibrometery and fiber optic pressure gauges within both the chinchilla animal model and human temporal bones. The outer ear is modeled as an acoustic lumped element network, the middle ear as a nonlinear transfer function, and the inner ear using an auditory nerve model.

Timeline and Cost

Activities / CY	15	16	17	18
Blast Characterization through HPD				
Quantifying Middle Ear Dynamics				
Measuring Auditory Response				
Improve AHAAH Model				
Estimated Budget ($K)	**$748**	**$547**	**$504**	**$521**
Updated: October 31, 2018				

Goals/Milestones

CY15 Goal – Evaluate pressures in the EAC to various levels of blast with and without hearing protection

- ✓ Quantified pressures in EAC with and without HPD using PMHS and began implementing findings into enhanced AHAAH Model
- ✓ Fabricated Shock Wave Emulator for Year 2-4 Testing

CY16 Goals – Quantifying Middle Ear Dynamics using Both PMHS and Chinchilla Models

- ✓ Quantify differences between Human and Chinchilla middle ears
- ✓ Address non-linearities of AHAAH middle ear

CY17 Goal – Measuring Auditory Response using Chinchilla Model

- ✓ Measure ABR and DPOAE response to blast using Chinchilla Model

CY18 Goal – Predict damage correlated to central auditory function

- ✓ Extend AHAAH model further into brain's neural network

Budget Expenditure to Date

Projected Expenditure: $2,320,452

Actual Expenditure: $2,314,753

15.2 Appendix 2: Hearing Protection Evaluation Protocol

Protocol for the Evaluation of Level-Dependent Hearing Protection Devices

Revision 0

October 31, 2018

Prepared for:
Richard Shoge, Ph.D.
Portfolio Manager
Injury Prevention and Reduction Program
Military Operational Medicine Research Program
U.S. Army Medical Research and Materiel Command

Authors:
Ted Argo, Ph.D., and Tim Walilko, Ph.D.
Applied Research Associates, Inc.

Jim Easter
Cochlear Boulder, LLC

Nathaniel T. Greene, Ph.D., and Daniel J. Tollin, Ph.D.
University of Colorado School of Medicine

Assistance Agreement W81XWH-15-2-0002

Table of Contents

List of Figures

List of Tables

Protocol for the Evaluation of Level-Dependent Hearing Protection Devices

1. Introduction

1.1. Background and Roadmap

Hearing injury due to exposure to repeated impulse noise is a high risk in the military. Hearing loss and tinnitus are two of the most common injuries experienced by US service members and represent the most prevalent service-connected disabilities of all recipients, with over 35% reporting tinnitus and 25% reporting hearing loss (U.S. Dept of Veterans Affairs, 2017). Military hearing conservation programs (HCPs) have been established to address the issue of hearing loss in the military with specific limits placed on the total acoustic exposure per day for personnel and noise limit design criteria established for new equipment [(U.S. Dept of Defense, 2010), (U.S. Dept of Defense, 2015)].

Existing weapons systems, such as mortars, present impulsive noise exposures in excess of 183 dB, which exceed the established acoustic exposure guidance even when hearing protection devices (HPDs) are properly employed by all personnel (NATO, 2010). Army HCPs specify that single hearing protection is required for impulse exposures above 140 dB and double hearing protection is required for impulse exposures above 165 dB—and only for the specific types of impulses outlined in MIL-STD-1474D [(U.S. Dept of Defense, 2015), (U.S. Dept of the Army, 2015)]. Impulsive sound as low as 132 dB is likely to impact the inner ear even when hearing protection is optimally employed. In practice, the National Institute for Occupational Safety and Health (NIOSH) recommends that the Noise Reduction Rating (NRR) for hearing protection devices for all exposures, which estimates expected performance of HPDs, should be de-rated by 25%–70% based on type [(ANSI, 1974), (Chan H. S., 1998)]; therefore, for Peltor ComTac IV earmuffs (NRR 30) and 3M Combat Arms Earplugs (NRR 7), common Army-issue hearing protection devices, the max attenuation that should be expected (assuming additive NRR) should be 25 dB. The resulting sound pressure level in the ear for the 183-dBP exposure, even when protected, is 158 dB—well above the 140-dB injury threshold; therefore, it is necessary to predict the probability and extent of injury due to high-amplitude impulsive noise exposure.

This protocol outlines the use of one model, the Auditory Hazard Assessment Algorithm for Humans (AHAAH), and specifically, use of a modified hearing protection module that generates waveforms for use by the balance of AHAAH. Multiple models have been proffered to predict hearing injury based on different metrics; a selection of models is described in this chapter. Methods for testing hearing protection and deriving the model coefficients is discussed in Chapter 3. Results for a set of four hearing protection devices is also presented in Chapter 4.

1.2. Comparison of Hearing Injury Prediction Models

Multiple models exist for the prediction of hearing injury focusing on different aspects of damage to the auditory system. The four models summarized in Table 1 describe the breadth of the types of hearing injury models and demonstrate the different types of inputs and outputs that may be used in predictions. A discussion of each of these models, including application, limitations, and validation, are presented in the following sections.

Table 1: Hearing injury prediction models

Model	Predicts	Basis	Input	Output	Source
Hirsch	Probability of tympanic membrane (TM) rupture	Empirical equation from human data	Peak pressure	Probability of TM rupture	Hirsch (1968)
Auditory 4.0	Probability of Temporary Threshold Shift (TTS) and Permanent Threshold Shift (PTS)	Empirical equations from human and chinchilla data	A-Weighted Sound Exposure Level [SELA]	Probability of a specified level of TTS/PTS	Chan et al. (2012)
$L_{IAeq100ms}$	Total allowable daily noise dose	Empirical equation from human data	Peak pressure and duration for impulse noises, sound pressure levels and durations for continuous noises	Percent of allowable daily noise dose	MIL-STD-1474E (U.S. Dept of Defense, 2015)
AHAAH	Compound threshold shift derived from displacement of the basilar membrane	Empirical model from cat and human data	Acoustic waveform measured in the freefield	Auditory risk units (ARUs)	Kalb & Price (2015)

1.2.1. Hirsch

1.2.1.1. Model Description

The Hirsch model for probability of tympanic membrane rupture was developed by Hirsch (1968) after performing a literature review of existent data on tympanic membrane rupture. Three major sources of data were utilized in the model's development:

1. The threshold for 8% probability of rupture of the tympanic membrane was taken from Vadala's 1930 study (Vadala, 1930) of men exposed to 37-mm antiaircraft fire. In this study, the 6-psi exposure generated six cases or tympanic membrane rupture over 75 subjects.
2. The threshold for 50% probability of rupture of the tympanic membrane was taken from Henry's 1945 study (Henry, 1945) of men exposed to explosions of landmines, 500-lb. bombs, or 3-inch mortar shells. In this study, the approximately 17-psi exposure generated 152 perforations of the tympanic membrane over 292 subjects.
3. The threshold for 85% probability of rupture of the tympanic membrane was taken from Reider's comments (Reider, 1966) in 1966 regarding explosions during industrial accidents. In an accident of note, a 30-psi event generated 19 perforations of the tympanic membrane over 22 exposed ears.

Hirsch collected these results as shown by the black points in Figure 1. To allow for estimation, Hirsch provided a trendline, shown in red. This trendline is accurate for estimation only in the 2- to 90-psi incident pressure range. Due to the axis chosen by Hirsch (1968) in his original report, outside of this pressure range, there will always be a probability of injury greater than 0%, and at no point is the probability of injury 100%. We developed a regression in log space, shown in blue, to better capture this behavior, as described below.

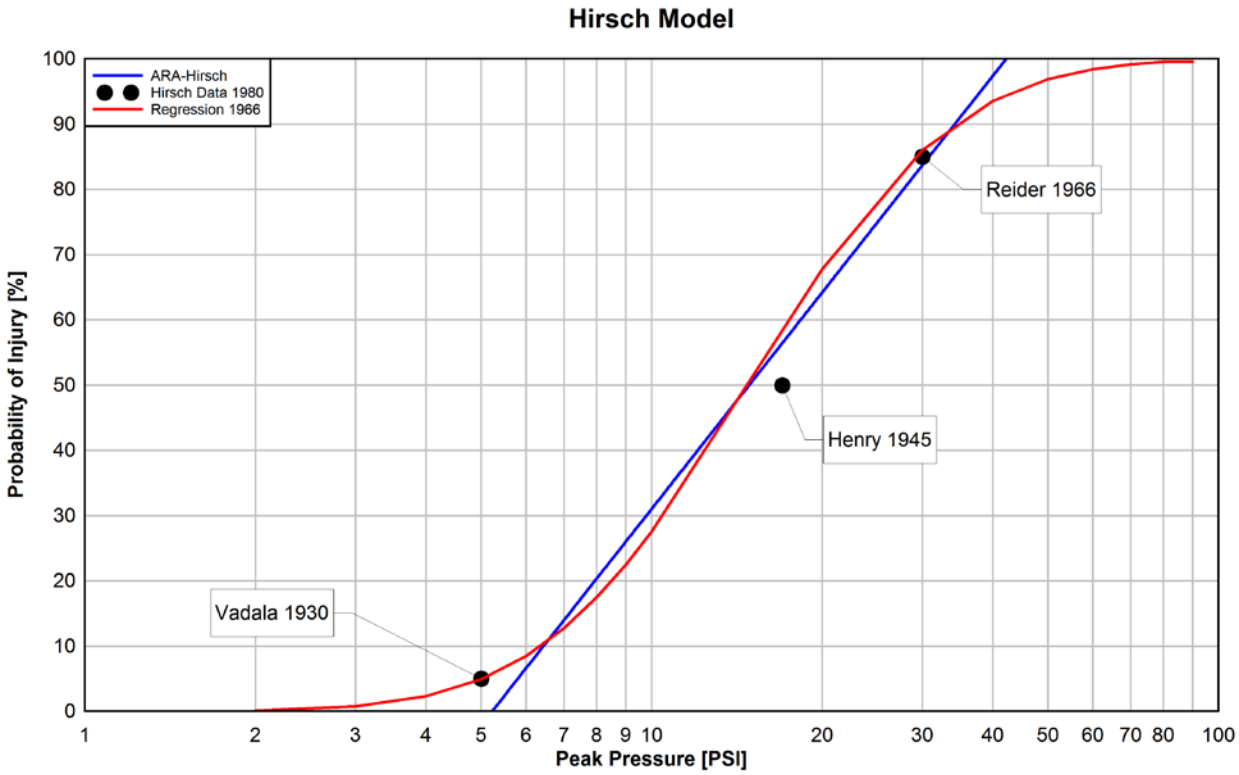

Figure 1: Plot of probability of human tympanic membrane rupture taken from Hirsch (1968).

To better implement this model for use at all relevant incident pressure levels, the blue nonlinear regression line shown in Figure 1 was developed. If the peak overpressure is less than 5.23 psi, there is zero probability of tympanic rupture whereas a peak overpressure greater than 42.25 psi results in 100% tympanic rupture probability. With peak overpressures between 5.23 psi and 42.25 psi, the probability of tympanic membrane rupture is computed as follows.

$$\text{Prob}(\text{Tympanic Membrane Rupture}) = -0.7917 + (1.102 * \log_{10} P) \quad (1)$$

where P is the peak overpressure in PSI. The result of this equation is shown in Figure 2, with the blue line denoting the result of the equation and the grey lines denoting the peak pressure and probability. (For example, for this 187 dB exposure, the probability of TM rupture is on the order of 15%.)

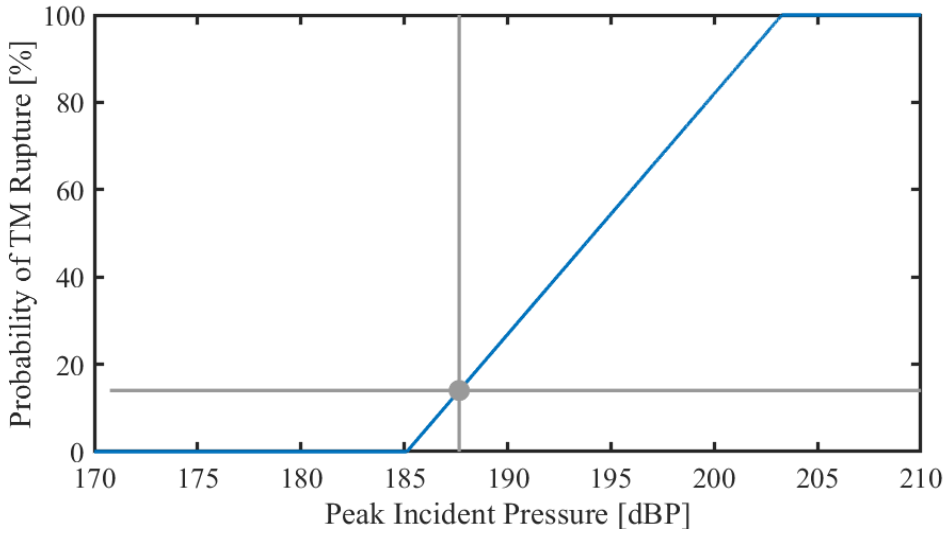

Figure 2: The output of the adapted Hirsch model.

1.2.1.2. Limitations

- Only the peak pressure is taken into account; no pressure-time information such as A-duration is considered.
- The Hirsch model (1968) is assumed to be valid over the full range of potential incident pressures; however, Hirsch's initial model is only valid across a 2- to 90-psi incident pressure range.
- The empirical equation is based on regression through the averages of three datasets with no formal scientific exploration of the parameter space.
- Only unilateral tympanic membrane rupture is predicted; probability of bilateral rupture is not implemented.
- There is no accounting for the effect of direction of incidence for the pressure wave; the head or body may shield the ear from the incident pressure, thereby reducing the probability of rupture. See Chandler & Edmond (1997) for these effects.

1.2.1.3. Validation

The original Hirsch regression and ARA's regression are shown in Figure 1. An extension of this model developed by ARA to remove the discontinuous points at low and high pressures will under-predict injury in the 4- to 6-psi incident pressure range and over-predict injury in the 35- to 70-psi range. Maximum deviation from the Hirsch model occurs at 5.23- and 42.25-psi exposures with approximately 5% under/over prediction. In contract to this model, in testing performed on post mortem human ears, the likelihood of rupture at 8-psi was found to be nearly 100% (Greene, et al., 2018).

1.2.2. AUDITORY

1.2.2.1. Model Description

AUDITORY 4.0 was developed by L-3 Communications/Jaycor (Chan, Ho, & Ryan, 2012) for the Joint Non-Lethal Weapon Directorate to assess the potential Temporary Threshold Shift (TTS) and Permanent Threshold Shift (PTS) due to exposure to high-amplitude sound. In addition, version 4.0 of this model predicts recovery time from an event causing TTS. This model is based

on TTS/PTS measurements performed on chinchillas exposed to impulsive noise in a laboratory setting. Dose-response curves based upon the A-weighted Sound Exposure Level (SELA) are produced for SELA values from approximately 102 dB to 135 dB.

To determine SELA from the incident pressure signal, the SEL is computed according to

$$\mathrm{SEL} = 10\log_{10}\left(\frac{1}{T_0}\int_{-\infty}^{+\infty}\frac{p^2(t)}{p_o^2}dt\right) \quad (2)$$

where T_o is a reference duration of 1 second, $p(t)$ is the A-weighted pressure of the incidence sound pressure event, and p_o is the reference pressure of 20 μPa. A weighting is applied to the incident pressure signal using IEC 61672:2003 (IEC, 2003) to ensure the calculation is representative of human perception of the acoustic event rather than the raw acoustic event.

The SELA is used as the sound exposure metric in an attempt to normalize the response of the model for all exposure types. Use of the SELA, however, is not truly representative of the sound pressure level experienced by the subject. As presented by Smoorenburg (2003), the peak sound pressure level (P) and the A-weighted sound exposure level (SELA) differ by as much as 40.7 dB, as shown in Table 2; therefore, when using this model, the pressure-time history converted to the SELA must be considered instead of peak sound pressure level.

Table 2: Comparison of A-weighted Sound Exposure Level (SELA) to peak pressure (L_p). Table taken from Smoorenburg (2003).

Source	*P* – SELA	Publication
Friedlander wave, 0.5 ms A-Duration	40.7	Auditory 4.0 Manual
Explosions (near Friedlander wave)	39.5	Parmentier *et al.* (1995)
Rifle (energy specified in J/m²)	40.0	Price *et al.* (1989)
Rifle, instructor	37.3	Dancer and Franke (1994)
Rifle, shooter	34.6	Dancer and Franke (1994)
FNC rifle	36.8	Brinkmann (2000)
Rifle with reflections	33.9	Dancer *et al.*

To determine the amount of TTS/PTS, the SELA is calculated given the pressure-time history for the compartment. Note that this is only available for custom attacks and not for ASAP runs. The SELA is then used as the input to the AUDITORY 4.0 module.

The AUDITORY model is based on the measured TTS of chinchillas when exposed to high-amplitude impulsive stimuli. The effects on over 900 chinchillas were studied with sources ranging from shock tubes to fast-acting valves. SELA values adjusted for number of shots,

$$\mathrm{SELA} = \mathrm{SELA} + 10\ \log_{10}(Nshots/25), \quad (3)$$

ranging from 102 to 135 dB were used. These levels correspond to the range of exposures at 15 feet recorded in a test series of Flashbang devices.

The probability of a given level of TTS shift is governed by ordered logistic regression on the chinchilla data. The probability of TTS is calculated as

$$\mathrm{Prob}(TTS) = \frac{e^L}{1+e^L} \quad (4)$$

where

$$L = \begin{cases} \alpha(\mathrm{SELA} + 3.44\log_{10}(N/25)) + \beta & N \le 25 \\ \alpha(\mathrm{SELA} + 3.44\log_{10}(25) + 10\log_{10}(N/25)) + \beta & N > 25' \end{cases} \quad (5)$$

α and β are regression coefficients from the chinchilla data, and *N* is the number of shots. Note that the correlations were obtained from the chinchilla data and shifted upward by 28 dBA to account for the scaling from chinchillas to humans.

The result of example AUDITORY calculations are shown in Figure 3 for *N*=1. The blue and green curves represent the probability of 10 and 40 dB of TTS, respectively. For a SELA of 140 dB presented normal to the ear, the red dashed line is observed. Based on the AUDITORY 4.0 model, there is a 78% probability of 10 dB TTS and a 15% chance of 40 dB TTS shift. Note that the model provides probability curves (outputs) for TTS levels of 1 dB, 5 to 90 dB in steps of 5 dB, and 90 dB as well as PTS levels of 1 dB and 5 to 70 dB in steps of 5 dB.

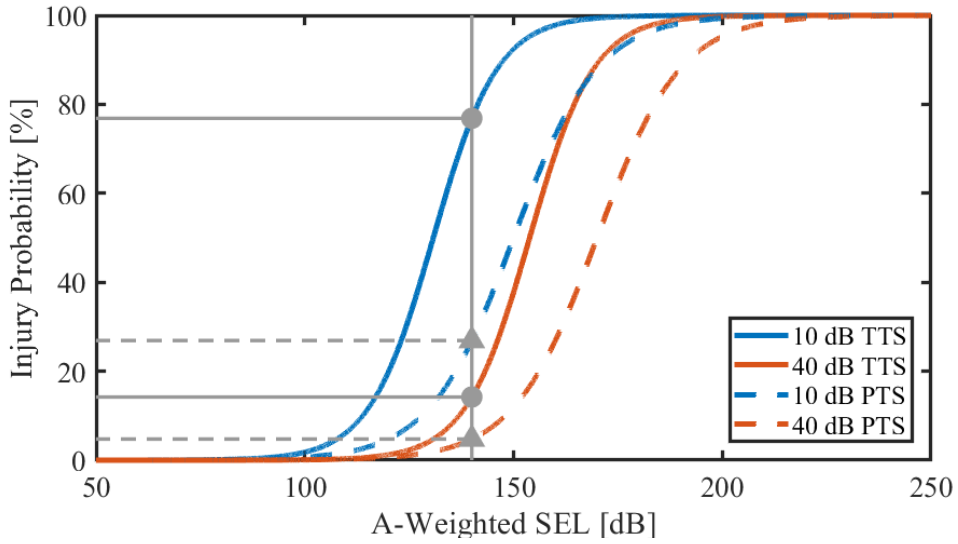

Figure 3: Result of sample calculations using the AUDITORY 4.0 Model.

1.2.2.2. Results

The model is calculated for the appropriate SELA; the model produces the probability of TTS and PTS of a given level. The amount of injury must be selected based upon this probability.

1.2.2.3. Limitations

- This model requires a pressure-time (P-t) recording or an ad hoc method to create the SELA for a single transient event.
- The validated SELA values for this model are up to 140 dB. For a higher SELA, this model is unvalidated. Hearing injury from weapons, such as the MAAWS, can produce SELAs in excess of 150 dB. In this range, however, the model is unvalidated, yet the probability of injury approaches 100%.
- This model can only account for normal incidence and grazing incidence to the ear.
- If performing a calculation for normal incidence, the opposing ear will be shielded from the pressure wave by the head and the results may not be accurate.

1.2.2.4. Validation

The AUDITORY 4.0 model was based on measurements performed using chinchillas as surrogates for the human auditory system. Due to the regression analysis performed, the data from each animal was used to develop each probability curve. The 95% confidence interval for a representative TTS is shown in Figure 4. The extent of the confidence interval is typical for each of the TTS levels. Given this interval, a maximum deviation of ± 5% with respect to the probability threshold can be expected with 95% confidence. This maximum potential deviation can be expected in approximately the 15% to 55% probability range.

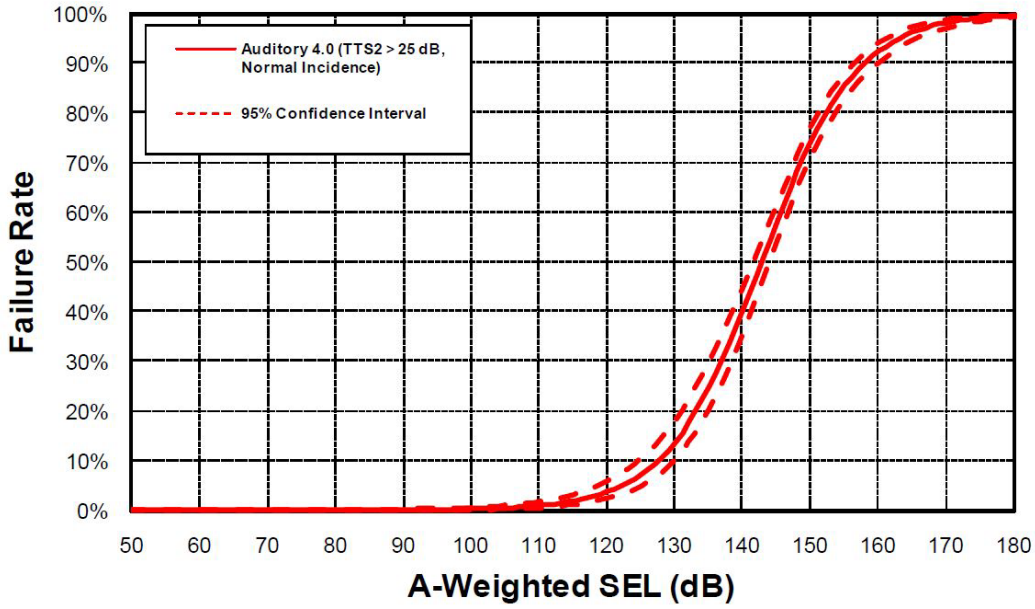

Figure 4: Confidence intervals for the 25-dB SELA exposure level (Coles, Garinther, Rice, & Hodge, 1967).

The model developed using the chinchilla exposures was validated by two sets of historical human data collected from volunteers. The first was a combined study of German rifle noise exposures without hearing protection collected by Pfander *et al.* (1980) and from the Committee on Hearing and Bioacoustics (CHABA) performed by Coles (1967). The second was from the USAMRMC Blast Overpresure Project (BOP), where volunteers were exposed to high intensity noise with hearing protection as described by Chan *et al.* (2001) [see (Patterson Jr. & Johnson, 1994) (Patterson Jr. & Johnson, 1994), (Johnson & Patterson, 1997), (Patterson Jr., Mozo, Gordon, Canales, & Johnson, 1997)]. The information gleaned from these studies improved the AUDITORY model by adding a 4-dB increase to SELA for sound exposures normal to the ear and validate TTS and recovery time experienced by the chinchillas.

The comparison of the AUDITORY model with rifle exposures is shown in Figure 5 and Figure 6. Figure 5 shows the data obtained by Coles (1967) from CHABA. AUDITORY 4.0 is shown in blue with a fit to the data shown in red with corresponding confidence intervals. For each of the populations presented, the AUDITORY model falls well within the confidence limits of the fit. Note that these curves are the TTS experienced by 10%, 25%, and 50% of the populations rather than the probability curves calculated by the AUDITORY model itself; the output of AUDITORY is used to generate these curves.

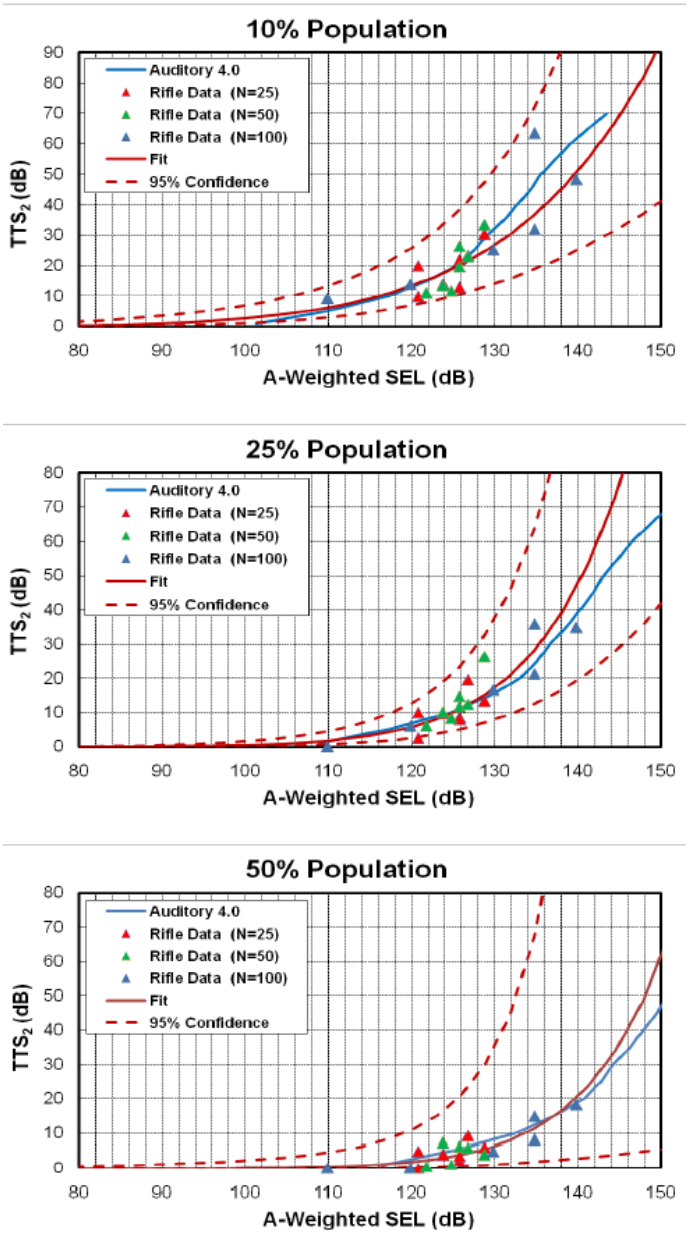

Figure 5: Comparison between the AUDITORY 4.0 model and CHABA data (Coles, Garinther, Rice, & Hodge, 1967).

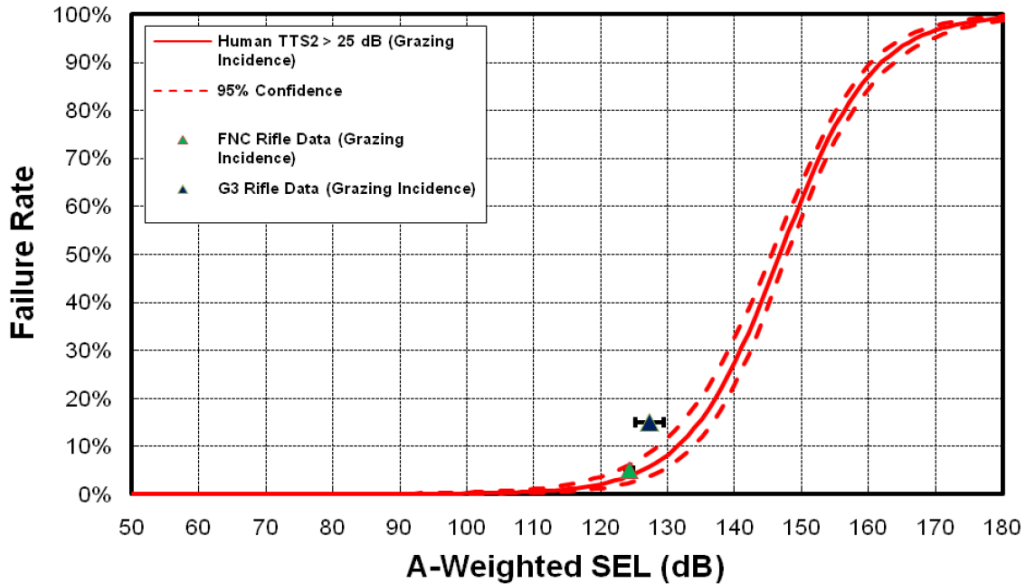

Figure 6: Comparison between the AUDITORY 4.0 model and German rifle data (Coles, Garinther, Rice, & Hodge, 1967).

Figure 6 shows the probability of injury for 25-dB TTS generated from the chinchilla regression compared to two sets of rifle data presented by Pfander et al. (1980) and Brinkmann (2003). Probability of injury associated with the FNC rifle is well predicted by the AUDITORY model. The impact of the G3 rifle, however, is not well predicted by the AUDITORY model as shown by the lack of overlap in the measurement uncertainty and the model 95% confidence interval. Note that this comparison is still considered valid since the TTS standard employed during the FNC and G3 measurements was the amount of shift recovered in 24 hours, not the TTS measured at two minutes used in AUDITORY; therefore, the deviation of the data from the model curve can be accounted for in this manner.

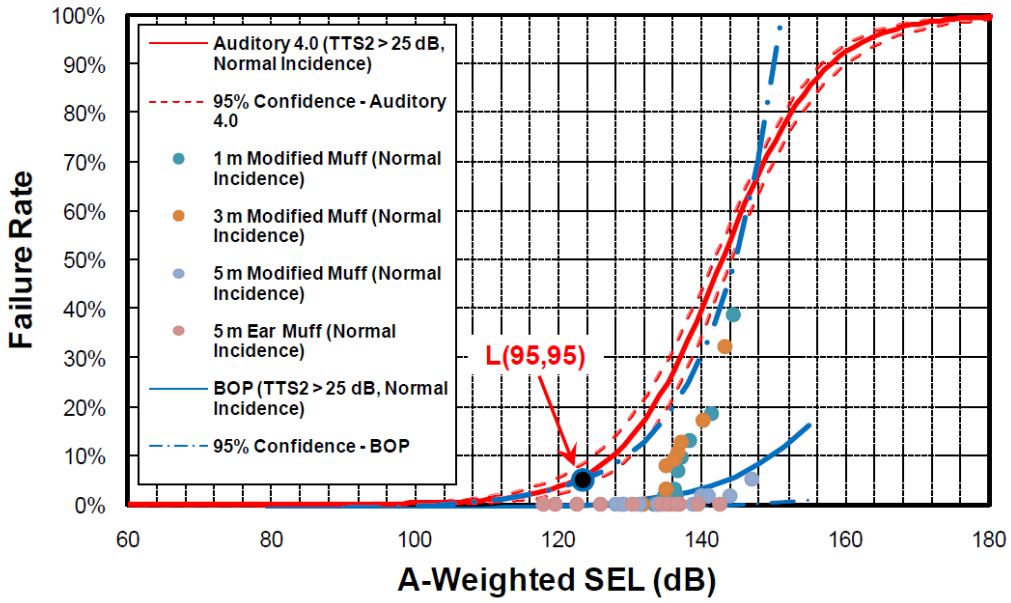

Figure 7: Comparison between the AUDITORY 4.0 model and BOP data [Reprinted from (Coles, Garinther, Rice, & Hodge, 1967)].

Data from the Albuquerque BOP tests is shown in Figure 7. There is no direct comparison between the AUDITORY model and this data set due to the use of hearing protection during this test series. Shown are the pressures measured under the hearing protection devices (unmodified) and the same recordings converted to freefield pressures using the ear canal transfer function (modified). Note that there is overlap between the AUDITORY and BOP 95% confidence intervals, despite the difference in regression lines. In addition, the calculated L(95,95) threshold, the point at which 95% of the population is protected 95% of the time, is well within the tight confidence interval of the AUDITORY model. Therefore, AUDITORY would have calculated a threshold shift estimate protecting 95% of subjects 95% of the time and assume up to 5% remain unprotected.

1.2.3. Equal Energy Equivalent Averaged over 100-ms Intervals ($L_{IAeq100ms}$)

1.2.3.1. L_{Aeq8}

The L_{eq} hearing injury risk model is an impulsive noise adaptation of the L_{eq8} used by an array of governments and agencies to evaluate risk from continuous noise and protect workers from hearing losses resulting from occupational noise exposure. A time-weighted average of measured A-weighted sound pressure levels is calculated and averaged over an eight-hour exposure time (T_0), to produce a noise dose (D) as a percentage of the maximum recommended exposure using:

$$D = 100 \sum_{n=1}^{N} \frac{C_n}{T_n(SPL_n)} \quad (6)$$

where N is the total number of different noise exposures experienced in the eight-hour time period, C_n is the total exposure time period in hours, and $T_n(SPL_n)$ is a reference duration for exposure to sound pressure level SPL_n in hours. The reference duration is based upon a recommended exposure limit (REL) sound pressure level, which will produce 100% noise dose for an eight-hour exposure and an exchange rate that increases or decreases the permissible exposure time for a non-REL sound pressure level. The permissible exposure time for each exposure is found using

$$T_n(SPL_n) = \frac{C_n}{2^{(SPL_n - SPL_0)/R}} \quad (7)$$

where SPL_0 is the REL sound pressure level and R is the exchange rate.

Organizations have specified different RELs and exchange rates. For example, the National Institute for Occupational Safety and Health (Chan H. S., 1998) recommends an REL of 85 dB and an exchange rate of 3 dB whereas the Occupational Safety and Health Administration (2013) recommends an REL of 90 dB and an exchange rate of 5 dB. A comparison of these two common REL/R combinations is found in Table 3.

Table 3: Comparison of time duration for 100% noise dose for common Recommended Exposure Levels and Exchange Rates

Exposure Level (in dB)	REL = 90 dB R = 5 dB	REL = 85 dB R = 3 dB
80	32 hours	25 hours, 24 minutes
85	16 hours	8 hours
90	8 hours	2 hours, 31 minutes
95	4 hours	47 minutes, 37 seconds
100	2 hours	15 minutes
105	1 hour	4 minutes, 43 seconds
110	30 minutes	1 minute, 29 seconds
115	15 minutes	28 seconds
120	7.5 minutes	9 seconds

This table provides the total allowable noise dose for an eight-hour period, assuming that the balance of the day is spent in quiet, below the REL. For example, personnel operating in a machine shop may be exposed to continuous noise of 100 dB during some machining operations. According to OSHA, that person may be exposed for up to two hours, whereas NIOSH limits the same individual to 15 minutes. For daily exposures encompassing multiple sound pressure levels, the time weighted average (TWA) is calculated:

$$\text{TWA} = SPL_0 + 10\log_{10}\left[\sum_{n=1}^{N} \frac{T_i}{T_0} 2^{(SPL_n - SPL_0)/R}\right]. \quad (8)$$

To implement hearing protection in the exchange rate scheme, the sound pressure level reaching the tympanic membrane should be used. If an in-ear dosimeter is available, the pressure may be recorded directly. If such a dosimeter is not available, the measured exposure level should be decreased by the expected insertion loss for the specific properly fitted hearing protection to be used. Various schemes exist for the calculation of the expected insertion loss; OSHA recommends the following formula:

$$REL = TWA - \frac{(NRR - 7)}{2} \quad (9)$$

The 7 dB of insertion loss should be subtracted to account for noise spectrum variations between general use and that used in calculation of the NRR of the hearing protection device. The derating by a factor of two should be used to account for the use of the “experimenter fit” method utilized in the evaluation of the NRR, which is unlikely to reflect the insertion loss experienced in the field.

1.2.3.2. $L_{IAeq100ms}$

The L_{IAeq8} is adapted for use in impulsive noise environments and is outlined in MIL-STD-1474E (U.S. Dept of Defense, 2015). For impulsive noise with peak pressures over 140 dBP, the $L_{IAeq100ms}$ is calculated using

$$L_{IAeq100ms} = 10\log_{10}\left[\frac{1}{p_0^2 T}\int_0^T p_A^2(t)dt\right] \quad (10)$$

where $p_A(t)$ is the A-weighted time domain pressure signal in Pascals, T is a time constant of 100 ms, and p_0 is the reference pressure of 20 µPa. To incorporate hearing protection, $L_{IAeq100ms\ protected}$ is calculated using

$$L_{IAeq100ms\ protected} = 10\log_{10}\left[\frac{1}{p_0^2 T}\int_0^T \left(p_A(t) - 10^{IPIL(p_{max})/20}\right)^2 dt\right] \quad (11)$$

where $IPIL(p_{max})$ is the Impulse Peak Insertion Loss (IPIL) metric defined by ANSI S12.42 (2010) at the standard exposure level (137, 155, or 173 dBA peak) most closely matching the peak pressure of the exposure. If the peak pressure is above 180 dB, the IPIL for the hearing protection must be evaluated at this level to determine nonlinear protection effects of the hearing protection and the potential loss of acoustic seal due to the blast overpressure. Note that the maximum IPIL to be used in this calculation is 41 dB, which is the bone conducted sound limit (U.S. Dept of Defense, 2015).

The equivalent L_{Aeq8} is then calculated based on the A-duration (T_A) of the time domain pressure signal defined as the first time at which the pressure signal crosses zero after arrival of the peak:

$$L_{Aeq8} = L_{IAeq100ms} - 54.6 - 1.5 \times 10\log_{10}\left(\frac{T_A}{T_{Amin}}\right) \quad (12)$$

$$L_{Aeq8} = L_{IAeq100ms} - 71.0 \quad (13)$$

where $L_{IAeq100ms}$ may be the protected or unprotected value and T_{Amin} is a minimum A-duration of 0.2 ms. Equation 12 is to be used for A-durations less than 2.5 ms and Equation 13 is to be used for A-durations greater than 2.5 ms to ensure the L_{Aeq8} is not overestimated.

The noise dose for each impulsive event (D_I) based on the equivalent L_{Aeq8} is

$$D_I(\%) = 100 \times 2^{\frac{-(85 - L_{IAeq8})}{3}} \quad (14)$$

with a full daily noise dose equal to 100%.

1.2.3.3. Limitations

- Corrections for duration of noise events must be applied. A default of 0.2-ms A-duration is used when duration information is not available. When duration information is available, the A-duration is limited to 2.5 ms regardless of signal characteristics.
- Hearing protection is incorporated using ad hoc corrections based on available data and the expected exposure level. When IPIL values are available, the closest IPIL value to the expected exposure is used. If the exposure will be over 180 dBP, IPIL values must be

obtained for exposure levels outside of ANSI S12.42 guidance. Measurements under the hearing protection device may also be used to predict injury.

- Bone conduction limits when using hearing protection are likewise applied ad hoc following the limits set forth in ANSI S12.42.
- The $L_{lAeq100ms}$ is designed for recordings of 100 ms. If durations greater than 100 ms are used, a correction must be applied.

1.2.3.4. Validation

L_{eq} is an established standard in the European Union used for the evaluation of risk of hearing injury, however, it has not been validated through peer-reviewed research. Despite the lack of peer-reviewed research, an independent American Institute of Biological Sciences review (Wightman, Flamme, Campanella, & Luz, 2010) of the L_{eq} recommended its use in predicting hearing injury. The $L_{lAeq100ms}$ is derived from the L_{eq} and recommendations for its use follow from the support for use of the L_{eq}.

1.2.4. AHAAH

1.2.4.1. Model Description

The AHAAH model was developed by the Army Research Lab (ARL) in an effort to address inadequacies and inaccuracies in prior impulse noise damage risk criteria [(U.S. Dept of Defense, 2015), (Price, 2007), (Fedele & Kalb, 2015)]. This model is a lumped element circuit model representation of the human auditory system, shown in Figure 8, which is designed to predict the risk of hearing injury due to an arbitrary sound exposure. An arbitrary pressure-time signal is input into the model and produces an output of Auditory Risk Units (ARUs), a quantity based on maximal displacement of the basilar membrane. The development and implementation of this model is described below.

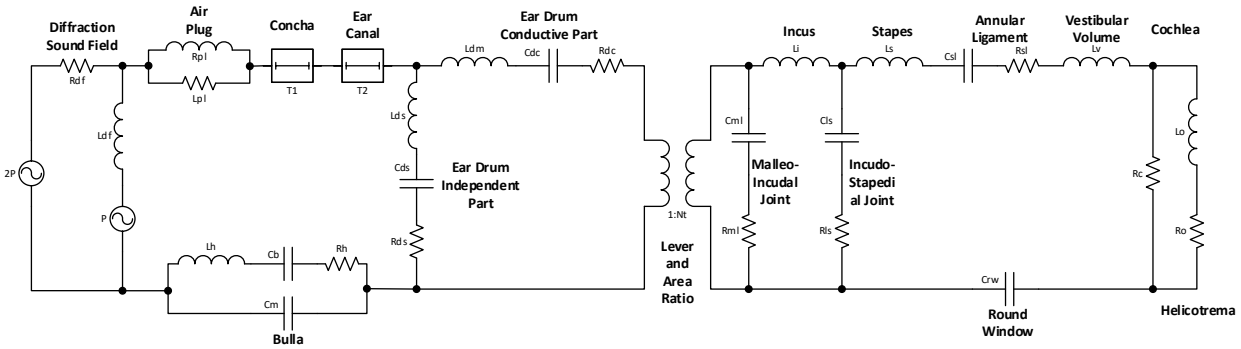

Figure 8: The AHAAH model is composed of electroacoustic elements representing the anatomy of the human auditory system.

1.2.4.2. Model Component Derivation

AHAAH is composed of elements intended to represent the various physiological structures of the human auditory system. Beginning on the left side of Figure 8, the direct and diffracted sound fields are incident on the outer ear. The pressure propagates through elements representing the auditory bulla and a plug of air at the entrance to the ear canal connected to delay lines representing the ear canal proper. A set of elements then represents the complex behavior of the ear drum. Elements representing the mass of the ossicles and the restoring force provided by the

ligaments of the middle ear transmit the sound from the ear drum to the vestibular volume via the oval window. The cochlea is by a load representing the total cochlear impedance without a more detailed description of the physiology within the cochlea.

Element parameters are derived from a variety of studies, and are primarily based on measurements in cats, as summarized in Price *et al.* (1991) and Price (2011) . A discussion in Price 2017 justifies the model developers' claims that the elements derived from the cat model accurately reflect human physiology. A discussion of some of the finer points of the model features can also be found in Price 2017, including support for their selection of physiological variables and datasets incorporated into the model for validation.

There are multiple potential test cases presented when using AHAAH. First is the normal or grazing incidence of the sound exposure, which changes the sound field impacting the ear. Second is the assumption of a *warned ear response*. This response assumes that hearing protection is provided to personnel who know an acoustic exposure is imminent through the contraction of the middle ear muscles. For the unwarned case, the muscle contraction activates over the 9.2-ms to 11.9-ms time window following an exposure over 134 dB. For the warned ear, it is assumed the muscle contraction is active before arrival of the sound exposure. In both cases, the muscle remains contracted through the end of the stimulus presentation. Finally, hearing protection is simulated with a lumped element model, as described in Chapter 2.

1.2.4.3. Use and Interpretation of AHAAH

Exercising this model requires the use of a computer running the AHAAH software distributed by ARL. The model input is a pressure-time recording for a sound exposure of interest that is propagated through the model to the cochlea. At the cochlea, ARUs are calculated based on the maximum of the squared displacement of the simulated basilar membrane. According to the authors, a noise dose of up to 500 ARUs (occasional) and 200 ARUs (occupational) represent a risk of 25 dB of TTS, which will recover over the course of 24 hours. As an example, an exposure with a 171-dBP (1-psi) overpressure and an A-duration of 4 ms can produce approximately 812 ARUs, thus exceeding the typical daily ARU limit for an occasional exposure. ARUs for multiple exposures are additive and accumulate.

1.2.4.4. Limitations

- Model parameters were primarily derived from the cat. Assumptions regarding the similarity of human and feline physiology may confound the model predictions [(Zagadou, Chan, Ho, & Shelly, 2016), (Greene, Jenkins, Tollin, & Easter, 2017)].
- A warned middle ear reflex is assumed, which may over-predict the protection afforded by the response of the middle ear muscle contraction [(McGregor, et al., 2018), (Flamme, Deiters, Tasko, & Ahroon, 2017), (Jones, Greene, & Ahroon, 2018)].
- Some element parameters were derived from quasi steady-state measurements of tissue properties, which may not adequately represent response under high-rate pressure changes.
- The ARU metric proposed for predicting hearing injury has not been adequately validated against known injurious exposures.
- The AHAAH model requires a computer to run such that measurements made in the field must be considered after recording and analyzing the full time domain waveform.
- It is assumed that all hearing protection, including circumaural muffs, maintain a seal with the head despite evidence that, under high-intensity pressure loads above 185 dBP, the acoustic seal may fail.

1.2.4.5. Validation

Performance of the AHAAH model has not been validated for prediction of hearing injury, though it has been applied to various datasets for comparison. An American Institute of Biological Sciences review was conducted (Wightman, Flamme, Campanella, & Luz, 2010), which recommended assumptions made during development of the model should be studied further before adoption. Additional research has discovered additional issues which should also be addressed and research is ongoing. Examples of recent research performed to address these assumptions and issues are as follows:

- *Middle ear reflex:* These studies all address the middle ear reflex as implemented in AHAAH. The main goal of this research was to determine (1) if the middle ear reflex is pervasive in the population and (2) if one can be trained to develop a middle ear reflex. The outcomes of this research to date have proven that the middle ear reflex is not pervasive enough to be considered a protective mechanism in the AHAAH model and that one cannot be trained to develop a middle ear reflex [(Jones, Greene, & Ahroon, 2017), (Ahroon, 2017), (Flamme, Deiters, Tasko, & Ahroon, 2017)].
- *Use of auditory risk units:* Wu and Qin (2013) examined the effects of the positive and negative phases of an incident blast wave to determine the rigor of the ARU metric. Through laboratory testing and exercising the model with synthetic data, it was determined that an increase source duration does not necessarily produce higher auditory hazard, whereas an increase in peak pressure will increase auditory hazard.
- *Non-physical physiological measurements:* Zagadou *et al.* (2016) discuss the issues with assigning parameters from the cat to the human AHAAH model. These include both the physiological measurements as well as the time constants and rate limiting of the middle ear muscle reflex. In addition, the stapes motion is limited to a small fraction of observed stapes motion in post mortem middle ears [(Greene, et al., 2018), (Greene, Jenkins, Tollin, & Easter, 2017), (Peacock, Al Hussaini, Greene, & Tollin, 2018)].

2. Description of the AHAAH Hearing Protection Module

2.1. Overview

The Electro-Acoustic 3-Piston Hearing Protector Model shown in Figure 9 is a standard analytical technique used the field of acoustics (Olson, 1957). The three-piston linear hearing protection model has been adopted for use in predicting the performance of HPDs (Kalb, 2013). In the model, 11 parameters determine sound transmission through three branches of the circuit: HPD material impedance (upper branch); plug mass and skin (middle branch); and the leak path (lower branch). In this study, these parameters were derived from the insertion loss curves generated from the whole-head post mortem human subject (PMHS) testing as well as from headform testing using the ANSI S12.42-compliant shock tube. While the curve fitting of these parameters was observed to be very accurate in the frequency domain, when transposed to the time domain errors were observed.

Currently all 11 electro-acoustic component values (EACV) shown in Figure 9 have been derived from insertion loss curves measured using standard Real Ear Attenuation at Threshold (REAT) or similar methods. As the methodology was determined for calculating the EACVs, it was observed that the order in which they are determined influences the values selected. This suggests that the number of EACVs to be determined is too large for the curves generated by the insertion loss (IL) curves. The section below describes how the methodology developed under this effort will reduce the number of derived EACVs from 11 to 6 to reduce the complexity and increase the accuracy of the predictions.

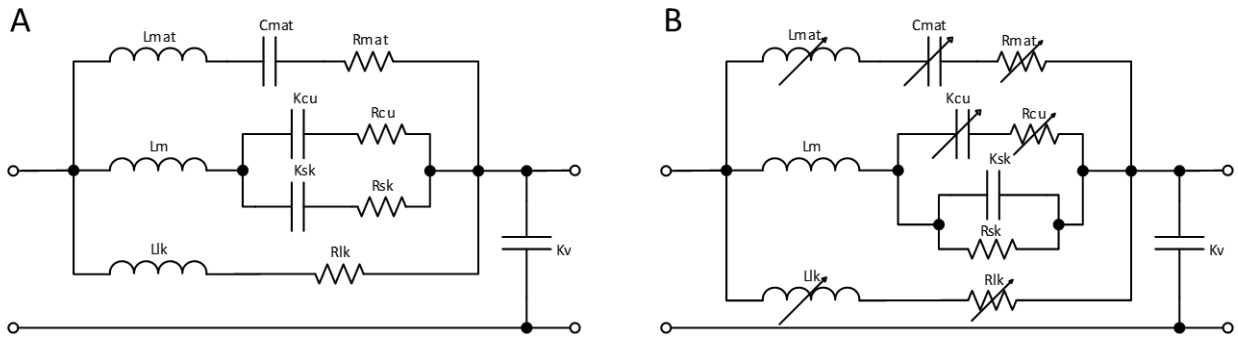

Figure 9: Hearing protection modules for the AHAAH model are composed of linear and nonlinear electroacoustic elements. Left – HPD module proposed by Kalb & Price (2015). Right – Modified HPD module developed under this program.

2.2. Descriptions of Model Branches

2.2.1. Leak

The leak path consists of an inductor/resistor pair (Llk, Rlk) representing the movement of air between the hearing protection and the skin. A capacitor (Kv) representing the compliance of the air in the ear canal cavity is also included in this path.

The compliance of the air in the ear canal cavity is based on the compressibility of gas and the volume of the gas behind the hearing protection. The gas volume for each hearing protection device was measured and found to be similar for each device. The value for the compressibility is held fixed at 1e5 dyne/cm^5. This reduces the ear canal from a variable to a fixed value.

The leak inductor/resistor path is modeled by separate inductance and resistance models for fluid flow through a slot as a function of pressure. The resistive (real) portion of this impedance (Z_{RE}) is modeled using the same function as Fedele & Kalb (2015), taken from Sivian (1935),

$$Z_{RE} = 150\left(1 + \frac{U}{203}\right)^{1.17}, \tag{15}$$

where

$$U = \frac{P}{\rho c} \tag{16}$$

for pressure P, air density ρ, and speed of sound in air c.

The inductive (imaginary) portion of the impedance (Z_{IM}) is modeled after Sivian's work as well. In this case, the imaginary portion of the fluid flow through a rectangular slot is used. It is assumed that the slot is bent into an annulus and that the impedance of the annulus is equivalent to the impedance of a slot. The imaginary portion of the impedance is defined by Sivian as

$$Z_{IM} = \rho\omega\left\{\frac{1}{4g_w g_h} + \frac{1}{3\pi g_w^2 g_h^2}\left[\left(g_w^2 + g_h^2\right) - \left(g_w^2 - g_h^2\right)^{3/2} + 3g_w g_h\left(g_h \log\frac{g_w\left(g_w^2+g_h^2\right)^{1/2}}{g_h} + g_w \log\frac{g_{wh}\left(g_w^2+g_h^2\right)^{1/2}}{g_w}\right)\right]\right\} \tag{17}$$

for g_h and g_w defined as the slot height and width, respectively. For this algorithm, the gap width is equivalent to the circumference of the ear canal and gap height is the difference in radius between the ear canal and the HPD. In this algorithm, the diameter of the ear canal is held fixed at 0.83 cm, but the gap height is allowed to vary from an initial value of 0.75e-3 cm. This reduces the leak path from two undetermined variables to one.

2.2.2. Material

This branch consists of an inductor (Lmat), capacitor (Cmat), and resistor (Rmat) representing the mass, compliance, and resistance of the hearing protection device. Each of these values are allowed to vary in the optimization algorithm.

2.2.3. Rigid Body

The rigid body branch is composed of an inductor representing the mass of the HPD (Lm), a resistor (Rsk) and capacitor (Csk) representing the viscosity and elasticity of the skin supporting the HPD, and a resistor (Rcu) and capacitor (Ccu) representing the viscosity and elasticity of the ear cup supports present for earmuffs. These elements are represented as follows.

- The cushion of the ear cup supports is composed of a compliance and resistance pair. These values are allowed to vary when using the optimization algorithm.
- The mass of the hearing protection was determined experimentally for each HPD tested. These values were held fixed in the optimization algorithm, thereby reducing the free variables by two.
- The Maxwell model (Kwon, Kwon, & Kim, 2006) for the skin is shown in Figure 10; this is a validated biomechanical model for skin based on small deformations. These values are

held fixed in the optimization algorithm, thereby reducing the number of parameters by one.

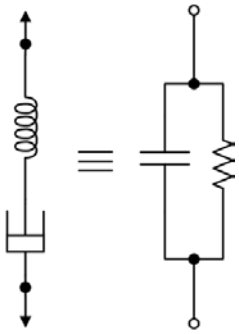

Figure 10: Mechanical Maxwell model representing the response of the skin to high intensity blast and the equivalent electrical model.

3. Steps for Evaluation of Hearing Protection Devices

The goal of this hearing protection device evaluation protocol is to obtain the level-dependent, frequency-dependent insertion loss over the 100-Hz to 10-kHz frequency band over a range of exposure levels relevant to those at which predictions will be conducted. The insertion loss values will then be incorporated into the nonlinear hearing protection module.

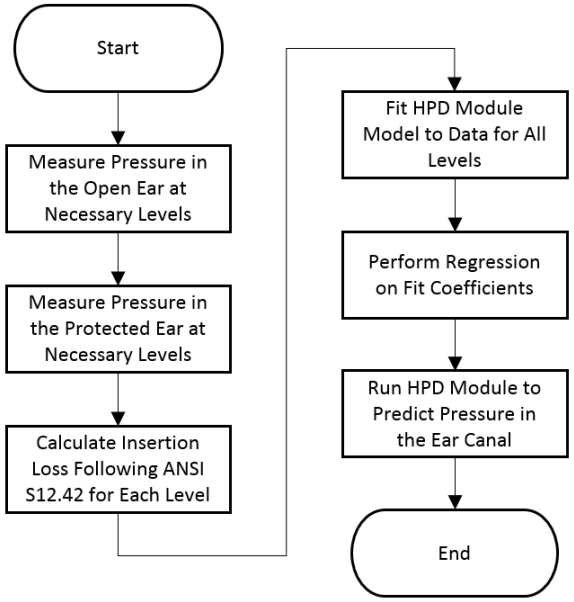

Figure 11. Flow Chart of Analysis Steps

To achieve this goal, the series of steps shown in Figure 11 are followed. These steps span the process for implementing a hearing protection device into the hearing protection module of AHAAH. The process outlines required data collection and analysis of level-dependent insertion loss for the hearing protection device. The free coefficients in the hearing protection module are then fit to the level dependent data for each level tested. A regression is then performed to determine predict the HPD module coefficients at untested exposure levels. This regression is then implemented into the HPD module and predictions of the incident waveform after passing through the HPD module are produced for processing by the remainder of the AHAAH model, regardless of the injury risk criteria of interest. Each of these steps is described in the following sections.

3.1. Measurement of Level-Dependent Impulse Response

To determine the level-dependent impulse response for a HPD, measurements of the blast wave in the freefield and under the hearing protection are collected using an impulsive noise source. Specifically, measurements outside hearing protection made in the freefield, and under the

hearing protection in the ear canal, must be performed simultaneously. Selection of source and target must be made by taking into account the pressures of interest, available facilities, and need for biofidelity and reproducibility. Each of these characteristics are described in the following sections.

3.1.1. Sources

Either compressed gas shock tubes or explosives may be used as a source of impulsive shock waves for the pressure ranges of interest in the HPD evaluation community. The use of shock tubes will be discussed in this protocol due to the ability for laboratories to operate shock tubes without special licensure.

3.1.1.1. ANSI-Compliant Shock Tube

The 4-in diameter shock tube manufactured by B/C Precision Tool shown in Figure 12 is pneumatically controlled to produce shots at intervals as short as 20 seconds. The tube, as purchased, is capable of producing blast overpressures of 132 dB, 150 dB, and 168 dB at 0.5- to 2.0-ms A-duration, meeting the requirements of ANSI/ASA S12.42.

ARA has modified the shock tube to perform additional functions. Computer operation of the shock tube has been enabled to puncture the membrane at specified driver pressures to achieve arbitrary peak free-field pressures from 132 dBP to 183 dBP. The maximum peak pressure for the shock tube has also been increased to 183 dB for use in Ultra level hearing protection testing.

This shock tube utilizes a catenoidal horn to better couple the pressure wave generated by the shock tube to free space by decreasing the impedance mismatch at the end of the tube and reducing turbulence noise from the sharp discontinuity. The horn flares from the 11.4-cm diameter circular pipe to a 1.09-m square cross-section at a length of 2.1 m and is covered with sound dampening material to ensure the pressure wave does not excite resonant modes in the cone walls [36]. When testing, the centerpoint of the ear canal axis of the test fixture is placed 30 cm from the plane of the horn output. Placement of the test fixture and freefield pressure probe should be carried out in consultation with ANSI/ASA S12.42.

Freefield pressures are measured above the center of the ear canal axis using a pencil-style pressure probe containing a high pressure microphone (e.g. G.R.A.S 45BH), oriented with the sensor surface 90° to the long-axis of the shock tube. The shock tube is driven with compressed air for incident pressures below 171 dBP and helium above 171 dBP. The pressure within the driver section of the shock tube is monitored and Mylar (Biaxially-oriented polyethylene terephthalate; greater than 160 dBP) and Acetate (less than 160 dBP) membranes are pierced at a predetermined driver pressure depending on the desired incident pressure level. Recordings are triggered by the drop in pressure in the driver section generated when the membrane ruptures.

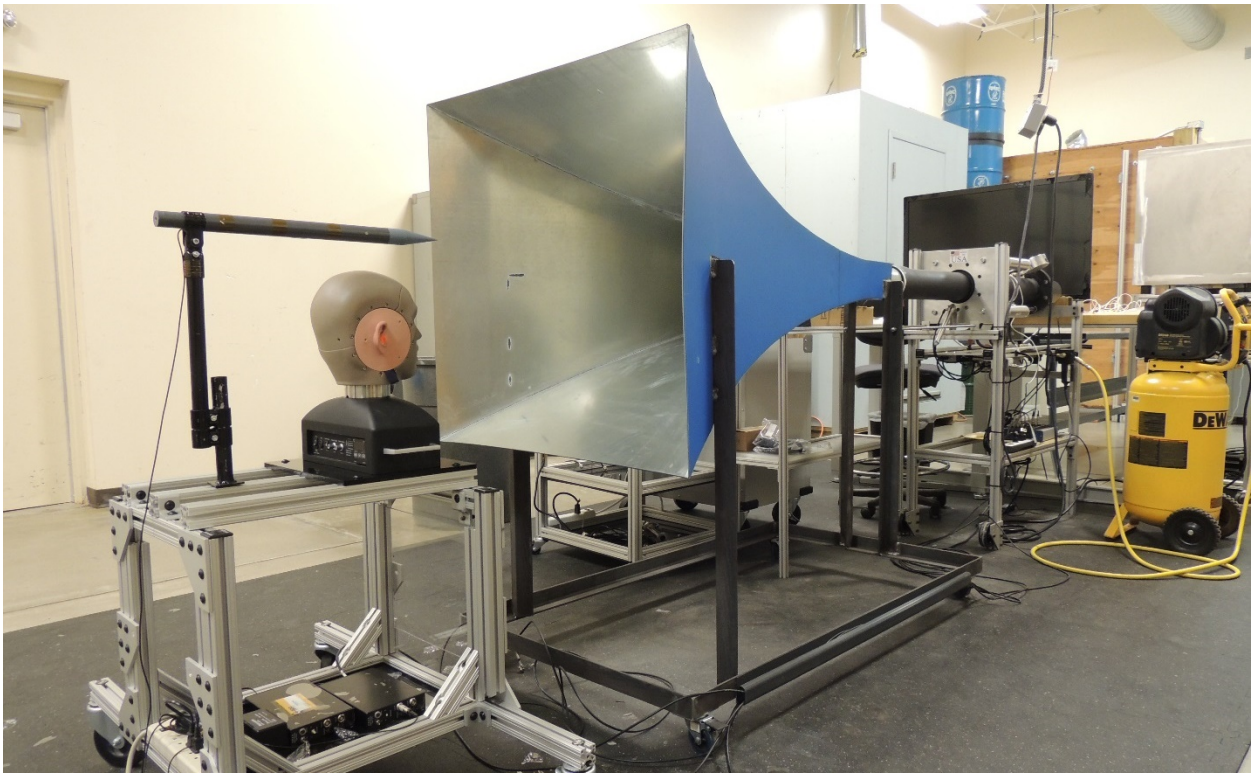

Figure 12: A modified ANSI S12.42-compliant shock tube is capable of exposing a target to incident pressures of 132 dBP to 183 dBP.

3.1.1.2. Mobile Shock Tube

The Mobile Shock Tube (MST) is a compressed-air shock tube designed to replicate the pressure wave produced in the freefield blast environment. The shock tube is capable of producing pressure waves having a characteristic Friedlander waveform with peak pressures and impulse (total energy) characteristic of a free-field blast wave [(Needham, 2010), (Baker, 1973), (Stuhmiller, Phillips, & Richmond, 1991), (McEntire, et al., 2010)]. The shock tube has a 17-inch inner diameter and an eight-foot-long expansion cone at the end of the driven section. This design accommodates large test subjects, such as a full-size human head form, without blocking the tube. In the standard setup, shock waves with peak pressures up to 40 psi and about 4 ms duration are obtainable.

The MST is housed in a semi-trailer that allows the MST to be transported to any research facility. This allows access to advanced medical facilities across the country while maintaining a method to deliver a shock wave that is consistent across many studies and biological models.

Figure 13: ARA's Mobile Shock Tube is capable of exposing a target to incident pressures of 168 dBP to 209 dBP.

Freefield pressures are measured adjacent to the forehead with a "pancake"-style pressure probe (PCB Piezoelectronics), oriented with the sensor surface 90° to the long-axis of the shock tube. The shock tube is driven with compressed air and uses Mylar (for 171 dBP) or aluminum (for higher exposures) membranes that are allowed to rupture spontaneously. A wire mesh screen near the membrane prevents membrane material from contacting the specimen. Pressure is monitored in both the driver and driven segments, near the membrane. Recordings are triggered by the pressure sensor adjacent to the specimen's forehead.

3.1.2. Targets

Both mechanical test fixtures and PMHSs may be used as targets for the evaluation of hearing protection devices. Each type of target has a different preparation and test procedure necessitated by the differences in geometry and material properties, as described below.

3.1.2.1. ANSI S12.42-Compliant Mechanical Test Fixture

Mechanical test fixtures, or headforms, are typically used in mechanical testing laboratories. Little preparation must be performed before testing and a high degree of accuracy and repeatability can be expected using this type of target. However, an idealized measurement of sound reaching the inner ear is recorded with no provisions for bone conduction or realistic tissues.

3.1.2.1.1. Fixture Description

ANSI S12.42 outlines requirements for a test fixture for measuring the IPIL of hearing protection devices. Since this HPD evaluation method uses a similar analysis method, test fixtures developed to meet the Standard guidelines will also provide an appropriate level of performance. The main requirements are as follows, with specifics detailed in the standard.

- Symmetrical ears composed of pinnae, conchae, and ear canals
- Simulated flesh for the ears, including the lining of the ear canals
- Instrumented ear canal couplers containing microphones, which approximate human hearing A-weighted tuning
- The remainder of the fixture must be anthropometrically representative
- The fixture must be maintained at 37 ± 2°C

It should be noted that the test fixture does not provide accurate levels of bone-conducted sound. Instead, when using these headforms, the bone conduction limits must be applied *post hoc* using known bone conduction limits. See Berger (2003) for a development of the limits applied in the standard.

3.1.2.1.2. Instrumentation Example

A G.R.A.S. 45CB conforms to all of the requirements is ANSI S12.42. The microphones, which terminate the ear canals of the 45CB, are designed to mimic the human hearing tuning curves. Standard microphones (40BP) seated in the ear canal couplers are capable of recording up to 174 dB. When performing tests using this test fixture, however, incident pressure levels must remain well below this level due to the acoustic gain provided by the ear canal. The microphones are connected to a G.R.A.S. 26AQ power module to provide external polarization and variable gain which may be needed at lower exposure levels.

Although use of this device and results generated from this device are presented in the balance of this protocol, other test fixtures also meet the ANSI S12.42 requirements (ANSI, 2010).

3.1.2.2. Post Mortem Human Subjects

PMHSs may be used when realistic geometry and tissue properties are of interest. True bone conduction limits are represented and alternative acoustic propagation pathways to the otic capsule are allowed. HPD fit and mechanical behavior under blast loading are also accurately represented; however, a higher degree of preparation is required for these targets and, due to the differences between specimens, a higher degree of variability in measurements is to be expected.

3.1.2.2.1. PMHS Temporal Bone Preparation

Temporal bone preparation procedures are similar to Greene et al. (2017), Greene et al. (2015), Mattingly et al. (2015), Tringali et al. (2010), etc. Briefly, the temporal bones are prepared bilaterally: The pinna and surrounding skin are reflected during preparation but left intact. Temporal bones are prepared with a canal-wall-up mastoidectomy with an extended facial recess. The facial canal is opened and the facial nerve removed to maximize exposure and visibility of the middle-ear structures, which are inspected for damage and abnormalities. The ossicular chain is not disturbed (including the stapedius muscle/tendon). The cochlear promontory is thinned near the oval and round windows in preparation for pressure probe insertion.

3.1.2.2.2. Instrumentation Example

Sensor placement used in Greene (2018) is illustrated in Figure 14 as an example of methods capable of measuring pressure outside and under HPDs. In Figure 14A, specimens were outfitted with an array of sensors in the ears bilaterally, as well as on the surface of the skull, and in the air adjacent to the front surface of the head. This report will only describe measurements from the pressure sensors. Surface sensors were attached above the pinna (in line with the entrance of the ear canal) outside the area of coverage by a set of ear muffs, as well as centered on the forehead. The skin overlying the skull in these locations was reflected. Strain gauges (not utilized in this protocol) were secured to the skull with cyanoacrylate adhesive, and were covered with the reflected flap of skin which was sutured into place. Pressure gauges (Endevco 8515C-15) were similarly affixed to stainless steel plates, which were likewise secured to the skull with

cyanoacrylate adhesive, and the overlying skin removed (Figure 14B). Wires were tightly sutured to the surface of the skin along the circumference of the head.

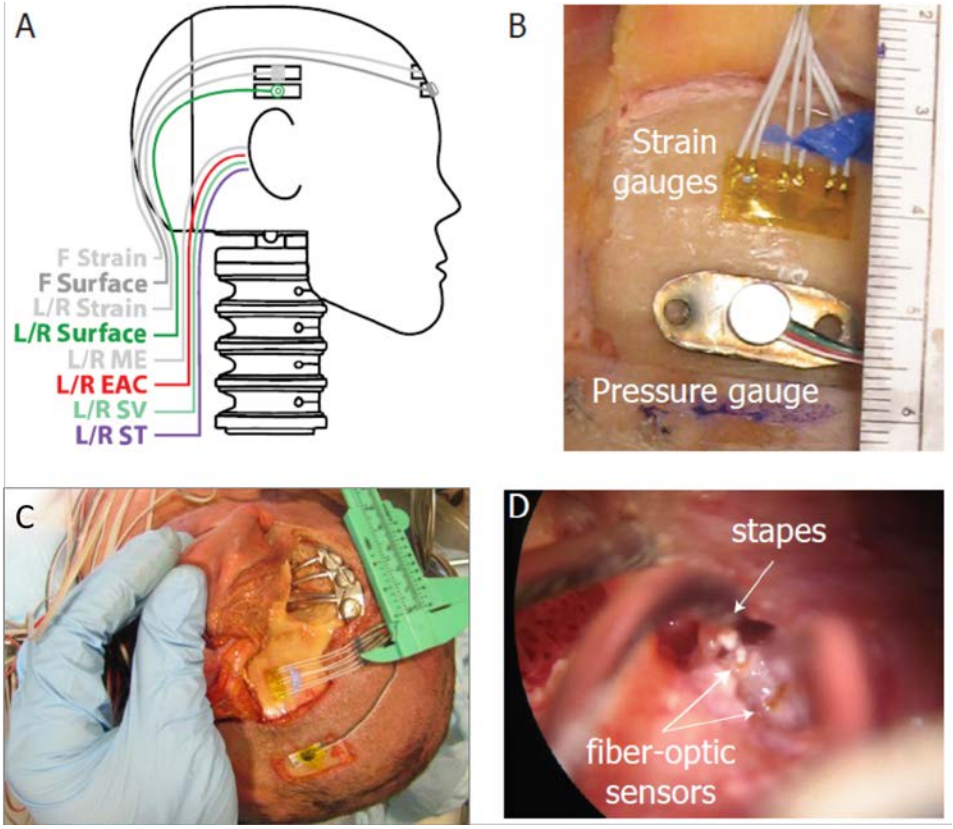

Figure 14: (A) Strain gauges and surface-mount pressure gauges were placed on the skull and fiber-optic pressure sensors were placed into both ear canals, middle ears and cochlea. (B) Strain gauges and surface-mount pressure gauges were fixed to the surface of the skull. (C) Stainless steel tubing was securely mounted to the skull to guide and protect the fiber-optic pressure sensors. (D) Fiber optic pressure sensors were inserted into the cochlea.

Fiber-optic pressure sensors entering the ear (in the ear canal, P_{EAC}; the cochlea in the scala vestibuli, P_{SV} and scala tympani, P_{ST}; and in the middle ear cavity, P_{ME}) were run through custom-fitted stainless steel guide tubes that were affixed to the skull in two positions with stainless steel retaining straps, which were screwed onto the skull with stainless steel screws (Figure 14C). The guide tubes were run under the skin from the base of the skull into the mastoidectomy (through a channel cut in the bone), and fitted such that no deformation was introduced around the pinna (which could interfere with ear muff placement). The end of the guide tube terminated in a hole cut in the bony wall of the ear canal (for P_{EAC}), and less than 1 cm from the intended cochlear target, P_{SV} and P_{ST} (Figure 14D). Fiber-optic sensors (FISO FOP-M-BA for P_{EAC} and P_{ME}, and FOP-M260-ENCAP for P_{SV} and P_{ST}; FISO Inc., Quebec, Canada) were inserted through the guide tubes, inserted underwater into the cochlea via small cochleostomies made with a sharp pick (for P_{SV} and P_{ST}), or until the sensor tip could just be seen (~100 µm) extending from the probe tube into the middle ear (P_{ME}) or the ear canal (P_{EAC}). P_{SV} and P_{ST} probes were sealed in place in the cochlea with alginate dental impression material (Jeltrate). Once placed, fiber-optic sensors were affixed in the guide tubes by applying cyanoacrylate adhesive to the far end of the guide tubes such that the liquid adhesive wicked into the guide tube via capillary action, and the pre-test velocity measurements repeated. The reflected skin and pinna were then fixed back into place

over the mastoidectomy with heavy suture, and the skin margin re-sealed with cyanoacrylate adhesive. Optic fibers and sensor wires were then bundled together at the back of the head, and affixed to the specimen support structure (shielded by the head and rubber/plastic covers), out of the shock tube. In this manner, the sensors and the optic fibers were securely fixed in place and protected from damage.

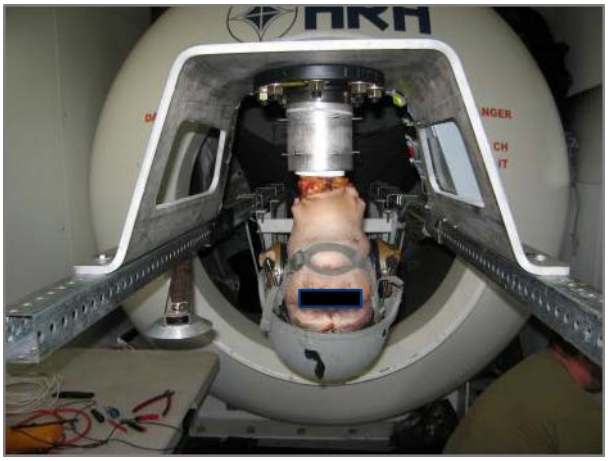

Figure 15: For testing, instrumented PMHS may be suspended within the expansion cone of the mobile shock tube.

3.1.3. Test Procedure

For each hearing protection device or mode of hearing protection device to be tested, an open ears test is performed as a baseline for comparison and a protected ear test is performed to determine the amount of insertion loss/attenuation provided by the hearing protection device. For mechanical test fixtures, open ear tests may be performed up to 150 dBP (or higher, depending on manufacturer specifications of the instrumentation). For PMHSs, open ear tests may be performed up to 183 dB; above this level, there is a high probability of TM rupture, which would render the specimen useless. Protected ear tests for both target types may be conducted to the limits of the instrumentation.

For each test, the following procedure is recommended as a template. Consult the standard operating procedures for the specific equipment being used to ensure any apparatus-specific requirements are met.

1. Align the target such that it is in at normal incidence in relation to the shock tube opening.
2. Clear the target ears of any hearing protection devices.
3. Ensure the ears are in working order. For mechanical headforms, ensure the microphones are responding properly. For PMHSs, monitor the condition of the TM and note any changes.
4. Execute a low level shock tube test with the target ears open to be used as a baseline.
5. Re-check the target to ensure it continues to be in working order.
6. Insert hearing protection devices into the ears of the target according to manufacturer instructions
7. Execute tests with the target ears occluded. These may exposures may follow a prescribed pattern (e.g., increase in pressure) or may be randomized.

8. Periodically, hearing protection should be removed, the ears inspected, and a low level shock tube test with open ears should be repeated to ensure no changes are occurring within the experimental setup.

3.1.4. Typical Data

Typical data collected using the ANSI headform and the ANSI-compliant shock tube are shown in Figure 16. Each subplot shows the received pressure signal in kPa for each of three tests denoted by differences in color. The first column is measurement of the freefield pressure using the pencil probe for each the four different exposure levels (132 dBP, 150 dBP, 168 dBP, and 183 dBP) and are typical of the waveforms produced by the shock tube. The middle and right columns are the received signals under the ARA ShotShields hearing protection. The shape and amplitude of these signals vary based on the type of hearing protection being tested.

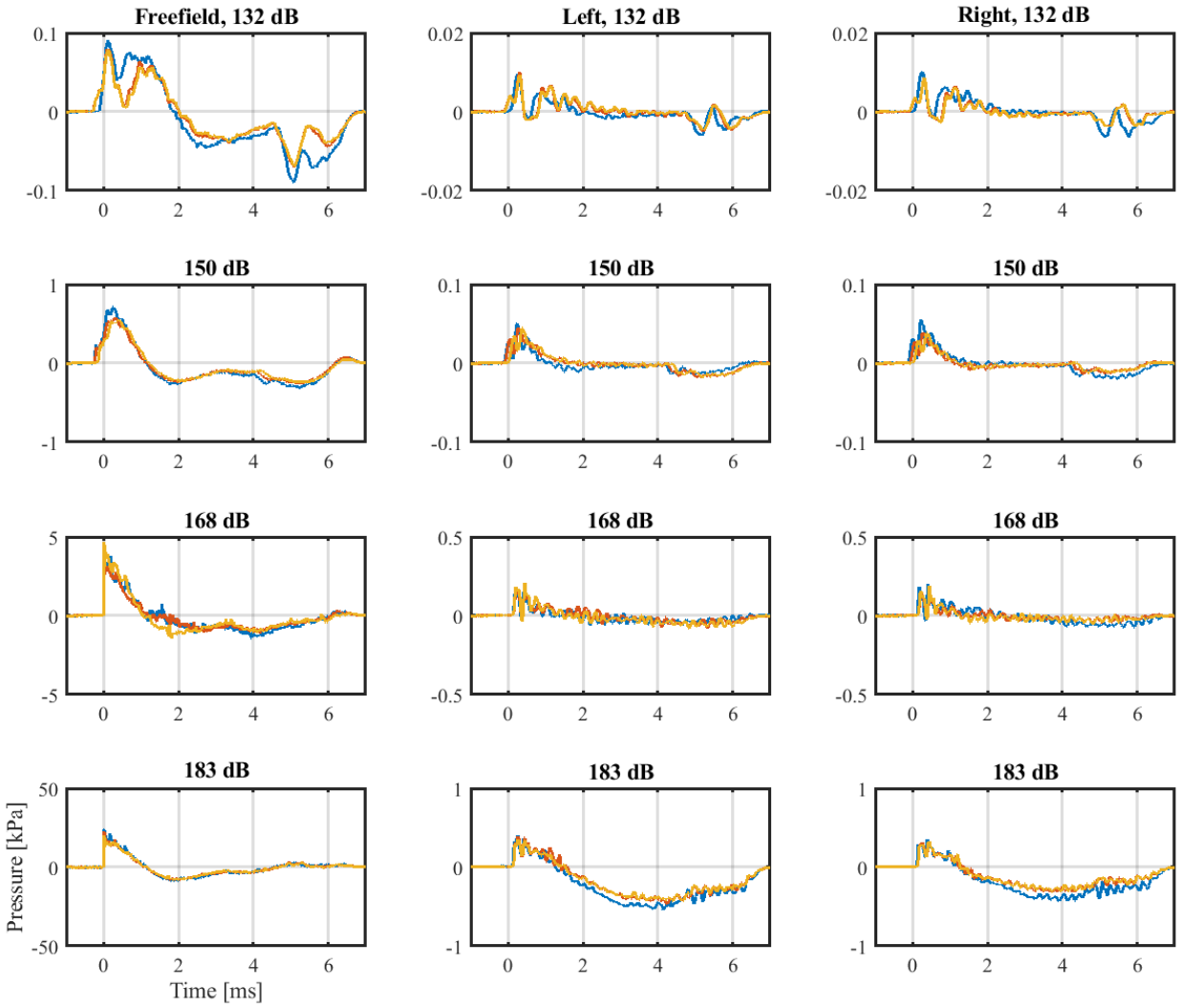

Figure 16: Raw data from IBR testing of the ShotShields HPD with the ANSI shock tube. Rows – 132-dB exposure (Top), 150-dB exposure, 168-dB exposure, 183-dB exposure (Bottom). Columns – Freefield (left), Left Ear, Right Ear (Right). The three tests at each level are shown in different colors: yellow, orange, and blue.

3.1.5. Analysis

When evaluating the effectiveness of hearing protection, ANSI S12.42 reports the IPIL, which is the difference in the received levels in the ear with and without hearing protection present. Measurements similar to those in Figure 16 are collected for the open ear at the 132-dBP and 150-dBP exposure levels. IPIL is calculated by direct comparison of the peak pressures for the 132-dBP and 15-dBP levels and by use of the Transfer Function of the Open Ear (TFOE) for higher levels due to dynamic range limitations of the microphones in the test fixture. In this case, the open ear is compared to the freefield for a lower level (132-dBP or 150-dBP) exposure and added to the comparison between the protected ear and the freefield at a higher (greater than 150 dBP) exposure level. For consistency, when using PMHS specimens, the TFOE is used for each IPIL calculation since all exposures were greater than 150 dBP.

In this program, calculation of IPIL is inadequate to describe the frequency-dependent protection of the hearing protection devices used in the AHAAH model; therefore, each of the recorded waveforms is decomposed into its frequency components to generate a frequency-dependent insertion loss, as described in Figure 17, for each exposure level and trial. A brief description of the processing steps is as follows.

1. The signal is detrended to remove any baseline shift.
2. A third order Butterworth filter is applied to the signal over the 100-Hz to 10-kHz band to isolate the frequency range of interest to the AHAAH model.
3. Each recorded signal is windowed using a Tukey window with a 10% cosine taper to a region 1 ms before and 7 ms after arrival of the peak pressure. This range is adequate to capture the frequency content of the direct arrival while preventing reflected signals and shock tube resonance effects from corrupting the frequency content.
4. A Fast Fourier Transform is applied to the signal to produce the frequency-dependent signal magnitude.
5. The frequency content is averaged over standard 1/3-octave and full octave bands and converted to decibels to produce the frequency-dependent spectrum in 1/3-octave bands and full octave bands. Full octave bands are used for further analysis in AHAAH and 1/3-octave bands are used for qualitative assessment of HPDs. The further analysis steps are applied to both types of spectra.
6. Depending on source level, compute the IL.
    a. For exposure levels less than or equal to 150 dBP, subtract the protected ear spectrum from the open ear spectrum to produce the IL. Subtract the open ear from the freefield to produce the TFOE, the frequency-dependent gain due to the outer ear.
    b. For exposures greater than 150 dBP, standard microphones may be damaged; therefore, the protected ear is subtracted from the freefield and the TFOE generated from a lower level exposure is subtracted from the result. Since the TFOE is assumed to be independent of level, this produces the IL for the higher level exposure.
7. This process is repeated for all trials at each exposure level and for all exposure levels.

Results of this analysis for a level-dependent insert HPD is shown in Figure 18. The freefield blast wave is shown for the protected and unprotected cases (top). Decomposition of these waves into 1/3-octave band averages are shown (middle). Upon combination of the 1/3-octave band averages to create the frequency-dependent attenuation for this exposure, the level-dependent behavior of this HPD is demonstrates by the increasing attenuation with increasing additional exposure levels (bottom).

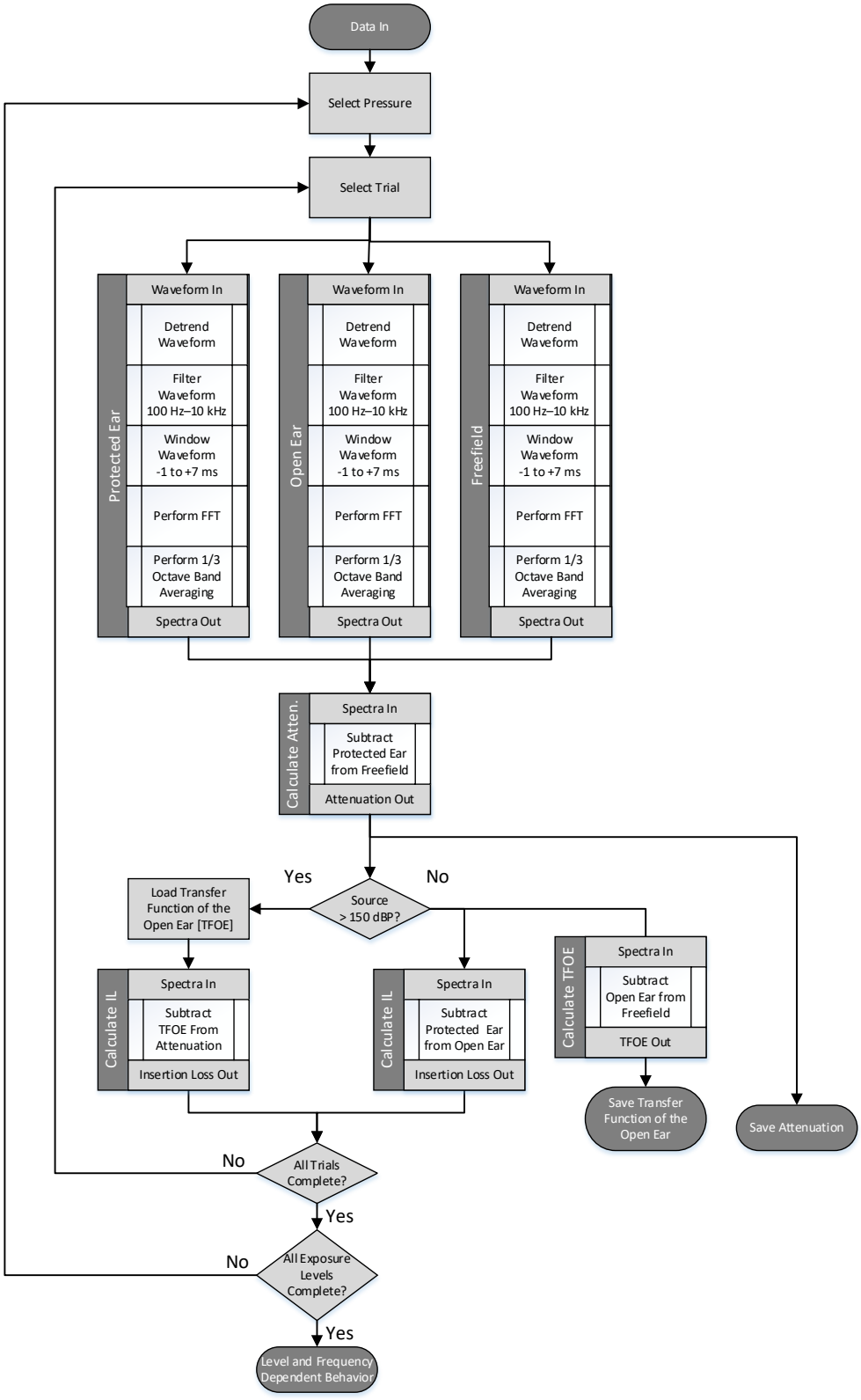

Figure 17: Flow chart describing the calculation steps necessary to determine the level and frequency dependent insertion loss from the impulse waveforms.

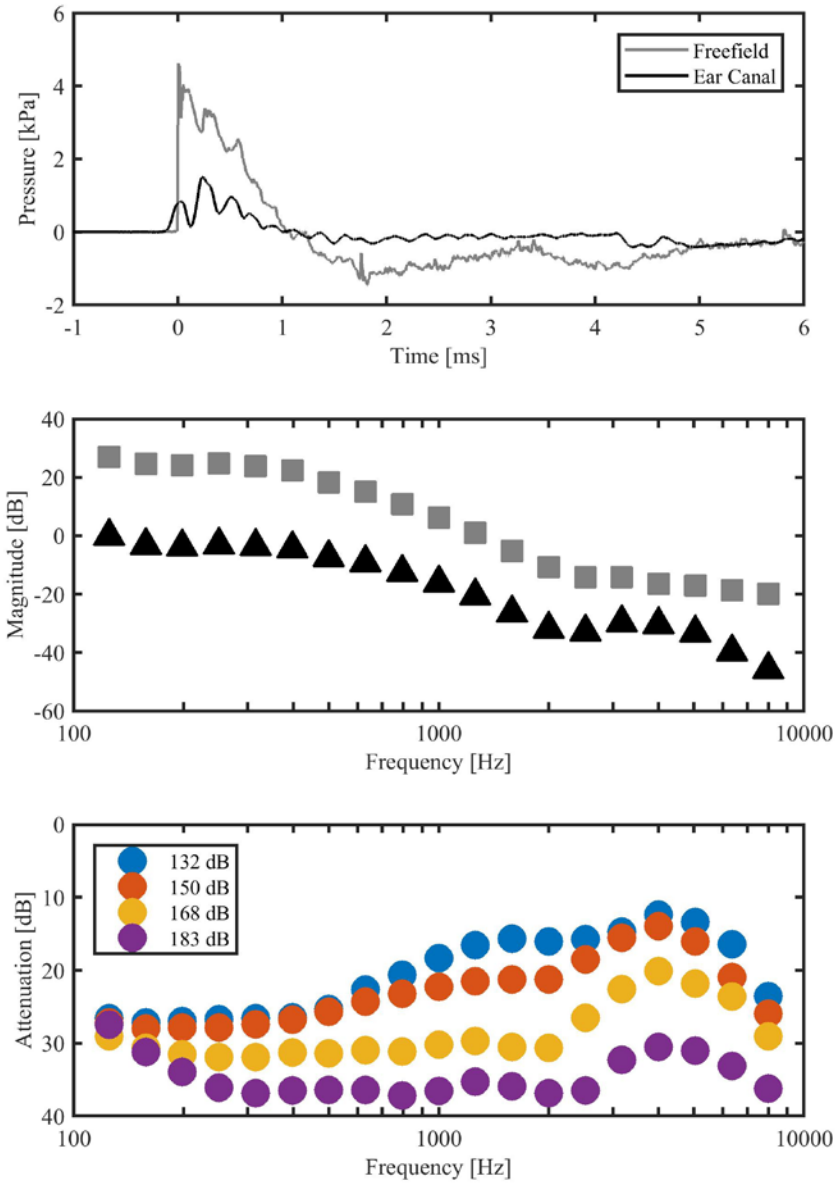

Figure 18: Freefield and protected ear waveforms are collected (top) and decomposed into their 1/3-octave band average frequency components (middle) in dB re 1 Pa. Subtraction of these frequency components for each exposure level demonstrates a device's level- and frequency-dependent attenuation in dB re exposure pressure.

3.2. Fit the HPD Module to the Measured Insertion Loss

To predict the performance of HPDs, the eleven electroacoustic parameters in the linearized hearing protection module are adjusted until the IL prediction matches the measured octave band IL values. This match is optimized through a combination of reduction in the number of fit parameters and by applying an automated fit routine that systematically adjusts the model parameters until the difference between the model and the octave band insertion loss is minimized. The optimized parameters are then used in the regression analysis to model their level-dependent behavior.

3.2.1. Determine Fixed Parameters

To reduce the number of free parameters available in the fitting routine, parameters in the hearing protection module may be fixed as constants based on measurements or tabulated physical values as follows.

- M_m: HPD mass is derived from physical measurement of the mass of the hearing protection device (insert devices) or individual ear cup (circumaural devices). Converted to specific acoustic impedance L_m by dividing by the cross sectional area of the HPD.
- K_{sk}: Stiffness of the skin in the Maxwell skin model (Jones, Greene, & Ahroon, 2017) is taken from Kwon et al. (2006). Conversion to specific acoustic impedance through division by cross sectional area of skin yields 5e-12 cm^5/dyne.
- R_{sk}: Resistance of the skin in the Maxwell skin model is taken from Kwon et al. Conversion to specific acoustic impedance through division by cross sectional area of skin yields 2.03e6 dyne-s/cm^5.
- K_V: The occluded volume under the hearing protection was measured for a variety of insert hearing protection devices and fixed at a value of 1e5 dyne/cm^5.

3.2.2. Optimize for Free Parameters

After assigning values to the fixed parameters, the remaining free parameters are systematically varied to match the modeled attenuation to the measured attenuation values for each exposure level. As the parameters are varied, the resulting frequency-dependent pressure in the ear canal behind the hearing protection is calculated. This pressure is then propagated to the tympanic membrane and middle ear of the AHAAH model.

A flow chart depicting the steps for optimizing the fit parameters is shown in Figure 19. Each step is designed to minimize the total error between the modeled attenuation and measured attenuation. Each branch of the model is sequentially optimized in a ‘fit step,’ which is repeated for four iterations.

3.2.2.1. Initialization

Fitting coefficients will be performed for the lowest exposure level first. Once the optimization routine is completed for an exposure level, the next higher exposure level will be optimized using the previous fit as its initial parameters. For the first fit, the model is initialized with the default coefficients in Table 4 which are based on the specific hearing protection device. ARL-TR-6748 [24] contains tables of coefficients for an array of hearing protection devices derived from fits to REAT (ANSI S12.6) (1984) insertion loss measurements. These coefficients should be used for all hearing protection devices included in the tables with the “generic” muffs and plugs used for devices that have not been included.

Table 4: Initial parameters for the optimization routine are selected from the fixed model parameters described in Chapter 2 and Fedele & Kalb (2015).

Branch	Element	Initial Value	Source
1	L_{mat}	Device-Specific	Fedele 2013
1	M_{mat}	Device-Specific	Fedele 2013
1	R_{mat}	Device-Specific	Fedele 2013
2	L_m	Device-Specific	Lab Measurement
2	K_{cu}	Device-Specific	Fedele 2013
2	R_{cu}	Device-Specific	Fedele 2013
2	K_{sk}	2e11 dyne/cm^5	Kwon 2006
2	R_{sk}	2.03e6 dyne-s/cm^5	Kwon 2006
3	L_{lk} (Imaginary Impedance)	0.75e-3 cm gap height	Sivian 1935
3	R_{lk} (Real Impedance)		Sivian 1935
3	K_v	1e5 dyne/cm^5	Lab Measurement

Once the initial coefficients have been selected, the frequency-dependent lumped element impedance for each element should be calculated as follows:

Resistance: $$Z_R = R_{ac} = \frac{R}{S^2} \quad (18)$$

Compliance: $$Z_K = \frac{K_{ac}}{j\omega} = \frac{K}{j\omega S^2} \quad (19)$$

Mass: $$Z_L = j\omega L_{ac} = \frac{j\omega L}{S^2} \quad (20)$$

In the element impedances, the subscript ac refers to the specific acoustic impedance and is equivalent to the element value normalized by the cross-sectional area *S*. In these formulas, *j* is the imaginary constant and ω is the angular frequency in radians/second. Upon calculating the element impedances, standard methods for solving electrical circuits can be used to determine the impedance for each branch and for the system as a whole.

The intent of this model is to determine the amount of pressure arriving in the ear canal behind the hearing protection such that it can be propagated through the middle and inner ear sections of the model to predict hearing injury. Therefore, the output of the hearing protection module, the attenuation due to the HPD, is the pressure drop across the K_v element compared with the freefield value which is analogous to the voltage drop in a standard electrical circuit formulation compared with the source voltage.

3.2.3. Model Iteration

To find a global minimum for the model, the elements in the branches are systematically fit in steps to the frequency range in which they govern the response. First, the gap height in the leak branch is varied to fit the 125-, 250-, 500-, and 1000-Hz octave band portion of the attenuation. Then, the three material parameters in the material branch are varied to fit the 1000-, 2000-, 4000-, and 8000-Hz octave band portion of the attenuation. Finally, the earmuff suspension parameters are varied to fit the 500-, 1000-, and 2000-Hz band portion of the attenuation.

The iteration cycle is repeated four times to systematically increase the goodness of fit of the model-data comparison. To determine the goodness of fit between the calculated attenuation and the experimentally measured attenuation, an error estimate is made. An average of the deviation

of the modeled attenuation from the measured attenuation is used. In each iteration, this elements resulting in the minimum of this value are propagated to the next fitting step.

Due to the large number of fit parameters and the smaller number of data points, the fit parameters are allowed to vary widely during each iteration cycle. In the first of the four iterative cycles, allowable values for each parameter are allowed to span six orders of magnitude centered on the value propagated from the previous fit step. In subsequent iterations the allowable span is reduced such that in iteration two, the span is three orders of magnitude, iteration three is 1.5 orders of magnitude, and iteration four is one order of magnitude. This scheme allows the parameters for each branch to affect the fit of subsequent fit steps while being affected by previous fit steps.

To ensure the calculated values are physically reasonable, the resonance frequency and quality factor of the oscillator formed by each of the three branches is also calculated:

$$f_{res} = \frac{1}{\omega}\sqrt{\frac{K}{L}} \tag{21}$$

$$Q = \frac{1}{R}\sqrt{KL} \tag{22}$$

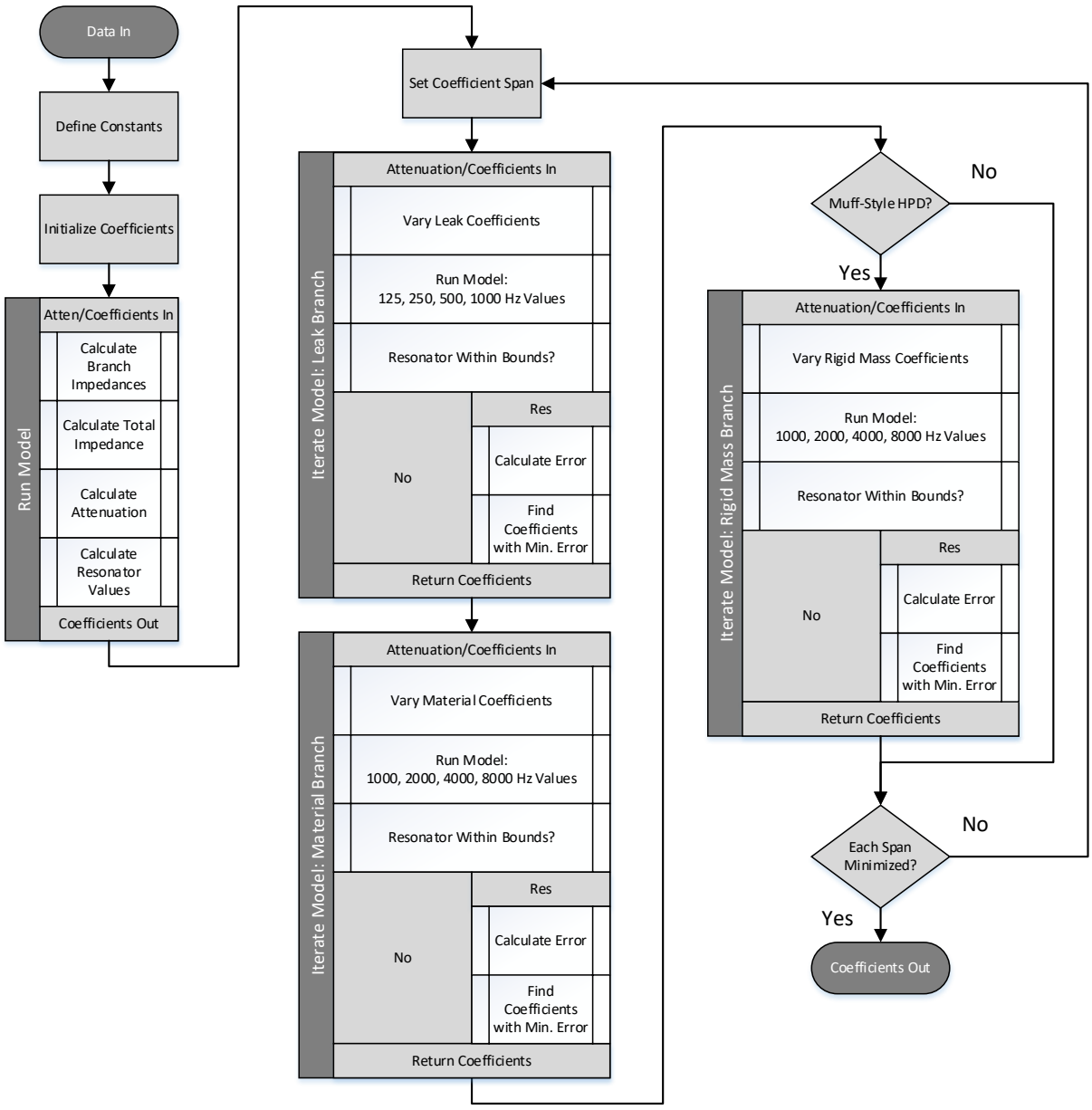

Figure 19: The coefficient optimization routine for a given HPD and exposure level is performed using this sequence of steps.

The resonance frequency and quality factor for each branch is bounded to a physically reasonable range and limited from values outside of these bounds. The bounds for the resonance frequencies and quality factors for each branch are shown in Table 5. Fit steps generating element values, which caused the quality factor and resonance frequency to fall outside of these ranges, were discarded and the coefficients from the previous fit step were carried forward.

Table 5: The resonance frequency and quality factor of the oscillator formed by each branch is bounded to ensure the elements maintain physical relevance.

Branch	Q_{min}	Q_{max}	f_{min} (Hz)	f_{max} (Hz)
Material	0.5	10	1000	20000
Rigid Mass	0.5	10	1000	5000
Leak	0.01	10	None	2000

3.2.4. Fitting Results

An example output of the fitting routine is shown in Figure 20 for a nonlinear universal fit insert HPD for four sequential exposure levels from 171 dBP to 192 dBP. The model has fit the gray triangles to the data represented by the black squares in octave bands. In each case, the orange line represents the contribution of the leak branch to the total impedance, the blue line represents the contribution of the material branch to the total impedance, and the black line represents the continuous impedance curve. A line representing the rigid body branch is not visible at this scale for this HPD. In this example, the leak branch varies little, behaving as a leak with a consistent gap width around the device. The material branch demonstrates increased attenuation with exposure level as intended by the level-dependent design of the device.

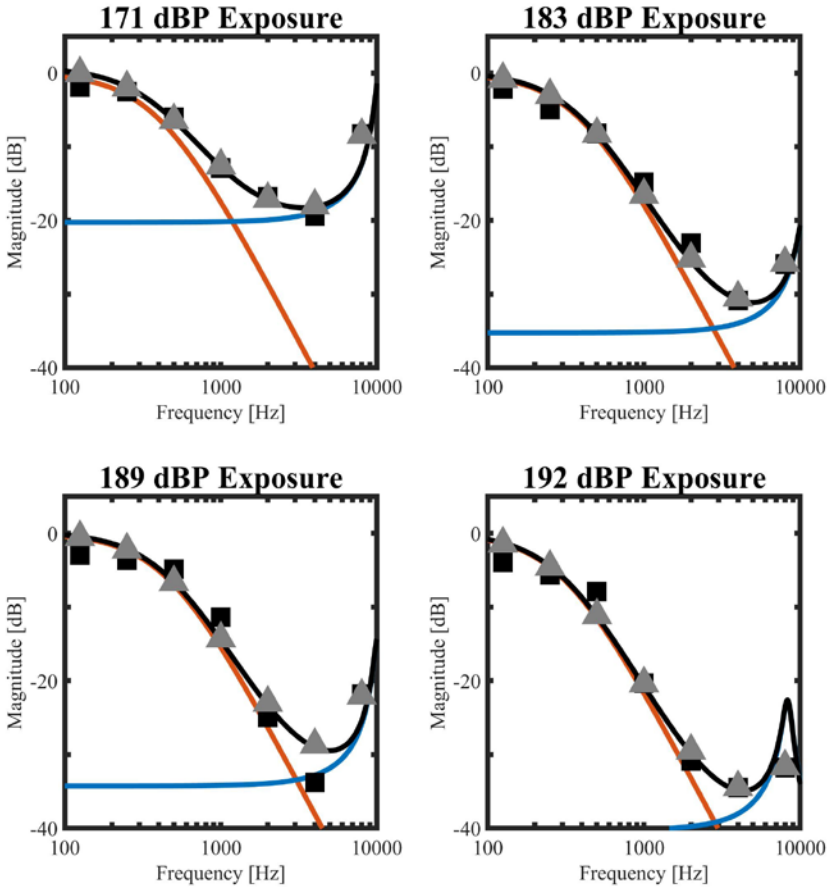

Figure 20: The optimization routine varies the elements of the HPD module to compare the module result (gray) with the measured data (black). Each branch of the model is varied sequentially; the resultant response for the low frequency (orange) and high frequency (blue) are shown. This process is repeated for each exposure level.

3.3. Regression Analysis of Model Coefficients

The optimization routine produces the elements of the HPD module that most closely resemble the measurements for each exposure level. Nonlinear behavior of the elements, however, must be determined by finding a relationship that can be implemented in the Simulink model. Element values for a given test fixtures and source may be determined by the optimization routine. However, since the routine optimizes attenuation, a relative measurement independent of source or test fixture, rather than pressure, an absolute measurement varying from fixture to fixture or source to source, the results may be combined to form one set of coefficients; these may then be applied to a given fixture or source.

To determine the behavior of the elements at levels that were not tested, a linear regression is performed on each element with respect to exposure level in dBP,

$$E = e^{A*P+B} \tag{23}$$

where E is the element value, P is the exposure level in dBP, and A and B are the linear fit coefficients. Figure 21 demonstrates a fit (gray lines) to PMHS data for 171-dBP, 183-dBP, 189-dBP, and 192-dBP exposures (black dots). Linear elements such as K2 and R3 do not vary with the fit, generating a pressure-independent line at a single element value. Nonlinear elements demonstrate slopes with both positive and negative behavior and are implemented in the model regardless of the sign of the coefficient.

The regression analysis performed on each coefficient demonstrates a limitation of this approach. The slopes of the coefficients may produce nonphysical element values when extrapolating the coefficients outside the range of incident pressures measured; therefore, model predictions for incident pressures outside of the range used in the regression analysis should be considered carefully to ensure that the coefficients generate physical predictions.

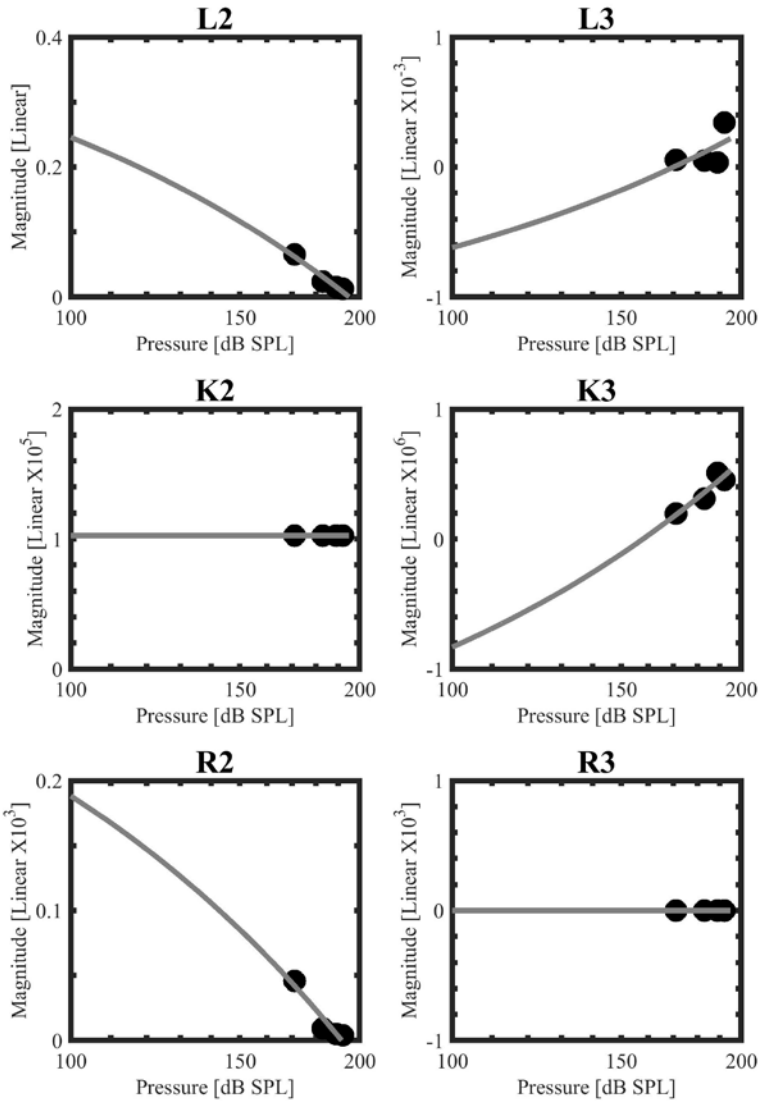

Figure 21: Linear regressions were performed on each of the calculated coefficients to determine how the nonlinearity was is included in the appropriate elements. Some elements remain linear while others display nonlinear behavior.

3.4. Implement the Regression Coefficients into a Simulink Model of the HPD Module

The Simulink model block diagram representing the ARA nonlinear hearing protection model is shown in Figure 22. A pressure source is programmed to import a pressure-time history recorded from a freefield measurement and the solver is programmed to find a solution at each time step. Nonlinear elements are arranged in the same manner as the circuit schematic of the nonlinear model shown in Figure 9. Other model elements are probes to observe the instantaneous pressure, including a probe to measure the pressure delivered to the ear canal compliance. This pressure is equivalent to the pressure measured in the ear canal during testing and is used as the solution to the model.

A typical implementation of a nonlinear element is shown in Figure 23. Coefficients for the element are imported and interpolated based on the instantaneous pressure, then combined using Equation 23. The linear coefficients are implemented using the same elements as the nonlinear coefficients, but using $A = 0$ for the linear term. Use of the same element construct allows the model to be used for linear and level-dependent devices with no changes. The coefficient is then applied to the element; in this example, the element is an inductor.

Exercising the model for a pressure-time history of interest produces the information shown in Figure 24. In each subplot, the blue lines represent the model output and the orange lines represent the measurement. The top pane shows the general time-domain agreement between the model and measurement for a level-dependent earplug at a 183 dBP (4 psi) exposure. The center subplot shows the frequency-domain spectrum for both measurement and model which is further decomposed into one third octave bands in the lower subplot. In this example, good agreement between the measurement and model is seen in the time domain signals; the frequency spectra show good agreement between 1 kHZ and 3 kHz with the model over-predicting the amount of pressure propagating through the HPD above and below this band.

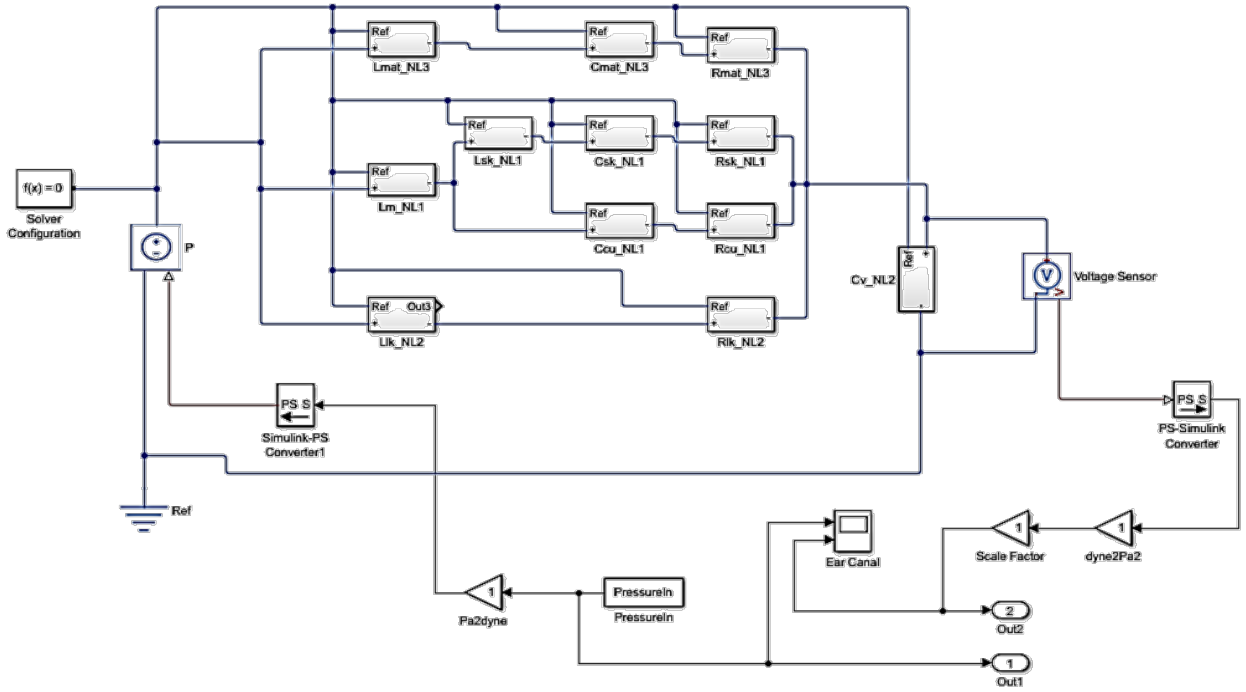

Figure 22: ARA's Nonlinear HPD Simulink Model consists of the nonlinear elements, solver, and monitoring probe points.

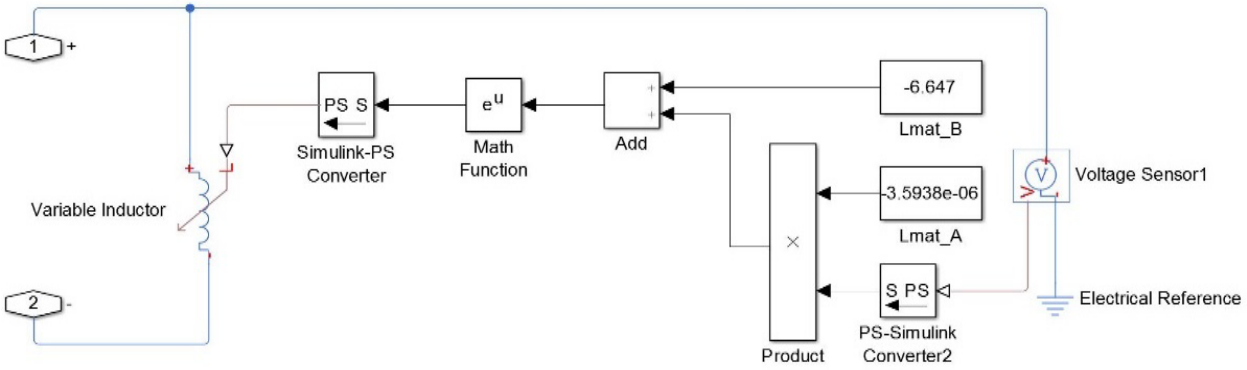

Figure 23: Element implementation for ARA's Simulink model consists of coefficient lookup and interpolation routines.

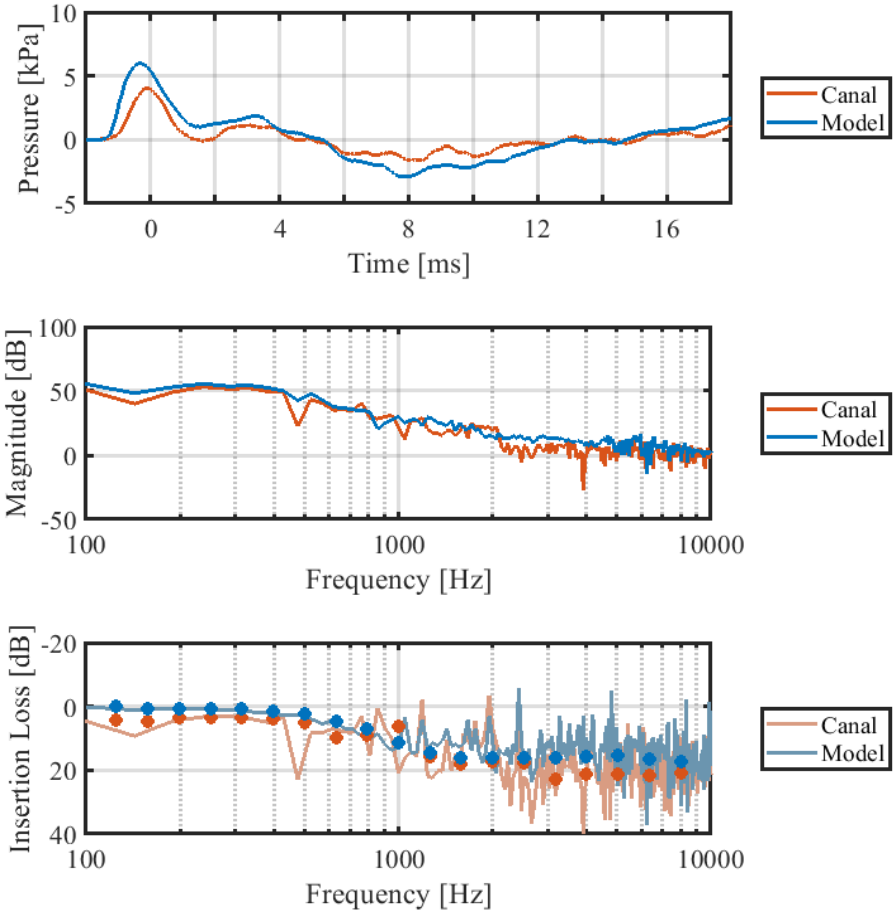

Figure 24: Simulink Model Output. Top – Time domain waveform. Center – Frequency Spectrum. Bottom – Continuous frequency and one-third octave band-limited IL.

3.5. Validation

An example of validation of the ARA nonlinear model is shown in Figure 25. Data measured in the ear canal of a PMHS specimen exposed to a 183-dBP blast overpressure is shown in blue. Model predictions using the linear AHAAH model are shown in orange. Model predictions for the

ARA model with linear (yellow) and nonlinear (purple) coefficients are shown. The peak pressure in the ear canal is well predicted by the ARA nonlinear model, though the ARA linear and AHAAH linear models capture more of the fine structure of the received signal. Results for other devices and levels are consistent with this example. Further data-model comparisons were performed for four hearing protection devices and the open ear and are shown in detail in Chapter 4.

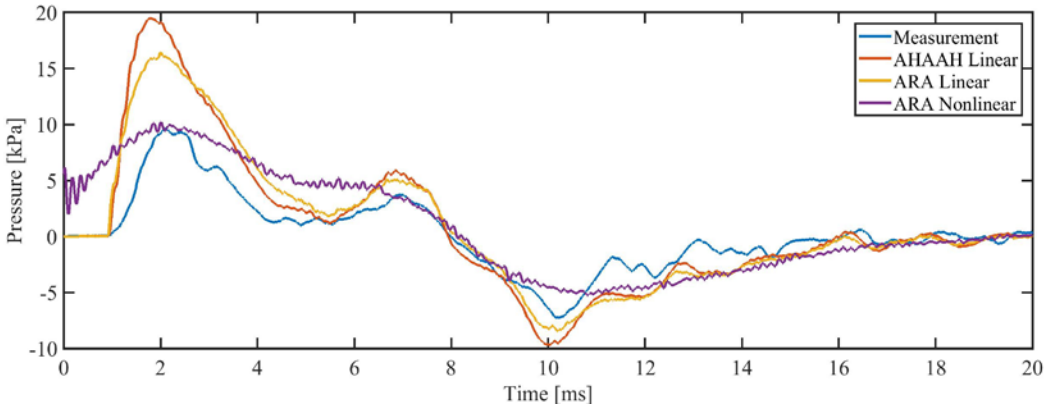

Figure 25: Model predictions were validated by comparing model predictions to data for the linear AHAAH model, the linearized ARA model and the nonlinear ARA model. The ARA nonlinear model produced model predictions equivalent to or exceeding the linear AHAAH model.

3.6. Limitations of the Updated HPD Module

- Measurements and regressions were only performed over the 85- to 192-dB exposure range. Results may not be valid for exposures outside of this pressure range.
- Coefficients were derived for four hearing protection devices. Use of other devices will require collection of additional data.
- Measurements within PMHSs may produce insertion loss values which differ from those obtained using mechanical test fixtures due to the differences in material properties. Combination of insertion loss data from both sources may produce regressions with higher error than if each dataset were treated separately.
- The order in which the fitting routine conducts its optimization search may affect the results for some hearing protection devices due to the presence of local minima in the model parameter space.

4. Application of the Level-Dependent HPD Module

Measurements of four hearing protection devices and the open ear were conducted to validate the model. Each of these devices is commonly used by the U.S. Army or was developed at the Army's behest. Table 6 is a brief description of each of the hearing protectors. Each of these devices was evaluated using both PMHS and ANSI test fixtures; results from PMHS testing are shown in the following sections.

Table 6: Descriptions of hearing protection devices tested using this protocol

<table>
<tr><th>Equipment</th><th>Real Ear Attenuation at Threshold (ANSI, 1984)</th><th>Picture</th></tr>
<tr><td>• 3M E-A-R Classic
• In-the-Ear
• Universal Fit
• Roll-Down Foam Earplug
• Level-Independent Performance</td><td>
<table>
<tr><th></th><th>125</th><th>250</th><th>500</th><th>1000</th><th>2000</th><th>3150</th><th>4000</th><th>6300</th><th>8000</th><th>NRR</th></tr>
<tr><td>Mean</td><td>37.4</td><td>40.9</td><td>44.8</td><td>43.8</td><td>36.3</td><td>41.9</td><td>42.6</td><td>46.1</td><td>47.3</td><td rowspan="2">29</td></tr>
<tr><td>S.D.</td><td>5.7</td><td>5</td><td>3.3</td><td>3.6</td><td>4.9</td><td>3</td><td>3.1</td><td>3.5</td><td>2.7</td></tr>
</table>
</td><td>  </td></tr>
<tr><td>• 3M Combat Arms Earplug
• In-the-Ear
• Universal Fit
• Tested Open (Nonlinear) Position
• Level-Dependent Performance</td><td>
<table>
<tr><th></th><th>125</th><th>250</th><th>500</th><th>1000</th><th>2000</th><th>3150</th><th>4000</th><th>6300</th><th>8000</th><th>NRR</th></tr>
<tr><td>Mean</td><td>4.1</td><td>4.5</td><td>11</td><td>18.7</td><td>24.9</td><td>29.8</td><td>25.8</td><td>18.7</td><td>26.5</td><td rowspan="2">7</td></tr>
<tr><td>S.D.</td><td>2.7</td><td>2.8</td><td>3.9</td><td>3.2</td><td>3.3</td><td>2.7</td><td>3.3</td><td>3.6</td><td>3.3</td></tr>
</table>
</td><td>  </td></tr>
<tr><td>• ARA ShotShields
• In-the-Ear
• Universal Fit
• Tested Open (Nonlinear) Position
• Level-Dependent Performance</td><td>
<table>
<tr><th></th><th>125</th><th>250</th><th>500</th><th>1000</th><th>2000</th><th>3150</th><th>4000</th><th>6300</th><th>8000</th><th>NRR</th></tr>
<tr><td>Mean</td><td>22.4</td><td>21.3</td><td>24.2</td><td>22.2</td><td>22.6</td><td>27.5</td><td>23.5</td><td>31.1</td><td>38</td><td rowspan="2">15</td></tr>
<tr><td>S.D.</td><td>3.9</td><td>3.8</td><td>4</td><td>3.5</td><td>3.3</td><td>3.8</td><td>3.1</td><td>4.4</td><td>3.8</td></tr>
</table>
</td><td>  </td></tr>
<tr><td>• 3M ComTac III
• Over-the-Ear Muff
• Tested with Power Off
• Level-Independent Performance</td><td>
<table>
<tr><th></th><th>125</th><th>250</th><th>500</th><th>1000</th><th>2000</th><th>3150</th><th>4000</th><th>6300</th><th>8000</th><th>NRR</th></tr>
<tr><td>Mean</td><td>15.2</td><td>17.6</td><td>24.9</td><td>30.5</td><td>33.4</td><td>39.3</td><td>41.4</td><td>46.2</td><td>45.8</td><td rowspan="2">21</td></tr>
<tr><td>S.D.</td><td>4.2</td><td>2.7</td><td>2.3</td><td>3.8</td><td>4.1</td><td>3</td><td>3.4</td><td>3</td><td>4.7</td></tr>
</table>
</td><td>  </td></tr>
</table>

In the following sections, model predictions are compared to the measured pressure in the ear canal behind the HPDs in PMHS specimen targets using the Mobile Shock Tube as a source. Incident pressures used to form the regression coefficients were from 171-, 183-, 189-, and 192-dBP tests. In each of the results figures for the specific HPDs, blue lines represent the measured pressure in the ear canal, orange lines represent the predictions of the linear AHAAH HPD module, yellow lines represent the predictions of the ARA model presented in this protocol with all coefficients held constant, and purple lines represent the results from application of the full nonlinear model.

4.1. Open Ear

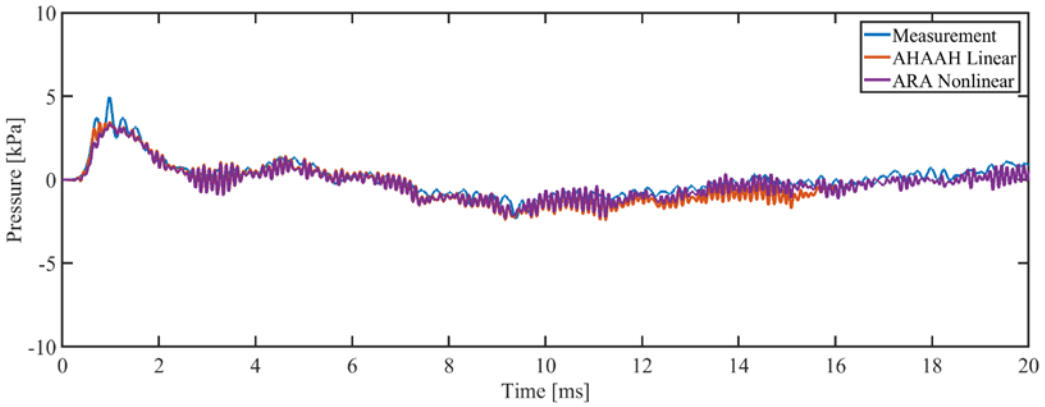

Figure 26: Data-model comparison for the Open Ear for a 171-dBP exposure sows good agreement between the measurement, AHAAH Linear and ARA nonlinear models.

Open ear measurements were performed for the 171-dB exposure only. Higher exposure levels with the open ear usually damaged, but did not rupture, the tympanic membrane; hence, regression through multiple exposure levels was not possible. For this reason, the ARA linear and nonlinear models are the same.

The data-model comparison for the open ear for one example 171-dBP exposure is shown in Figure 26. The peak pressure and A-duration are accurately captured by both the AHAAH linear and ARA models. Overall trends in the shape, even at long durations (~15 ms to 20 ms) are accurately recorded. Both the AHAAH linear and ARA Nonlinear models demonstrate a small amount of extra high frequency energy which is apparent periodically throughout the waveforms, such as that apparent near 3 ms. This noise is at approximately 100 kHz, well above the range of human hearing and may be related to the time step utilized when running the models. Regardless, it would be imperceptible to humans.

4.2. Over-the-Ear HPD

The data-model comparison for the Peltor Comtac III earmuff with gel cushions is shown in Figure 27 for a 183-dBP exposure. The ARA model with linearized elements matches the measured A-duration well, however, the peak pressure is over-predicted by a factor of two and the strength of the shock is much stronger. The AHAAH linear model and the ARA model with nonlinear elements both capture the general shape of the measured pressure consisting of two gentle humps and a return to a near-quiescent state after approximately 12 ms. The peak pressure using these models is over-predicted by approximately 10%.

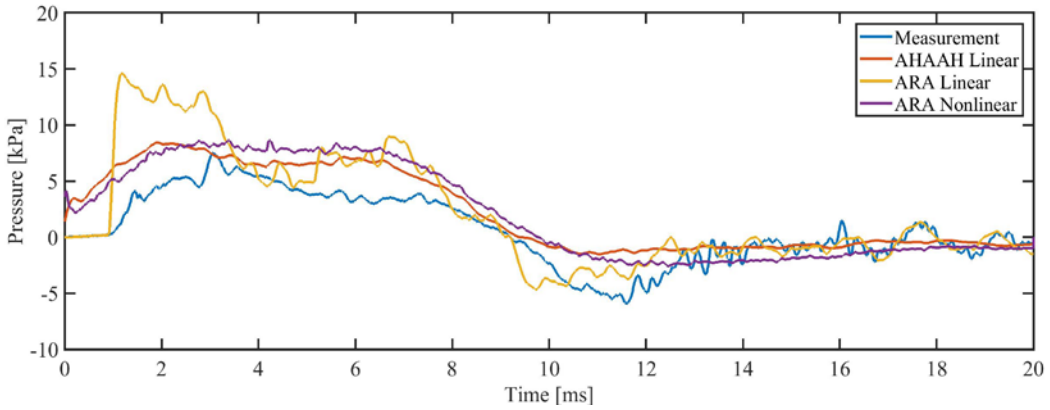

Figure 27: Data-model comparison for the Comtac III for a 183-dBP exposure. The peak pressure is matched well by the ARA nonlinear model and the AHAAH linear model. The ARA model with linear coefficients does not well represent the peak pressure.

4.3. In-the-Ear HPDs

The data-model comparison for the 3M Combat Arms is shown in Figure 28 for a 183-dBP exposure. The linear AHAAH model and linearized ARA model both accurately predict the A-duration and shape of the measured pressure as demonstrated by a two hump positive phase and negative phase, all arriving at equivalent times. These models over-predict the peak pressure, however, by 100% for the AHAAH linear model and 60% for the ARA linear model. The ARA nonlinear model accurately predicts the peak pressure and the general shape of the measured pressure, but prediction of the fine structure is poor.

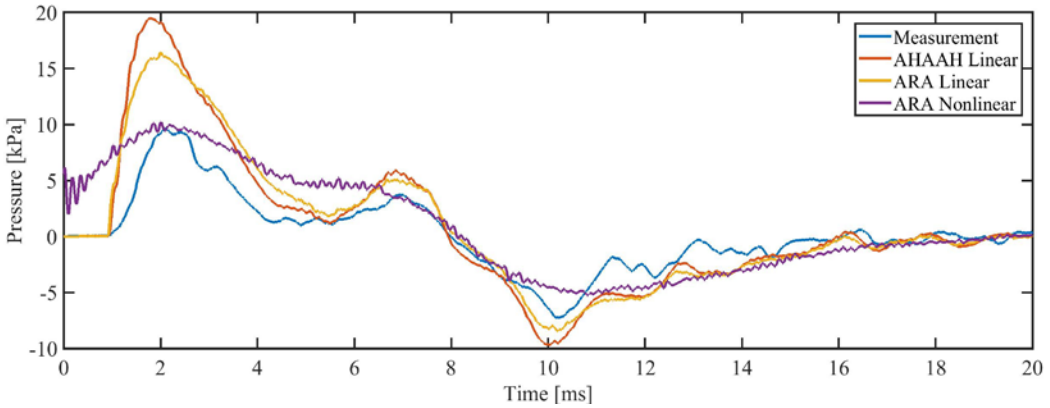

Figure 28: Data-model comparison for the 3M Combat Arms for a 183-dBP exposure. The A-duration is well captured by the AHAAH and ARA linear models, but the peak pressure is well captured by the ARA nonlinear model.

The data-model comparison for the ARA ShotShields is shown in Figure 29 for a 183-dBP exposure. The AHAAH linear model was implemented with the generic insert HPD coefficients for this case and the data-model comparison is poor. The ARA linear and ARA nonlinear models both capture more of the structure with the linear ARA model providing the best prediction of both A-duration and peak pressure. This hearing protection device has a constant attenuation down to low frequencies at approximately 15 dB to 20 dB. In the HPD model. The low frequency leak branch must use a very small gap to produce this attenuation; physically unrealistic artifacts may

appear as a result when the linear regression extrapolates for lower pressures, such as the small jump near 7 ms.

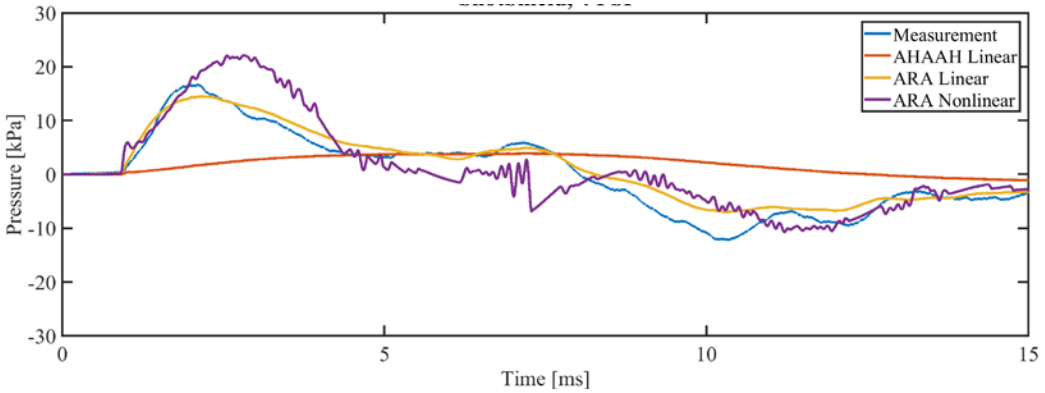

Figure 29: Data-model comparison for the ShotShields for a 183-dBP exposure. The behavior of the measured pressure is poorly predicted by the linear AHAAH model, but predicted more accurately by the ARA model.

The data-model comparison for the 3M E-A-R Classic foam earplugs is shown in Figure 30 for a 183-dBP exposure. The AHAAH linear model predictions are poor and do not represent the measured pressure. The ARA linear model under-predicts the peak pressure by 30%, yet captures the general shape of the measured pressure with respect to the A-duration and negative phase. The ARA nonlinear model accurately predicts the peak pressure and negative phase peak pressure of the measurement, though it over-predicts the A-duration by approximately 20%.

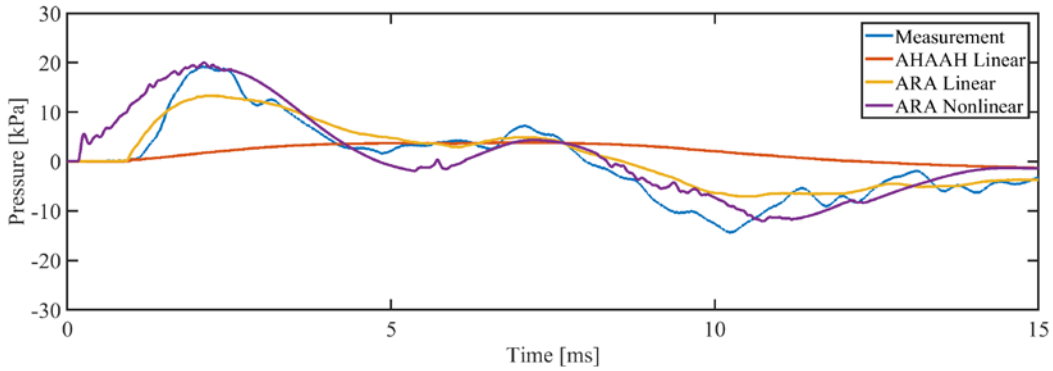

Figure 30: Data-model comparison for the E-A-R Classic for a 183-dBP exposure. The ARA nonlinear model captures the peak pressure and fine structure of the measured pressure with the ARA linear and AHAAH linear models providing poorer predictions.

4.4. Comparison between Test Fixtures and PMHSs

This protocol presents a method for evaluating hearing protection devices that is not tied to either the source generating the overpressure or the target holding the hearing protection. As an example of the comparison between PMHSs and a test fixture, the results of a data-model comparison for a 183-dBP exposure is shown in Figure 31. In each of these cases, the nonlinear model was used and the regressions were performed over the 132-dBP to 183-dBP band for the test fixture and over the 171-dBP to 192-dBP band for the PMHSs. As shown, both sets of equipment produce reasonable predictions of the measured pressure; each captures the general shape, peak pressure, and A-duration. The ANSI test fixture under-predicted the peak pressure

by approximately 10%, but matched the amplitude of the remainder of the measured pressure wave. The PMHS prediction matched the peak pressure, but overestimated the A-duration by approximately 15%. The PMHS prediction does not match the shape of the measured pressure as well, likely due to the coefficient regression being performed over multiple PMHSs with different physiology and tissue properties, which would introduce more variability into the data. The predictions based on the test fixture data were acquired using a much more consistent piece of test hardware which generated better behaved coefficients as demonstrated by the tighter fit.

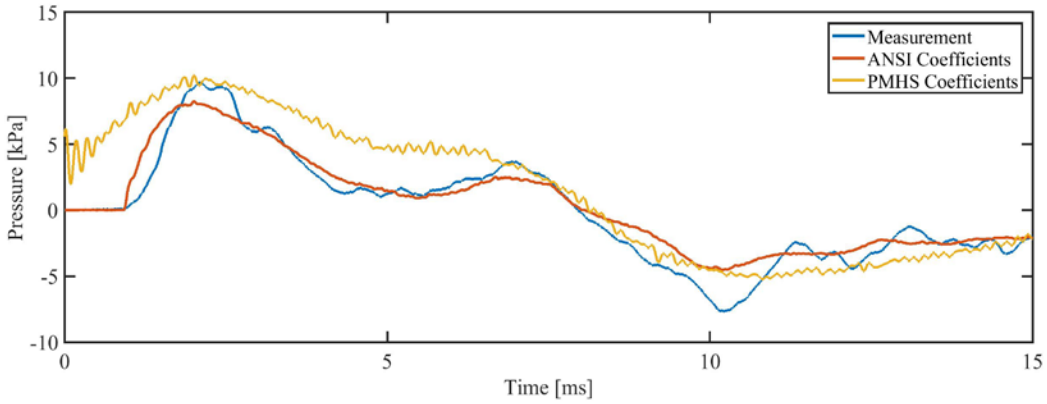

Figure 31: Measured pressure in a PMHS (blue) compared to model predictions for coefficients generated from ANSI test fixture (orange) and PMHS (yellow) measurements produce different predictions for a 183-dBP exposure. The ANSI coefficients better predict the measured pressure in the ear canal compared to the PMHS coefficients due to the variability in PMHS geometry and tissue parameters.

5. Conclusion

5.1. Implications and Application of the HPD Evaluation Protocol

The protocol presented here implements a nonlinear model of hearing protection devices and the method for obtaining the model parameters for each device so that it can be accurately implemented into the model. The optimization routine may be run on measured data from arbitrary source levels while maintaining physical relevance for each parameter. These physically relevant parameters, coupled with the laboratory-based measurements of other parameters, reduce the number of free variables in the fitting from 11 to 6, thereby providing more confidence in the optimization routine's ability to produce a globally minimized fit of the model to the data.

This protocol provides a straightforward means of implementing hearing protection devices into a range of hearing injury without requiring specific equipment for validation measurements. The regression analysis used for estimating the response of the devices at source levels not measured is a means to reduce the size of the overall testing program when evaluating a large range of devices. These features both reduce the burden on model developers by reducing the equipment footprint, time, and cost necessary for validation studies.

In summary, the hearing protection device evaluation protocol and model presented here is agnostic of source and target and produces results equivalent to or exceeding those of a linear model. This protocol and model is extremely flexible as demonstrated by its ability to produce accurate predictions for any hearing protection device. Finally, due to the modular nature of the model itself, it can be integrated into any model capable of utilizing the pressure in the ear canal as an input to downstream prediction of hearing injury, thereby allowing the greater hearing injury prediction community to experiment with different model formulations depending on the model architecture and type of injury predicted.

5.2. Recommended Future Work

Two major avenues of inquiry would enhance the applicability and benefits provided by this protocol. At present, this protocol is capable of predicting only the protection afforded by hearing protection devices as it pertains to hearing injury from the air conducted pathway through the auditory system. Advancement of a model capable of predicting vestibular injury from blast overpressure, described in Figure 32, would allow for prediction of balance disorders, as well as hearing loss, resulting from blast exposure. This effort would require the implementation of a hearing protection module to accurately assess injury probability. Study of the alternative paths for acoustic wave propagation from freefield to the hair cells throughout the human labyrinth, described in Figure 33, would determine under which conditions the PMHS versus mechanical targets would be appropriate. Each of these programs is a logical extension of this work and would allow operators to employ weapons systems without increasing risk of injury, possibly increasing accuracy of determination of safe return to duty times when injuries due to blast overpressure exposure are correctly classified.

SOLVING PROBLEMS OF GLOBAL IMPORTANCE

Follow-on Work

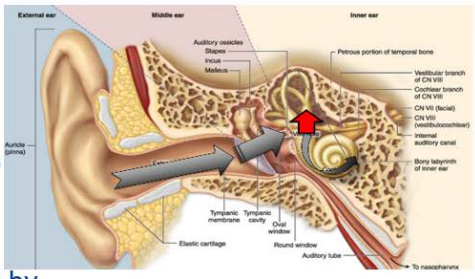

Problem Addressed No injury threshold for vestibular neurotrauma exists. Without, some Traumatic Brain injuries (TBI) symptoms are being misinterpreted since vestibular neurotrauma produces outcomes similar to TBI.

Hypothesis: Vestibular blast Injury model can be developed by scaling physiological damage observed from chinchillas exposure to overpressure. Clinical relevance of the damage can be quantified through the application of clinical evaluations performed on injured animals and humans exposed during combat

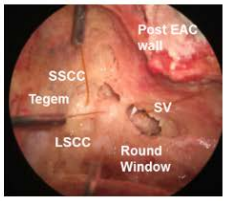

Specific Aims

1. Quantify Damage to the Peripheral System
2. Determine Clinical Relevance of Injuries
3. Develop a Human Injury Threshold & Model

Vestibular disorders are preventable and evidence suggests damage is reversible with pharmaceutical therapies if diagnosed early

ARA
www.ara.com

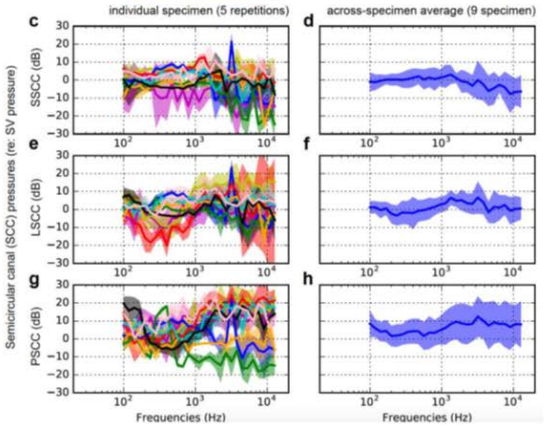

Figure 32: Understanding injury thresholds for the vestibular system and study of the protective power of hearing protection devices for preventing vestibular injury should be undertaken to prevent misdiagnosis of vestibular disorders as traumatic brain injury and allow operators to return to duty more quickly.

SOLVING PROBLEMS OF GLOBAL IMPORTANCE

Follow-on Work: Bone Conduction Pathways

Problem Addressed Current standards for predicting the risk of auditory injury only take into account energy transmitted from the pressure source, through the ear canal and the ossicular transmission chain, and into the inner ear. This is just one of the five pathways by which acoustic energy reaches the inner ear. The remaining four pathways are related to bone conduction: 1) motion of the middle ear ossicles relative to their surroundings caused by inertial reaction as the skull is vibrated; 2) inertial reaction of the inner ear fluid; 3) compression and expansion of the otic capsule; and 4) transmission of pressure waves through the skull.

Specific Aims

- Quantify the energy transmitted through each of the identified air and bone conduction pathways by measuring pressures within the cochlear and vestibular labyrinthine system.
- Extend current models for predicting blast-induced hearing and vestibular injury to include energy transmitted through bone conduction for improving the accuracy of protective equipment evaluations that includes in-ear plugs, over-the-ear muffs, and military helmets.

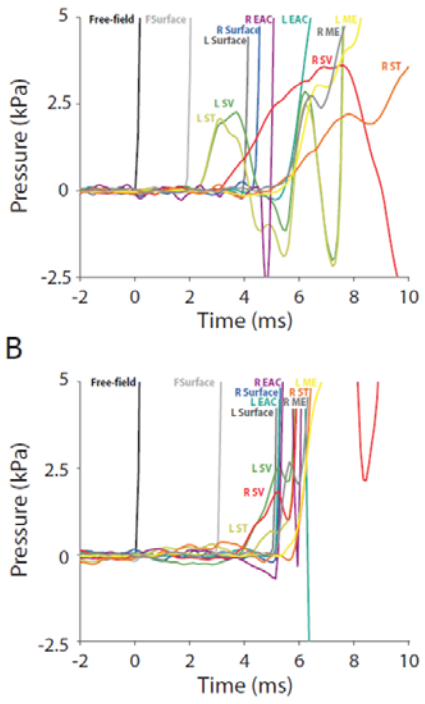

ARA www.ara.com

SCHOOL OF MEDICINE
Department of Physiology and Biophysics
UNIVERSITY OF COLORADO ANSCHUTZ MEDICAL CAMPUS

Figure 33: Measurement of the alternative pathways for sound propagation to the middle ear would allow for the design of protective systems and engineering controls for high amplitude exposures, deployment of which would allow operators more freedom to utilize potentially injurious weapons systems.

6. Acknowledgements

Development of modifications to the AHAAH model and the protocol for measuring the level dependent response of hearing protection devices was performed under Assistance Agreement W81XWH-15-2-0002 from Dr. Richard Shoge, U.S. Army Medical Research and Materiel Command.

7. References

Ahroon, W. (2017). *Effects of acoustic impulses on the middle ear.* U.S. Army Medical Research and Materiel Command. Tacoma, WA: The Geneva Foundation.

ANSI. (1974). *Method for Measurement of Real-Ear Protection of Hearing Protectors and Physical Attenuation of Earmuffs (ANSI S3.19).* New York, NY: American National Standards Institute (ANSI).

ANSI. (1984). *Method for the Measurement of the Real-Ear Attenuation of Hearing Protectors (ANSI S12.6-1984).* New York, NY: American National Standards Institute (ANSI).

ANSI. (2010). *American National Standard Methods for the Measurement of Insertion Loss of Hearing Protection Devices in Continuous or Impulsive Noise Using Microphone-in-Real-Ear or Acoustic Test Fixture Procedures (ANSI S12.42).* New York, NY: American National Standards Institute (ANSI).

Baker, W. E. (1973). *Explosions in air.* Austin, TX: University of Texas Press.

Baker, W. E., Kulesz, J. J., Westine, P. S., Cox, P. A., & Wilbeck, J. S. (1981). *A manual for the prediction of blast and fragment loadings on structures (SWRI-02-5594).* San Antonio, TX: Southwest Research Institute.

Berger, E. H., Kieper, R. W., & Gauger, D. (2003). Hearing Protection: Surpassing the Limits to Attenuation Imposed by the Bone-Conduction Pathways. *The Journal of the Acoustical Society of America, 114*(4), 1955-1967.

Brinkmann, H. (2003). Chapter 4: Supplementary investigation of the German Damage Risk Criterion with the Belgian NATO small arms rifle FNC. In NATO, *Reconsideration of the effects of impulse noise [Technical Report TR-017].* Neuilly-Sur-Seine, France: North Atlantic Treaty Organization (NATO).

Chan, H. S. (1998). *Occupational Noise Exposure: Criteria for a recommended standard (DHHS (NIOSH) Publication No. 98-126).* Cincinnati, OH: NIOSH.

Chan, P. C., Ho, K. H., Kan, K. K., Stuhmiller, J. H., & Mayorga, M. A. (2001). Evaluation of impulse noise criteria using human volunteer data. *The Journal of the Acoustical Society of America, 110*(4), 1967-1975.

Chan, P., Ho, K., & Ryan, A. F. (2012). *Auditory 4.0 Impulse Noise Injury Model [J0563-12-509-R1].* San Diego, CA: SPAWAR.

Chandler, D. W., & Edmond, C. V. (1997). Effects of Blast Overpressure on the Ear: Case Reports. *Journal of the American Academy of Audiology, 8*, 81-88.

Coles, R. R., Garinther, G. A., Rice, C. G., & Hodge, D. C. (1967). *U.S. Army Technical Memorandum 13-67: Criteria for Assessing Hearing Damage Risk from Impulse-Noise Exposure.* Abderdeen Proving Ground, MD: U.S. Army Human Engineering Laboratories.

Ethridge, N. H., Lottero, R. E., Wortman, J. D., & Bertrand, B. P. (1984). *Computational and Experimental Studies of Blockage Effects in a Blast Simulator (ARBRL-TR-02564).* Aberdeen Proving Ground, MD: U.S. Army Ballistic Research Laboratory.

Fedele, P., & Kalb, J. (2015). *Level-Dependent Nonlinear Hearing Protector Model in the Auditory Hazard Assessment Algorithm for Humans [ARL-TR-7271].* Adelphi, MD: U.S. Army Research Laboratory.

Flamme, G. A., Deiters, K. K., Tasko, S. M., & Ahroon, W. A. (2017). Acoustic reflexes are common but not pervasive: Evidence from the National Health and Nutrition Examination Survey, 1999–2012. *International Journal of Audiology, 56*(sup1), 52-62.

Greene, N. T., Alhussaini, M. A., Easter, J. R., Argo IV, T. F., Walilko, T., & Tollin, D. J. (2018, August). Intracochlear pressure measurements during acoustic shock wave exposure. *Hearing Research, 365*, 149-164.

Greene, N. T., Jenkins, H. A., Tollin, D. J., & Easter, J. R. (2017). Stapes displacement and intracochlear pressure in response to very high level, low frequency sounds. *Hearing Research, 348*, 16-30.

Greene, N. T., Mattingly, J. K., Jenkins, H. A., Tollin, D. J., Easter, J. R., & Cass, S. P. (2015). Cochlear implant electrode effect on sound energy transfer within the cochlea during acoustic stimulation. *Otology & Neurotology, 36*(9), 1554.

Henry, G. A. (1945). Blast injuries of the ear. *The Laryngoscope, 55*(11), 663-672.

Hirsch, F. G. (1968). Effects of Overpressure on the Ear—A review. *Annals of the New York Academy of Sciences, 152*(1), 147-162.

IEC. (2003). *Electroacoustics — Sound level meters.* Geneva, Switzerland: International Electrotechnical Commission (IEC).

Johnson, D. L., & Patterson, J. H. (1997). *Effectiveness of a leaking earmuff versus a leaking earplug (USAARL-97-23).* Fort Rucker, AL: U.S. Army Aeromedical Research Laboratory.

Jones, H. G., Greene, N. T., & Ahroon, W. A. (2017). *Assessment of Middle Ear Function during the Acoustic Reflex Using Laser-Doppler Vibrometry [USAARL-2017-16].* Fort Rucker, AL: U.S. Army Aeromedical Research Laboratory.

Jones, H., Greene, N., & Ahroon, W. A. (2018). Human middle-ear muscles rarely contract in anticipation of acoustic impulses. *The Journal of the Acoustical Society of America, 143*(3), 1962.

Kalb, J. T. (2013). *An electroacoustic hearing protector simulator that accurately predicts pressure levels in the ear based on standard performance metrics [ARL-TR-6562].* Aberdeen Proving Ground, MD: U.S. Army Research Laboratory, Human Research and Engineering Directorate.

Kalb, J. T., & Price, G. R. (2015). *Mathematical Model of the Ear's Response to Weapons Impulses [ARL-RP-0521].* Aberdeen Proving Ground, MD: U.S. Army Research Laboratory.

Khan, A., Murphy, W. J., & Zechmann, E. L. (2012). *Design and construction of an acoustic shock tube for generating high-level impulses to test hearing protection devices (EPHB Report No. 350-12a).* National Institute for Occupational Safety and Health (NIOSH).

Kwon, H. J., Kwon, Y. H., & Kim, Y. H. (2006). Biomechanical skin measurement system for analysis viscoelasticity. *Key Engineering Materials, Vols. 326-328*, pp. 777-780.

Mattingly, J. K., Greene, N. T., Jenkins, H. A., Tollin, D. J., Easter, J. R., & Cass, S. P. (2015). Effects of skin thickness on cochlear input signal using transcutaneous bone conduction implants. *Otology & Neurotology, 36*(8), 1403.

McEntire, B. J., Chancey, V. C., Walilko, T., Rule, G. T., Weiss, G., Bass, C., & Shridharani, J. (2010). *Helmet Sensor - Transfer Function and Model Development.* San Antonio, TX: True Research Foundation.

McGregor, K. D., Flamme, G. A., Tasko, S. M., Deiters, K. K., Ahroon, W. A., Themann, C. L., & Murphy, W. J. (2018). Acoustic reflexes are common but not pervasive: evidence using a diagnostic middle ear analyser. *International Journal of Audiology, 57*(sup1), S42-S50.

NATO. (2010). *Hearing Protection—Needs, Technologies and Performance (TR-HFM-147).* Neuilly-Sur-Seine, France: North Atlantic Treaty Organization (NATO).

Needham, C. E. (2010). *Blast Waves (Shock Wave and High Pressure Phenomena).* London & New York: Springer.

Olson, H. F. (1957). *Acoustical engineering.* Princeton, NJ: van Nostrand Company.

OSHA. (2013). *Authority for 1910 Subpart G.* Washington, DC: Occupational Safety and Health Administration (OSHA).

Patterson Jr., J. H., & Johnson, D. L. (1994). *Actual Effectiveness of Hearing Protection in High Level Impulse Noise (USAARL-94-48).* Fort Rucker, AL: U.S. Army Aeromedical Research Laboratory.

Patterson Jr., J. H., & Johnson, D. L. (1994). *Temporary threshold shifts produced by high intensity freefield impulse noise in humans wearing hearing protection (USAARL-94-46.* Fort Rucker, AL: U.S. Army Aeromedical Research Laboratory.

Patterson Jr., J. H., Mozo, B. T., Gordon, E., Canales, J. R., & Johnson, D. L. (1997). *Pressures measured under earmuffs worn by human volunteers during exposure to freefield blast overpressures (USAARL-98-01).* Fort Rucker, AL: U.S. Army Aeromedical Research Laboratory.

Peacock, J., Al Hussaini, M., Greene, N. T., & Tollin, D. T. (2018). Intracochlear pressure in response to high intensity, low frequency sounds in chinchilla. *Hearing Research, 367*, 213-222.

Pfander, F., Bongartz, H., Brinkmann, H., & Kietz, H. (1980). Danger of auditory impairment from impulse noise: A comparative study of the CHABA damage-risk criteria and those of the Federal Republic of Germany. *The Journal of the Acoustical Society of America, 67*(2), 628-633.

Price, G. R. (2007). Validation of the auditory hazard assessment algorithm for the human with impulse noise data. *The Journal of the Acoustical Society of America, 122*(5), 2786-2802.

Price, G. R. (2011). *The auditory hazard Assessment Algorithm for Humans (AHAAH): Hazard Evaluation of Intense Sounds [ARL-TR-5587].* Aberdeen Proving Ground, MD: U.S. Army Research Laboratory.

Price, G. R., & Kalb, J. T. (1991). Insights into hazard from intense impulses from a mathematical model of the ear. *The Journal of the Acoustical Society of America, 90*(1), 219-227.

Price, G. R., Kalb, J. T., & Jokel, C. R. (2017). *Critical Examination of the Article Impulse Noise Injury Prediction Based on the Cochlear Energy by Zadadou, Chan, Ho, and Shelly [ARL-TR-7958].* Aberdeen Proving Ground, MD: U.S. Army Research Laboratory.

Reider, R. H. (1966). Personal communication concerning data from two industrial explosions. Los Alamos, NM: Los Alamos National Laboratory.

Sivian, L. J. (1935). Acoustic impedance of small orifices. *The Journal of the Acoustical Society of America, 7*(2), 94-101.

Smoorenburg, G. F. (2003). *Risk of hearing loss from exposure to impulse sounds: Reconsideration of the Effects of Impuse Noise [RTO Technical Report TR-017].* Neuilly-Sur-Seine, France: North Atlantic Treaty Organization (NATO).

Stuhmiller, J. H., Phillips, Y. Y., & Richmond, D. R. (1991). Chapter 7: The Physics and Mechanisms of Primary Blast Injury. In R. F. Bellamy, R. Zajtchuk, & T. M. Buescher, *Conventional Warfare: Ballistic, Blast, and Burn Injuries* (Vol. 5, pp. 241-270). Washington, DC: Walter Reed Army Institute of Research, Walter Reed Army Medical Center.

Tringali, S., Koka, K., Deveze, A., Holland, N. J., Jenkins, H. A., & Tollin, D. J. (2010). Round window membrane implantation with an active middle ear implant: a study of the effects on the performance of round window exposure and transducer tip diameter in human cadaveric temporal bones. *Audiology and Neurotoloty, 15*(5), 291-302.

U.S. Dept of Defense. (2010). *Department of Defense Instruction 6055.12: DoD Hearing Conservation Program (HCP).* Washington, DC: U.S. Dept of Defense.

U.S. Dept of Defense. (2015). *Department of Defense Design Criteria Standard Noise Limits (MIL-STD-1474E).* Washington, DC: U.S. Dept of Defense.

U.S. Dept of the Army. (2015). *Army Hearing Program [Pamphet, DA PAM 40-501].* Washington, DC: U.S. Government Printing Office.

U.S. Dept of Veterans Affairs. (2017). *Veterans Benefits Administration Annual Benefits Report: Fiscal Year 2016.* Washington, DC: U.S. Dept of Veterans Affairs.

Vadala, A. J. (1930). Effects of Gun Explosions on the Ear and Hearing Mechanism. *Mint. Surgeon, 66*, 810-822.

Wightman, F. L., Flamme, G., Campanella, A. J., & Luz, G. A. (2010). *American Institute of Biological Sciences Peer Review of Injury Prevention and Reduction Research Task Area: Impulse Noise Injury Models.* Retrieved from https://www.arl.army.mil/www/pages/343/AHAAH_AIBS_revew_Public_Release_11Aug14.pdf

Wortman, J. D., & Lottero, R. E. (1982). *Comparison of HULL Hydrocode Computations of Shock Tube Blockage Effects on Target Loading for Step Shocks and Rapidly-Decaying Shocks (ARBRL-MR-03232).* Aberdeen Proving Ground, MD: U.S. Army Ballistic Research Laboratory.

Wu, Q., & Qin, J. (2013). Effects of key parameters of impulse noise on prediction of the auditory hazard using AHAAH model. *International Journal of Computational Biology and Drug Design, 6*(3), 210-220.

Zagadou, B., Chan, P., Ho, K., & Shelly, D. (2016). Impulse noise injury predection based on the cochlear energy. *Hearing Research, 342*, 23-38.

Improvement and Extension of Auditory Hazard Models

ERMS/Log Number **13063022**

Award Number: **W81XWH-15-2-0002**

PI: Tim Walilko, Ph.D. **Org:** Applied Research Associates, Inc. **Award Amount: $** 2,320,452

Study/Product Aim(s)

- Develop a neuro-functional understanding of acoustic injury encompassing the dynamics of the peripheral auditory system, through sensory transduction, to central auditory processing.
- Develop an animal model, correlating human and animal auditory mechanisms and physiological responses to noise and blast events.
- Develop a robust, validated system for the evaluation of hearing protective systems across the broad range of intensities and frequency spectra seen in real-world exposures.

Approach

Phase 1 – Simulation of blast through EAC to improve cochlea parameters in AHAAH model as well as validate output from in-ear shock emulator.

Phase 2 – Quantify middle ear bone dynamics to increase the fidelity of the parameters in the model representing the stapes and annular ligament

Phase 3 – Extend AHAAH model using auditory evoked potentials and behavior data from Chinchilla model to improve the understanding of cognition of high amplitude sound including any nonlinear effects:

Phase 4 – Improve AHAAH model to predict risk of injury for high impulse noise and identify the appropriate type of hearing protection for real-world exposures

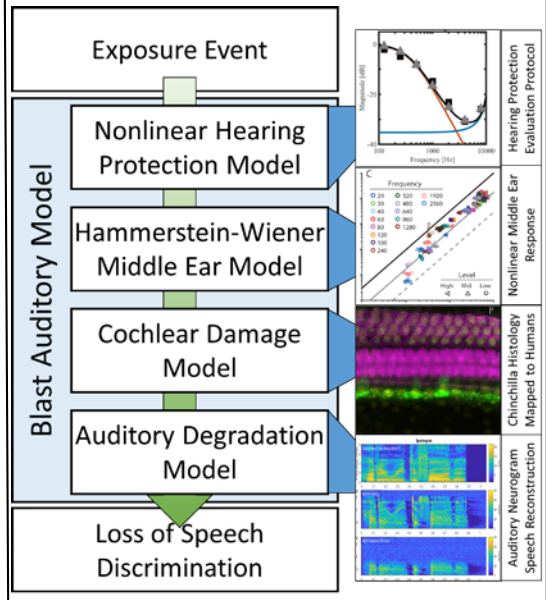

The Blast Auditory Model developed under this program predicts the propagation of a blast wave through the auditory system using a series of sequential submodels. The outputs of the model were verified experimentally using laser Doppler vibrometery and fiber optic pressure gauges within both the chinchilla animal model and human temporal bones. The outer ear is modeled as an acoustic lumped element network, the middle ear as a nonlinear transfer function, and the inner ear using an auditory nerve model.

Timeline and Cost

Activities / CY	15	16	17	18
Blast Characterization through HPD				
Quantifying Middle Ear Dynamics				
Measuring Auditory Response				
Improve AHAAH Model				
Estimated Budget ($K)	**$748**	**$547**	**$504**	**$521**
Updated: October 31, 2018				

Goals/Milestones

CY15 Goal – Evaluate pressures in the EAC to various levels of blast with and without hearing protection

- ✓ Quantified pressures in EAC with and without HPD using PMHS and began implementing findings into enhanced AHAAH Model
- ✓ Fabricated Shock Wave Emulator for Year 2-4 Testing

CY16 Goals – Quantifying Middle Ear Dynamics using Both PMHS and Chinchilla Models

- ✓ Quantify differences between Human and Chinchilla middle ears
- ✓ Address non-linearities of AHAAH middle ear

CY17 Goal – Measuring Auditory Response using Chinchilla Model

- ✓ Measure ABR and DPOAE response to blast using Chinchilla Model

CY18 Goal – Predict damage correlated to central auditory function

- ✓ Extend AHAAH model further into brain's neural network

Budget Expenditure to Date

Projected Expenditure: $2,320,452

Actual Expenditure: $2,314,753